Development of a Rock Mass Boreability Index for the Performance of Tunnel Boring Machines

By

Saad Cheema

A thesis submitted to the faculty and board of trustees of the Colorado School of Mines in partial fulfillment of the requirements for the degree of Doctor of Philosophy (Mining and Earth Systems Engineering).

Golden, Colorado

Date: _07 - 26 - 99_

Signed: _____
Saad 'Cheema

Approved: _____
Levent Ozdemir
Thesis Advisor

Golden, Colorado

Date: _07/26/99_

_____
Dr. Tibor G. Rozgonyi
Professor and Head
Department of Mining
Engineering

ii

ABSTRACT

The ability to accurately predict TBM performance allows for more reliable estimates of the project completion time and costs, hence the increased confidence in the application of this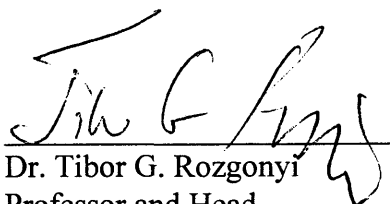 technology to a wider sector of the underground construction market. One of the key parameter in all performance predictor models is the geological and geotechnical input represented by the strength of the formation to be bored.

The strength of rock is a function of intact properties and rock mass characteristics. To establish the relationship between the intact rock properties and the existing geologic features, such as joints, bedding and foliation, a Rock Mass Boreability Index (RMBI) has been developed in this thesis. This index is determined from elasticity modulus, Poisson's ratio and a size reduction factor which has the greatest effect on boreability. The size reduction factor is calculated from UCS, RQD, and joints spacing, conditions and orientation. The foliation effect is taken into account by the indirect tensile strength test.

To validate the concept and the developed index, extensive field TBM performance data were collected from a tunnel recently completed in Boston, Massachusets. In addition, cores were taken at fixed intervals along the tunnel to establish a database of rock properties. This database included intact rock properties, such as unconfined compressive strength, tensile strength, elasticity modulus and Poisson's ratio, as well as rock quality designation (RQD), joint spacing, orientation, condition and the foliation. The machine performance data included motor amps, propel pressure and the achieved penetration rate throughout the 10-mile long tunnel. The goal was to evaluate the machine performance during actual boring and its relation to the developed rock mass boreability index.

The RMBI was derived by applying regression analysis to the extensive database of rock intact and mass properties collected from the entire length of this tunnel. This index was then incorporated into the existing CSM model designed to predict the TBM performance as a function of the measured rock properties and the encountered geologic features. A very close correlation was obtained between the model predictions and the actual field performance of the Boston TBM.

TABLE OF CONTENT

LIST OF FIGURES

LIST OF TABLES

ACKNOWLEDGMENTS

1. INTRODUCTION

Mechanical excavation today has become a common aspect of underground development. Its role in the development of underground space, from tunnels, shafts, inclines to mining applications has gained increasing importance over the past few decades. The growing degree of successful experiences with mechanical excavators in numerous projects has moved them from "novel techniques" in the past, to more of a today's "conventional" method. They are expected to take a greater share of the underground construction market in the future compared to drill and blast as advancements and improvements continue to occur in different aspects of the mechanical excavation technology.

One of the major issues in the successful application of mechanical excavators has been the design optimization and the accurate performance prediction of these machines. Design optimization refers the requirement for a thorough study of the anticipated ground conditions and design of the cutterhead for achieving optimum performance. Design and performance optimization ultimately dictates the attainable production rates, hence determining the cost and the economics of the project.

Tunnel Boring Machines (TBM), which are the main focus of this study, have achieved remarkably high advance rates in tunnel construction, not matched by any other means of excavation. They are the most popular mechanical excavators and the prime choice for tunnel construction in practically any ground conditions, ranging from soft to very hard rocks. Nonetheless, the existing capabilities for an accurate and reliable performance prediction of these machines still need further improvements.

Tunnel Boring Machines now dominate the excavation of long tunnels throughout the world. According to the American Underground-Space Association (AUA) each year, the US public sector awards between 20-30 major underground projects with a diameter of over 1.5 m (5 ft) and a combined value of over one billion dollars. This is a small portion of the US investment in its physical infrastructure which has been estimated at $20 trillion, much of it in transportation and utility service networks constructed in urban environment (CERF 1994). With the increasing competition for surface space and the growing concerns on the environmental issues pertaining to urban development, the share of underground construction in the construction infrastructure is expected to increase (Nelson 1996). Additional tunneling activity is carried out in diameters below 1.5 m (5 ft) in the utility sector which, according to the National Research Council (NRC), amounts to over 2 billion dollars. AUA tunnel demand forecast based on the study of eight years of tunneling activity indicates an increasing demand for infrastructure development and enhancement. This study shows the market expects sporadic growth with an average rate of 8% over the next decade. Also, based on AUA forecast, hard rock tunneling amounts to just under 15% of the major underground projects or about $140 Million each year. The worldwide market for civil hard rock tunnels is assumed to be 3 to 4 times the US market and estimated at $420-470 million. (Handewith 1995)

In mining applications, virtually all-underground development in hard rock is done with drill and blast at the present time. Little information is available regarding the actual development footage of mine drifts. However, one can conservatively assume that each year about 50 miles of tunnels are driven by the mining sector in hard rock in North America. Due to their short service life, mine drift development costs are only about 30-40% that of civil tunnels. This leads to estimates of about $270 million for the value of North American hard rock tunneling in mining sector and about $810 million world wide. This market is not expected to show significant growth, rather a steady demand for

underground hard rock tunnels in mining is anticipated. Therefore, the estimated worldwide market for hard rock tunnels is about $1.2 billion per annum. (Handewith 1995)

The share of TBMs in underground civil construction is significant. Yet the application of TBMs in underground hard rock development in mining is limited to a few cases. One of the main obstacles in further growth in the market share of TBMs in mine development is the high capital investment together with the time and costs associated with their mobilization. This puts a heavy burden on the project finances, which does not justify application of TBMs in tunnels shorter than 2 km (1.5 miles). This limit can be partially improved as the percentage of capital investment for TBMs to the total project costs decreases due to increases in labor costs, reduced machine prices, application of used TBMs, and improvements in machine design which allow for rapid mobilization and start of boring operations.

Another major impediment stems from the lack of general knowledge about the operational capability of mechanical tunnel boring. This refers to limited exposure of owners and some contractors to these machines and their potential. The enormous positive impact of mechanical excavation in tunneling and underground development has been over shadowed by many years of experience with drill and blast and the hesitation to implement a new method. This problem is rapidly diminishing as more and more tunnels are successfully completed by the TBMs and both owners and contractors continue to gain experience with this technology. Also, the substantial advances in information and communication systems in recent years have been instrumental in removing the barriers for technology transfer and in building a bridge between the parties involved in decision making for the selection of excavation method. The familiarity with the significant benefits of these systems should improve as the new generations of engineers, more educated about these systems, enter the job market.

Despite these advancements in mechanical excavation technology, there is still an important issue that must be addressed. A large majority of the tunneling contracts end up in major disputes and claims. Some of these claims are resolved between the contractors and the owners while some are referred to the Disputes Review Boards (DRB), and some make their way to courts. These claims/disputes consume a significant amount of time and energy form all the parties involved and impose additional financial burden on the projects. This can range from a few percent to over 100% of the total estimated project budget or contract value (bid). This burden is commonly passed on to the taxpayers since in most of the cases, the owner is public sector (i.e. cities, public utility, water authorities, etc.).

Some of these disputes are over the change order and ground conditions, which is normally easy to resolve. When an unpredicted situation such as high ground water inflow, a fault zone, different rock type, etc. is encountered in the tunnel, both parties investigate the situation and typically a settlement is reached to compensate the contractor for the losses of time and incurred extra costs.

The other type of dispute arises from the TBM achieving a lower performance than anticipated based on the information provided in the Geotechnical Data Summary Reports (GDSR). The same forums that discussed and suggested use of baseline performance in the GDSRs a few years ago, are discussing to improve the information provided as a baseline in the geotechnical reports now due to problems experienced in project development and contracting practice. This refers to the estimated performance of TBMs in a given rock type and ground conditions. Typically a baseline performance and penetration rate is provided in the GDSRs to allow for uniform costing of tunneling jobs by contractors. This baseline, which is simply a performance prediction for a typical machine specification in the given rock types, is normally used by contractors for preparing their bids. If for some reason, the

achieved penetration rates do not match the predicted baseline, there is a ground for dispute or claims.

A part of the problem stems from the limited funds generally allocated for geotechnical investigations. Typically, the cost of geotechnical investigations and the design is about 4-6% of the total project costs. Only a portion of these funds is allocated for actual drilling and testing of the samples. It is not uncommon to drill very limited number of exploration holes along the tunnel alignment and to test only a certain portion of the samples recovered to develop geological and geotechnical maps. Consequently, there are many occasions where the insufficient amount of data available can lead to incomplete interpretation of the subsurface conditions. To further compound the problem, in most tunneling jobs, only certain rock properties are measured which fall short of providing an accurate assessment of rock boreability. The most common rock property given in the geotechnical data reports is the unconfined or uniaxial compressive strength (UCS). The second property normally reported in the GDSRs is the quartz content. Other parameters, such as rock tensile and shear strength, grain size and shape, intergranular bonds, porosity, abrasivity indices such as Cerchar index, and the rock fracture properties are not normally measured in the geotechnical investigations. Moreover, rock mass properties including direction and frequency of joints, fractures, bedding and foliation are not always considered in pre-construction investigations.

The type of tests performed on rock samples collected from a tunneling site or on the cores retrieved from bore holes are usually dictated by the type of performance prediction method to be used. As stated earlier, in most cases, all required information for the use of a specific TBM performance model may not be available. In such cases, the missing properties have been estimated from data available in similar rock formations. Given the

fact that no two-rock types have the same boreability characteristics, assumptions on unmeasured rock properties could lead to inaccurate performance predictions for TBMs.

The preceding discussion places a sharp focus on the importance of accurate and reliable performance prediction models in tunneling projects. These models have a major impact on every stage of tunnel development, from the initial pre-feasibility studies, to GDSR reports, engineering design and cost estimates, to bid preparation by the contractors, and finally, to resolution of claim disputes. Shortcomings of these models in accounting for any of the influencing parameters could result in errorous performance estimates and potential claims. Unfortunately, all the models available to date have some limitations depending on the basis used for their development. This is due to the very complex nature of the problem which involves a wide range of parameters including cutter geometry, rock cutting parameters (i.e. spacing between the cuts), rock mechanical properties affecting rock failure and chipping, fracture initiation and propagation, dynamic nature of chipping, and rock mass properties and imperfections. A valid solution to this problem will certainly help improve the utilization of mechanical excavators in tunneling operations both in civil and mining, by providing more accurate performance estimates towards developing more reliable costs and schedules for the projects.

As noted earlier, several models have been developed over the years for performance prediction of hard rock TBMs. These models can be divided into two main groups, empirical and semi-theoretical. The empirical methods are based on the observed performance of TBMs in the field and interpretation of the relationships amongst the influencing parameters. The semi-theoretical models are based on the testing and measurement of forces acting on individual cutters. Cutting forces, which are predicted from the geological and geometric parameters, are then related to the machine performance and penetration rates. The main advantage of the latter type of models is their ability to

provide reasonable estimates of machine performance while assisting engineers in machine design and providing the means for design optimization.

1.1 Objectives of the Thesis

The existing TBM performance prediction model developed by the Colorado School of Mines (CSM) has had great success in providing a reasonable estimate on penetration rate of the machines in massive rock formation. However, for rocks exhibiting unusual boreability characteristics in terms of fractures, thin bedding and joints / foliation, the existing model is still sometime unable to producing accurate TBM performance estimates. The current study is an attempt to address this problem and improve the capabilities of the performance prediction model by providing a better insight into interaction between the machine and the rock. The main objective of this study to develop a rock mass boreability index to incorporate the effects of joints and foliation into the existing CSM predictor model to improve the accuracy of the model. The objectives of this study can be summarized as follows:

1. Develop a rock mass boreability index based on intact and rock mass characteristics.

2. Collect and analyze field TBM data to verify the developed index.

3. Develop guidelines for recommended rock testing for tunnel boring projects.

These objectives are designed to provide a guideline for future TBM projects and to enhance the predictive capabilities of the current performance prediction models to achieve higher levels of accuracy and reliability. Moreover, an accurate estimate of cutting forces is essential in optimization of cutterhead design. Optimization means achieving maximum

performance for a given machine thrust and power with subsequent reductions in project costs and completion time.

Accuracy of the TBM performance estimate is crucial in conducting a reliable feasibility assessment of TBM application in a project. The direct impact of penetration rate on the design of machine back up systems and tunnel utilities, the timing and planning of the project, and finally, the projected costs and schedules is well established. In order to extend the areas of application for TBMs in the future, reliable performance prediction arises as one of the key issues impacting the future growth of this highly promising and successful technology.

1.2 Scope of the Proposed Thesis Research

The above mentioned objectives can be met by following a thoroughly developed plan for identifying the basic parameters, using the available information, and conducting additional theoretical and experimental studies. the following describe the specific steps to fulfill the objectives of this study. This comprises of conducting a laboratory testing and field measurements and utilizing the results towards the modification of existing TBM performance prediction model, as follows:

a) A literature review to identify the parameters influencing the performance of TBMs and considered in available performance prediction models.

b) To develop a rock mass boreability index to accommodate rock mass properties into the existing predictor model.

c) Development of the laboratory and field testing plans for achieving the objectives of this dissertation.

d) To analyze the database of physical properties and rock mass information to validate the developed rock mass boreability index.

e) Applying the developed concept to existing TBM performance prediction model to evaluate the machine performance.

f) Recommending guidelines for pre-bid investigations for future projects in foliated rock conditions.

1.3 Thesis Organization

The current thesis is organized with the intention to provide a logical sequence for reviewing the issues and developing the solutions. The first chapter is the preface to the proposed study and its importance. It contains the introduction to the field of mechanical excavation and tunneling, especially TBMs brief review of the issues, definition of the problem, and the general approach taken to address these issues. It also states the objectives of the proposed work and the means to achieve these objectives.

Chapter 2 is a review of the pertinent literature, particularly focusing on the issue of performance prediction models for TBMs using disc cutters, cutting force estimation, and influencing parameters.

Chapter 3 describes the existing CSM predictor model for tunnel boring machines, based on intact rock properties.

Chapter 4 describes the relevant rock mass classifications and their utilization in developing the rock boreability index. It also describes the general equation for the index.

Chapter 5 describes the source of field data and rock properties collected to verify the developed rock mass boreability index. It includes a detailed introduction to the tunnel

project where data were collected. This includes the pre-bid investigation, establishment of geo-technical data survey report, and selection of machine based upon given information.

Chapter 6 describes the laboratory-testing program performed to evaluate the performance of the machine. This includes the brief description of each test performed to identify the rock mass behavior and analysis of the laboratory testing.

Chapter 7 describes the field-testing program including equipment and the special instrumentation used for the test program to evaluate the performance of the tunnel-boring machine. This includes description of drag test and the strip chart data collection and covers the analysis of the machine performance from field data.

Chapter 8 includes the discussion of the model results for the project in light of new index equation applied to the existing CSM predictor model to incorporate the rock mass behavior while predicting the performance of machines in future projects with jointed and foliated rock. It also includes the hypothetical case to analysis the rock mass behavior on the performance of the machine.

Chapter 9 includes the suggested testing methods to determine the rock properties in the laboratory to evaluate the behavior of rock mass.

Chapter 10 summarizes the results of the thesis work and lists the conclusions and chapter 11 contains the recommendation for the follow up studies.

2. LITERATURE REVIEW

2.1 Background

All the tunneling projects have a common aim, namely that of successfully mastering the range of geological difficulties encountered. The geological problems, however, differ from site to site and each site. The type of difficulties experienced may not necessarily be anticipated. The geological environment presents the major challenge to both the tunnel designers and the builders. Additionally there is often a measure of uncertainty concerning the response of the rock mass to the chosen tunneling method. Although there is, however, general recognition of the importance of knowledge on the geological aspects of tunneling projects, the depth of such knowledge and its appreciation in respect of particular sites frequently gives rise to different opinions.

The nature of the geological setting of a tunneling site has a major bearing on the choice of construction method and many aspects relating to safety, design and subsequent service, operation and maintenance. Detailed geological factors essentially influence the choice of a particular tunneling method and in some cases govern the feasibility of an entire project.

The extent of prior knowledge of geological aspects of the proposed tunneling site is frequently governed by economic consideration. Consequently while the site exploration stage is accepted as providing vital data to judge tunneling design proposals, due account needs to be taken of the limitations of prior exploration in providing a complete assessment of the various geological factors of relevance to the project. In many tunneling projects, the main detailed geological data only becomes available during the tunneling construction phase.

All the stages of a tunnel project, from preliminary design considerations through design evaluation and final design selection, to assessment and choice of construction method, and finally through to commissioning and operation of the tunnel, the designers need to be prepared to revise their thinking on final designs in the light of geological information that emerges subsequent to the design stage. Therefore it is of paramount importance to tunnel work that a through geological investigation is conducted before the commencement of construction work, and this would involve producing geological sections along proposed tunneling alignment. Additionally the engineering behavioral characteristics of the rocks are also equally important to provide a basis for making judgements on the practical and economical feasibility of the project.

The general aim of the preliminary geological investigation is to provide the nature of the ground forming the route of the tunnel. It is frequently difficult to correlate surface knowledge of the geology with that anticipated along the planned route of the tunnel. The cost of such preliminary work which includes geological surveys, test pits, drilling, geophysical surveys and any additional measurements may arise in special situation is likely to cost 2 to 8 percent of the total cost of the project.

The investigation should proceed from general to specific according to the following steps.

First step involve literature search survey to review the published and unpublished information on project area, including general history and appreciation of previous significant undertakings and construction works of the site. Aerial photographs are good source to obtain broad overview of project area and identify geomorphological aspects.

Second step should include reconnaissance of surface geology and geophysical survey. Surface geology provides general appreciation of rock types, constituent make-

up and structural properties, geomorphological and weathering aspects. Geophysical survey offers advantages of being non-destructive, relatively fast and generally of low unit cost especially advantageous for tunnels in locating anomalous conditions which would need detailed identification by direct methods. Methods include seismic refraction and reflection surveys, electrical resistivity soundings, gravity surveys and magnetic surveys. An application of geophysical methods includes identification of material type, location of anomalous geological conditions, location of bedrock horizon and assistance in choice of drill hole sites. Down-hole geophysical techniques have proved useful in studying stratification, geological structures, and rock types and possible existence of cavities and old mine workings. Down-hole cameras have proved useful in supplementing such work in specific cases.

Third step is to perform exploratory drilling, which is the most common exploration method used in civil works and provides geological information specific to the drill hole area. The location of drill holes needs careful consideration in order to maximize the information yielded and this does not necessarily mean arbitrarily spaced holes along the tunnel line. Drill holes should provide detailed exploration of portals, topographic lows, locations where deep weathering is suspected, water-bearing locations and shear zones. The rock-drilling program provides information to identify the geological types, stratigraphy and structure at the tunneling horizon. It also helps in process of determination of physical properties of rocks, establishing fracture pattern data for main rock types and evaluation of rock strength characteristics.

Next step in site investigation involves *In situ* testing. In situ rock mechanics investigations provide:

(a) Evaluation of rock support and reinforcement requirements for temporary and permanent phases of construction.

(b) evaluation of rock stability

(c) assessment of suitability of various excavation construction methods

(d) Provision of rock physical properties to assist tunnel construction evaluation.

Laboratory work is performed for:

(i)   Determination of rock strength values and deformational behavior in uniaxial and triaxial stress conditions for pre- and post- failure states,

(ii) Determination of elastic constants for the rocks,

(iii) Assessment of creep behavior characteristics,

(iv) Determination of rock joint strength values and influence of joint in-filling,

(v)   Determination of permeability and porosity values,

(vi) Assessment of density and susceptibility to loss of strength due to weathering and other factors,

(vii) Rock hardness and abrasive properties.

Full-scale models are sometimes employed to assess the merits of particular aspects of the detailed design. Small-scale models are useful for testing particular features of the design, and offer a relatively low cost means of assessment. Models are useful for conveying a visual impression of the overall geological setting along the route of the tunnel.

Detailed assessment of geological features as exposed during actual construction needs to be recorded and taken into account in updating existing records; this involves

regular and systematic inspection of the tunnel face by a geologist. The implications of changes in rock types and their condition, in geological structure and in hydro-geological character need assessment by a geologist in relation to the overall tunneling project and associated works. Monitoring to judge that the tunnel post-construction monitoring and condition satisfies the expected stability, performance and performance levels of safety as anticipated by the design forms an important part of the overall project.

2.2 Rock Fragmentation

Mechanical tools have been used in rock fragmentation for a long time. Ranging from drill bits and point attack cutters to roller cutters and discs, they all share the same principle of penetrating into the rock under a force and causing it to break. Over the years, the cutting tools and machines have undergone significant technological evolution. Today's mechanical excavators have become highly productive, efficient, and reliable while growing in application in a wide variety of ground conditions. At present, disc cutters are the most efficient tools among the different types of cutters employed in hard rock excavation. They are also the cutters of choice in many other applications due to their capability to cut a wide range of rock types ranging from soft to very hard, larger product size, and the lower specific energy requirements. Discs were first installed on the tunneling machines around 1950's and became more popular as improvements were made in bearing design and disc material coupled with a better understanding of the rock fragmentation process. Today, disc cutters are widely used on mechanical excavators of different types. Figure 1 shows a disc cutter used on the tunnel boring machines in recent years to improve the performance of the machines.

Disc cutters have proven to be superior to drag type tools in cutting hard rock formations due to their prolonged wear performance and efficiency. They can cut a wide

variety of rocks of different strength and are more durable than pick cutters. Picks can not be used in hard rocks because of the high wear rates and loss of carbide tip caused by shock loads or the excessive heat generated during the cutting process. Therefore, disc cutters are the only alternative for successfully excavating hard and abrasive rocks and provide the highest efficiency among roller cutters. Today, the cutting tools utilized on hard rock TBMs are almost exclusively single disc cutters with replaceable disc rings.
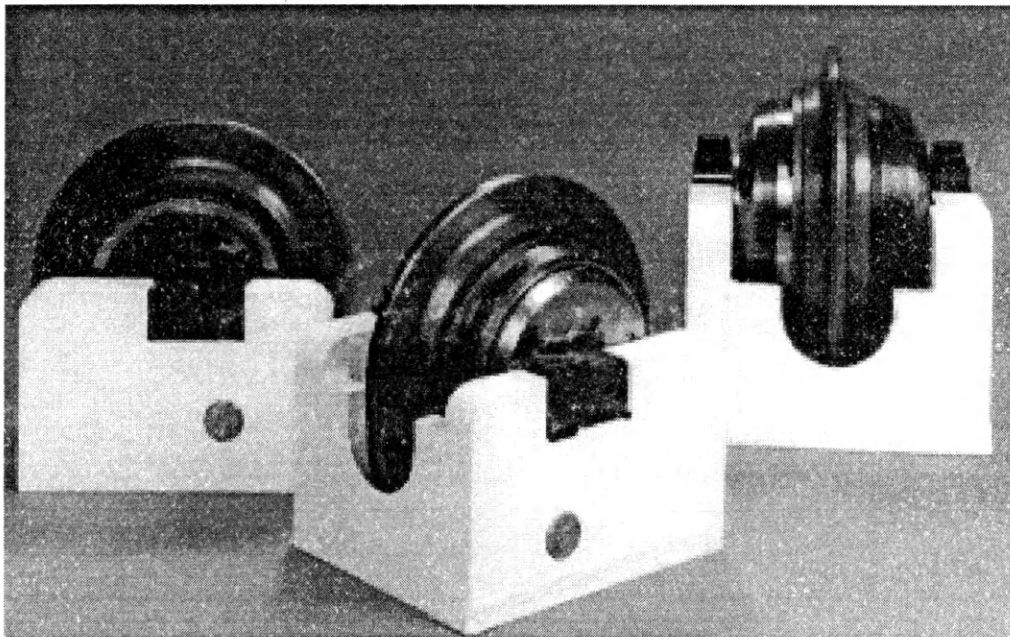
Figure 1: The disc cutter used on tunnel boring machines for hard rock.

Over the years, disc cutters have significantly improved in performance as a result of the development and utilization of more wear resistant materials and steel alloys, increased bearing capacity, and a more efficient cutting edge profile. Early disc cutters had a V-profile (V-shape) which caused rapid loss of efficiency as the tip wear occurred. Starting in the late 1970's V-shape ring profiles were replaced by constant cross section (CCS) profiles to maintain the nearly same cutting efficiency as the tip wore out. A

superimposed drawing of the two profiles is shown in Figure 2. Present day TBMs almost exclusively use CCS cutters, which are also the dominant type of cutters installed on various types of underground hard rock excavators. Figure 3 shows a picture of tunnel boring machine fitted with disc cutters. Each cutter cuts a concentric kerf, as shown in Figure 4. As it will be discussed in more detail later, the spacing of the kerfs and their relation to cutter penetration is a very important parameter influencing machine performance.
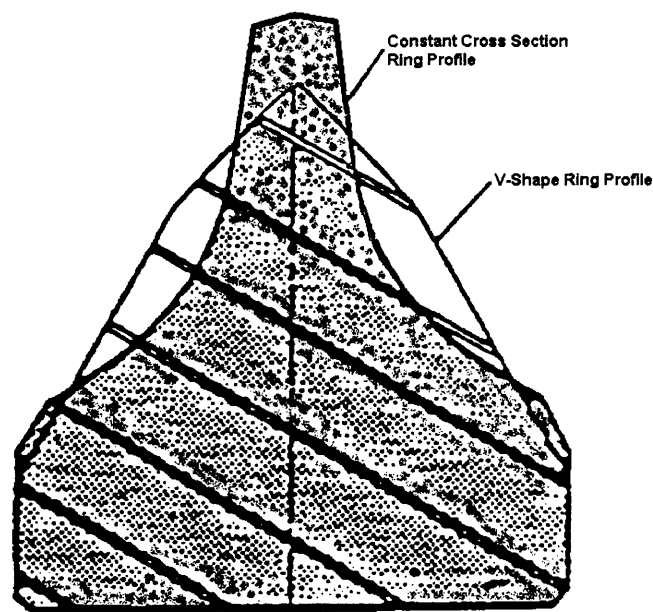
Figure 2. Superimposed drawing of a V-shape and CCS disc cutter (after Ozdemir 95)
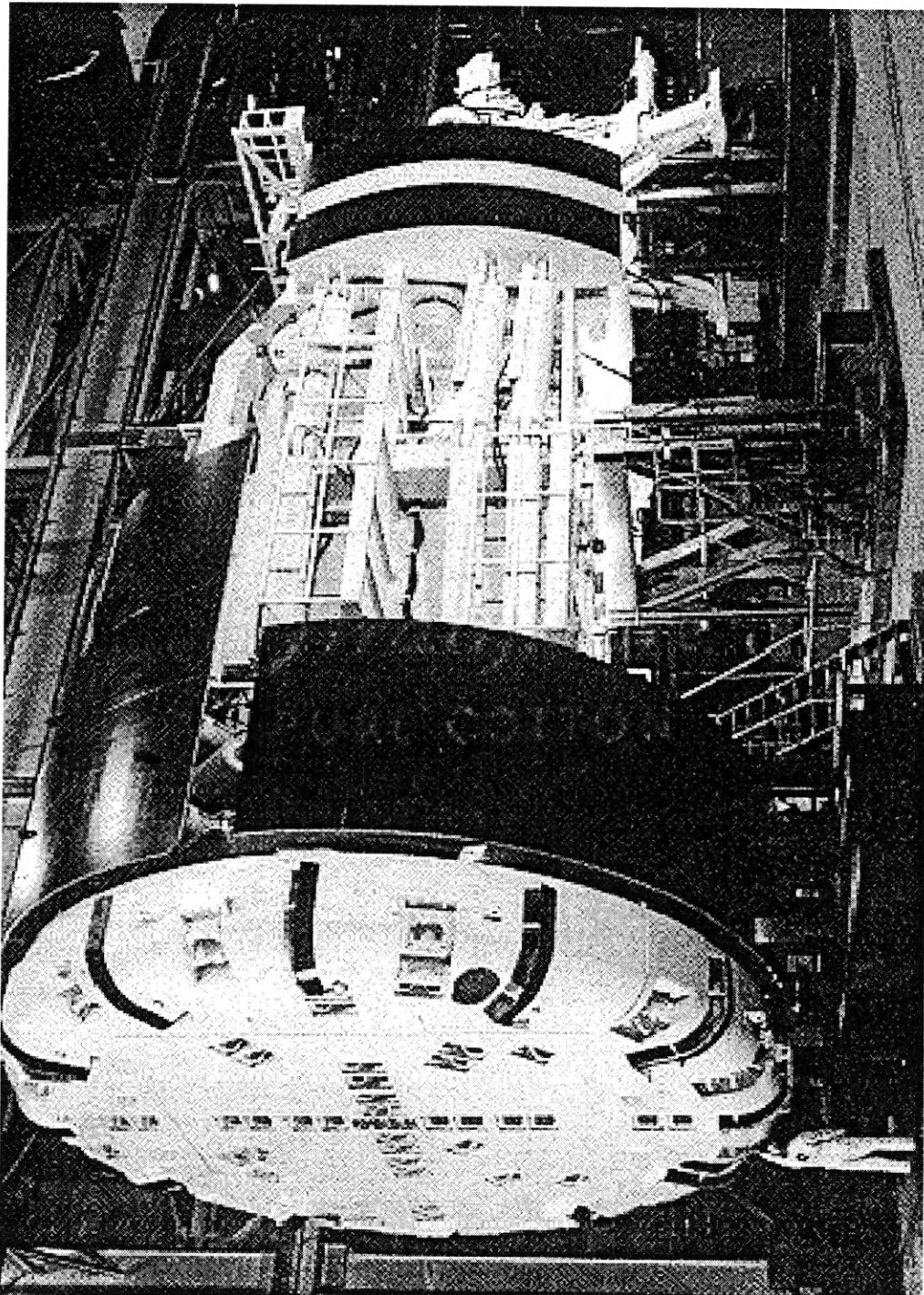
Figure 3: Modern day tunnel boring machine with disc cutters.
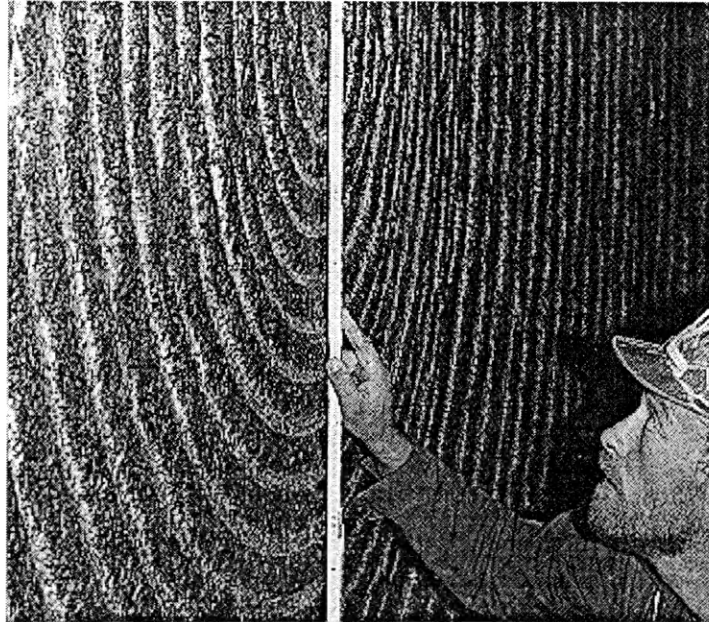
Figure 4: Tunnel face excavated by disc cutters on a TBM.

Studies on the rock fragmentation process can be divided into the following categories.

i)   Study of the indentation process in small-scale laboratory tests,

ii)   Investigation of the rock cutting process by using full-scale tests under controlled conditions in the laboratory,

iii)   Evaluation of the machine performance and geological parameters in the field.

Study of the indentation process has created a great deal of knowledge on the mechanism of crushed zone formation and the development of cracks, but it has failed to adequately explain the broader picture of chip formation and the interaction of all cutting parameters involved in disc cutting. The field studies have been useful for observation of interaction between the machine and the rock under real conditions. However, the

geologic complexity and constantly varying rock properties together with machine and operator induced errors have increased the complexity of the problem, thereby making it difficult to draw firm conclusions or derive reliable formulas to estimate machine performance. The laboratory testing of full size cutters has served as the link between these two ends by allowing a closer examination of the rock-cutter interaction under controlled test parameters and cutting conditions. The need for more research in this area has been very apparent to those involved in the subject and has been deemed crucial to advancement of the understanding of rock fragmentation principles (Nelson 1996).

Despite the commonality of the indentation process, the cutting phenomenon is drastically different between drag bits and disc cutters. In the case of drag bits, the crushed zone is very small and localized, thus the developed cracks are relatively shallow. The component of the force parallel to the cutting path is relatively high, meaning low normal and significant drag forces. The concentration of stresses in the direction of cutting is very high and therefore, cracks propagate in this direction to form chips. This mandates a smaller cut spacing because the lateral development of cracks between the cuts is very limited. Overall, the cutters in this category tend to scratch the rock more than stressing it to failure (Figure.5).

For disc cutters, the mode of cutting is different since the component of normal force is much higher than the rolling force. Due to the available bearing capacity of these cutters, higher loads can be applied on the disc to meet the high normal force requirements for cutting hard rock. The rock is subjected to significant stresses and deep cracks up to several centimeters (or inches) can develop under disc cutters. Longer cracks mean increased spacing between the cuts and the creation of larger chips (Figure 6). Since the cutter rolls over the rock, less scratching and much less cutter wear occurs.
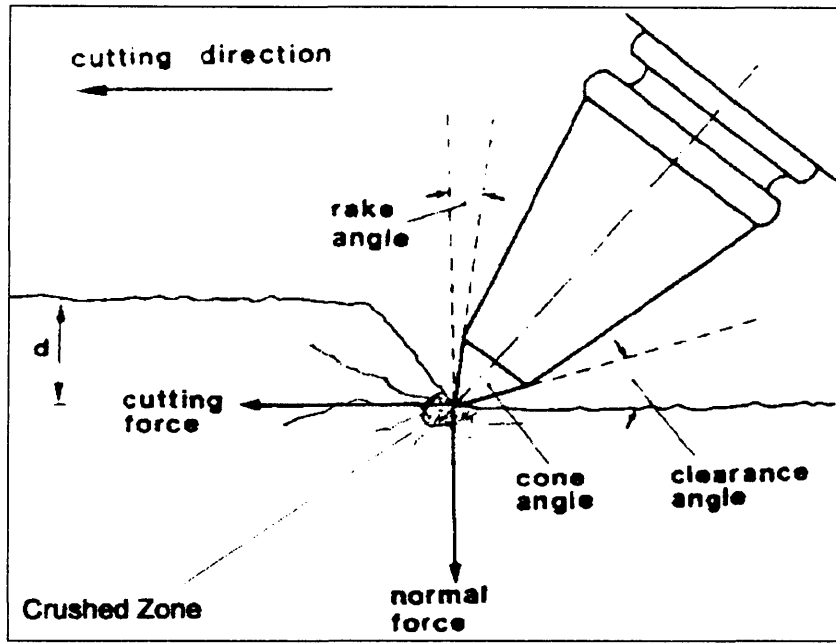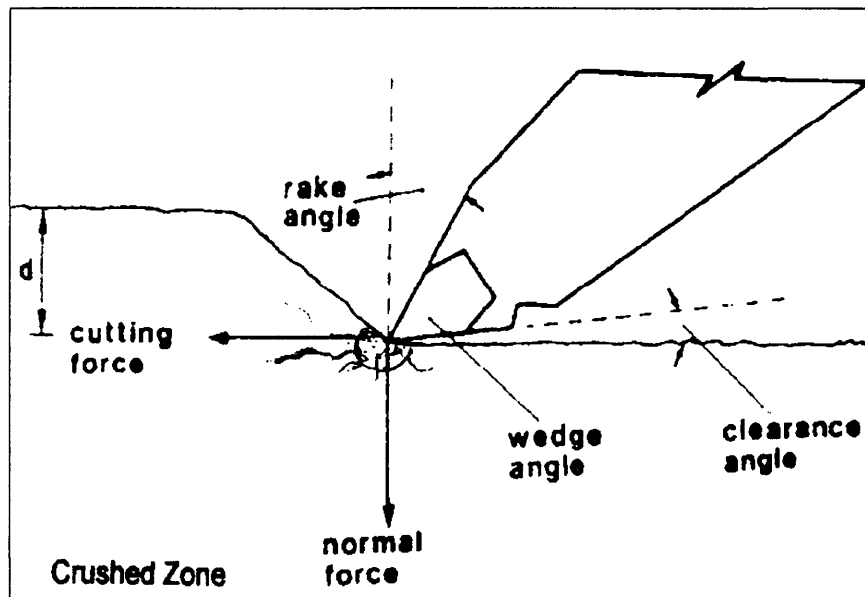
Figure 5: Schematic drawing of the cutting mechanism for a) point attack cutter, b) drag bit (After Goktan 1992)
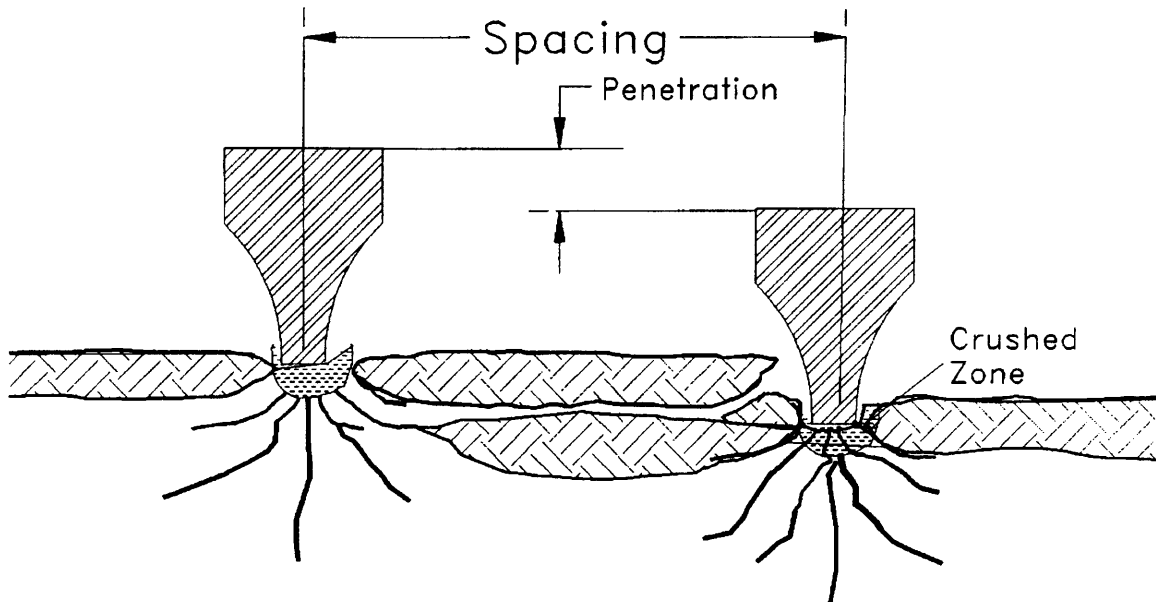
Figure 6: Disc cutting process.

Cutting forces acting on a disc cutter, the normal, rolling, and side forces are essential inputs to the cutterhead design and layout of hard rock mechanical excavators. Figure 7 shows these force components on a disc cutter. Normal forces constitute the thrust requirement of the machine and rolling forces determine the torque and power requirements of the machine. Side forces are usually random, since chips can form on either side while the pressure is maintained on the opposite side. The exception to this rule is the side forces on the center and gage cutters (installed at an angle), that act outwards toward the periphery of the tunnel. These cutters often can experience significant side loads.

There have been extensive studies over the years to determine the forces acting on disc cutters as they cut through the rock. These forces are used in optimization of the cutter head design and layout, and the overall machine design. Also, they are used to provide an estimate of the machine performance and the attainable production rates. This

is a critical issue in assessing the feasibility of applying mechanical excavators in an underground construction project.
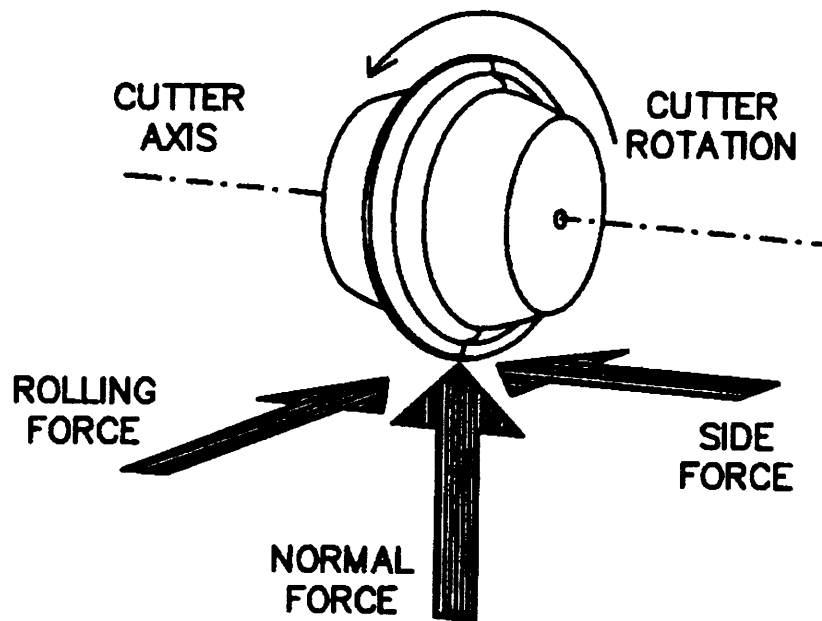
Figure 7: Schematic drawing of the cutting forces on a disc cutter (Rostami 97).

For the estimation of cutting forces, different investigators have used different approaches. On one hand, numerous tests in various scales have been conducted on individual cutters to identify those parameters affecting the cutting forces and their interactions. On the other hand, field studies using the geological and machine parameters have been performed to estimate the cutting forces and to observe the relationships between influencing parameters. The latter approach has always involved the complexity of interaction between the machine and the rock mass, level of machine thrust and torque used, the accuracy of the records maintained for machine performance, the effect of worn and new cutters working together, and other related factors. Overall,

these issues combined have generally masked the accurate determination of cutter forces in the field. Further, the accumulated data was used towards development of empirical models calibrated with reference to a small data set, without verification on a larger scale (Nelson 1996). There have also been attempts made to measure the forces directly under the disc mounting assembly on the face of TBMs. These measurements have proven that the results obtained from the laboratory linear cutting tests are accurate enough for the type of studies on cutting forces.

It has been observed that the cutting forces are a function of cutter and cutting geometry, as well as the rock physical properties. The cutter geometry refers to the disc diameter, the tip width and the geometry of the ring profile. The cutting geometry includes the spacing between the cuts and the depth of penetration. Rock physical and mechanical properties include primarily the unconfined compressive strength and the tensile strength of the rock. Other parameters, such as Young's elastic modulus, Poisson's ratio, internal angle of friction, are also known to influence the cutting forces, but to a much lesser degree. In addition, the effects of grain size and shape, porosity and rock hardness indices on the cutting forces have not been thoroughly studied in previous research efforts. This is partly due to the fact that some of these parameters are not commonly found in the geo-technical reports and are seldom measured in the field.

Since fractures are the primary means of forming chips between the adjacent cuts, one of the major rock characteristics influencing the cutability is initiation and propagation of fractures in a given state of stress. Although there have been several attempts made to take these parameters into account (Nelson et. al. 1985, Sanio 1985, Whittaker et. al. 1992), there is still no existing model which can fully explain, formulate, and utilize the rock fracture parameters in estimation of cutting forces.

Following is a summary of the research performed in different scales to identify the

parameters influencing the performance of TBMs using disc cutters to provide a basis for understanding of the process towards developing accurate tools for performance prediction and analysis.

2.3 Rock Indentation and Disc Cutter Theories

Reichmuth (1963) considers a crushed zone under the cutter based on the experimental evidences. He assumes that the crushed zone is a triaxial compression region that generates tangential tensile stress field, the material behaves elastically, two-dimensional tensile strain failure criterion is valid, and the maximum tangential tensile strength is generated right underneath the wedge tip. The initial crack starts under the wedge tip, as shown in Figure 8.

The initial crack extends into the medium till the tensile strain at the crack tip reaches below the point that required for fracture development. Reichmuth developed a stress estimation formula for initiation of the first crack that is independent of wedge angle and wedge penetration as follows:

$$\sigma_R = \frac{2P}{\pi t}\left(\frac{\cos\alpha}{R}\right) \tag{2.1}$$

The parameters of the equation 2.1 are given in Figure 9. The initial crack divides the stress fields into two quarter-spaces and the secondary cracks develops and extend to the surface to form chips, as shown in Figure 10. In this condition, the stress estimation is expressed by equation 2.2. It should be noted that in equation 2.2, it does not take into account for penetration, which is a deficiency of this theoretical model.

$$\sigma_R = \frac{4P}{Rt}\left[\frac{Nz'\cos\{\alpha - (\pi/4)\}}{\pi + 2} + \frac{Nx'\sin\{\alpha - (\pi/4)\}}{\pi - 2}\right] \qquad 2.2$$
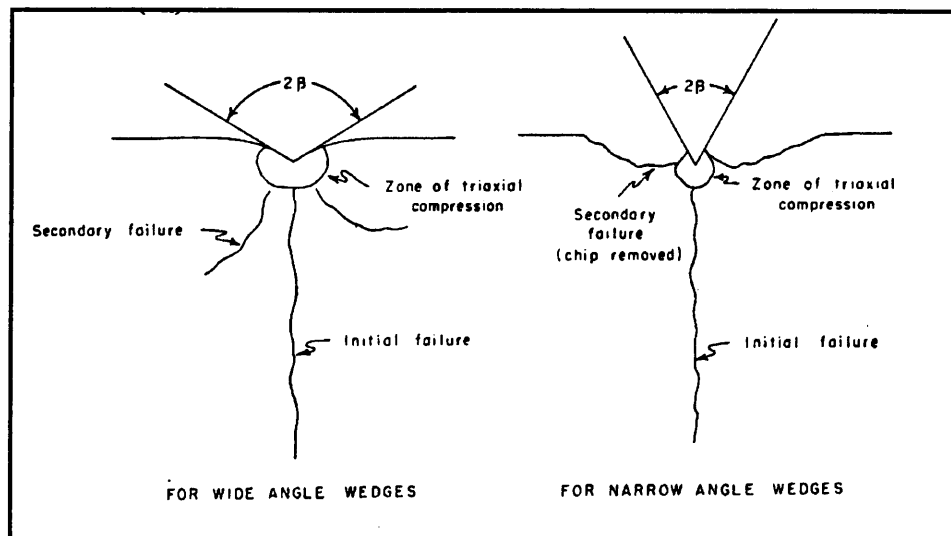
Figure 8: Fracture development induced by wedge indentation (Reichmuth, 1963)
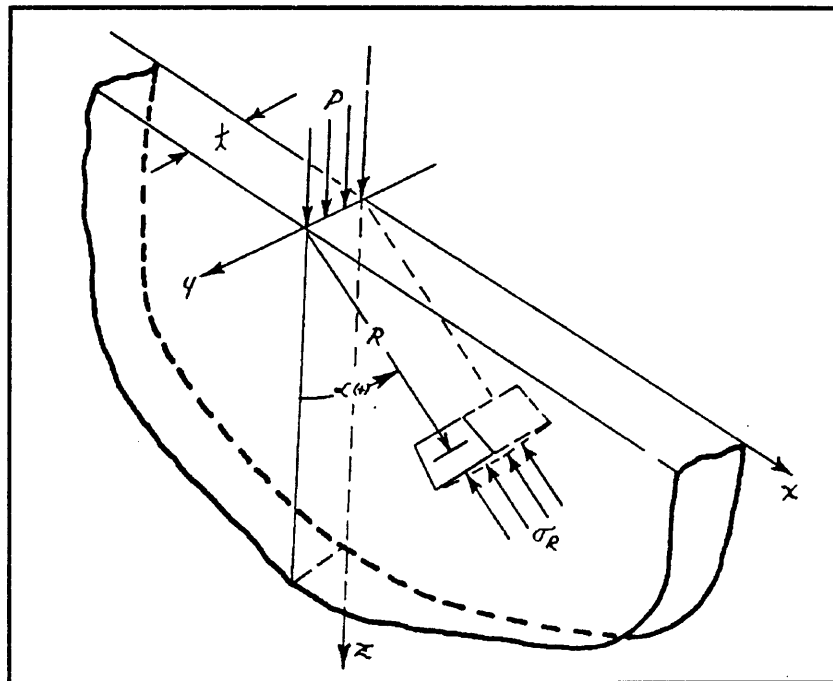
Figure 9: Nomenclature for a half-space under concentrated load (Reichmuth, 1963)
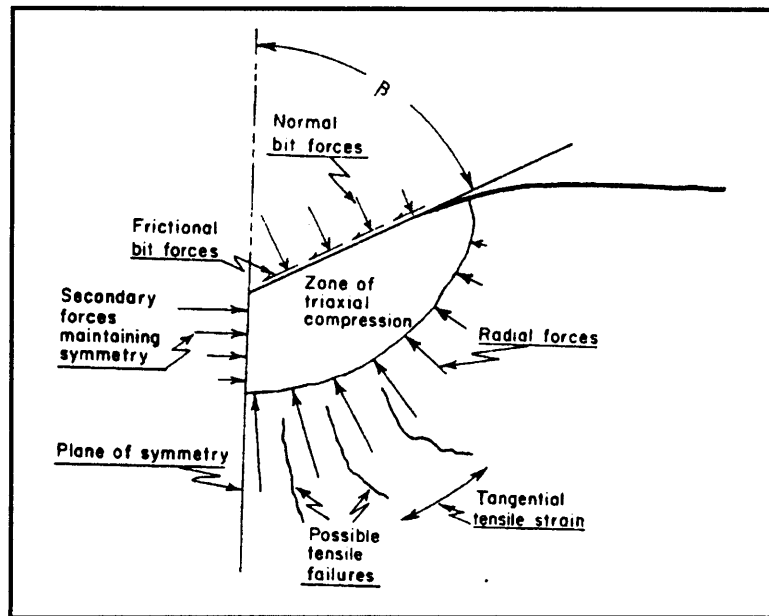
Figure 10: Quarter-space under indentation loading (Reichmuth, 1963)

where :

for $\tan \beta \leq \dfrac{\pi - 2\mu B}{2 + \pi\mu B}$

$$Nz' = \frac{\sqrt{2}}{4}\left(\frac{1 - \mu B \tan \beta}{\tan \beta + \mu B} + 1\right)$$

$$Nx' = \frac{\sqrt{2}}{4}\left(\frac{1 - \mu B \tan \beta}{\tan \beta + \mu B} - 1\right)$$

for $\tan \beta \rangle \dfrac{\pi - 2\mu B}{2 + \pi\mu B}$

$$Nz' = \frac{\sqrt{2}}{4}\left(\frac{2 + \pi}{\pi}\right)$$

$$Nx' = \frac{\sqrt{2}}{4}\left(\frac{2 - \pi}{\pi}\right)$$

and $\beta = bit\ semi - angle$, $\mu B = bit - medium\ friction\ coefficien\ t$

$\sigma_{\alpha'} = 0$ *and* $\tau R_{\alpha'} = 0$

Paul and Sikarskie (1965) omitted the crushed zone occurrence phase and only concentrated on brittle chip occurrence phase for brittle isotropic rocks. They assumed a two-dimensional and direct loading of the chip by the penetrating wedge, causing a shear failure. They set the mathematical model as shown in Figure 8 and assumed that the experimental force-penetration data, i.e. slope k and slope K, is known for constant penetration rate conditions, as illustrated in Figure 11. It should be noted that the slopes k and K could be estimated for constant loading conditions. The resulting chip formation forces are derived from Mohr-Coulomb failure criterion assuming a uniform shear and normal stress distribution along the potential failure line.

The chipping angle ψ is estimated from equation 2.3. The force (P^*_{i+n}) necessary to obtain the $(i+n)^{th}$ chip is estimated from equation 2.4, if the penetration depth (d^*_i) of the previous chip is known. The penetration depth (d^*_{i+n}) of the $(i+n)^{th}$ chip is estimated from equation 2.5, if the penetration depth (d^*_i) of the previous chip is known.

$$\psi = 45° - \frac{\theta + \phi_f + \phi}{2} \tag{2.3}$$

$$P^*_{i+n} = K \left(\frac{k}{k-K} \right)^n d^*_i \tag{2.4}$$

$$d^*_{i+n} = \left(\frac{k}{k-K} \right)^n d^*_i \tag{2.5}$$

Where:

θ = wedge semi-angle (degrees)

ϕ = angle of internal friction of rock (degrees)

ϕ_f = angle of friction between indentor and rock (degrees)

k = slope of force-penetration curve during crushing periods (psi)

K = slope of line connecting peak forces (psi)

K value is also given as follows:

$$K = \frac{4c\sin(\theta + \phi_f)\cos\phi}{1 - \sin(\theta + \phi_f + \phi)} = \frac{P*_{i+1}}{d*_{i+1}}$$

Where:

c = cohesion of rock in lbs./inch square.
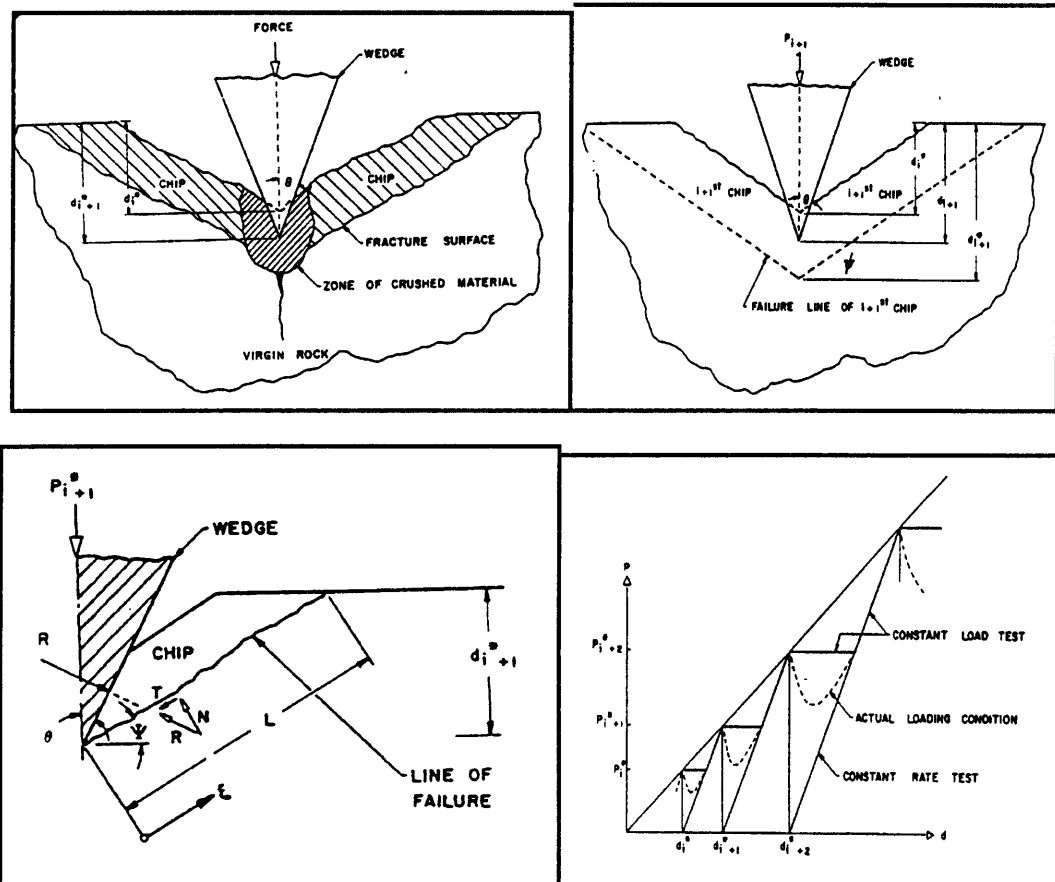
Figure 11. Mathematical idealization of the model by Paul and Sikarskie (1965)

The theory gives higher force values than the authors' experimental results. The authors thought that this was because of the oversimplification of the theory by assumptions such as uniform shear and normal stress distribution along the potential failure line.

Miller and Sikarskie (1968) extended the theory developed by Paul and Sikarskie (1965) for three-dimensional cone, sphere and pyramid shape indentor. They compared the indentor by experimentally estimating the force increase rates for initial crushing and post chipping phases.

Benjuma and Sikarskie (1969) extended Paul and Sikarskie's theory for non-isotropic (bedded) brittle rocks. Dutta (1972) extended Paul and Sikarskie's theory by including both crushed zone occurrence and chipping phases.

Ozdemir (1977) developed theoretical models for predicting the forces acting on sharp and dull V-shape disc cutters for indexed cutting (includes spacing between the cutters). He assumed that the failure of the ridge between the cuts was a shear failure, there was a pressure bulb (crushed zone) under the cutter, and the rock was isotropic and brittle (Figure 12). If the spacing were too small or too large, the cutting would be inefficient. There is an optimum spacing to penetration ratio that makes specific energy optimum. The vertical (normal) and rolling forces acting on a sharp V-shape disc cutter are estimated with equation 2.6 and equation 2.7.

$$VF = D^{1/2} p^{3/2} \left[\frac{4}{3} C + 2\tau \left(\frac{s}{p} - 2\tan(\alpha/2) \right) \right] \tan(\alpha/2) \qquad (2.6)$$

$$RF = \left[Cp^2 + \frac{4\tau\phi \left(s - 2p\tan(\alpha/2) \right)}{D(\phi - Sin\phi Cos\phi)} \right] \tan(\alpha/2) \qquad (2.7)$$
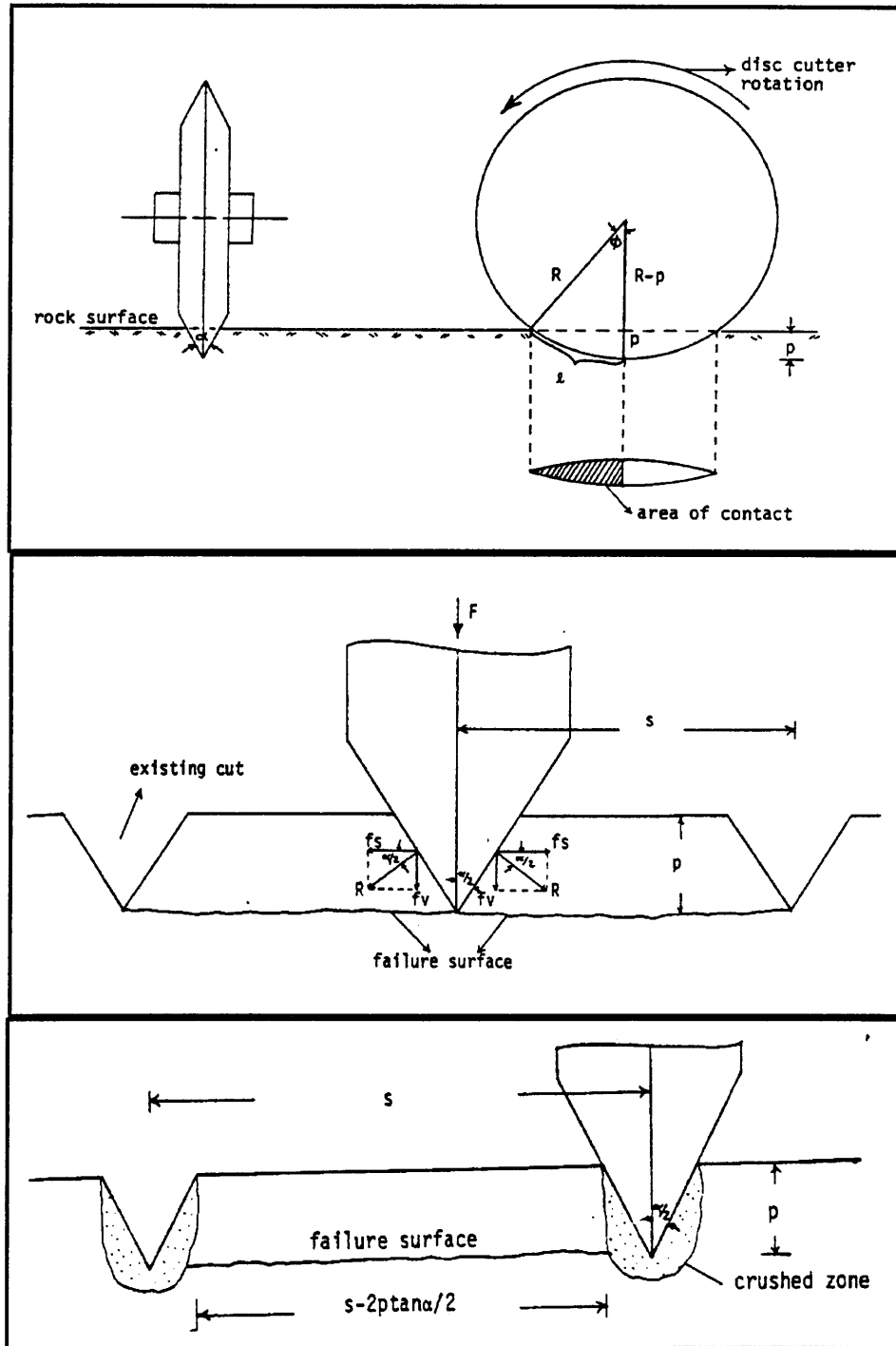
Figure 12: Mathematical idealization of the model by Ozdemir (1977)

Where:

VF = mean vertical force on the cutter (lbs.)

RF = mean rolling force on the cutter (lbs.)

C = rock uniaxial compressive strength (psi.)

τ = rock unconfined shear strength (psi.)

D = cutter diameter (inches)

α = cutter edge angle (degrees)

s = spacing of cuts (inches)

p = cutter penetration (inches)

$\phi = ArcCos[(R-p)/R]$

R = cutter radius (inches)

The analytical solution for the case of indentation of mechanical tools into the rock begins with the analysis of stresses in an elastic media under a point load. Boussinesq offered the first formulation of the stresses under a point load and the related stress field was calculated and analyzed by Lawn and Swain (1975). In essence, all the mechanical rock cutting tools share the same principle and consequently, a great deal of efforts have been dedicated to developing models which can offer an explanation for the force-penetration behavior of rocks. When an indentor penetrates the rock, a zone of crushed material is developed immediately under the tip, consisting of fine material, which in turn transfers the load to the surrounding area. Radial cracks are created around the crushed zone and then propagate as the applied load and pressure in this zone increases. The forces increase until a chip is formed and then the stresses are released. The chip formation is due to initiation and propagation of cracks under the applied load. These cracks grow until they reach a free surface, which could be the rock surface or another fracture in the rock. This phenomenon has been observed and confirmed by almost all researchers in a variety of rock cutting and indentation tests. Despite the extensive

studies, there is still a difference of opinion as to the dominant mode of failure, whether it is tensile or shear.

Based on experimental results of wedge indentation and full-scale cutting tests with disc cutters and on a basic theoretical analysis of the interaction between tool and rock, predictor equations for the calculation of tool forces in bedded rock were developed. In contrast to predictor equations derived by Roxborough and Phillips or Ozdemir et al, the equations derived by Sanio(1985) are based on the assumption that tensile rather than shear failure is the dominant chip forming mechanism of disc cutters is the base of these equations. This fundamental assumption is justified by the evidence of typical tensile failure characteristics at the chip surfaces and by the fact that the experimental results can best be correlated to the tensile strength of the rock. The cutting process can be explained in Figure 13. As a direct result of high stress concentration, the rock is first crushed in a zone just below the tool. An approximate hydrostatic state of stress exists within this crushed zone causing tangential tensile stresses to be generated in the surrounding undamaged rock. When these reach the tensile strength, tensile cracks develop which extend in radial direction from the cutting edge. Once such a crack reaches the free surface of the rock, a chip is formed which removes the rock between the neighboring cuts. It is assumed that the crushed zone is circular in shape. Its radius is to be a constant fraction q of the penetration depth h. The critical hydrostatic pressure within the crushed zone is to be a characteristic constant of the rock, i.e. it is independent of the geometry of the tool. Multiplication of this hydrostatic pressure by the projected area of contact between the tool and the rock equals the penetration force f_N (Figure 13).

$$f_N = 2 * h * \tan\left(\frac{\varepsilon}{2}\right) * \sigma_0 \qquad (2.8)$$

Where:

f_N = penetration force

h = depth of penetration

ε = wedge angle and

σ_o = hydrostatic pressure in the crushed zone.
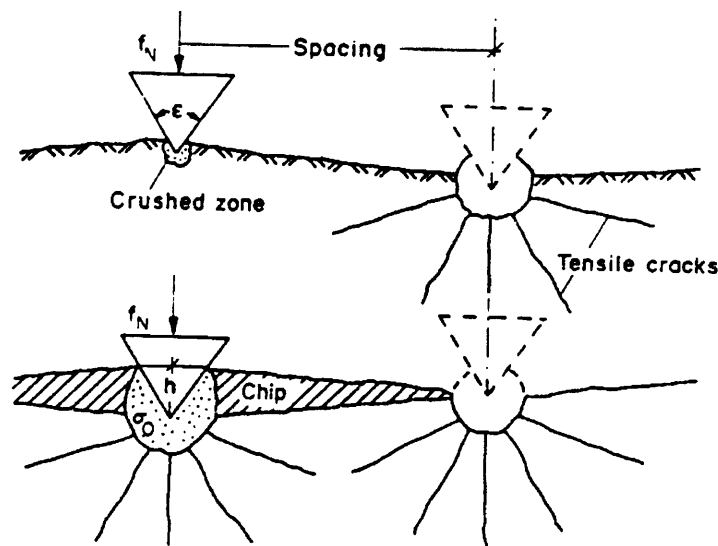
Figure 13: Schematic representation of wedge penetration and chip forming process (After Ouchterlony).

Ouchterlony carefully studied different expansion loaded radial crack systems, which are very similar to the Situation presented in Figure 13. His findings can be used to determine the unknown hydrostatic pressure σo in equation 2.8. Ouchterlony deduced the following correlation between the length of the crack and the radius of the hole and σo for a pressurized circular hole with pressure less radial cracks in an infinite plate (Figure 14).
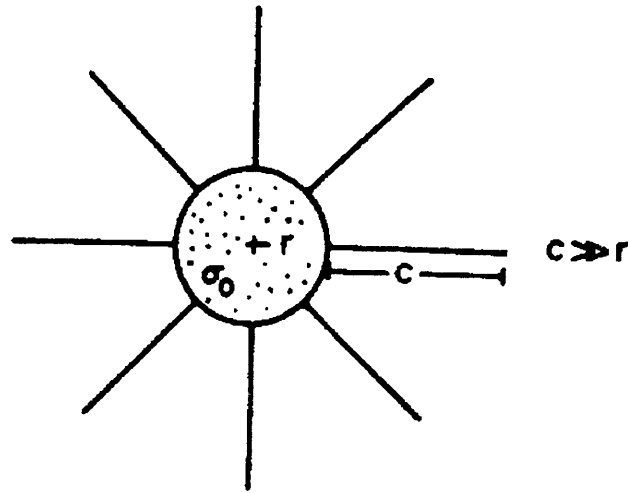
Figure 14: Crack propagation from a circular hole in an infinite plate (After Ouchterlony)

$$2 * \sigma_0 * r = k * c^{0.5}$$ (2.9)

Where:

r = radius of the hole

k = critical stress intensity factor, dependent on the rock and the number of cracks

c = length of crack

If the influence of the free surface on the rock on the state of stress at the crack end is neglected, and r = q * h, penetration force can be expressed as follows:

$$f_N = \frac{k}{q} * \tan\left(\frac{\varepsilon}{2}\right) * c^{0.5}$$ (2.10)

With the use of equation 2.10, the equilibrium of forces acting on a disc cutter can be determined as shown in Figure 15. Approximating the area of contact between the

tool and the rock by thin wedge elements arranged in the form of steps with a width dx, the penetration force FN at the tool is given by equation 2.11.

$$FN = \int_0^{(d*p-p^2)^{0.5}} f_N(x)dx \qquad (2.11)$$

$$FN = \frac{k}{q} * \tan\left(\frac{\varepsilon}{2}\right) \int_0^{(d*p-p^2)^{0.5}} c(x)dx$$

Where:

      FN = penetration force

      d = diameter of the tool (disc)

      p = penetration of tool (disc)
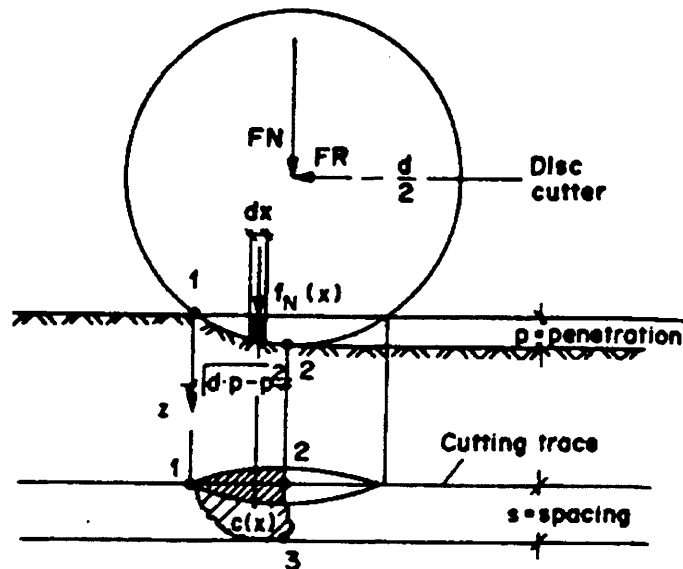
Figure 15: Cutting process of a disc cutter.

A single wedge element starts its penetration at point (1) in Figure 15. At this point the length of crack is zero. The wedge element at point (2) generates crack of length s in order to enable continuous removal of rock between two neighboring cuts. If the length of the crack increases between points 1 and 2 linearly with x, the following is attained:

$$c(x) \cong \frac{s}{(d*p - p^2)^{0.5}} * x \qquad (2.12)$$

By incorporating equation 2.12 into 2.11 and integrating over the area of contact between tool and rock the normal penetration force is estimated from the following:

$$FN = \frac{2*k}{3*q} * \tan\left(\frac{\varepsilon}{2}\right) * (d*p - p^2)^{0.5} * s^{0.5} \qquad (2.13)$$

The rolling force (FR) can be calculated from the penetration force. If the friction at the bearing of the tool is neglected, the resultant of FN and FR must pass through the rotation center of the tool as shown in Figure 16, so the moment around the tool axis must be zero.

$$FN*h + FR*t - FR*\frac{d}{2} = 0,$$

with $h = (d * p - p^2)^{0.5} - b$ it is follows that

$$FR = \frac{\left[(d*p - p^2)^{0.5} - b\right]*FN}{\left(\frac{d}{2} - t\right)}$$

Since the resulting normal force FN must yield the same static moment around point 2 as the sum of all moments generated by the normal forces of the infinitesimal small wedges, b can be derived as:

$$b = \frac{1}{FN} * \int_{0}^{(d*p-p^2)^{0.5}} f_N(x)dx$$

then

$$FR = \frac{2}{5} * \frac{\left[(d*p-p^2)^{0.5}\right]*FN}{\left(\frac{d}{2}-t\right)}$$

(2.14)

Cook et. al. (1984) performed a series of tests to observe the crack growth in hard rock loaded by an indentor. They proposed a formula for estimating the stress needed under an indentor to penetrate a certain amount into the rock as follows:

$$\sigma = \frac{E.p}{0.54(1-v^2)a}$$

(2.15)

Where:

σ_n= Normal stress under indentor

E = Elastic modulus

p = Average displacement of the punch

v = Poisson's ratio

a = Area of indentor

It was also found that the rock deforms elastically until the applied load exceeds

45% of the maximum. After that, a crack is initiated around the perimeter of the punch and propagates in the well-known Hertzian manner.
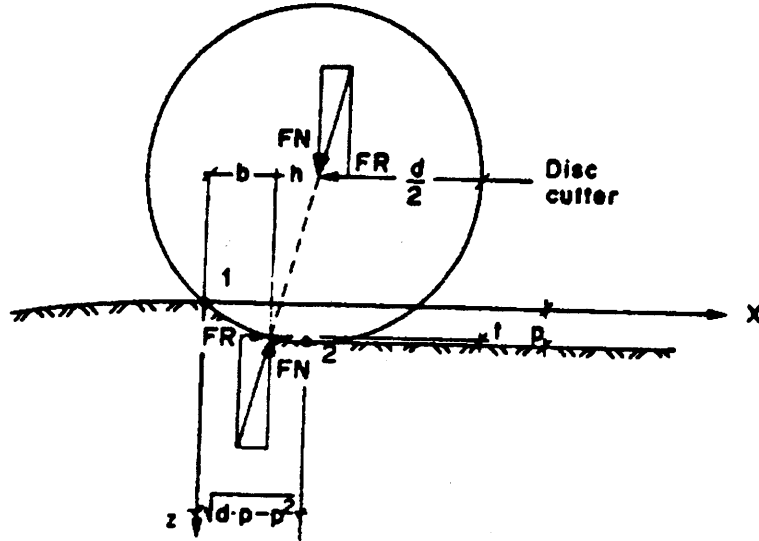
Figure 16: State of equilibrium of a disc cutter.

A force-deformation model has also been developed for localized loading of brittle rocks by Pang et. al. (1989). In this model, conical and wedge shape indentor were considered and a model was proposed for simulating the force indentation behavior which mainly depends on the geometry of the tip-rock contact area. The force requirement for a wedge shape indentor was calculated as follows:

$$F_s = \sigma_o(Sin\theta + \mu Cos\theta)\left(\frac{2wx}{Cos\theta}\right) \qquad (2.16)$$

And for conical shape indentor:

$$F_s = \left[\sigma_o(Sin\theta + \mu Cos\theta)\left(\frac{\pi Tan\theta}{Cos\theta}\right)\right]x^2 \qquad (2.17)$$

Where:

F_S = Normal Force

σ_0 = Constant stress in crushed zone

θ = Half-cone angle

w = Width of indentor

x = Depth of indentation

Peng et. al. also offered some equations for estimating force requirements on blunt indentor. These models show a linear force for wedge indentation and a quadratic relationship for conical indentor. The resistive stress, is yet to be determined by testing or other studies and the proposed model only provides a means to simulate the force indentation behavior. The model also provides envelopes for upper and lower band of forces as the indentation into the rock proceeds. The model was verified by comparing the results with some experiments, showing a satisfactory agreement.

There have also been several attempts to apply numerical methods to rock indentation and fragmentation under different types of cutters. Among the numerical methods, the most widely used is the Finite Element Method (FEM). FEM is very powerful and flexible in most stress field simulations and particularly useful under complex geometry and loading conditions. The main underlying assumption in the model, however, is the continuity of the media. In spite of the new developments in FEM to include gap elements or other means of simulating discontinuities, it can not, under normal circumstances, allow for initiation and propagation of cracks. As a result, the path for the cracks and discontinuities has to be defined, which inherently causes a bias in the results. A special study conducted by Souma (1984) is an example of the many attempts to simulate rock cutting and related crack propagation process by FEM. A program was specifically developed for this purpose and was capable of re-meshing the

domain to include the crack tip growth. Yet, due to the complexity of the process, the 2D model could only account for a predetermined crack path.

For the problem of rock cutting, other methods, such as the Displacement Discontinuity Method (DDM), are preferred. This method was developed by Crouch (1976), and is similar to the integral equation method using a special Green function. It allows the use of influence functions to set up a system of simultaneous algebraic equations involving only the boundary conditions while singularities are represented algebraically in the analytical solution and the finite displacement of a line segment replaces the infinite displacement of the point solution.

The numerical procedure involves descretizing a certain number of elemental displacement discontinuities along the boundaries and then producing a system of simultaneous algebraic equations to find the discontinuity values, which cause prescribed stresses or displacements at the boundaries. This procedure has been found to be particularly applicable to the crack propagation problem. It allows the calculation of displacements normal and/or parallel to the crack plane, facilitating the determination of stresses and displacements for a curved crack, as well as an intercept crack and a crack with frictional forces along its faces. This method has been used for solving the rock cutting problems by several groups, including Sun et. al. (1992) and Guo et. al. (1992) who applied DDM for the modeling of rock chip formation by drag bits and disc cutters.

2.4 Full Scale Tests and Laboratory Studies

There have been a number of research studies performed on the estimation of disc cutter forces since their introduction in mid 1950's. Murhead and Glossop (1968) and Hustrulid (1970), Temporal & Snowdon (1983), obtained a good correlation between the rock compressive strength and the Specific Energy (SE), defined as the amount of energy

to excavate a unit volume of rock. Effects of joints and planes of weakness were examined by Benjumea and Sikarski (1965), Miller (1974), Ozdemir (1975), and Howarth and Roxborough (1982), and Sanio (1986). They all observed and reported a significant reduction in cutting forces in presence of joints in the rock except for the joints oriented normal to the cutting surface (parallel to loading).

The exact mechanism of how rock failure occurs under the action of a disc cutter is a subject that has been studied in great detail over the last two decades. As a result of these efforts, several theories have been developed with the objective of modeling and explaining the rock failure process, which were discussed earlier. The theories differ primarily in the way which chipping is assumed to take place to an adjacent cut. Some theories are based on the occurrence of a shear failure while others use a tensile mode of failure for chip formation between neighboring cuts. Which type of failure predominates is still a subject of intense research and controversy. Mechanical rock failure is a complex process influenced by nearly all rock physical and geologic properties. Naturally, more brittle rocks will tend to fail by tensile fracturing while a shear type failure may predominate in rocks exhibiting a more plastic behavior. In general, evidence produced from high-speed movies of the cutting process and the examination of the chip failure surfaces all support the occurrence of a tensile failure for rocks. In soft rocks lacking brittle behavior, chipping is believed to occur by a combination of shear-tensile failure, one proceeding the other depending on rock characteristics and the cutting geometry. One aspect shared by all these theories is the existence of a zone of highly crushed rock material beneath the cutter tip prior to chipping (Figure 17).

As the cutter penetrates the rock, a crushed zone is formed due to extremely high stresses generated in the rock. This crushed zone is also commonly referred to as the pressure bulb. The tensile strain generated in the crushed zone causes tensile cracks to

initiate and propagate into the rock mass. The cracks continue their propagation until the tensile strain at their tip falls below the tensile strength of the rock. If the stresses developed in the crushed zone are sufficiently high, one or more cracks extend far enough to reach one of the tensile cracks developed from the adjacent cut, causing rock failure in the form of chipping, as shown in Figure 18.
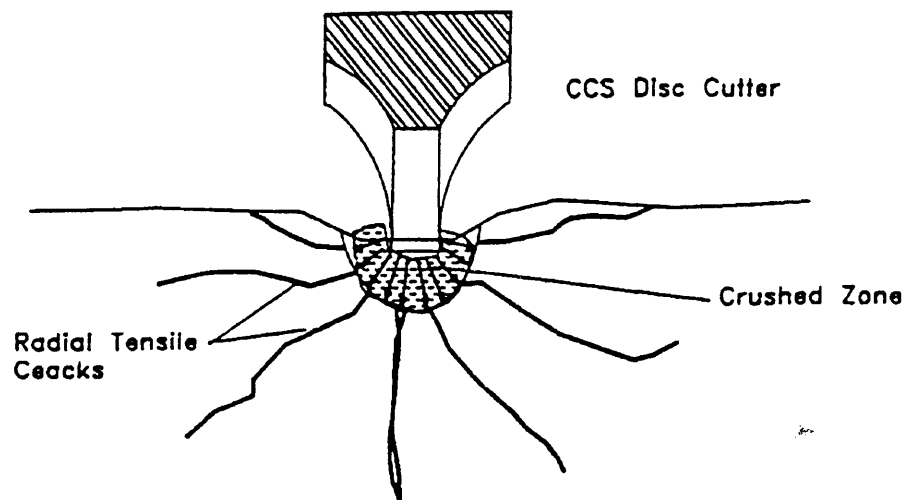
Figure 17: Brittle chip formation with crushed zone (after Ozdemir 96).
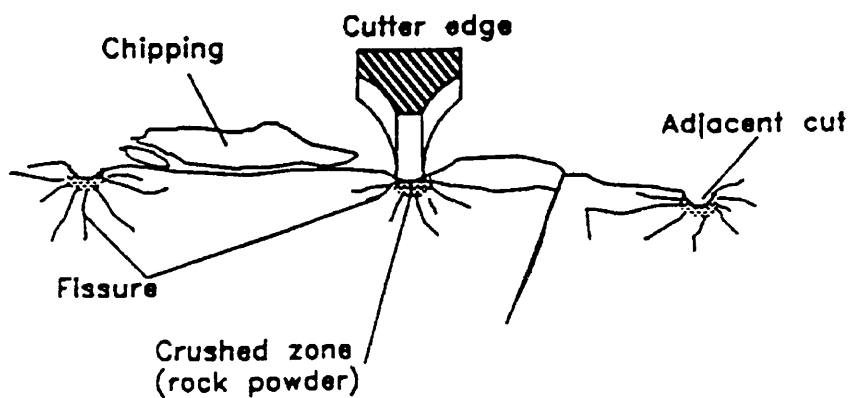
Figure 18: Chipping mechanism (after Ozdemir 96).

As for the cutting geometry, effects of spacing and penetration along with the cutter type and geometry have been studied by Ozdemir et al (1978). It has been established that the magnitude of cutting forces increases with the increase in the spacing between the cuts. Depth of penetration also was shown to have the same effect on the cutting forces. This includes both the normal and the rolling forces which increase in a relatively linear fashion with spacing and penetration. The observed behavior of cutting forces with regard to spacing can be divided into three zones, as shown in Figure 19. The first zone corresponds to small spacing, and is characterized by the localized crushing with little or no chip formation and excessive crushing, resulting in high specific energy requirements and low efficiency accompanied with rapid increase in cutting forces. The second zone features increased spacing, where chipping begins to occur and becomes the principle mechanism of rock failure while forces continue to increase in a more or less linear fashion with spacing. In the third zone, due to increased spacing and lack of interaction between the cracks, chip formation ceases to occur for each pass of the cutter while forces increase until they reach a certain level.
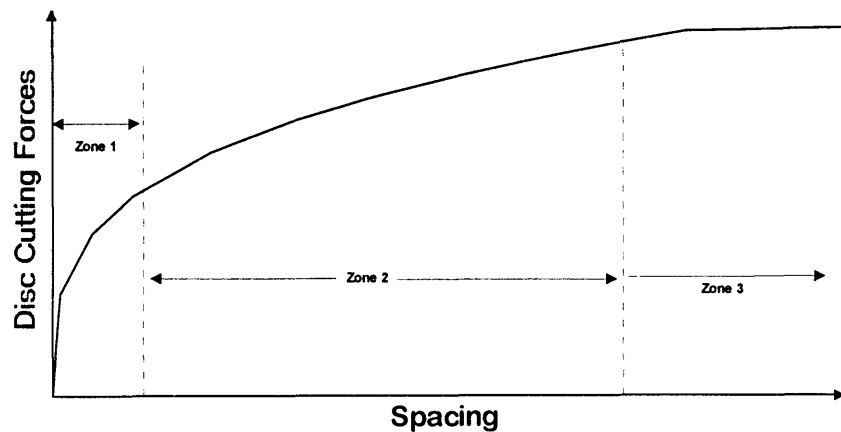
Figure 19: Variation of cutting forces with spacing between the cuts (Rostami 97).

At larger spacing beyond this zone, cuts become isolated and cutters continue to deepen their grove without chip formation as shown in Figure 20. For disc cutting, there is a range of spacing to penetration (S/P) ratio where the specific energy of cutting is minimized and the most efficient cutting is achieved. This range is normally between S/P ratios of 10 to 20. This relationship is schematically shown in Figure 21.

Cutter tip geometry has been shown to have a major impact on the cutting forces. Increased tip angle in V-shape cutters and the greater tip width in CCS cutters can drastically increase the cutting forces. Cutter radius also impacts the forces required to penetrate the rock. In this case, the forces increase almost proportional to cutter radius.

The rate of production in any mechanical rock excavation system is directly proportional to the amount of energy transfer to the rock. Thus, there exist two options for increasing the rate of penetration in a rock boring operation. First is to optimize the cutting process to enable system operation at its minimum specific energy. This is accomplished by determining the optimum spacing of cuts once an estimate is made of the depth of penetration which a cutter will achieve for a given thrust load. The optimum spacing is selected by using the s/p ratios discussed above taking into account rock hardness and brittleness. The second option is to transmit more power into the rock by increasing the thrust, torque and /or the rotational capacity and therefore, the power of the machine. Naturally, the machine may already be operating at its maximum thrust or torque/power capacity and this option may not be available. In general, TBMs become thrust limited in hard rocks. In soft formations where higher rates of penetration are feasible, the machine usually reach their torque/power capacity before becoming thrust limited. Of course, a well-balanced design would allow the machines thrust and torque capacity to be reached at approximately the rate of penetration. The thrust / torque vs. specific energy relationships for TBM performance. is shown in Figure 22 and Figure 23.
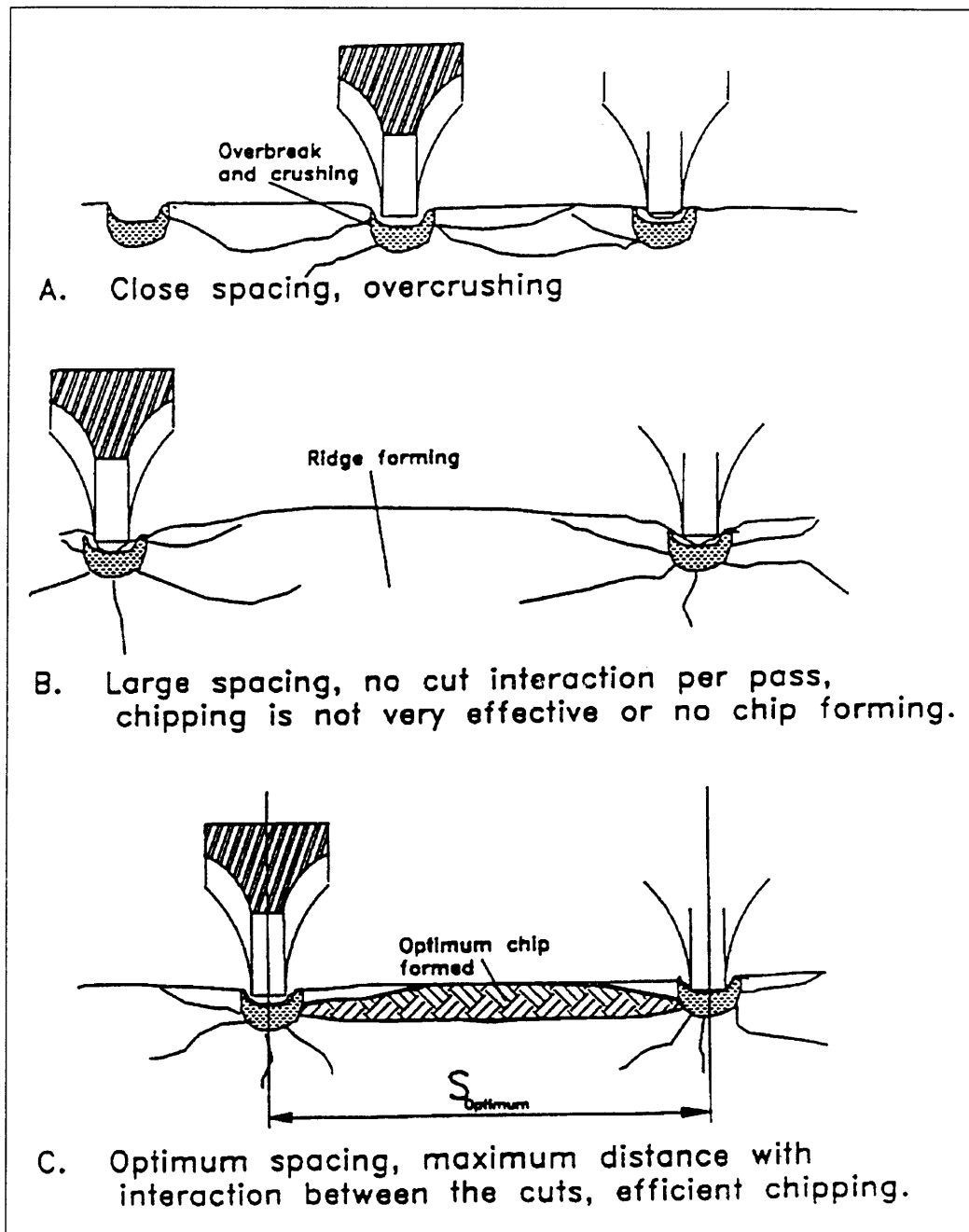
Figure 20: Effect of spacing on the chip formation (after Ozdemir 96).
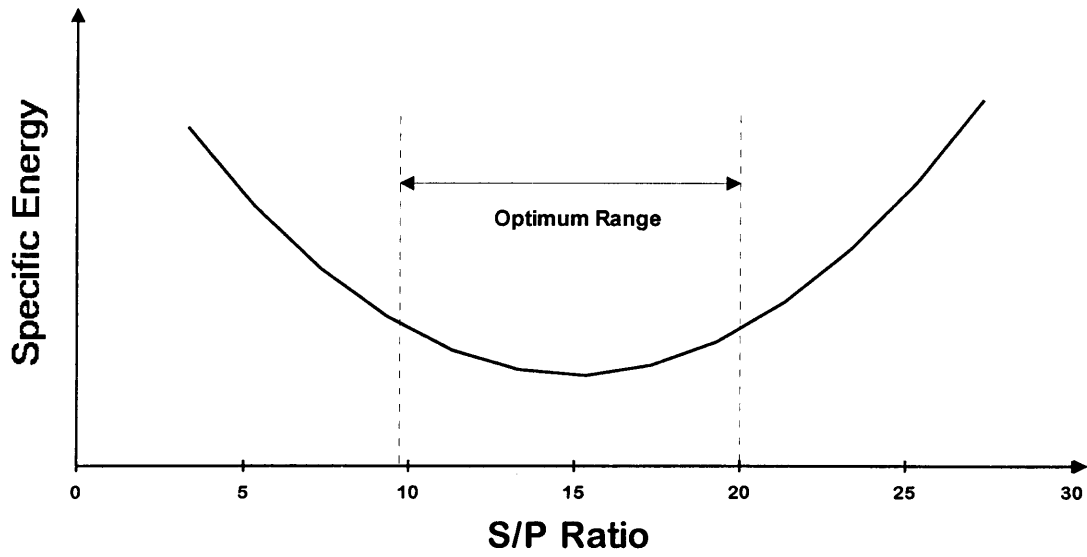
Figure 21: Variation of Specific Energy (SE) with S/P ratio (Rostami 97).
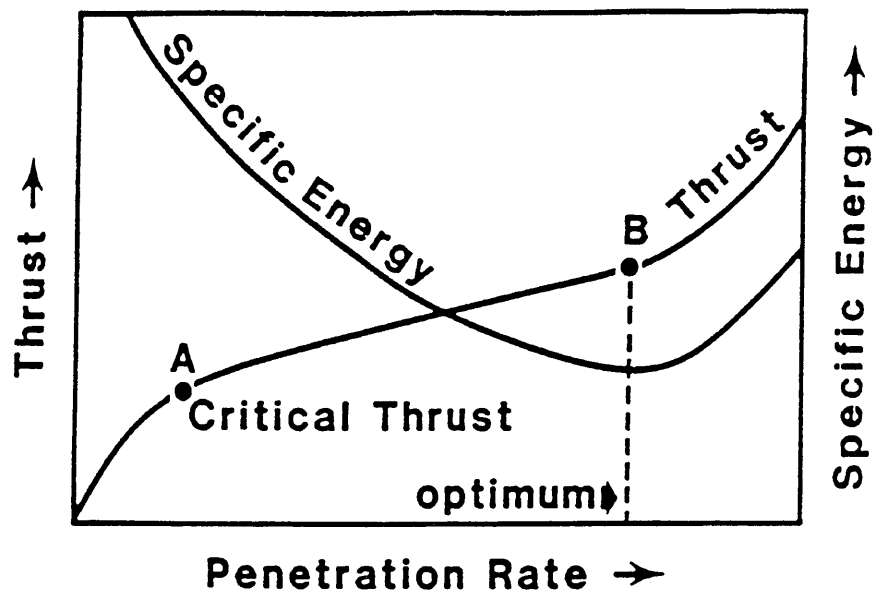
Figure 22: Optimum penetration with respect to specific energy and thrust (Ozdemir 96).
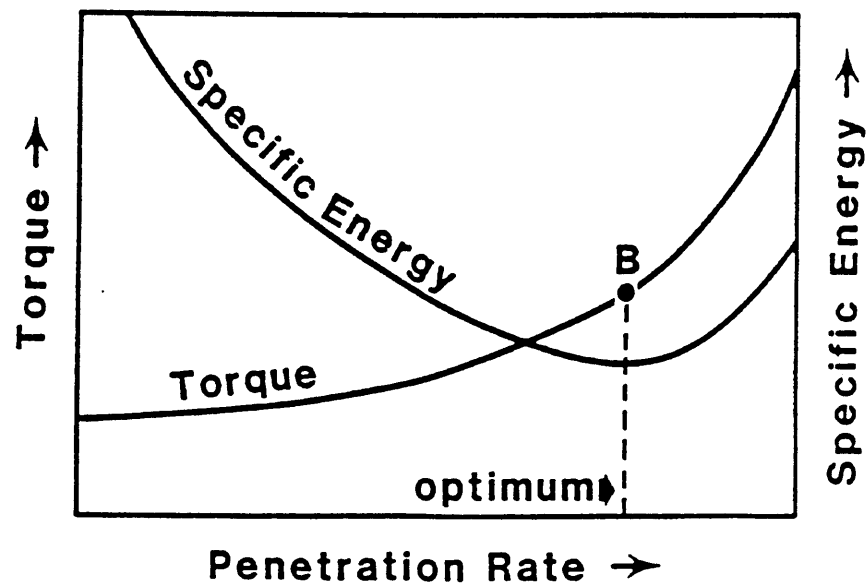
Figure 23: Optimum penetration with respect to specific energy and torque (Ozedmir 96).

Note that the torque increases curve linearly with thrust. This is because the cutting (drag) coefficient increases with depth of penetration. This is the reason why the machines generally become torque and power limited in the excavation of softer rock formations or those with high degree of jointing.

One of the fundamental rules governing efficient rock excavation states that the cutter penetration should be as deep as the bearing capacity and the available machine power would allow. Deeper cutter penetrations not only increase the attainable penetration rates, they also enable the cutter to take maximum advantage of the internal weaknesses present in the rock due to existence of micro-fractures, joints, bedding and foliation. Moreover, deeper penetrations mean larger cutter spacing can be utilized while still maintaining optimal cutting geometry. This in turn enables each cutter on the machine to produce more tonnage for a given lineal travel distance or the hours of operation. This leads to reduce cutter costs per unit volume of rock excavated. Since

deeper penetrations allow for the use of wider cutter spacing for the same optimum S/P ratio, the machine can be fitted with a lesser number of cutters, again contributing to lower cutter costs. These are some the main reasons why the manufacturers have continued to develop and use bigger disc cutters on TBMs over the years.

Another critical aspect of mechanical rock excavation is that a threshold cutter force needs to be exceeded before efficient chipping of the rock begins to occur. As shown in Figure 24, penetration increases very slowly at low cutter loads until a threshold load is reached. At this point, efficient rock chipping initiates such that penetration begins to increase at a much higher rate with increasing load on the cutter. Thus, the machine must have the thrust capacity required to operate above the critical thrust range. It should also be noted that the threshold force is a function of cutter size, geometry, spacing and the degree of wear, as shown in Figure 25.
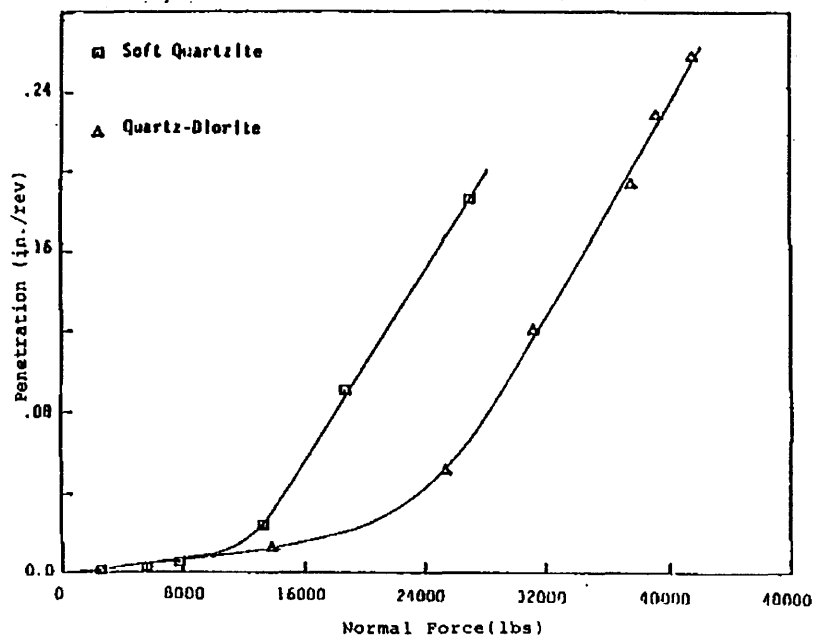
Figure 24: TBM performance for two different rock types (Ozdemir 96).
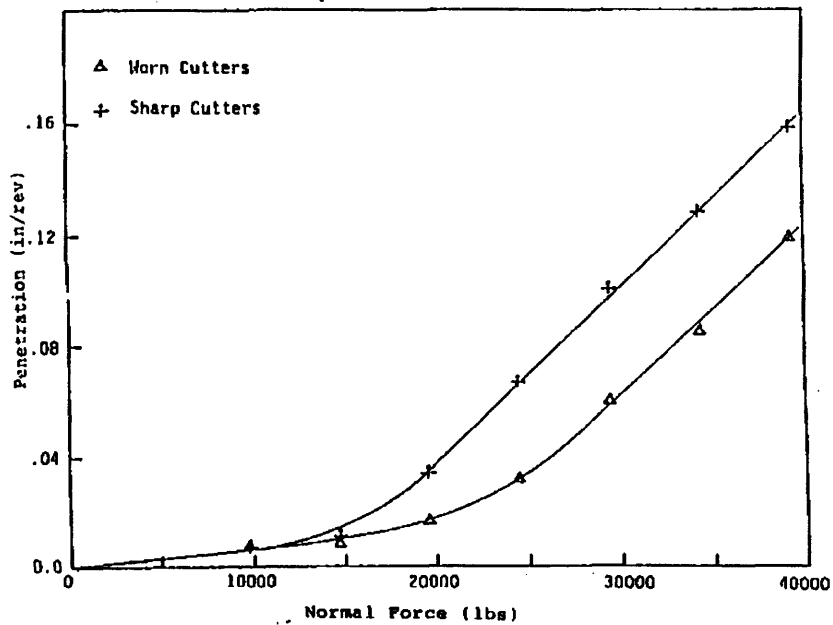
Figure 25: TBM performance for two types of cutters (Ozdemir 96).

The wear factor needs to be taken into account when determining the critical thrust requirements of the machine in a given rock formations. The average chip size become larger as cutter penetration depth increases. Figure 26 displays chip size distributions for different penetrations for a series of linear cutting test performed in a welded tuff formation with a 17-inch CCS cutter. As can be seen, deeper penetrations produce a higher percentage of bigger chips, meaning more efficient cutting process.

Various models and equations have been developed based on the observations made in the laboratory, each supported by testing of different discs and rock types. The parameters used for the estimations vary between the models. Some of the models are purely based on the rock properties, which obviously do not reflect the effects of cutting geometry. A few other models lacked the effect of spacing, and merely focused on penetration, resembling the indentation process. This means that these models have been

developed and validated with a set of varying parameters, while some other parameters were kept unchanged (mostly for simplification) and therefore, were not included as input variables into these models. Some examples of the most frequently cited research studies and models are discussed as follows.
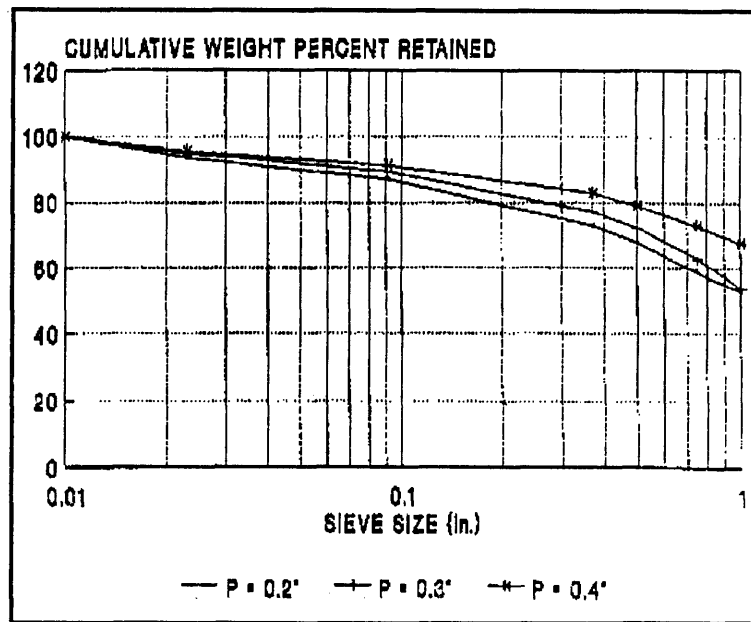
Figure 26: Sieve analysis results in welded tuff with constant spacing (Ozdemir 96).

Miller (1974) and Roxborough (1975), using different approaches developed theoretically derived predictor equations, but they did not include the spacing effects. Roxborough and Phillips (1975) developed equations for estimation of the cutting forces of a V-shape disc using the rock compressive strength together with the disc diameter and the tip angle. Howarth and Roxborough (1982) followed this work to include the effects of joints. Ozdemir (1978) developed a set of predictor equations for V-shape cutters using the cutting geometry (spacing, penetration) along with rock uniaxial compressive and tensile strength to calculate the cutting forces (normal and rolling) for both new and

worn cutters. Sanio (1985) proposed a tensile failure model for the chip formation and introduced some equations for estimation of cutting forces, as follows:

$$f_n = 2.h.Tan\left(\frac{\varepsilon}{2}\right)\sigma_o \qquad (2.18)$$

Where:

f_n = Penetration force

h = Depth of penetration

ε = Tip edge angle

σ_o = Hydrostatic pressure in crushed zone

Sanio also used Ouchterlony's (1974) solution for a circular hole under pressure (blasting) to back calculate the pressure from the rock fracture toughness and crack length equal to spacing. The solution is:

$$2.\sigma_o r = K_{IC}.\sqrt{c} \qquad (2.19)$$

Where:

r = Radius of the hole

K_{IC} = Critical intensity factor

c = Length of crack

The combination of the two equations yields:

$$f_n = \frac{K_{IC}}{q}Tan\left(\frac{\varepsilon}{2}\right)\sqrt{c} \qquad (2.20)$$

with q = r/h. The next step is integrating these penetration forces over the area of contact which yields:

$$F_n = \frac{2K_{IC}}{3.q} Tan\left(\frac{\varepsilon}{2}\right)\sqrt{(d.p - p^2)S}$$

(2.21)

and

$$F_r = \frac{4}{5}\sqrt{\frac{p}{d}}.F_n$$

(2.22)

Where:

F_n = Normal Force

F_r = Rolling force

d = Cutter diameter

p = Depth of penetration

S = Spacing.

The equations were then extended to account for joint effects, simply by using a factor, which was a function of joint orientation.

Sato et. al. (1991) followed Sanio's work and using the same approach, but on a rotary cutting machine (not linear cuts), offered the following equations:

$$F = kP^a S^b$$

(2.23)

Where:

F = Force

k = Coefficient of cutting

P = Penetration

S = Spacing

a = Penetration coefficient, ~0.5 for normal force , ~1 for rolling force.

b = Spacing coefficient, ~ 0.5 (0.43) for both forces.

They concluded that the rolling coefficient (Fr/Fn) is independent of spacing and it increases with the square root of penetration. The coefficients a and b are almost independent of rock type, whereas k is a function of rock and cutter geometry. In this study, k was found to have little or no correlation with fracture toughness, as stated by Sanio, nor with fracture surface energy, as mentioned by Nelson. Also, k had no significant correlation with rock uniaxial and tensile strengths. Specific energy of cutting, however, has shown a good correlation with rock uniaxial compressive strength. To estimate the ratio of peak to mean forces, a linear relationship was suggested to predict peak or maximum forces as a function of the measured or estimated mean force.

The same group, Sato et. al. (1993) followed their studies to include the effects of tool oriented at an angle to the cutting surface. The following equations are the modified version of their previous formulae for force estimation.

$$F_n = AP^m \tag{2.24}$$

and

$$F_r = BP^n \tag{2.25}$$

Where: m, n = Coefficients of penetration for normal and rolling forces (~ 0.5 and 1.0, respectively)

$$A = K_n \, \text{Tan}(\frac{\varphi}{2} + \alpha)\sqrt{D.S}$$

$$B = K_r \, \text{Tan}(\frac{\varphi}{2} + \alpha)\sqrt{S}$$

$K_n = 0.13 \, E^{0.36} K_{Ic}^{0.23}$ (kN/mm$^{1.5}$)

$K_r = 0.11 \, E^{0.4} K_{Ic}^{0.28}$ (kN/mm$^{1.5}$)

K_{Ic} = Rock fracture toughness to be determined from ISRM method.

α = Angle to the cutting surface

φ = Angle of cutter tip.

All the models mentioned above, even the most recent ones, are for V-shape cutters whereas these cutters are hardly found on present day TBMs or other mechanical excavators. As noted earlier, for a number of reasons, particularly the long term wear and performance, constant cross section (CCS) cutters have been favored over V-shape cutters by nearly all machine manufacturers. Rostami (1991, 1993) developed a model for cutting force estimation of CCS disc cutters based on tensile failure mode for chip formation. As opposed to V-shape cutters, CCS cutters cause no wedging effect, and the shear forces induced by cutter within the rock media is therefore minimal. The suggested tensile failure was based on the observation of radial cracks propagating from the crushed zone developed under tip of the cutter. The total estimated resultant cutting force (Figure 27) was derived as follows:

$$F_t = \int_0^{\phi} TPR d\theta = \int_0^{\phi} TRP^\circ \left(\frac{\theta}{\phi}\right)^{\psi} d\theta = \frac{TRP^\circ \phi}{1+\psi} \qquad (2.26)$$

Where:

Ft = Total resultant force

T = Cutter tip width

R = Cutter radius

θ = Angle from normal (variable)

ϕ = Angle of contact area between rock and cutter, $Cos^{-1}[(R-p)/R]$

P = Pressure of crushed zone, defined by a power function as $P = P^0\left(\dfrac{\theta}{\phi}\right)^{\psi}$

ψ = Power of pressure function

P' = Base pressure in the crushed zone at the point directly underneath cutter.
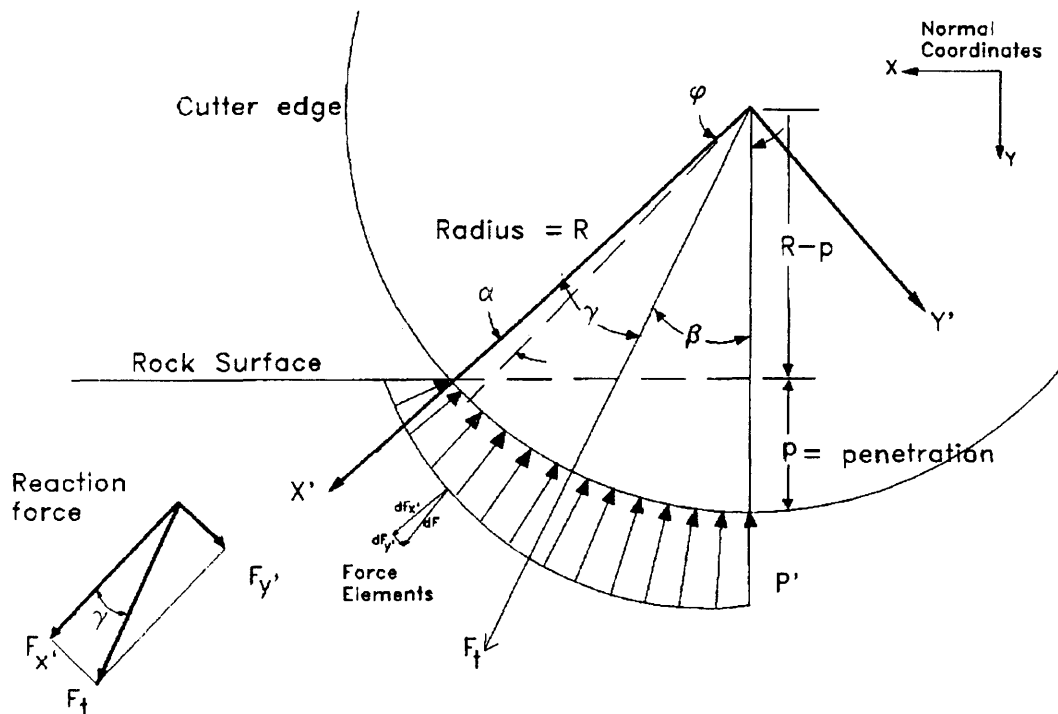
Figure 27: Longitudinal cross section of cutter-rock contact area for CCS disc cutters (after Rostami 97).

In this equation, T and R are cutter geometry parameters, which are known. The

angle ϕ can also be calculated once the penetration is known. The power of the pressure function, ψ, varies between 1.0 for V-shape and very sharp cutters to -0.25 for wider tip cutters. Using the equations derived from regression analysis of measured forces, base pressure P^0 can be estimated as a function of following parameters.

$$P^0 = f(S, \sigma_c, \sigma_t, R, T, p) \tag{2.27}$$

Where:

    S = Spacing between the cuts

    p = Penetration

    σ_c = Uniaxial compressive strength of rock

    σ_t = Tensile strength of rock.

It should be mentioned that the same model can be used to estimate the forces for a V-shape cutter given that tip width at contact area, T', is estimated using tip angle α:

$$T' = p\, Tan(^\alpha/_2)$$

In effect, this implies that the tip width is the effective width of the trajectory of the contact area between rock and the cutter.

The normal and rolling forces can be directly estimated from the force distribution profile, using the integration of the infinitesimal components of normal and rolling forces, or can be estimated from the total force by using the angle of resultant force β, as follows:

$$F_n = \int_0^\phi dF Cos\theta \qquad \text{and} \qquad F_r = \int_0^\phi dF Sin\theta$$

Where: dF= TRP'$(^{\theta}/_{\phi})^{\psi}$ dθ or

$$Fn = Ft\,Cos\,\beta \quad , \quad Fr = Ft\,Sin\beta \quad , \text{and} \quad \frac{Fr}{Fn} = Tan\beta$$

This model has been validated by comparing the results with laboratory cutting tests on linear cutting test machine, as well as estimating the cutting forces for a given cutterhead layout and calculating achievable penetration rates in the field.

Rostami (1993) conducted initial studies using the results of linear cutting tests and measured forces for full size cutters, to correlate cutting forces with different rock fracture properties. This study was performed based on the assumption that the rock cutting and chip formation is strongly influenced by rock fracture mechanics. The relationship between cutting forces and rock fracture mechanic parameters was examined. An extensive database of cutting forces for various cutters, cutting geometry, and rock types was utilized to select a group of tests with the same parameters, except for rock type. The selected cutter was a 43-cm (17") diameter disc with a CCS profile and the tip width of about 1 cm (0.45"). The spacing of 7.5-cm (3") and penetration of 0.75 cm (0.3") was considered to provide more consistency. The cutting forces for two cases were estimated by extrapolation over the available data to match the selected depth of penetration.

Full-scale cutting tests were performed at the Earth Mechanics Institute (EMI) of the Colorado School of Mines (CSM). The rock physical properties, including the uniaxial compressive strength, Brazilian indirect tensile strength, rock density, dynamic modulus and abrasivity index were measured in these tests. The results of this study indicated that within the limited data available, the best correlation was found with the compressive

strength of rock. Tensile strength and elastic modulus showed no significant correlation with forces. More extensive studies along this line are required to confirm the results of this limited study.

Overall, the studies conducted by various research groups either in the field or in the laboratory have confirmed the effects of the following parameters on the cutting forces acting on disc cutters.

1. Intact Rock Properties (Quantitative):

a)   Unconfined (Uniaxial) Compressive Strength

b)   Brazilian Indirect Tensile Strength

c)   Elastic Modulus and Poisson Ratio

d)   Rebound and abrasion Hardness

e)   Porosity

2. Rock Mass Properties:

a)   Discontinuities such as joints, fractures and foliation

3. Disc Cutter Geometry

a)   Disc Diameter

b)   Tip geometry (width or tip angle to represent the width of the contact area)

4. Cutting Geometry

a)   Spacing

b)   Penetration.

2.5 Field Studies

Tunnel Boring Machine (TBM) performance and operational characteristics in the

field, and their relationships with the geological conditions and the rock physical and mechanical properties have been the subject of a large number of studies. The main advantage of field studies, over research investigations conducted in the laboratory is that they contain the complexity of the overall system. In other words, some of operational factors have already been accounted for in the test results and the measurements. Some operators, design engineers, and project planners accept this approach on the notion that they are based on the experiences obtained from actual tunneling operations. Further, the information generated in these studies can be used to confirm and validate the related studies in the laboratory using disc cutters. They provide a basis for extending the results of laboratory studies to the field TBM performance by offering required the correction factors to account for the added complexity of the overall excavation system.

One of the well-known models developed from field performance analysis is the University of Trondheim method, commonly known as the Norwegian or NTH model. This model has been used by the tunneling industry, particularly by Europeans for performance estimation of TBMs. The model uses machine specifications, including the cutter type, size, and number, thrust, torque, and power, as well as laboratory measured indices (drilling index DRI, abrasive index, and toughness index) together with geological and structural features (joints, laminations, faults etc.) to provide an estimate of machine performance. The relationships established between the parameters are in the form of equations and charts derived from regression analysis of the field data collected from a large number of TBM driven tunnels (NTH Report 1-94).

In the Norwegian model, the strength and toughness of the rock is accounted for by running several tests in which various rock indices are measured. These indices were originally developed for evaluation of rock drill-ability and include a miniature drilling, as well as an impact-crushing test to measure and represent rock characteristics. Over the

years, the measured indices along with machine information and the field penetration rates were compiled into a database to develop a performance estimation model. The measured indices on the rock type for a new project are utilized in conjunction with the equations derived from the existing database to estimate the performance of a TBM.

The model has been developed continuously since 1975. In this model two sets of parameters are involved to predict advance rate for the machine. First set of parameter consists of rock mass properties and second set consists of machine parameters. Rock mass parameters include fracturing, drilling rate index (DRI), abrasives and porosity.

In the NTH method, fracturing is the most important rock mass parameter for estimating penetration rate for tunnel boring machines. The estimated penetration rate (m/h) can increase by a factor of five from homogenous to well fractured rock mass. For homogenous rock mass, estimated penetration rate can increase by a factor of two from extremely low to extremely high DRI values. Fracturing means fissures or joints with little or no shear strength along the planes of weakness. Rock mass fracturing is characterized by degree of fracturing (type and spacing) and the angle between the tunnel axis and the planes of weakness. All the parameters are presented in form of graphs and equations. The graph in Figure 28 gives factor for fracturing depending on joint or fissure class and angle between the tunnel axis and plane of weakness. The upper graph provides the DRI factor for given value of fracture factor for the project.

The use of Schmidt hammer for boreability prediction was proposed by Ross (1970), but has found limited success as a reliable indicator of boreability. Shore scleroscope hardness in combination with rock density has also been used in a predictor equation. Another example of performance prediction models based on the field experiment is relating machine advance rate to the rock total hardness index, as proposed by Tarkoy (1973, 75, 79, 86). Tarkoy developed an empirical relationship between total

hardness and TBM rate of penetration. Total hardness is a combination of the Schmidt hammer rebound and the square root of modified Tabor (abrasion) hardness.
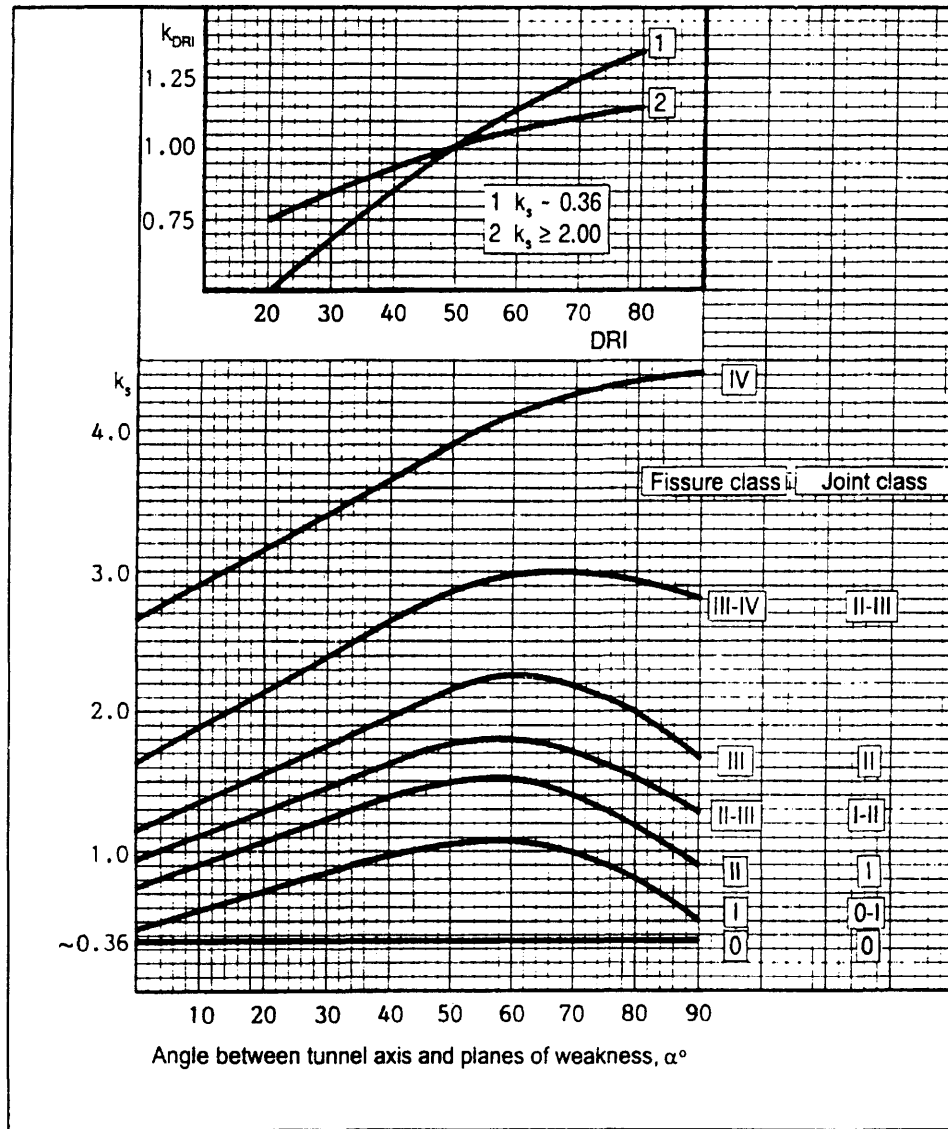
Figure 28: Fracturing factor and DRI correction factor (after NTH I-94).

Nelson et. al. (1983a, 1985) studied TBM operations at several tunneling projects in sedimentary formations by comparing the instantaneous penetration rate achieved with different rock properties. The results of their study showed that there is no significant correlation between the penetration rate and the rock compressive or tensile strength, point load index, or fracture toughness K_{IC}. On the other hand, a good correlation with a combination of rebound and abrasion hardness, as well as rock critical fracture surface energy G_{IC}, was observed. A good correlation was found between the field penetration index (FPI), which is the penetration normalized for the thrust level, with total hardness index of the rock which confirms the observations of Tarkoy. The following equations were derived by regression analysis of the data to relate penetration rate P_r (mm/rev) and the field penetration index R_f (kN/mm) to the hardness indices measured (Nelson et. al. 1983).

$$P_r = 10.45 - 1.19 H_A \text{ and } R_f = 5.95 + 0.18 H_T$$

Where:

H_A = Taber abrasion hardness

H_T = Total hardness

This effort has continued by collecting and compilation of more field data to include a wider spectrum of rock types and machine parameters (Nelson et. al. 1994). The database of machine field performance is already being extended and analyzed to derive simulation models for TBM performance and project completion schedule.

The models based on the field studies are frequently updated to include new projects and advances in machine manufacturing technology. However, the application of these models is limited to the range of available data, and as a result, can experience difficulties

in accurately estimating the performance of newer machines. Also, they can not be used in optimizing machine cutter-head design or improving the performance of machines, which fail to achieve their expected performance. This is mainly owing to the fact that these models do not account for cutter head geometry or lacing and consequently, can not be used for machine modifications or design optimization.

2.6 Rock Properties and Geological Effects on Performance

As basic physical properties of rock such as the compressive and tensile strength, other rock properties and geologic factors can also have a significant influence on the boreability. This section presents a brief overview of the rock properties and certain geologic features commonly associated with various rock formations.

It is well known and established that compressive strength alone only provides an overall indication of rock boreability. That is, any boreability predictions relying solely on the compressive strength may not give accurate results. Tensile strength is another common rock property, which is widely used in making boreability predictions along with the compressive strength of the rock. Tensile strength is generally intended to provide an indication of rock toughness from a viewpoint of crack propagation between adjacent cutter paths. Modulus of elasticity, whether statistically measured or dynamically calculated also is utilized in some prediction techniques to give insight into rock brittleness or the lack thereof.

Perhaps one of the most crucial rock properties which affects its boreability by mechanical means is the brittleness or the plasticity which the rock exhibits when subjected to the mechanical forces generated by the cutting action of an excavator. The sensitivity of rock boreability to brittleness has been investigated in detail in various laboratory programs, as well as field machine performance analysis efforts. These studies

have resulted in the following general conclusions regarding brittleness effects on rock boreability:

(a) In general, rock cutting efficiency of any mechanical tool improves with increasing brittleness exhibited by the rock formation. That is, more brittle behavior makes it easier for chipping to occur between adjacent cuts. This is primarily because brittleness enhances crack propagation.

(b) Larger cut spacing can be employed in brittle materials as opposed to those exhibiting a more or less plastic behavior. This also improves boreability as larger spacing yield bigger chips and contribute to reduced specific energy requirements with the end result being higher rates of penetration and lower cutter costs per unit volume of rock excavated.

(c) In contrast, cut interaction may not occur in highly plastic rocks, such as those featuring a significant amount of clayey or silt material. Under these conditions, the so-called 'coring' action may develop such that due to lack of chip formation between adjacent cuts, ridges begin to build up. In extreme cases, these ridges may eventually contact the cutter saddle, causing the boring operation to essentially come to a stop.

(d) A termed commonly used to describe rocks exhibiting plastic behavior is 'spongy'. This implies that the rock is absorbing large amounts of energy before it chips. As a result, the crushed zone becomes larger which in turn consumes additional energy and creates accelerated wear on cutter ring.

Thus, brittleness is a highly desirable feature of the rock from a boreability standpoint. The question then becomes how to determine and at least provide an indication of rock brittleness or the lack thereof. Short of conducting actual laboratory

cutting tests, one of the best indicators of brittleness is the punch test which involves penetrating a small indentor into the rock and measuring the force vs. penetration behavior while observing the means by which chip formation takes place under the indentor. If such a test can not be carried out, the Modulus and the way a sample fails in compression testing can be used to gain insight into rock brittleness, but with less accuracy.

Porosity is another factor, which can have a major influence on rock boreability. In general, porosity enhances the boring performance by making it easier for the cutter to penetrate. On the other hand, porosity may also interfere with effective crack propagation from one cut to another. However, in general higher porosity has been found to augment rock cutability.

Moisture or the degree of rock saturation has been shown to affect cutability in soft rocks, in particular those exhibiting high porosity. This is because rock strength is reduced with increasing moisture. In hard rocks, however, no discernible effect of moisture was found to exist on machine performance.

Foliation has been shown to influence boreability greatly depending on its orientation with respect to direction of machine advance. Field observations together with extensive laboratory studies have clearly shown that cutting performance can be enhanced drastically if the foliation planes are nearly perpendicular to tunnel axis. Figures 29 and 30 shows the schematic sketches for plan view of tunnel boring machine excavating the rock perpendicular and parallel to foliation respectively.

As depicted in Figure 31, when foliation planes are parallel to tunnel face, crack propagation between adjacent cutter paths occur along foliation planes, significantly reducing the chip formation effort (Case A). In this case, foliation planes essentially act

as weakness planes in the rock in a direction very favorable for crack propagation.
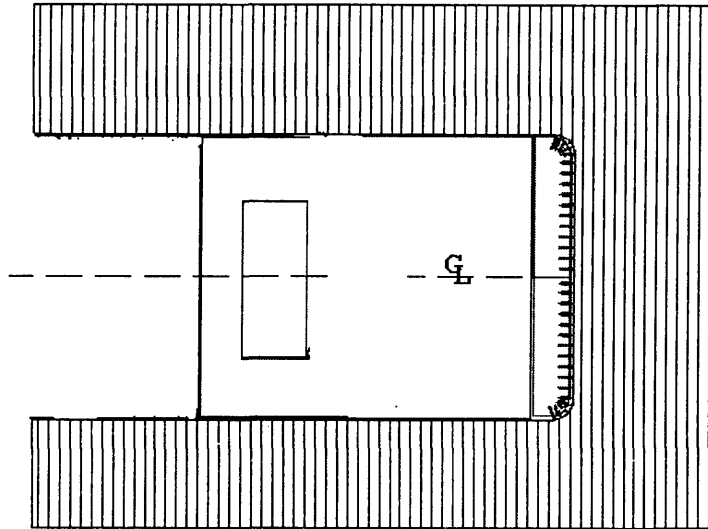
Figure 29: The schematic drawing for TBM excavating perpendicular to foliation (plan view)
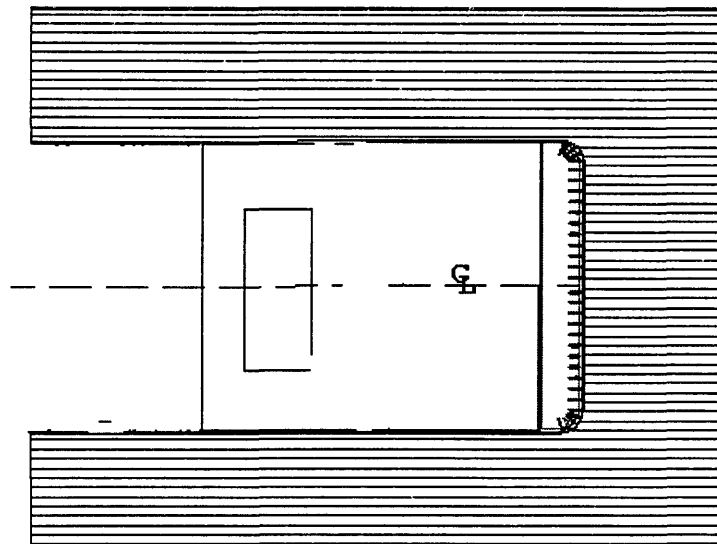
Figure 30: The schematic drawing for TBM excavating parallel to foliation (plan view)
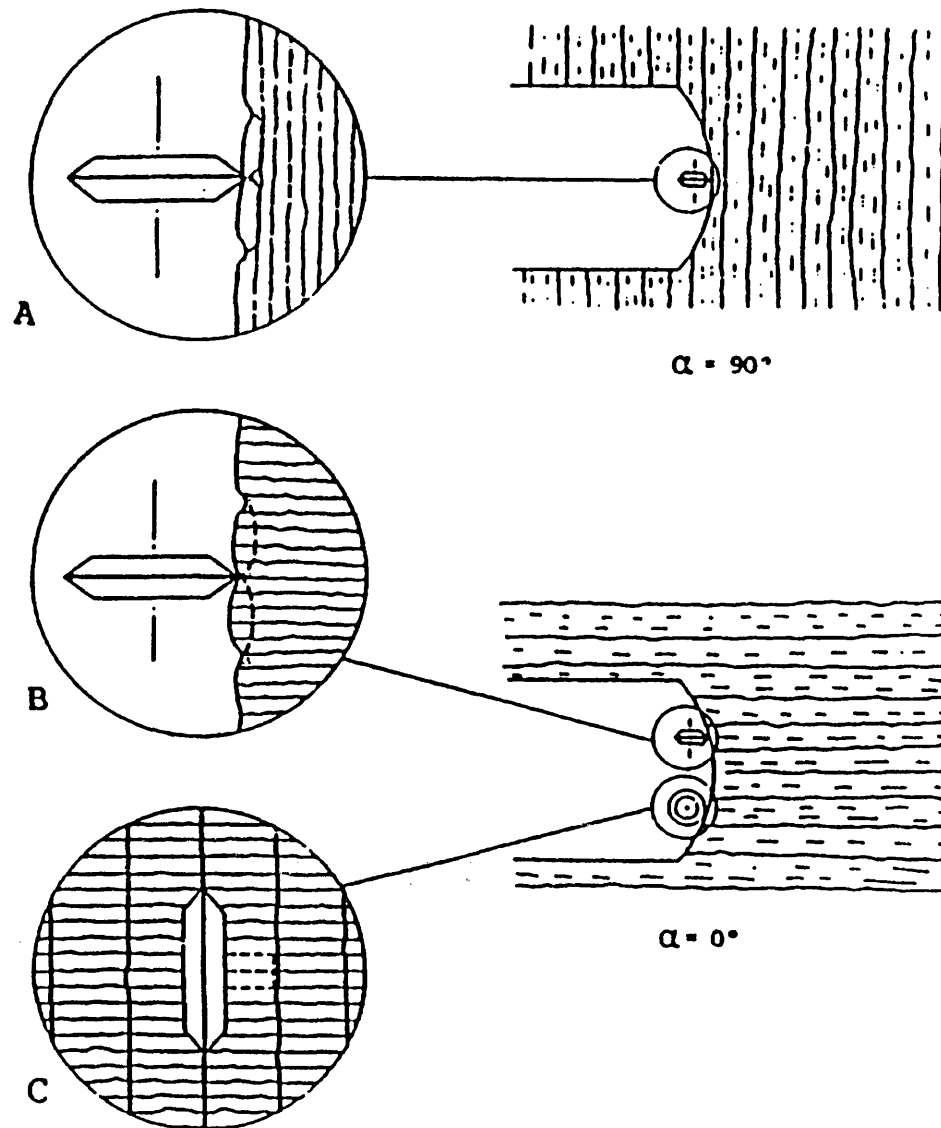
Figure 31: Various chipping patterns for boring in foliated rock (after Ozdemir 96).

If the foliation planes are perpendicular to the face being cut, they actually hinder boring performance since, in this case, they tend to impede crack propagation to adjacent cuts. Also, the average muck size produced from Case B and C is much smaller than case

A, another indication of the cutting inefficiency when foliation is present at a direction more or less perpendicular to tunnel face. The chipping mechanism for cutters acting perpendicular and parallel to the foliation is shown in Figures 32 and 33 respectively.
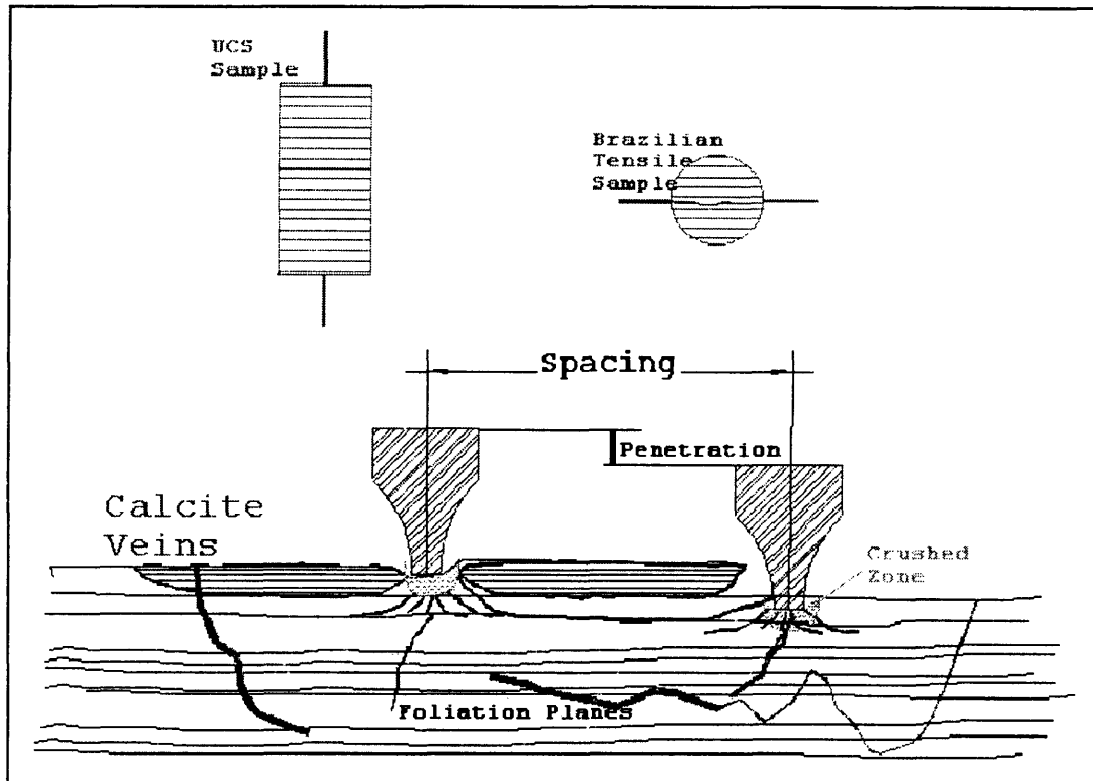
Figure 32: The chipping mechanism for disc cutters acting perpendicular to foliation.

It can be observed in Figure 33 that the chip formation is difficult, as the energy required to break the rock is absorbed by existing discontinuities and fracture propagation is inhibited and irregular cuttings are produced. In this case the compressive strength for the rock is measured parallel to bedding and tensile strength is perpendicular the bedding, which also indicates the rock will behave tough for cutting. On the other hand, a machine operating at 90 degree to the foliation the chips are formed along the bedding and needs less energy to prolong fracture due to favorable conditions.
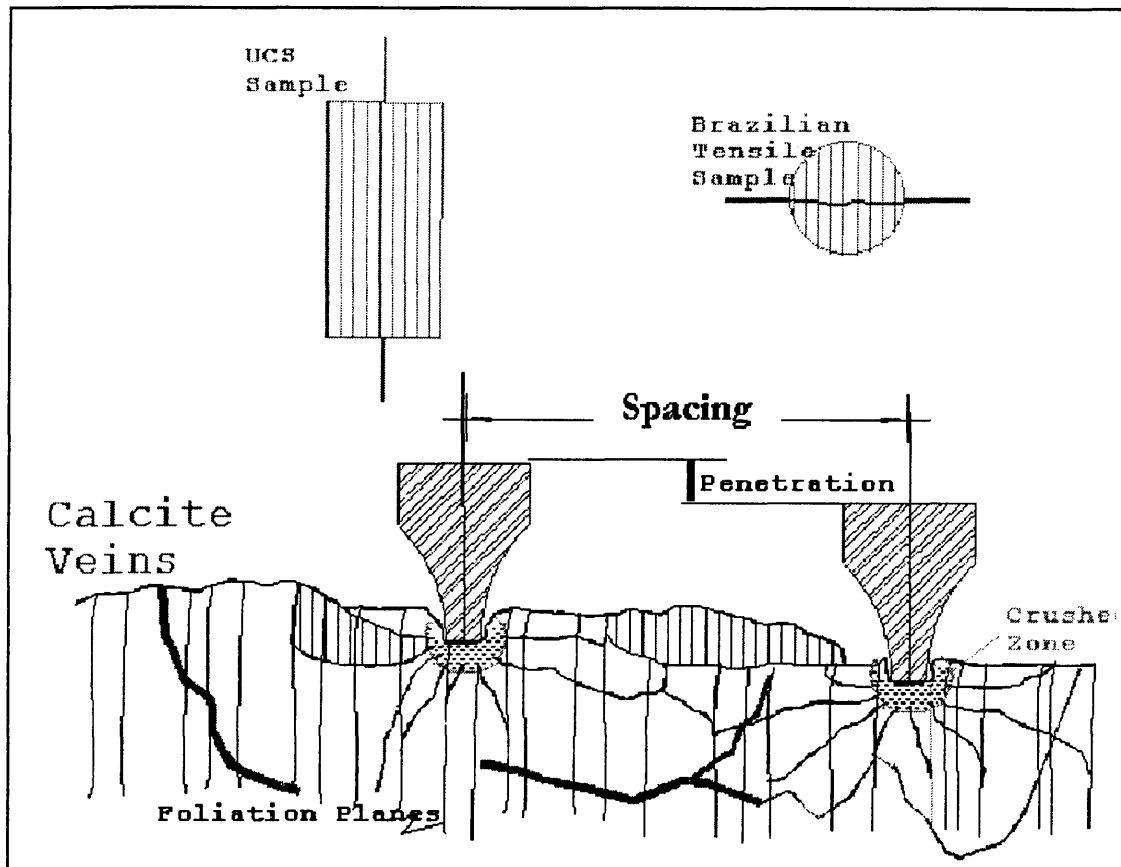
Figure 33: The chipping mechanism for disc cutters acting parallel to foliation.

Laboratory and field studies have also shown that in most cases, rock compressive strength was not affected by the direction of foliation in core samples tested. That is, the compressive strength was nearly the same whether the foliation was parallel or perpendicular to core axis. Tensile strength is, of course, affected by the direction foliation in the sample. Figure 34 shows rate of penetration vs. foliation angle for a tunnel bored in schist in Austria. Note that the cutting rate almost tripled when the foliation direction became nearly perpendicular to tunnel axis.

Bedding can also influence boreability depending on its thickness and orientation

with respect to direction of machine advance. For bedding to have any appreciable effect on boreability, bedding separation needs to be close, its thickness being on the same order of magnitude as the cutter penetration per cutter head revolution. Joints and fractures can effect boreability to a significant degree depending on their orientation, frequency and type. Obviously, tunnel stability and the support requirements are also affected by the presence of joints and fractures.
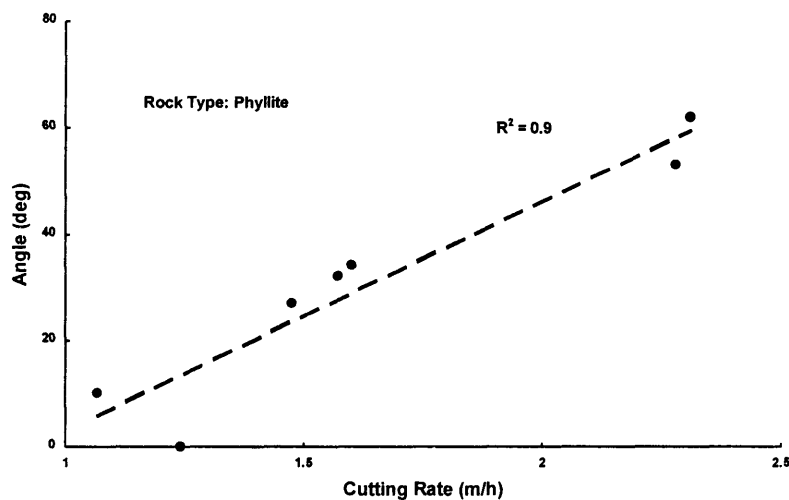
Figure 34: TBM cutting rate vs. rock schistosity and tunnel axis (after Warner 96).

2.7 Summary

In summary cutter loads on a TBM should be as high as possible to attain the highest rates of advance. This requires a machine with high thrust and torque capacity, as well the required rigidity to react to high cutting forces and the impact loads generated during the boring process. At a minimum, the TBM should be capable of developing cutter loads, which are above the threshold forces required for the start of efficient boring

cycle. Each rock type has a threshold load above which efficient chipping and fragmentation begin to occur. As can seen, very little cutter penetration occurs into the rock until the cutter load exceeds a certain value. Once the threshold limit is reached any unit increase in cutter load results in more than a unit increase in penetration depth. This threshold value depends on rock hardness and other physical properties with harder rocks, in general, requiring higher threshold forces before efficient excavation commences. Thus, it is imperative that the rock properties are thoroughly understood and the machines fitted with the sufficient thrust and torque capacity to allow operation above the threshold limit. Cutter spacing and layout need to be optimized for efficient boring. This requires the determination of the optimum cutter spacing for the rock formation to be bored. Otherwise, unnecessary waste of machine energy is bound to occur with a resultant decrease in boring performance. The cutter layout should be chosen so that each cutter more or less breaks the rock to a free face created by a leading cutter on one side. If possible, cutting into rock without any relief on either side of the cutter should be avoided as this would result in high loads to be imposed on the cutter. Naturally, the cutter layout should also provide the best balancing of the cutter head in order to minimize the cutter head vibrations during the boring process. Cutter head vibrations not only accelerate cutter wear, but they also adversely affect the boring performance and can result in premature failure of various machine components, in particular the main bearing.

Deep penetrations require high cutter rolling forces and hence, high machines torque requirements. Thus, the machine needs to incorporate the torque and power capacity required maintaining high thrust operation. Otherwise, the attainable production rates can be limited by the available torque and /or power capacity of the system. This is the reason for the high performance TBMs being packed with as much power as it is physically possible to install on the machine. System rigidity is another factor, which can play a key role in the achievable machine performance. The cutting system should

incorporate as high stiffness as possible to minimize energy losses and to maximize the boring performance. In particular, the stiffness of the cutter head should be maximized. This may require a support system immediately at or behind the cutter head. A stiff cutting system also lowers cutter costs by reducing the vibrations and shock loads experienced by the cutters during boring. Higher system stiffness also allows for the use of wider cutter spacing, meaning reduced number of cutters on the machine.

The review of the literature on hard rock excavation using TBM and the research study focusing on the performance of the machines leads to the conclusion that this subject still needs extensive further studies. In general, all the above models and related research investigations are useful in identifying some of the influencing parameters, but they can not offer a solution to the question of rock mass behavior during actual excavation with full face machine.

The aim of current dissertation is to develop a rock strength index to accommodate the rock mass characteristics in the existing CSM predictor model for estimating the performance of machine more accurately in foliated/jointed rock formation.

3. REVIEW OF EXISTING CSM PERFORMANCE PREDICTOR MODEL

3.1 Introduction:

As discussed in previous chapter, efforts have been made to develop models to predict the performance of tunnel boring machine in term of penetration rate. The semi theoretical model developed at CSM is based on intact rock properties and does not directly include the effect of rock mass behavior in predicting the performance of the machine. At its current form, the effects of rock mass is factored into the predicted performance of the machine later to account for these effects as a whole and not on the cutting forces. The purpose of this study is to modify the existing model so as to accommodate the rock mass properties such as joints, fractures and foliation directly into the predictions. The brief description of the existing model is given in this section.

3.2 Description of the Model

The existing predictor model uses compressive strength and tensile strength as principal rock properties representing its boreability and cutting behavior. A database of measured cutting forces using disc cutters in different rock types has been developed and continuously updated at the Earth Mechanics Institute of the Colorado School of Mines (Rostami 1991,97). The data and information was generated by the Linear Cutting Machine (LCM) for use in this database, which includes a variety of rock types. These tests were accompanied by the physical property testing of the same rocks to measure the compressive and tensile strength of the samples. Occasionally, some other rock properties, such as acoustic wave velocity, dynamic rock modulus, and shear characteristics were measured

along with the rock strength. The latter test data, however useful and essential, have not been measured for all rock types. Also, they are not commonly provided in the geo-technical investigation and testing programs and reports. As a result, the database of the cutting forces was established with the information on the cutter geometry, cutting parameters, rock strength measurements, and finally, the measured cutting forces.

The database was initially used to derive new formulation for cutting forces using linear and polynomial relationship between the influencing parameters. The data was arranged in columns including the spacing, penetration, cutter diameter and tip width, rock compressive and tensile strength, and average normal and rolling forces. This information was then used to determine the average resultant force. The pressure of the crushed zone could be estimated given that a form of load distribution could be universally adopted for this purpose. Running multiple variable regression analysis to find the best combination of parameters to develop a relationship between the forces and the input parameters performed the analysis of the existing database. Normally, the relationships found between the parameters are linear functions. In other words, the program finds the best-fit regression between the parameters in a linear combination, as follows:

$$F = f(X_1, X_2, ...) = A_1.X_1 + A_2.X_2 + ...$$

Where: F = Objective Parameter

$X_1, X_2, ...$ = Independent variables

$A_1, A_2, ...$ = Calculated coefficients

The nonlinear relationships between the parameters can also be determined by defining a new set of variables (new columns) in the program from the original set of variables. For example, a new variable X_j can be defined as a function of original parameter X_i ($X_j = f(X_i)$). This allows defining other parameters in various forms, such as

polynomials, exponential, and logarithmic functions of the original parameters. In order to determine the correct power to be used for each variable in a polynomial equation, the new variables can be set to different powers of the original parameters (i.e. instead of using X_i, its square or square root is used). This method requires several iterations and comparison between the correlation of different powers of a parameter with the forces. An alternative to this method is to use the logarithmic analysis and use the logarithm of each parameter in a linear relationship. This allows obtaining the correct power for each parameter using the characteristics of logarithmic functions.

3.3 Estimation of Forces:

The force estimation formulas were derived from the regression analysis, by using the database of disc cutting forces (Rostami 97). Some of these formulas are discussed here. The simplest formula includes the linear relationship between the parameters. Obviously, such formulas are dimensionally incorrect. In other words, one side of equation was the force (MLT^{-2}) and the other side was a mixture of parameters ranging from length (S, R, etc.) to stresses. In addition, these equations give erroneous answers when the value of the parameters is near boundary conditions (i.e. if any of the parameters is set to zero). The linear relationship for the normal force estimation was as follows: (Correlation Coefficient $R^2 = 78\%$)

$$F_N = -31620 + 2182.S + 5538.P + 2.6.\sigma_t + 0.357.\sigma_c + 71621.T + 1162.R \quad (3.1)$$

Where: F_N = Normal Force (lbs.)

S = Spacing (in)

P = Penetration (in)

σ_t = Tensile Strength (Psi)

σ_c = Uniaxial Compressive Strength (Psi)

T = Tip Width (in)

R = Cutter Radius (in)

When analysis was performed in a logarithmic scale, the relationships included power functions instead of linear functions. The advantage of this type of analysis was that it may yield or lead to equations that were dimensionally correct. The result of the logarithmic analysis produces the following equation: (Correlation Coefficient R^2 = 86%)

$$F_N = 8.76.T^{0.797}.R^{0.788}.\Phi^{0.602}.S^{0.28}.\sigma_c^{0.629}.\sigma_t^{0.195} \qquad (3.2)$$

As can be seen, this equation offers a better correlation with the data. Moreover, it was reasonably close to the right dimension while fulfilling the required behavior of the correct functions at marginal values of the input parameters. This equation was modified to obtain the correct dimensions. To meet this objective, the equation was rearranged as follows:

$$F_N = T.R.\Phi.P_r \qquad (3.3a)$$

Where: P_r = Pressure (psi) and

$$P_r = C.T^{-0.2}.R^{-0.21}.\Phi^{-0.4}.S^{0.28}.\sigma_c^{0.629}.\sigma_t^{0.195} \qquad (3.3b)$$

Where: C = Constant

Examining the powers used in the formula, they were replaced by a set of fractions (such as 2/3 for compressive strength and 1/3 for spacing, tensile strength etc.). Therefore, the pressure equation was rewritten as follows:

$$P_r = C.T^{-\frac{1}{6}}.R^{-\frac{1}{6}}.\Phi^{-\frac{1}{3}}.S^{\frac{1}{3}}.\sigma_c^{\frac{2}{3}}.\sigma_t^{\frac{1}{3}} \qquad (3.3c)$$

or

$$P_r = C.\sqrt[3]{\frac{S.\sigma_c^{\,2}.\sigma_t}{\Phi.\sqrt{R.T}}}$$ (3.3c)

This equation has the correct dimensions ($ML^{-1}T^{-2}$, pressure or stress) and the correct behavior as observed in testing. The coefficient for this equation was calculated to be $C = 2.12$. The rolling forces can be estimated by using the rolling coefficient, which is the ratio of rolling to normal forces, as follows:

$$RC = \frac{F_R}{F_N}$$ (3.4a)

or

$$F_R = F_N.RC$$ (3.4b)

In order to estimate rolling coefficient, there are several reliable formulations. Some of these equations are listed below:

Sugden 1977, $$RC = \sqrt{\frac{p}{D}}$$ (3.5)

Roxborough 1975, Rostami (1993) $$RC = Tan\left(\frac{\Phi}{2}\right)$$ (3.6)

Where:

p = penetration

D = Cutter Diameter.

Φ = Angle of the arc of contact

The later formula (Eqn. 3.6) was based on the assumption that the resultant force passes through the center of the arc or area of contact.

3.4 TBM Performance Predictor Model:

The force estimation formulas were utilized for performance analysis and prediction of various mechanical excavators fitted with disc cutters. As noted before, the most popular machine using disc cutter for hard rock application is the TBM. This section presents the general approach to TBM performance prediction by modeling, which uses the developed force estimation formulae.

The main concept used in the modeling was to program each individual cutter, estimate forces on each cutter, and subsequently determine the overall thrust, torque, and power requirements of the machine. These requirements can then be compared with the installed thrust and power of the machine on an iterative basis to estimate the achievable rate of penetration.

The model was mainly programmed in Microsoft Excel. Figure 35 shows an example of a TBM performance prediction model, printed from the spreadsheet specially developed for this purpose. In this spreadsheet, the upper portion contains general information about the machine, as follows:

•Machine specifications (i.e. diameter, thrust, power, rpm, torque, etc.),

•Cutter type (including diameter and tip width),

•Rock physical properties (UCS, Tensile),

•Nominal penetration per revolution and estimated penetration rates,

•Calculated machine thrust and power requirements,

•Limit check to compare the required and installed thrust and power.

Figure 35 — TBM performance prediction model spreadsheet.

Machine Specification:

Cutterhead Dia. (ft)	26.5	8.08 m
Cutterhead Radius (in)	159	3.98 m
Cutterhead RPM (Actual)	6.4	
No of Cutters (Actual)	50	
Cutter Type	Disc	
Average Cutter Spacing (in)	NA	
Maximum Cutter Load (lbs)	50000	

Calculated Specification:

Cutterhead Dia. (ft)	26.53	8.09 m
Cutterhead Radius (in)	159.2	3.98 m
Max. Cutter Spacing (in)	3.7	93.98 mm
Assumed Penetration (in/rev)	0.10	2.4 mm
No of Cutters	50	
Max. Cutter linear speed (ft/)	550	
Cutterhead RPM	6.4	6.60 Max
Cutter Dia (in)	17	432 mm
Approx. Cutting Coefficient	0.001	
Average Rolling Force (lbs)	3.184	

(center section)

Total Thrust (average)	2,500,000	
Total installed Thrust	2,500,000	
Cutterhead RPM	6.4	
Available Torque (ft-lbs)	2,482,000	
Usable Power (hp)	3024	
Cutterhead Power (hp)	3360	
Motor Voltage (Volt)	660	2520
Max. Advance Rate (pump limit)	25	

Cutting Forces Input Data:

Rock Type		
Rock UCS (psi)	35005	241.4 Mpa
Rock BTS (psi)	1955	13.5 Mpa
Cutter Tip width (in)	0.625	18
Angle of Contact (φ): (deg)	0.15	
Aprox. Ψ value for P'	-0.031	
Estimated P' for crushed zone		
Average (psi)		
Average Normal force (lbs)	46080	
Average Rolling force (lbs)	3450	
Average CC	0.07	

Machine Performance Evaluation:

Limit Check:		
Operating Thrust	O.K.	
Maximum Thrust	O.K.	
Maximum Torque	O.K.	
Max. Cutterhead Power	O.K.	
Max. Cutter Load Cap	O.K.	
Penetration Rate (IPR f)	3.04	

Penetration (in/rev): 0.095

Cutter Load: 46,076 Avg; 49,600 Max

Cutterhead Requirement:

Total Thrust required	2E+06	
Total Torque required	1E+06	
Power required (hp/e)	1461	146
Power for full cutter l	27.66	
Total installed power requirement (assuming a mechanical efficiency of): 90% (hp)	1620	
Electric power required in KW with assuming an electrical efficiency of 100% (KW)	1220	
(hp)	1620	
Center of mom (ft)	6.9	
(% of	52.0	

Per-cutter data table:

No	Location (in)	Angle α (deg)	TRUE r (in)	Ave. S (in)	Angle φ (Rad)	Normal Forces Cutter (lbs)	Normal Forces Sum (lbs)	Rolling Forces Cutter (lbs)	Rolling Forces Sum (lbs)	Torque Cutter (ft-lbs)	Torque Sum (ft-lbs)	Center of Moment ft	%	Power Required (ft-lb/min)	(hp)	Travel per Rev (ft)	coef	Rev	Time (hr)
1	3	0	0.10	3	0.15	46250	46250	3520	3520	880	880	0.3	2.3	5630	1	2	22	82480	215
2	6	0	0.10	3	0.15	46250	92500	3520	7040	1760	2640	0.4	3.0	11260	2	3	16.5	73310	191
3	9	0	0.10	3	0.15	46250	138750	3520	10560	2640	5280	0.5	3.8	16900	3	5	10	72580	189
4	12	0	0.10	3.1	0.15	46250	185000	3520	14080	3520	8800	0.6	4.5	22530	4	6	6	100810	263
5	15.2	0	0.10	3.25	0.15	46760	231760	3560	17640	4510	13310	0.6	6.0	28860	5	8	3	151210	394
6	18.5	0	0.10	3.4	0.15	47500	279260	3620	21260	5580	18890	0.8	6.8	35710	7	10	2	181450	473
7	22	0	0.10	3.5	0.15	48220	327480	3670	24930	6730	25620	0.9	7.5	43070	8	12	1.5	201610	525
8	25.5	0	0.10	3.5	0.15	48690	376170	3710	28640	7880	33500	1.0	9.0	50430	10	13	1.2	232630	606
9	29.2	0	0.10	3.6	0.15	49150	425320	3740	32380	9100	42600	1.2	9.8	58240	11	15	1.5	241940	630
10	32.9	0	0.10	3.7	0.15	49600	474920	3780	36160	10360	52960	1.3	11.3	66300	13	17	1	213470	556
11	36.6	0	0.10	3.7	0.15	49600	524520	3780	39940	11530	64490	1.6	12.1	73790	14	19	1	191000	497
12	40.3	0	0.10	3.7	0.15	49600	574120	3780	43720	12690	77180	1.8	13.6	81220	15	21	1	172810	450
13	44	0	0.10	3.7	0.15	49600	623720	3780	47500	13860	91040	1.9	14.3	88700	17	23	1	157780	411
14	47.7	0	0.10	3.7	0.15	49600	673320	3780	51280	15030	106070	2.1	15.8	96190	18	25	1	145160	378
15	51.4	0	0.10	3.7	0.15	49600	722920	3780	55060	16190	122260	2.4	16.6	103620	20	27	1	134410	350
16	55.1	0	0.10	3.7	0.15	49600	772520	3780	58840	17360	139620	2.4	18.1	111100	21	29	1	125140	326
17	58.8	0	0.10	3.7	0.15	49600	822120	3780	62620	18520	158140	2.5	18.8	118530	23	31	1	117070	305
18	62.5	0	0.10	3.7	0.15	49600	871720	3780	66400	19690	177830	2.7	20.4	126020	24	33	1	109970	286
19	66.2	0	0.10	3.7	0.15	49600	921320	3780	70180	20850	198680	2.8	21.1	133440	25	35	1	103690	270

Figure 35: Example of TBM performance prediction model

Cutters were individually programmed in subsequent rows, with each row representing one cutter and containing the required information for that cutter. The

positions of the cutters on the cutter head were defined by simple geometrical parameters. This includes spacing, which determines their distance from each other, radius of each cutter from the center, the angular position (in a polar coordinate system), and the tilt angle, which is the angle between the disc and the tunnel axis.

The cutter head geometry was defined in a polar coordinate system. This was sufficient for modeling most full-face machines with flat cutter heads since they can normally be considered a 2D problem.

Using the available information on the cutter geometry and rock type, the model then estimated the cutting forces required to penetrate in the rock for each cutter from the nominal value of penetration per revolution. The developed force estimation formula was used in this part to estimate normal and rolling forces for a given type of cutter at specified cutting geometry. The cutting force calculations also include the effect of various spacing values on the lacing pattern. Other parameters, such as different tip width or cutter diameter can be programmed for each individual cutter separately, if required.

The normal forces were all in a column and their summed value represents the machine thrust requirements. Likewise, the rolling forces were estimated and listed in another column. The rolling force, combined with the radial distance of each cutter from the center of the cutter head, determined the moment or torque required to overcome the rolling resistance for that position. The sum of moments for the cutters was the cutter head torque requirement. This value together with the rotational speed of the cutter head (rpm) was then used to calculate the cutter head power requirements.

This concept allowed modeling any cutter head layout, pattern, or configuration for design or performance prediction. It facilitated modeling new machine geometry, disc

cutter size and profile, and provided a basis for performance analysis. In comparison, the TBM models, which were developed empirically, can not account for the detailed cutter head design parameters. The models developed allowed analysis of forces on individual cutters and avoid overloading by making adjustments in the layout. Another area of application for the force estimation formula was in the models used for cutter head balancing. Using the geometry of the cutter head, position of the cutters, and the cutting forces, the balance of forces can be examined to avoid any eccentric force or moments. This can be accomplished by changing the position of the cutters to minimize the out of balance forces on the cutter head. This issue becomes important in improving the life of the main bearing and the cutters.

The developed performance prediction model was considered a semi-theoretical model, which used the cutting forces for cutter head design analysis and performance prediction. Some researchers and most machine manufacturers have employed this particular approach and the basic concept behind modeling. The systematic programming of the individual cutters and related force estimations used in these models have proven to be valid, while offering the means to perform necessary analysis of cutter head design, machine specification, and finally, the machine performance. Obviously, the formulae used for estimation of the cutting forces, the input parameters, the organization of the models and programs, and the output of the programs are different between the models.

The developed model was used for estimation of the penetration rate in several tunneling projects for the purpose of comparison and validation. Some examples include four completed TBM projects including Svarstisen Hydro tunnel project in Norway, the Cowles Mountain Project in San Diego, California, the Stanley Canyon tunnel project in Colorado Springs, Colorado, and the River Mountains No. 2 Tunnel in Las Vegas, Nevada.

The reason for selection of these particular tunneling projects was mainly due to the fact that the rock formations encountered in these tunnels were mostly massive with relatively little jointing. This allowed the modeling and performance prediction of these TBMs without a significant influence of joints and rock mass properties on machine performance. In addition, the geology of the tunnels and the resultant machine performance were studied in detail and reliable field performance data were collected in each project.

One of the important features of the prediction model was the ability to develop performance curves. This refers to the achievable rate of penetration as a function of various TBM and rock parameters. The model allowed a total performance analysis of a TBM for a tunneling project while identifying these conditions where the achievable rate of penetration becomes constrained by either the TBM thrust or power/torque capacity.

As mentioned above in this predictor model the effects of joints and discontinuities were not addressed by the developed force estimation formulae. These effects were not very well explored and quantified. The effects of joint direction and spacing have more or less been observed both in the laboratory and in the field. The common practice today is to use some factors for adjustment of the machine penetration and advance rate to account for joints. This is accomplished by adjusting the calculated penetration rate to account for field joint effects using empirically developed relationships between TBM performance and the rock mass properties. A good example of this practice is the Norwegian model (NTH 94).

In rock mass conditions the results of the model at current status were less accurate. The purpose of this study was to include the effect of rock mass properties in the existing CSM predictor model to achieve more accurate prediction for tunnel boring machines in

jointed rock mass conditions. To achieve this purpose a rock mass boreability index was developed to include the effect of discontinuities in the model.

4. DEVELOPMENT OF A ROCK MASS BOREABILITY INDEX

4.1 Introduction:

As discussed in the previous chapter, the existing CSM predictor model is based on the results of full scale laboratory cutting tests and therefore lacks the parameters associated with rock mass characteristics and their impact on the TBM performance in the field. The model in its current status utilizes intact rock properties, such as, the uniaxial compressive and the tensile strength for boreability evaluation and performance prediction. The rock formation / mass properties, i.e. discontinuities, joints, fractures, foliation and bedding are subsequently factored into result of the model to account for the impact of the rock mass on machine performance. These discontinuities are known to affect the behavior of rock during excavation. This means that the actual strength of the rock mass for boreability can be different from the strength of intact rock determined in the laboratory and, hence it should be factored into the performance prediction model through a proper index.

4.2 Background:

During the feasibility and preliminary design stages of a project, when very little detail information on the rock mass and in situ stresses are available, the use of rock mass classification systems can be beneficial to gather information about joint and foliation, which will effect the underground construction. At its simplest, this may involve using the classification scheme as a checklist to ensure that all-relevant information has been considered. Rock mass classification schemes also can be used to build up a picture of the composition and characteristics of a rock mass to provide initial estimates of the strength and deformation properties of the rock mass.

Rock mass classification schemes have been developed over the past 100 years since Ritter (1879) attempted to formalize an empirical approach to tunnel design, in particular for determining support requirements. While the classification schemes are appropriate for their original application, especially if used within the bounds of the case histories from which they were developed, considerable caution must be exercised in applying rock mass classifications to other rock engineering problems. The following sections briefly describe the rock classification systems developed over the years and concept of developing rock mass boreability index involving rock mass classifications.

4.3 Rock Mass Classifications:

Brief introduction to some important classification systems are presented in this section, and although every attempt has been made to present all of the pertinent data from the original texts, there are numerous notes and comments which cannot be included. The readers are referred to the cited references for a full appreciation of the use, applicability and limitations of each system.

Most of the multi-parameter classification schemes (Wickham et al (1972) Bieniawski (1973, 1989) and Barton et al (1974)) were developed from civil engineering case histories in which all of the components of the engineering geological character of the rock mass were included. Different classification systems place different emphases on the various parameters, and it is recommended that at least two methods be used at any site during the early stages of a project.

4.3.1 Terzaghi's Rock Mass Classification

The earliest reference to the use of rock mass classification for the design of tunnel support is in a paper by Terzaghi (1946) in which the rock loads, carried by steel sets, are

estimated on the basis of a descriptive classification. The rock mass description included in his paper characterizes the dominant rock mass behavior where the gravity constitutes the main driving force. The clear and concise definitions and the practical comments included in these descriptions are good examples of the type of engineering geology information, which is most useful for engineering design.

4.3.2 Rock quality designation index (RQD)

The Rock Quality Designation index *(RQD)* was developed by Deere (Deere et al 1967) to provide a quantitative estimate of rock mass quality from drill core logs. *RQD* is defined as the percentage of intact core pieces longer than 100 mm (4 inches) in the total length of core. The core should be at least NW size (54.7 mm or 2.15 inches in diameter) and should be drilled with a double-tube core barrel. The correct procedure for measurement of the length of core pieces and the calculation of RQD is summarized in Figure 36.
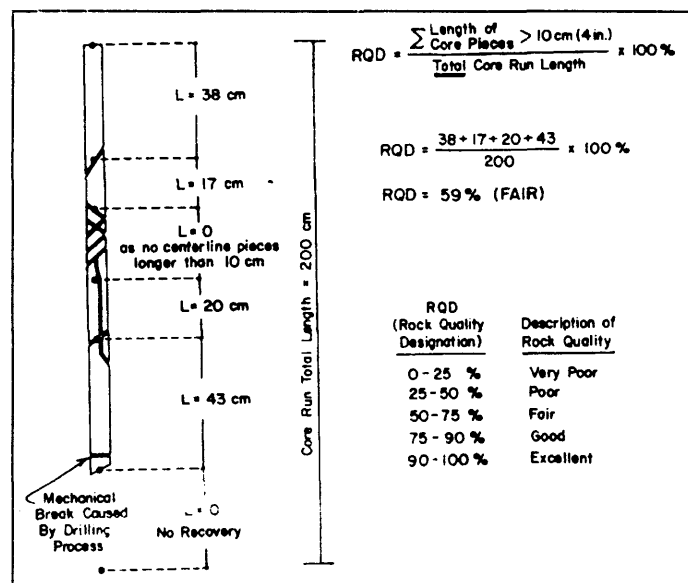
Figure 36: Procedure for measurement and calculation of RQD(After Deere,67)

Deere's RQD has been widely used, particularly in North America, for the past 25 years. Cording and Deere (1972), Merritt (1972) and Deere and Deere (1988) have attempted to relate RQD to Terzaghi's rock load factors and to rockbolt requirements in tunnels. In the context of this discussion, the most important use of RQD is as a component of the RMR and Q rock mass classifications.

4.3.3 Rock Structure Rating (RSR)

Wickham et al (1972) described a quantitative method for describing the quality of a rock mass and for selecting appropriate support on the basis of their Rock Structure Rating (RSR) classification. Most of the case histories, used in the development of this system, were for relatively small tunnels supported by means of steel sets, although historically this system was the first to make reference to shotcrete support. The significance of the RSR system is that it introduced the concept of rating each of the components.

4.3.4 Rock Mass Rating (RMR)

Bieniawski (1976) published the details of a rock mass classification called the geo-mechanics classification or the Rock Mass Rating *(RMR)* system. Over the years, this system has been successively refined as more case records have been examined and the reader should be aware that Bieniawski has made significant changes in the ratings assigned to different parameters. The following six parameters are used to classify a rock mass using the *RMR* system:

1. Uniaxial Compressive Strength (UCS) of rock material.
2. Rock Quality Designation *(RQD)*.
3. Spacing of discontinuities.
4. Condition of discontinuities.

5. Groundwater conditions.

6. Discontinuities orientation.

4.3.5 Rock Tunneling Quality Index (Q)

On the basis of an evaluation of a large number of case histories of underground excavations, Barton et al (1974) of the Norwegian Geotechnical Institute proposed a Tunneling Quality Index (Q) for the determination of rock mass characteristics and tunnel support requirements. The numerical value of the index Q varies on a logarithmic scale from 0.001 to a maximum of 1,000 and is defined by:

$$Q = \frac{RQD}{J_n} * \frac{J_r}{J_a} * \frac{J_w}{SRF}$$

Where:

RQD is the Rock Quality Designation

J_n is the joint set number

J_r is the joint roughness number

J_a is the joint alteration number

J_w is the joint water reduction factor

SRF is the stress reduction factor

4.4 Utilizing Rock Mass Classification systems

The two most widely used rock mass classifications are Bieniawski's *RMR* (1976, 1989) and Barton et al's Q (1974). Both methods incorporate geological, geometric and design/engineering parameters in arriving at a quantitative value of their rock mass quality. The similarities between RMR and Q stem from the use of identical, or very similar, parameters in calculating the final rock mass quality rating. The differences between the

systems lie in the different weightings given to similar parameters and in the use of distinct parameters in one or the other scheme.

RMR uses compressive strength directly while Q only considers strength as it relates to in situ stress in competent rock. Both schemes deal with the geology and geometry of the rock mass, but in slightly different ways. Both consider groundwater, and both include some component of rock material strength. Some estimate of orientation can be incorporated into Q using a guideline presented by Barton et al (1974): "the parameters *Jr* and *Ja* should ... relate to the surface most likely to allow failure to initiate". The greatest difference between the two systems is the lack of a stress parameter in the RMR system.

When using either of these methods, two approaches can be taken. One is to evaluate the rock mass specifically for the parameters included in the classification methods; the other is to accurately characterize the rock mass and then attribute parameter ratings at a later time. The latter method is recommended since it gives a full and complete description of the rock mass, which can easily be translated into either classification index. If rating values alone had been recorded during mapping, it would be almost impossible to carry out verification studies.

4.5 Rock Mass Strength Criterion

Understanding the behavior of jointed rock masses requires a study of the intact rock material and of the individual discontinuity surfaces which go together to make up the system. Depending upon the number, orientation and nature of the discontinuities, the intact rock pieces will translate, rotate or crush in response to stresses imposed upon the rock mass. Since a large number of possible combinations of block shapes and sizes exist, it is obviously necessary to find any behavioral trends which are common to all of these

combinations. The establishment of such common trends is the most important objective in this section.

Hoek and Brown (1980a, 1980b) and Hoek (1988) reviewed the published information on intact rock strength and proposed an empirical failure criterion for rock mass. In developing their empirical failure criterion, Hoek and Brown attempted to satisfy the following conditions:

a) The failure criterion should give good agreement with rock strength values determined from laboratory triaxial tests on core samples of intact rock. These samples are typically 50 mm in diameter and should be oriented perpendicular to any discontinuity surfaces in the rock.

b) The failure criterion should be expressed by mathematically simple equations based, to the maximum extent possible, upon dimensionless parameters.

c) The failure criterion should offer the possibility of extension to deal with the failure of jointed rock masses.

Based on their experimental and theoretical experience with the fracture mechanics of rock, Hoek and Brown (1980a, 1980b) experimented with a number of distorted parabolic curves to find one which gave good coincidence with the original Griffith theory (Griffith, 1921, 1924). Griffith was concerned with brittle failure in glass and he expressed his relationship in terms of tensile stresses. Hoek and Brown sought a relationship, which fitted the observed failure conditions for brittle rocks subjected to compressive stress conditions.

Note that the process used by Hoek and Brown in deriving their empirical failure criterion was one of pure trial and error. Apart from the conceptual starting point provided by the Griffith theory, there is no fundamental relationship between the empirical constants

included in the criterion and any physical characteristics of the rock. The justification for choosing this particular criterion over the numerous alternative lies in the adequacy of its predictions of observed rock fracture behavior, and the convenience of its application to a range of typical engineering problems.

The Hoek-Brown failure criterion for intact rock may be expressed in the following form:

$$RMS = \sigma_3 + \sigma_c \left(m_i \frac{\sigma_3}{\sigma_c} + 1 \right)^{0.5}$$

Where:

RMS is the intact rock mass strength at failure

σ_3 is the minor principal stress at failure

σ_c is the uniaxial compressive strength of the intact rock

m_i is the material constant for the intact rock

Whenever possible, the value of σ_c should be determined by laboratory testing on cores of approximately 50-mm diameter and 100 mm in length. In some cases, where the individual pieces of intact rock are too small to permit samples of this size to be tested, smaller diameter cores may be tested.

The most reliable values of both the uniaxial compressive strength σ_c and the material constant m_i are obtained from the results of triaxial tests. For typical igneous and metamorphic rocks and for strong sedimentary rocks, such as sandstone, these laboratory tests are customary and there are many laboratories around the world, which have excellent facilities for triaxial testing. In weak sedimentary rocks, such as shale and siltstone, preparation of specimens for triaxial testing can be very difficult because of the tendency of

these materials to slake and delaminate, when subjected to changes in moisture content. A solution, which has been used on several major engineering projects, is to carry out the triaxial tests in the field, usually in exploration adits or access tunnels.

The specimen for testing should be cored normal to significant discontinuities, such as bedding planes, and the tests should be carried out on specimens which have a moisture content as close to in situ conditions as possible. Although it is possible to obtain porous platens so that pore fluid pressures can be controlled, this control is not practical in field testing situations and a reasonable compromise is to keep loading rates low in order to avoid generation of dynamic pore pressures.

The triaxial test results can be processed using a program called ROCKDATA developed by Shah (1992). This program is based upon the simplex reflection statistical technique, which has been found to produce the most reliable interpretation of triaxial test data and is available from "The Rock Engineering Group" Canada.

When time or budget constraints do not allow a triaxial testing program to be carried out, the values of the constant σ_c and m_i can be estimated from Tables 1 and 2. Table 2 is based upon analyses of published triaxial test results on intact rock (Hoek, 1983, Doruk, 1991 and Hoek et al. 1992).

4.6 Geological Strength Index

The strength of a jointed rock mass depends on the properties of the intact rock pieces and also upon the freedom of these pieces to slide and rotate under different stress conditions. The geometrical shape of the intact rock piece as well as the condition of the surfaces separating the piece control this freedom. Angular rock pieces with clean, rough discontinuity surfaces will result in much stronger rock mass than one which contains

Term	UCS (MPa)	Point Load Index (MPa)	Field estimate of strength
Extremely strong	>250	>10	Rock material only chipped under repeated hammer blows, rings when struck
Very strong	100-250	4-10	Requires many blows of a geological hammer to break intact rock specimens
Strong	50-100	2-4	Hand Specimens broken by a single blow of geological hammer
Medium strong	25-50	1-2	Firm blow with geological pick indents rock to 5 mm, knife just scrapes surface

Table 1: Field estimates of uniaxial compressive strength of rocks

Rock type	Class	Group	Texture			
			Course	Medium	Fine	Very fine
SEDIMENTARY	Clastic		Conglomerate (22)	Sandstone 19	Siltstone 9	Claystone 4
				←— Greywacke —→ (18)		
	Non-Clastic	Organic		←— Chalk —→ 7		
				←— Coal —→ (8-21)		
		Carbonate	Breccia (20)	Sparitic Limestone (10)	Micritic Limestone 8	
		Chemical		Gypstone 16	Anhydrire 13	
METAMORPHIC	Non Foliated		Marble 9	Hornfels (19)	Quartzite 24	
	Slightly foliated		Migmatite (30)	Amphibolite 31	Mylonites (6)	
	Foliated*		Gneiss 33	Schists (10)	Phyllites (10)	Slate 9
IGNEOUS	Light		Granite 33		Rhyolite (16)	Obsidian (19)
			Granodiorite (30)		Dacite (17)	
			Diorite (28)		Andesite 19	
	Dark		Gabbro 27	Dolerite (19)	Basalt (17)	
			Norite 22			
	Extrusive pyroclastic type		Agglomerate (20)	Breccia (18)	Tuff (15)	

Table 2: Values of the constant m_i for intact rock, by rock.

rounded particles surrounded by weathered and altered rock material. The Geological Strength Index (GSI) introduced by Hoek *(1995)* and Hoek, Kaiser and Bawden *(1995)* provides a system for estimating the reduction in rock mass strength for different geological conditions. The parameters to estimate the GSI value includes as follows:

1) Uniaxial Compressive Strength of rock (UCS)

2) Rock Quality Designation (RQD)

3) Discontinuity Spacing

4) Discontinuity Conditions

5) Groundwater conditions considered being dry (constant).

The value of *GSI* can be estimated directly from the 1976 version of Bieniawski's Rock Mass Rating, with the Groundwater rating set to 10 (dry) and the Adjustment for Joint Orientation set to 0 (very favorable). The *GSI* value ranges from about 10 for extremely poor rock masses to 100 for intact rock. The RMR 1976 version classification can not be used to estimate the GSI value less than 25, Barton, Lein and Lunde's Q value should be used instead.

Once the geological strength index has been estimated, the mass size reduction factor for rock is calculated as follows:

$$S = \exp\left(\frac{GSI - 100}{9}\right)$$

The relationship between the GSI and reduction factor is shown in Figure 37
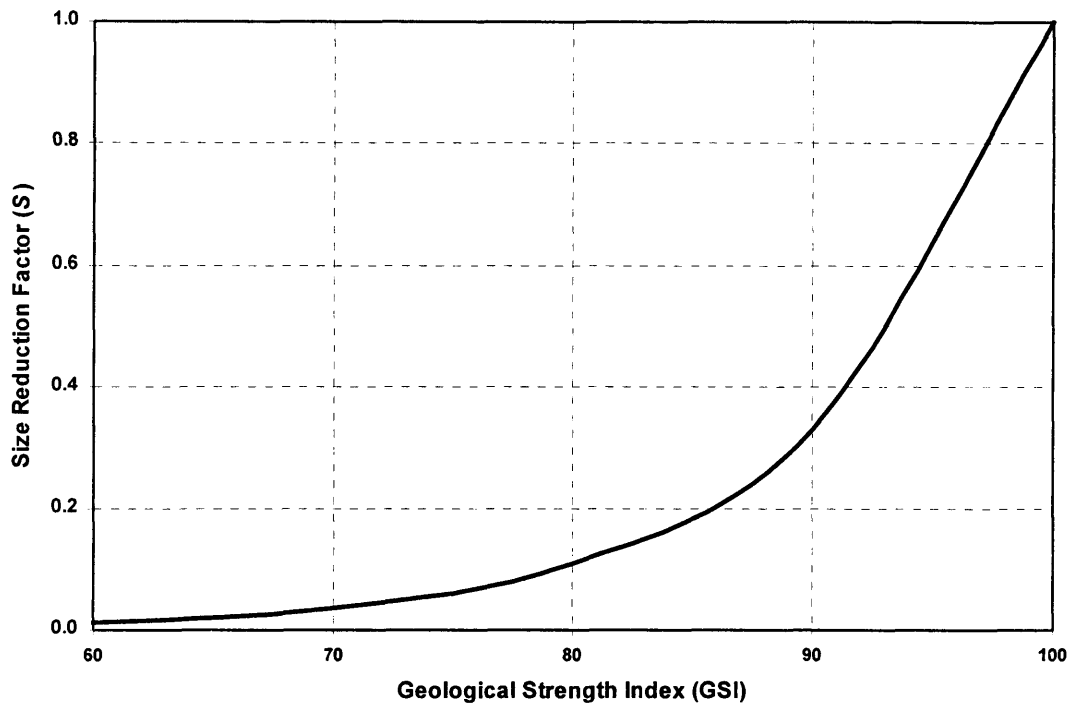
Figure 37: Effect of GSI on Size reduction factor (S)

4.7 Effect of Input Parameters on GSI

The input parameters to estimate the geological strength index (GSI) are unconfined compressive strength, rock quality designation (RQD), joint spacing and conditions. In this section effect of each parameter on the index is described briefly.

4.7.1 Unconfined Compressive Strength (UCS)

The unconfined compressive strength test is the most common way to determine the strength of intact rock. This is the rock strength most commonly used in estimating the performance of tunnel boring machines (TBM). The strength is determined by loading a cylindrical specimen of rock axially between two flat platens in compression with constant

loading rate. The stress value at failure gives the unconfined compressive strength of rock specimen.

It is very important to observe the type of failure during testing. If the sample fails along the existing fracture or bedding/foliation or any other weakness, it should be marked as structural failure. The samples with normal failure (non-structural) during the testing should be included in estimating the GSI. Otherwise, the actual strength of the rock will be underestimated, resulting in lower GSI estimate.

The unconfined compressive strength of rock can vary within a wide range of values. For very strong rocks, it may be around 45,000 psi (310 MPa) and for weak rocks, it may be around 1,500 psi (10 MPa). The classification of intact rock strength with rock mass rating is given in Table 3. The effect of UCS on the value of GSI is shown in Figure 38. This figure shows the relationship between GSI and UCS with change in other parameters.

Description	Unconfined Compressive Strength	RMR
Very High Strength	> 29,000 psi (> 200 MPa)	15
High Strength	14,500-29,000 psi (100-200 MPa)	12
Medium Strength	7,250-14,500 psi (50-100 MPa)	7
Low Strength	3,625-7,250 psi (25-50 MPa)	4
Very Low Strength	145-3,625psi (1-25 MPa)	2

Table 3: Deere and Bieniawski classification of intact rock strength (RMR 76)
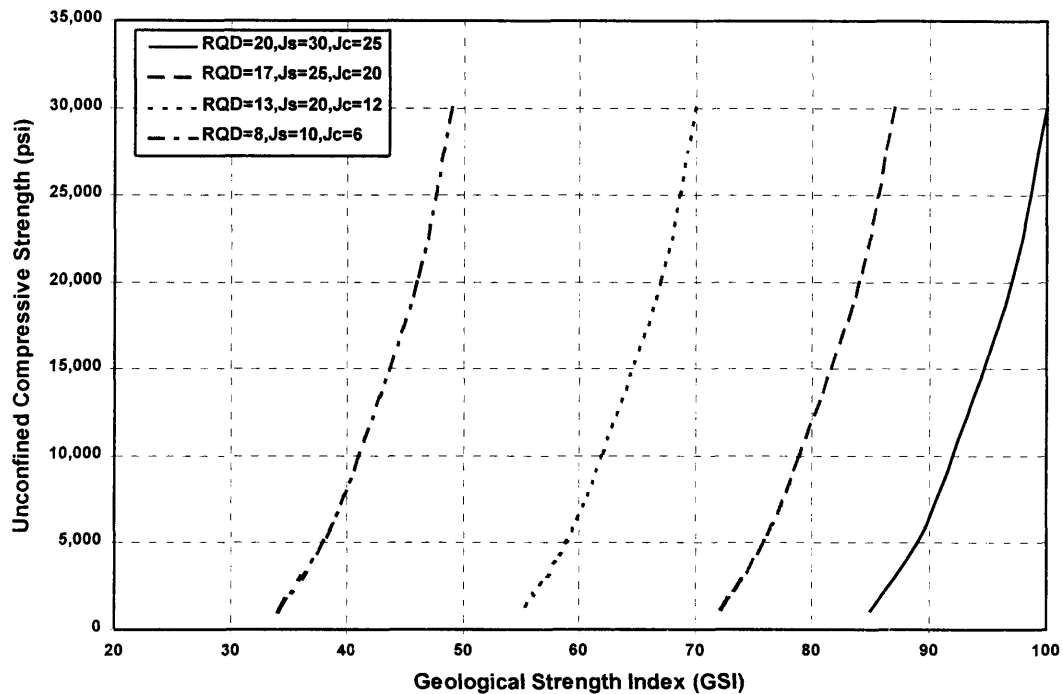
Figure 38: Relationship of GSI with UCS

The effect of decrease in UCS from 30,000 psi to 5000 psi on value of GSI is around 10 units when other parameters are in constant state (RQD etc). The decrease of 10 units in geological strength index reduces the value for reduction factor from 1 to 0.33 for perfect rock mass conditions and from 0.00224 to 0.00073 for worst rock mass condition. The overall decrease in reduction factor is about 67 percent with change in strength of rock. It is further notes that there is no effect of unconfined compressive strength on the GSI value above the value of 30,000 psi.

4.7.2 Rock Quality Designation (RQD)

The rock quality designation index (RQD) was developed by Deere to provide a quantitative estimate of rock mass quality from drill core logs. RQD is defined as the

percentage of intact core pieces longer than 4 inches (100 mm) in the total length of core. The procedures for measurement of the length of core pieces and the calculation of RQD are summarized in previous chapter. RQD intended to represent the in situ rock mass quality. When using diamond drill core, care must be taken to ensure that fractures caused by handling or the drilling process, are identified and ignored in determining the value of RQD. The classification and rock mass rating for RQD is given in Table 4. The effect of RQD on GSI is shown in Figure 39. This figure illustrates the relationship between RQD and GSI relative to other parameters.

The effect of decrease in rock quality designation (RQD) from 100 percent to 20 percent on value of GSI is around 15 units when other parameters are in constant state. The decrease of 15 units in geological strength index reduces the value for reduction factor from 1 to 0.19 for perfect rock mass conditions and from 0.00309 to 0.000584 for worst rock mass condition. The overall decrease in reduction factor is about 81 percent with change in the rock quality from 100 to 20 percent.

Description	Rock Quality Designation	RMR
Excellent	*90-100 %*	20
Good	*75-90 %*	17
Fair	*50-75 %*	13
Poor	*25-50 %*	8
Very Poor	*< 25 %*	3

Table 4: Deere and Bieniawski classification of rock quality designation (RMR 76).
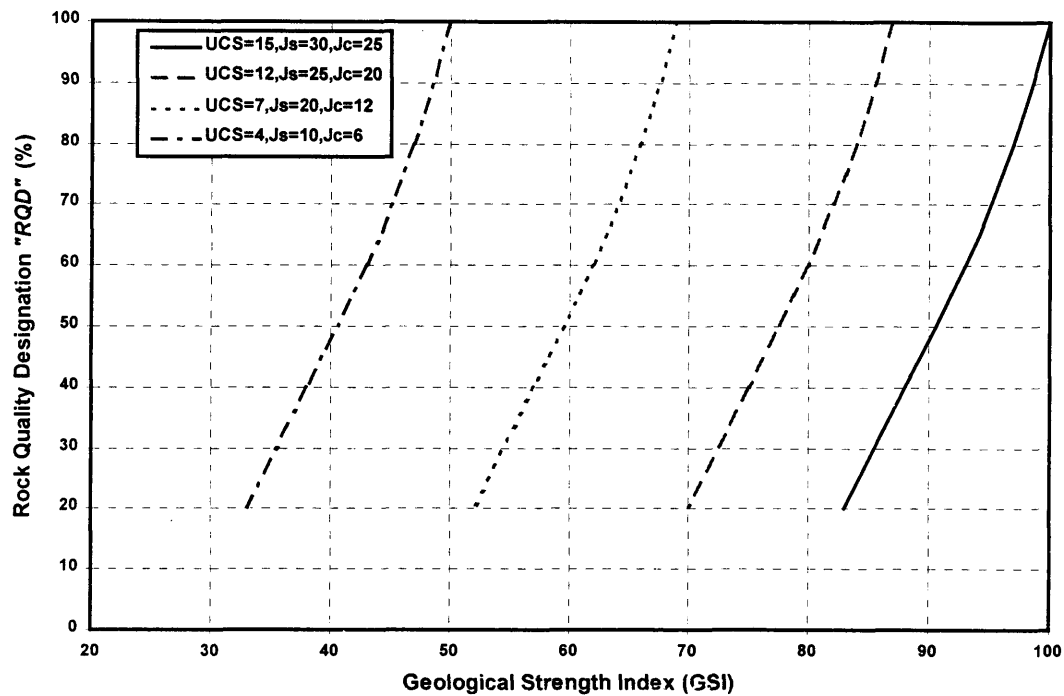
Figure 39: Relationship of GSI with RQD

This illustrates that unconfined compressive strength of the rock can not be considered sole indicator to predict the behavior of the rock during excavation.

4.7.3 Discontinuity Spacing (Js)

In this context, discontinuity can be joint, fault, bedding planes, foliation or any other surface weakness. The spacing between these discontinuities were classified by Deere. The classification for joint spacing is given in Table 5 along with rock mass rating developed by Bieniawski. The effect of these rating on GSI is shown in Figure 40 along with the effect of other parameters on the relationship.

Description	Joint Spacing	Rock mass grading	RMR
Very wide	*> 10 ft (3 m)*	*Solid*	30
Wide	*3 ft to 10 ft (1-3 m)*	*Massive*	25
Moderately	*1 ft to 3 ft (0.3-1 m)*	*Blocky/seamy*	20
Close	*2 in to 1 ft (50-300 mm)*	*Fractured*	10
Very close	*< 2 in (< 50 mm)*	*Crushed /shattered*	5

Table 5: Deere and Bieniawski classification for joint spacing (RMR 76).
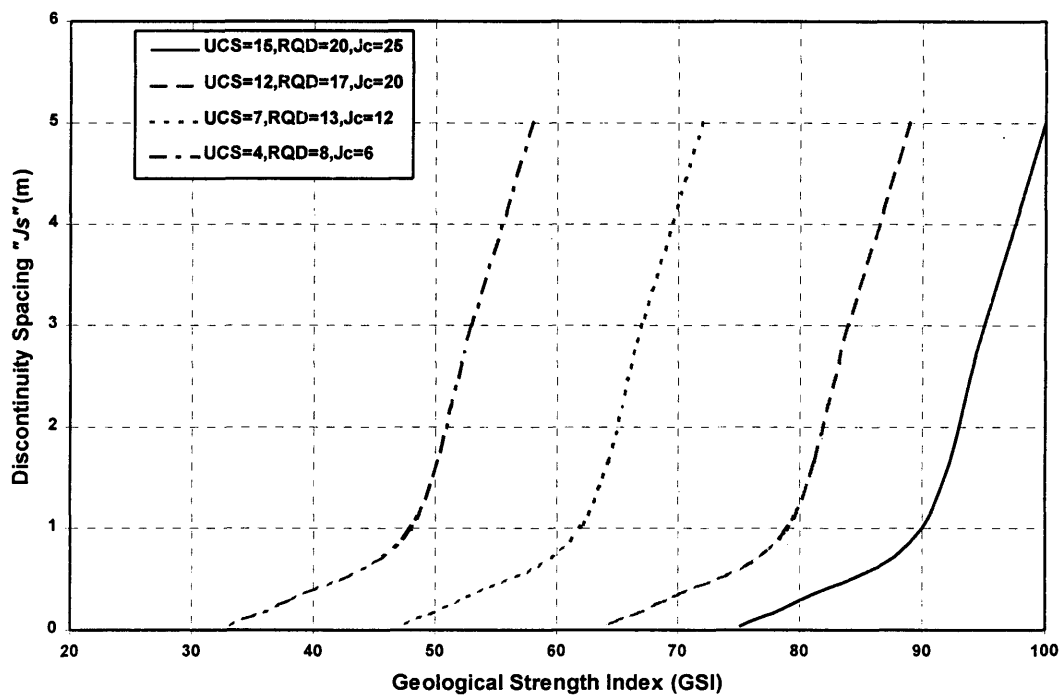
Figure 40: Relationship of GSI with discontinuity spacing

The effect of decrease in joint spacing from 5 to 1 meters on value of GSI is around 10 units, and with spacing less than 1 meter the effect is around 15 units when other parameters are in constant state. This illustrates that the rock mass strength is low for highly jointed or fractured rock.

4.7.4 Discontinuity Conditions (Jc)

This parameter accounts for the separation or aperture of discontinuities, their continuity or persistence, their surface roughness, the wall condition and the nature of any in-filling material present. The classification of this parameter with rock mass rating is given in Table 6. The effect of conditions of discontinuities on GSI with respect to other parameters is shown in Figure 41. This joint condition is based on observation of individual who classifies them to various categories, so the rating of this parameter can vary from person to person.

No	Description	RMR
1	*Very rough surface, No separation, Hard joint wall contact*	25
2	*Slightly rough surface, Separation < 1mm, Hard joint wall contact*	20
3	*Slightly rough surface, Separation < 1mm, Soft joint wall contact*	12
4	*Slickensided surfaces, Joints open 1-5 mm, Continuous Joints*	6
5	*Joint open > 5 mm, Continuous Joints*	0

Table 6: The Bieniawski classification for joint conditions (RMR 76).
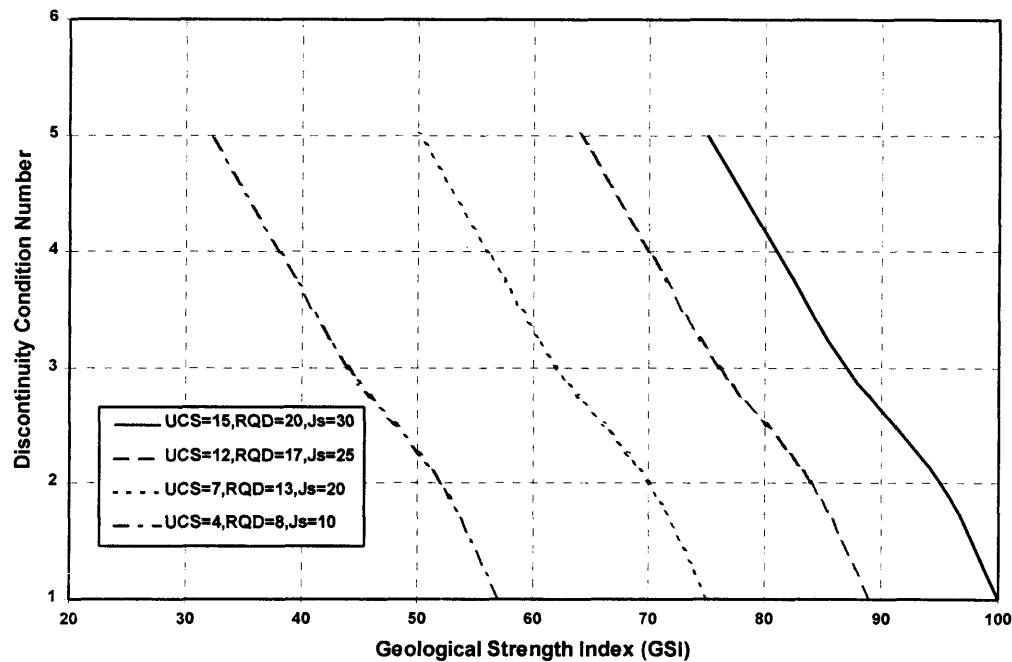
Figure 41: Relationship of GSI with discontinuity conditions

The effect of increase in discontinuity condition number on value of GSI is around 25 units when other parameters are in constant state. The decrease of 25 units in geological strength index reduces the value for reduction factor from 1 to 0.06 for perfect rock mass conditions and from 0.0094 to 0.000584 for worst rock mass condition. The overall decrease in reduction factor is about 94 percent with change in the joint conditions from best to worst. This illustrates that classification of joint conditions is very important in assessing the strength of rock mass for excavation purpose.

In summary the GSI values decreases as rock gets weaker due to decrease in any of the parameter. It is to note that rock mass rating has been divided into five categories for each parameter and combine effect of each category on GSI is linear as shown in Figure 42. The

approximate value of GSI can be estimated from graph shown in Figure 42 if general rock mass quality is known for the area under investigation for any project.
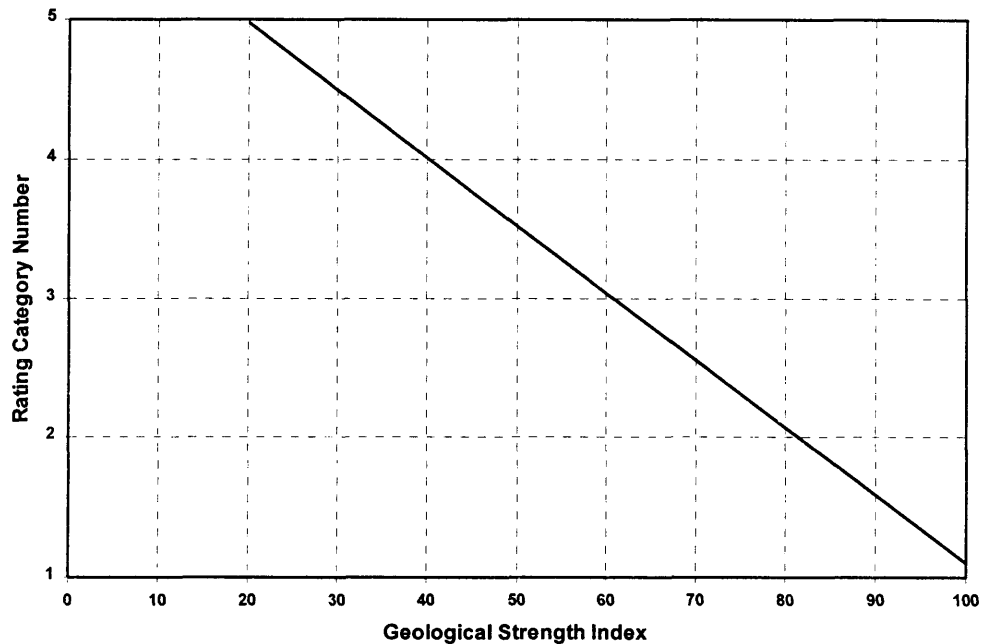
Figure 42: General relationship of GSI with rock mass rating parameter

4.8 Estimation of Rock Mass Boreability Index

As mentioned earlier, the rock strength is function of the rock characteristics and size of the rock, which represents those characteristics. In other words rock strength can be determined by its capacity to sustain stress and strain on minimum size of rock piece which behaves as intact rock within rock mass. Mathematically it can be expressed as follows:

$$RMBI = f(X_1, X_2, \ldots\ldots\ldots) = A_1 X_1 + A_2 X_2 + \ldots\ldots$$

Where:

RMBI = Objective parameter

$X_1, X_2, \ldots$= Independent variables

$A_1, A_2, \ldots$= Calculated coefficient.

This relationship between the parameters can be achieved by establishing a database of independent parameters including modulus of elasticity, Poisson's ratio and size reduction factor obtained from geological strength index. The objective parameter data can be established by applying existing rock strength criterion as mentioned earlier. The rock material constant m_i can be obtained from Table 2 or by triaxial strength tests and minor principle stress can be considered equal to hydrostatic pressure. The database can be arranged in sets of columns. By performing multiple regression analysis by using professional version of MINITAB®, which is a commercial software package for standard statistical analysis, to find the best combination of parameters to develop a relationship between the rock mass strength and the input parameters. Normally, the relationships found between the parameters are linear functions. In other words, the program finds the best-fit regression between the parameters in a linear combination as mentioned above.

The nonlinear relation between the parameters can be determined by defining a new set of variables in the program from the original set of variables. For example a new variable Y can be defined as a function of original parameter X ($Y = f(X)$). This allows defining parameters in various forms, such as polynomials, exponential and logarithmic functions of the original parameters. An alternative to this method is to use the logarithmic analysis and use the logarithm of each parameter in a linear relationship. This allows obtaining the correct power for each parameter using the characteristics of logarithmic function. Altogether, use of logarithmic method allows developing several combinations of

parameters in different mathematical forms. The result of this analysis for the rock strength database can be as follows:

4.9 Analysis of Results

The rock mass boreability index estimation formulas can be derived from the regression analysis, by using the database developed for rock mass strength and the software. Some of these formulas will be discussed here. The simplest formula includes the linear relationship between the parameters. These equations give erroneous answers when the value of the parameters is near boundary conditions (i.e. if any of the parameter is set to zero). The linear relationship for the rock mass boreability index estimation is as follows:

$$RMBI = C + aE + bS - cv$$

Where:

$RMBI$ = Rock Mass Boreability Index (psi)

E = Elasticity Modulus (ksi)

S = Size Reduction Factor

v = Poisson's Ratio

C = Constant Coefficient

a = Coefficient of elasticity modulus

b = Coefficient of size reduction factor

c = Coefficient of Poisson's ratio

If the analysis is performed in a logarithmic scale, the relationships will include power functions instead of linear functions. The result of the logarithmic analysis produces the following equation:

$$RMBI = C * E^a * S^b * v^{-c}$$

The negative power for Poisson's ratio shows that this parameter is inversely proportional to the strength of rock mass.

In summary, the estimation of rock mass boreability index (RMBI) from this new approach is developed to include the rock mass conditions in the existing CSM predictor model to predict the performance of tunnel boring machines in foliated / jointed hard rocks. To verify the concept, extensive data were collected related to actual machine performance and the encountered rock physical and mass properties from a TBM project recently completed in Boston, MA.

5. FIELD DATA COLLECTION

5.1 Introduction

As discussed in previous chapter, a concept was developed to include rock mass characteristic in the existing CSM predictor model through a newly developed index. To validate this concept, significant efforts were made to collect field data from past and ongoing TBM projects. Many tunnel projects were contacted for this purpose. The only project where detailed information about machine performance and rock conditions available was the Boston Harbor Outfall tunnel. The detail description of this project together with geological information is presented in this section.

5.2 Boston Harbor Tunnel Project

The dumping of untreated sewage and industrial waste in lakes, rivers and harbors has become a common phenomenon in major cities. Boston harbor is no exception, and over the years the problem has worsened, culminating in a series of legal actions. In 1985 the Federal District Court, Massachusetts District, ruled that the discharge of "primary treat effluent into Boston Harbor was unlawful" and the Massachusetts Water Resources Authority (MWRA) was established by the State Legislature. The mission of this newly created agency was to conceive designs and constructs the facilities to clean up the harbor. To fulfil this mission, a solution was designed that consisted of a pump station at Nut Island linked by a tunnel to a secondary treatment facility on Deer Island. The plant will also process the wastewater from other sections of the Boston area that currently is delivered to Deer Island through two existing tunnels. The treated effluent will then be discharged through a deep rock outfall tunnel extending about nine mines offshore to a diffuser area in Massachusetts Bay. The project consists of the inter-island conveyance

tunnel from the new headwork at Nut Island to the Deer Island Secondary Treatment Facility and the effluent outfall system. The layout plan of the project is shown in Figure 43.
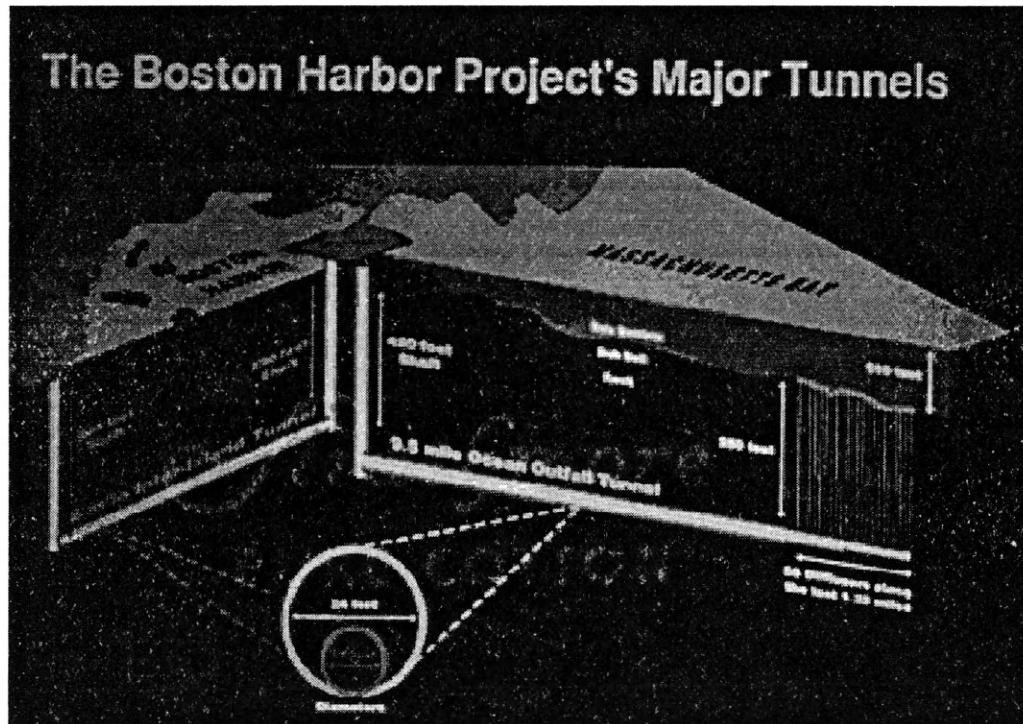
Figure 43: The Layout of Major tunnels for the project.

The Outfall tunnel is the centerpiece of this program. The work consisted of the construction of around 9.4 miles (49,630 ft.) of 24 ft. 3 inches finished diameter tunnel into Massachusetts Bay from a 420 ft. deep 30 ft. finished diameter shaft. The last 6,600-ft. of tunnel includes 55 diffusers. The first year and half was spent on construction of 420 ft. deep shaft, driving of some 265 ft of starter tunnel using a top heading and bench method and 200 ft of tail tunnel. These operations were performed conventionally with

hydraulic air tracks and jumbos. The tunnel was driven by a double-shield TBM fitted with disc roller cutters.

5.3 Geology

5.3.1 Regional Geology

Boston is located in the New England province of the Appalachian Highlands, an area characterized by complexly folded and faulted bedrock that has been worn down by surface erosion. The collision boundary between the Paleo-African and North American plates lies to the north and west of Boston. Bedrock southeast of the collision boundary consists largely of Precambrian igneous and metamorphic rocks. These rocks lie in three sedimentary basins, the Narragansett Basin, the Norfolk Basin and the Boston Basin (Figure 44).
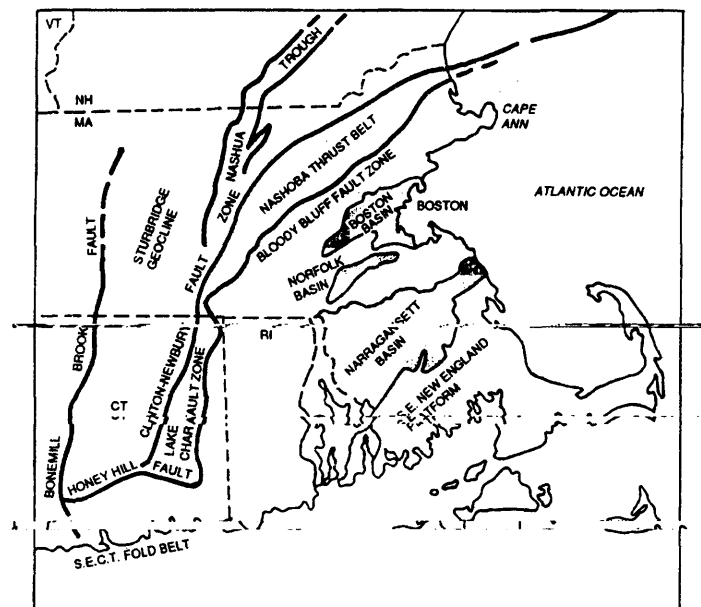
Figure 44: Major Tectonic Provinces and Structures of South Eastern New England (After Barosh, 1984).

The site area lies in the eastern portion of the topographic and structural depression known as the Boston Basin. On land the basin is about 25 miles long and approximately 1.5 miles wide. It extends underneath Massachusetts Bay and is believed to become wider to the east (Kaye, 1982). The boundaries are a series of faults that in places form steep escarpments. The bedrock in the basin is primarily sedimentary; mainly argillite, sandstone and conglomerate. Structurally the bedrock is folded and faulted longitudinally in an east-west direction.

Much of the topography seen today is the result of Pleistocene glaciation. Massive blocks of ice scoured the bedrock surface, eroding away the softer sedimentary rocks of the basin leaving the more resistant igneous and metamorphic rocks as topographic highs. The bedrock in portions of the Boston Basin are covered by glacially deposited soils up to 200 ft thick.

5.3.2 Stratigraphy

The largest portion of surficial materials found in the Boston Basin are Pleistocene in age. These deposits include glacial till, marine clays and glacial out-wash. The glacial till is typically a dense, non-stratified, variable mixture of sand, silt, clay, gravel, cobbles, and occasional boulders. The marine clay, known locally as the Boston Blue Clay, is a rock flour deposited in a quiet marine environment (Kaye, 1967). The marine clay was deposited in low areas between drumlins. Recent processes have deposited organic silt/peat, alluvium, and reworked sand and gravel.

The soil profile encountered in the diffuser area consists of relatively thin unconsolidated soft organic clay and silts overlying the marine clay. The marine clay overlies glacial till, ranging from 5 to 25 ft thick. The till occurs as a discontinuous blanket on top of the bedrock.

The bedrock in the Boston Area has been described in papers dating back to 1818. Despite this history, interpretation of the bedrock geology is still being revised. This is due to the complexities of the area and the lack of outcrops at critical locations. The single most important contribution to information on the bedrock geology has been the construction of the tunnels beneath Boston.

The Boston Basin contains a series of inter-layered sedimentary rocks intruded by igneous rocks, mainly diabase. The basin was originally thought to be a layered sequence of basal conglomerate, slate, and tillite (Roxbury Formation) overlain by fine grained shale and slate (Cambridge Formation). Work by Kaye (1984) has shown that the relationship between formations is not that simple. There are a greater variety of rock types than originally thought and units change composition.

The Roxbury Conglomerate occurs in the Southern half of the Boston Basin and primarily consists of conglomerate with inter-bedded units of argillite and sandstone. The conglomerate is gray, white, or maroon colored feldspathic sandstone containing well-rounded pebbles and cobbles 0.5 to 6 inches in diameter. The pebbles are chiefly quartzite, quartz monzonite, granite and felsite (Billings, 1976). Argillite associated with the Roxbury conglomerate is similar to the Cambridge formation but is maroon, pink, white, red or purplish gray in color.

The Cambridge formation occupies the northern half of the Boston Basin and overlies the Roxbury conglomerate in the southern half of the Basin. It is characterized by laminated bedding with alternating layers of light gray, sandy, and dark gray clayey argillite. Thicker beds up to 3 ft also occur, and the composition occasionally grades to sandstone. The outfall tunnel and shaft is excavated through the Cambridge Formation.

Igneous intrusions are also abundant in the Boston Basin. They occur as sills,

intruded along a weak bedding plane; as dikes, intruded along a fracture plane; or as irregularly shaped bodies (Rahm, 1962). The composition is mainly diabase, a dark colored, fine grained igneous rock containing feldspar and magnesium rich silicates. Basalt is also present, the basalt and diabase are chemically similar but have different textures. In the City Tunnel, which traverses the northern portion of the Boston Basin, basalt comprised about 24% of the rock excavated and diabase comprised about 4% (Tierney et al., 1968). At the Porter Square Station in Cambridge, igneous intrusions, mainly altered basalt, comprised about 10% of the rock excavated (Dill, 1986). Various extrusive igneous rocks are inter-bedded with the sedimentary rocks of the basin. A large diabase sill forms the Brewster Island Complex, including the Calf Island and the Graves. Mapping of these islands, indicated that some igneous activity may have occurred at the same time as deposition of the argillite, since slabs of argillite are found within the diabase with very little if any alteration. The diabase is also inter-layered with basalt, except for on the Graves. The sill that forms the islands may be up to 300 ft. thick.

5.3.3 Structural Geology

The dominant trend of bedrock structure in the Boston area is nearly east-northeast, ranging from N6SE to N85E. Offshore that regional trend is believed to be more northerly, N45E (Kaye, 1984).

Understanding the structural geology of the Boston Basin is made more difficult due to the folding, and faulting in the basin, and the slumped and distorted bedding of the argillite. Much of the data on the structural geology of the basin is from the eight-rock tunnel: built in Boston, since 1885. The major folds identified in the basin trend N6OE to N85E (Billings, 1976) with the majority of the folding occurring in the southern portion of the basin. The attitude of the bedding is variable. Typically the bedding strikes east west with moderate dips between 25 to 55 degrees either to the north or south. Faulting

is quite apparent throughout the area. A series of east-northeast trending faults divide the bedrock into elongate slices. However, due to the lack of exposure there is considerable disagreement on the number and locations of these faults. Another set of faults trend northerly and dip at high angles, either east or west.

5.4 Geotechnical Investigation

5.4.1 Geophysical Surveys

Prior to the start of exploration drilling a geophysical survey was performed. This survey consisted of 215 miles of seismic reflection profiling, 94.5 miles of seismic refraction profiling and 4.5 miles of side scan sonar and magnetometer data acquisition. The side scans sonar and magnetometer lines were performed in the proposed diffuser area for a preliminary archeological survey, and to determine the ground conditions in which the diffusers will be seated.

The refraction profile indicated that a large low velocity zone velocities between 10,000 and 14,000 ft/sec in the northern section of the study area (Figure 48). Typically the Cambridge Formation has seismic velocities between 14,000 and 16,000 ft/sec. The seismic survey also produced a top of bedrock contour map, which indicated that bedrock was at higher elevations in the southern portion of the study area. The sides scan sonar survey performed only in the proposed vicinity of the diffusers located numerous large boulders in the northern portion of the diffuser locations. A seafloor contour map indicated that drumlin shaped features are located in the far-eastern portion of the study area. No archeological features were located with this study.

5.4.2 Drilling Program

The marine-boring program was laid out to determine the nature of the geology and

the geotechnical characteristics of the soil and rock in the approved diffuser area and the corridor from that area to Deer Island. The depths of the borings were based upon the geophysical information, which indicated that there was bedrock low just off of Deer Island. The boring depth was determined assuming that the tunnel crown would be two tunnel diameters below the low point in the bedrock surface. The borings were then advanced two-tunnel diameter below the invert. Twenty-five borings were drilled ranging in depth between 275 ft to 450 ft.

Soil samples were taken at 10-ft interval for borings along the tunnel alignment and at 5-ft interval in the diffuser area. Undisturbed samples were taken in the marine clays. Once into rock, an NQ-wire-line system was utilized (core size 1.88 inch) to continuously recover core to the required depth. Oriented core was taken in selected borings near the anticipated tunnel horizon.

The focus of the drilling program shifted toward the southern portion of the approved diffuser area, as more information became available from the geophysical survey, revealing that the "low velocity zone" covered most of the northern portion of the diffuser area. Borings drilled in the low velocity zone yielded large sections of altered argillite. One boring encountered nearly 200 ft of altered material, and the boring was ended while still in it. The average core recovery range from 85% to 100%. The average Rock Quality Designation (RQD) for the borings ranges from 44% to 98%. The RQD usually increased with depth, with joint spacing being moderately close to close.

Additional boring was drilled at the outfall shaft. Techniques employed to complete this boring were similar to those of the marine borings. Standard penetration tests were taken at 5-ft interval. Once rock was encountered a NQ wire-line system was utilized. Oriented core was taken every other core run for a total of 54% of the core recovered. The boring was drilled to a depth of 470 ft. Argillite was the only lithology encountered

in this boring. The oriented core indicates that the bedding is very consistent in this location, with an orientation of N59W, 25NE, on average.

5.5 Geotechnical Investigation Summary

The design of the Outfall Tunnel was based on extensive geo-technical explorations conducted by Metcalf & Eddy in 1988 and Parsons / Brinckerhoff in 1989. The tunnel alignment and profile was established such that the "crown of the tunnel would be at least 100 ft. below the top rock.

The tunnel was driven mostly through the Cambridge Argillite. The Cambridge Argillite was a gray, layered, slightly calcareous rock with beds generally ranging 0.5 to 3 inches in thickness, with occasional thickness up to 5 ft. Volcanic flows or ash fall tuffs in thickness of 0.5 to 12 inches were occasionally inter-bedded with argillite, with occasional tuff deposits up to 275 ft. thick. Intruding the Cambridge Argillite were igneous dikes and sills, predominantly of diabase, with minor amounts basalt, andesite and felsite. Significant zones of alteration of both the argillite and the tuffs were occasionally present. The breakdown of the above rock formations along the tunnel alignment was projected as follows:

Argillite	56%
Sandy Argillite	23%
Tuffaceous Argillite	8%
Diabase, Felsite, Andesite	7.4%

In general, the boring were spaced some 1,000 ft. apart. Based on Geo-technical Interpretative Report (GIR), the rock quality was generally good to excellent, with

occasional poor rock areas. Measured permeability indicates that the rock mass has low permeability (10^{-5} cm/sec to 10^{-6} cm/sec).

The values of RQD, which represented quality of the rock varied between 10 to 100 percent at different coring locations. Figure 45 is the histogram showing the frequency of various RQD values. This graph shows that more than 50% of core footage had RQD greater than or equal to 90 percent. About 83 % of the core footage had RQD greater than 50, about 86 % greater than 40 and about 90 % greater than 30. No boring shows three significant joint sets, only one boring showed two sets, which were in diabase, reminder of the boring showed one set or random jointing. The spacing between the joints ranged between 3 ft to several feet apart. On conservative side the average spacing between the joints was around 3 ft to 5 ft. The joint roughness was rough to slightly rough surface for most of the locations. Most of the joints were unaltered, with some being slightly altered.
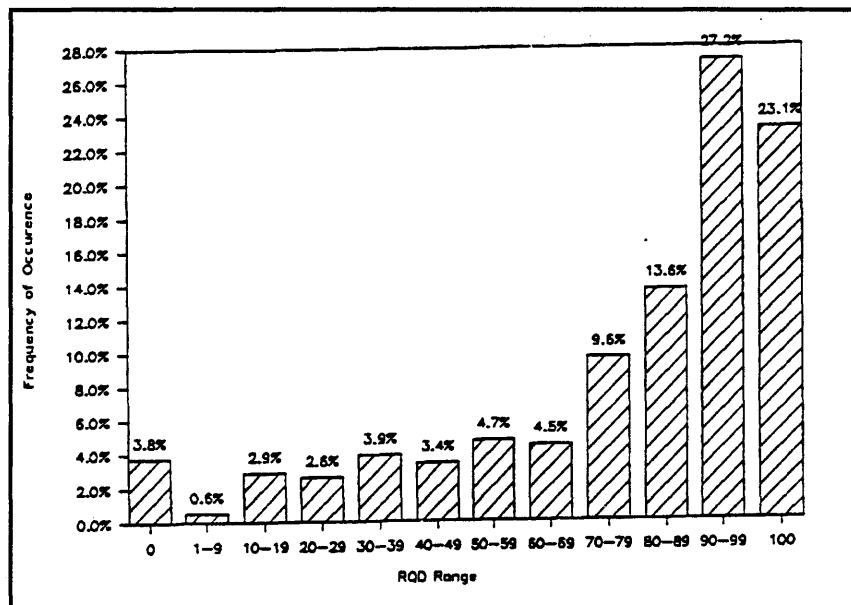
Figure 45: Histogram showing distribution of RQD values (GIR 1989).

5.6 TBM Design

The Outfall Tunnel TBM was a 26.5ft. diameter completely shielded TBM weighing some 700 tons. The machine was equipped with 50 of Robbins new 17-inch Duro cutters. These new disc cutters use an improved alloy, which allow for a narrower and longer ring, thus reducing the weight of the cutter. These cutters can be changed from either the front or the back of the cutter head. Figure 46 shows the photograph of the TBM for this project.

The machine was powered by eight (8) each 420-hp electric motor, which rotated the cutterhead at 6.4 revolutions per minute (RPM). Cutterhead thrust or forward movement was accomplished in one of two ways, either by 10 main-thrust cylinders or by 12 auxiliary-thrust cylinders. In competent ground or hard rock, thrust was transferred to the tunnel walls through hydraulically extended gripper shoes. The 10 main-thrust cylinders were connected between the forward shield and the gripper shield, allowing for 5 ft. of forward movement for each cycle. In unstable ground or soft rock, the gripper shoes were left retracted, and the twelve auxiliary thrust cylinders mounted at the rear end of the gripper shield were capable of pushing off the pre-cast concrete segments. Steering of the TBM was also accomplished by quadrant or section control of the thrust cylinders. The maximum cutterhead thrust was 2,500,000 lbs. based on a loading of 50,000 lbs. per cutter. The machine specifications are shown in Table 7.

The cutterhead assembly was mounted to the cup of the main bearing assembly, which accepts both radial and thrust loading. Drive torque for the cutterhead assembly was provided by eight, 3-phase, water-cooled AC electric motors, each delivering 420 HP at 1800 RPM. Those motors, driving through gear reducer assemblies into a main ring gear, which was attached to the cutterhead, rotate the cutterhead at approximately 6.4 RPM in a clockwise direction as viewed looking forward.
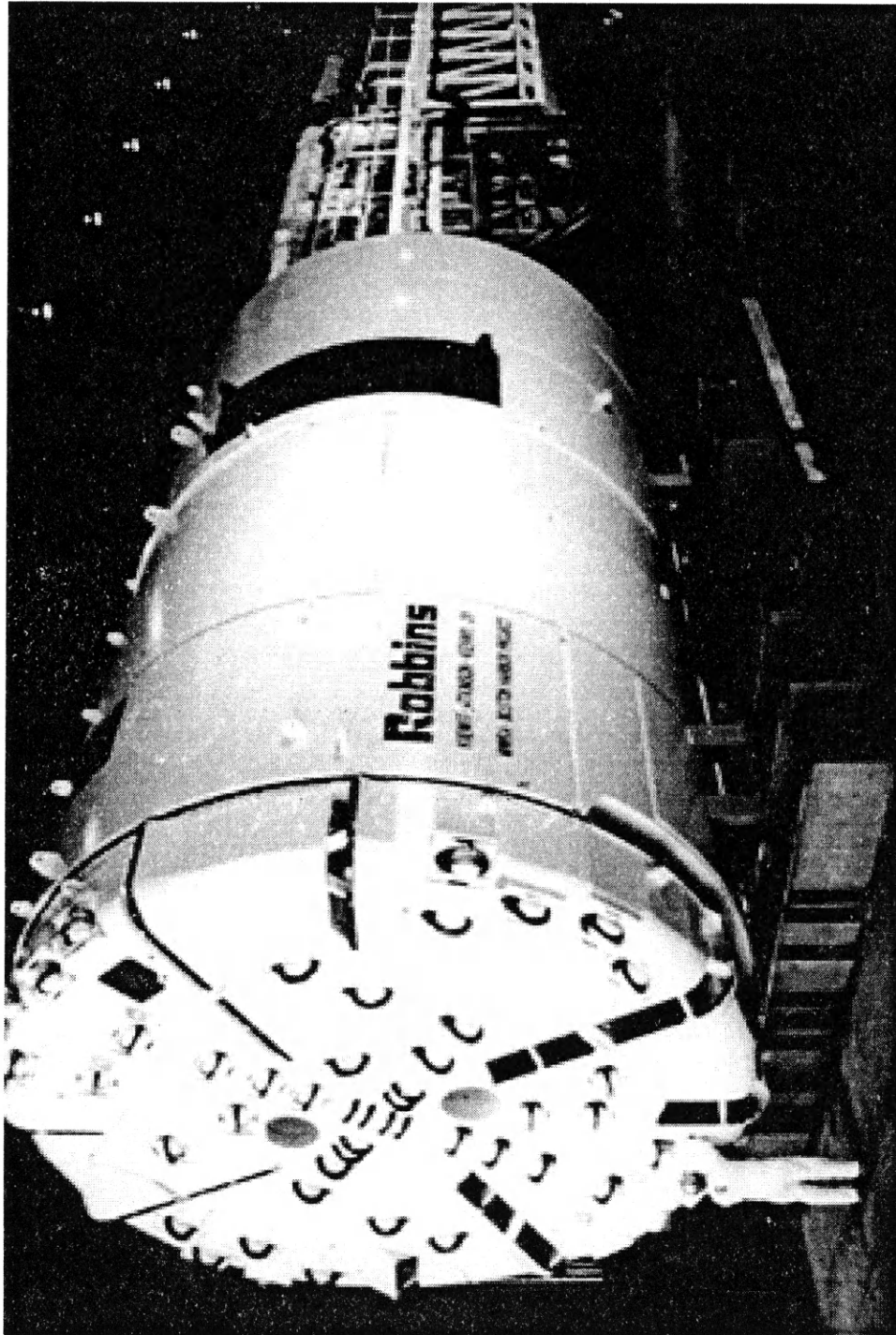
Figure 46: Photograph of Tunnel Boring Machine used in Outfall project

Boston Tunnel Boring Machine Features

Machine Diameter	26 ft 6 inches
Cutters	Disc cutters
Cutter Diameter	17 inch
No. of Cutters	50
Max. Load per Cutter	50,000 lbs.
Maximum Operating Thrust	2,500,000 lbs.
Maximum Shield Thrust	6,670,000 lbs.
Cutter head Drive	Electric Motors
Cutter head Power	3,360 hp (8*420 hp motors)
Cutter head Speed	6.4 RPM
Cutter head Torque	2,700,000 lb-ft.
Boring Stroke	65 inches
Conveyor Capacity	350 ft^3/min

Table 7: Specification of tunnel boring machine used in the project.

Structurally, the cutterhead assembly was made of heavy steel plates, internally reinforced, with integral buckets to remove the rock cuttings. The pickup devices, or

buckets, scoop up the material at the tunnel invert and deliver it by gravity into the conveyor system within the cutterhead support as each bucket rotated to the crown of the tunnel. These buckets were equipped with replaceable hard-faced lips for longer wear.

The cutterhead assembly was the mounting structure for the 46 cutter assemblies, having a total of 50 replaceable cutter rings, used on the machine. The eight cutter rings located at the center of the cutterhead were 17 inches in diameter and were twin-disc assemblies. The remaining 42 cutter rings were also 17 inches in diameter, but were single-disc assemblies. All cutter assemblies and housings were designed so the cutters may be changed from the rear of the cutterhead. For convenience the cutter assemblies at positions 9 to 42 (face cutters) could be removed and replaced from the front side of the cutterhead assembly. The individual cutter rings were numbered radial distance from the center outward from number 1 through number 50. Cutters number 43 through 50 were commonly referred to as gage cutters; however, cutter number 50, being the furthest outboard, was actually provided final sizing of the bore of the tunnel.

Each cutter ring described an individual radial pattern as the cutterhead rotated through a complete revolution. Spacing between cutter ring paths varied from approximately 3.5 inches at the center and face cutters, to approximately 0.25 inch as the pattern approached the final cutter ring. The cutterhead assembly also provided a mounting base for water spray nozzle and associated plumbing used with the water spray system.

The forward shield assembly supported the weight of the cutterhead support and cutterhead assembly and provided mechanisms for stabilizing it against movement within the bore section of the tunnel. The cutterhead support provided the primary structure for the cutterhead assembly. The cutterhead support provided a mounting base for the main drive assemblies, and a machined and drilled structure for mounting of the main bearing

assembly. The cutterhead support also included provisions for mounting of the conveyor, muck chute, and stabilizer cylinders and shoes.

Stabilization of the front shield was provided by two stabilizer shoes, which were attached to the cutterhead support in the upper left and right hand quadrants and extend through holes in the forward shield. Two stabilizer cylinders were connected to each shoe by stabilizer beams, and raise or lower the stabilizer beams, which react against the stabilizer shoes.

Ten thrust cylinders were mounted between the forward shield and gripper shield, each having a bore of 14.0 inches, a rod diameter of 9.0 inches, and a stroke of 60.0 inches. These cylinders had spherical ends, which mount into sockets on the forward and gripper shields.

The cylinders were installed at alternating angles between the gripper shield and the forward shield. This angular arrangement allowed the cylinders to react to cutterhead torque and transfer that reaction to the gripper shield, thereby provided roll control without the need for additional torque cylinders. The arrangement of the cylinders, along with the hydraulic circuit functions, permitted the cylinders to provide lateral and vertical steering of the forward shield and cutterhead.

The telescopic shield assembly provided the intermediate stage between the forward shield and the gripper shield. The telescopic shield was comprised of an inner shield and a outer shield. The inner shield was connected to the gripper shield assembly by cap screws, and provided coverage of the bored tunnel during thrust cylinder extension. The outer shield was connected to the forward shield assembly by the action of twenty articulation cylinders and extends around the inner shield. Total length of the telescopic shield assembly was 103.3 inches in the retracted mode and 169.8 inches in the extended

mode.

5.6.1 Back-up or Trailing Gear

Boretec, Inc. of Solon, Ohio, performed the design and manufacture of the trailing gear. A total of eight (8) 35 ft. long cars comprise the back-up train which was connected to the TBM via a retractable set of cylinders at the end of the bridge conveyor. A 45-ft. section from the tail shield of the TBM to the first back-up car was used to install the 80-lb. rail and longitudinal ties used for the rolling stock.

The trailing gear was a two-track system from Car No.1 to Car No.6. Six (6) segment cars carrying three (3) segments each were stored on one side with pea gravel cars, and flat cars with rail & ties on the other track. The upper deck of cars #1 and #2 contained two (2) 2000 KVA transformers along with all of the associated switch gear. The upper deck of the remaining cars contained the turbo filter dust suppression system and fan units, electric power cable storage, water system and an auxiliary hydraulic system for the probe drill. The ventilation system consisted of 60-in. diameter fire resistant bag line, which extended from the shaft to the last gantry car. It was supported by messenger cable from the tunnel crown. A replaceable bag line cassette containing 650 LF of bag was located on the upper deck of the last car and the bag line was pulled from the cassette as the backup moves forward.

All of the gantry cars were pre-assembled and ballast with sand and concrete on the surface. They were then lowered end-on-end down the shaft and placed on the rail at the shaft bottom. Associated outfitting equipment was then lowered onto the upper deck before moving the car forward to the TBM.

5.6.2 Muck Disposal System

The key to any successful tunnel excavation system generally lies in the efficiency of the muck removal. This commonly accepted rule was more critical on this unusually long single heading tunnel. In order to overcome this obstacle and negate the problems that eight (8) diesel locomotives would create to the ventilation requirements, a continuous conveyor system was opted on the job.

The complete system consisted of a horizontal conveyor designed by Long Air Dox, a vertical conveyor designed by "Trellex Flexowell" and a transfer and stacker conveyor also designed & built by Long Air Dox.

Horizontal Conveyor

The 36" continuous horizontal conveyor system comprised the following:

1. An advancing tail pieces where conveyor idlers were installed.
2. Continuous longitudinal channel frames with diagonal support frames.
3. Booster units (3 each) every 12,000 ft. with 2-200 HP motors to provide the required belt tension throughout.
4. Conveyor take-up and main drive motors unit.

The conveyor take-up unit was permanently located at the shaft bottom. It consisted of two opposing carriages with multiple rollers 10 provide storage capacity and to control the belt tension. The increase in belt tension resulted from the advancing tailpiece signals the take-up unit to released the belt in storage. It thus allowed the belt to extend forward without over-stressing.

The total storage capacity in the take-up unit was 2,000 feet up to ± 750 ft. of tunnel was serviced by it when full. As required, 1,000-ft. rolls of belt were added to the systems at a splice platform attached near the bottom of the shaft.

Two 200-hp motors drive the conveyor belt at the shaft similar to the 400 hp booster drive units. The system was designed to handle over 900 tons of material per hour, at a running speed of 600 feet per minute.

Vertical Conveyor

In order to transport the rock 420 LF up the shaft, a bucket-type Vertical Lift Conveyor System (S-Belt) was purchased from LakeShore Industries and was installed in the shaft. The system was driven by two (2) 250 hp motors which enable it to haul over 900 tons of rock per hour. The conveyor belt moved at 450 ft per minute and was completely shrouded to provide safety in the shaft. All of the conveyor systems were equipped with solid state controls, which vary the belt speed and synchronize different systems depending on actual loading conditions. The TBM operator controlled the operation of all systems. The Long Air Dox in feed conveyor fed the S-belt system at the tunnel level.

Surface Discharge

At the top of the shaft, an 85 LF transfer conveyor and a 130 LF stacker conveyor were installed to transport the tunnel muck from the vertical conveyor to a muck pile adjacent to the access road. The muck pile was removed on a daily basis using three 35-ton Volvo articulated trucks loaded by a CAT 980 loader.

6. LABORATORY ROCK TESTING PROGRAM AND RESULTS

6.1 Field Rock Coring Program

In order to provide an accurate assessment of actual rock conditions encountered, an extensive field core-drilling program was carried out to obtain rock samples in the tunnel to conduct an intensive laboratory test program. The cores were obtained at 250-ft. intervals along the entire tunnel length. Eight-inch diameter cores were retrieved from the tunnel at seven-o' clock position as shown in Figure 47. These core samples were then re-cored in the longitudinal and radial directions as shown in Figure 48. The radial cores were orientated in the direction of tunneling, where as the longitudinal cores were perpendicular to tunnel axis. The purpose of coring in the two directions was to assess any rock directional properties, which might exist and influence the machine performance.

6.2 Geological Features

As the tunnel was lined in the tail shield along with the advancement of the machine, it was not possible to gather any geological information from the walls of the tunnel. Therefore, all the information about geological features was obtained from coring locations. The geologic information collected included the orientation of bedding and foliation, fractures, and joints.

The collected data revealed that the rock was highly foliated and bedding/foliation varies in orientation along the tunnel axis. Rock also contains micro-fractures in few sections. Joints were closed and many were filled with intrusions of calcite and other minerals. The rock had low permeability.
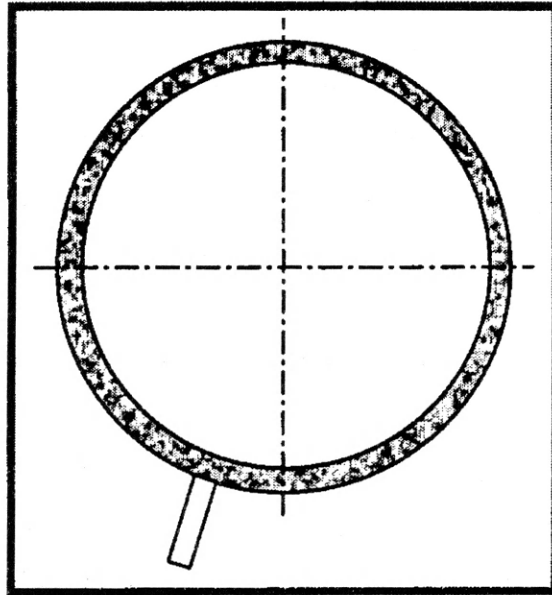
Figure 47: Location of Eight inches cores in the tunnel.
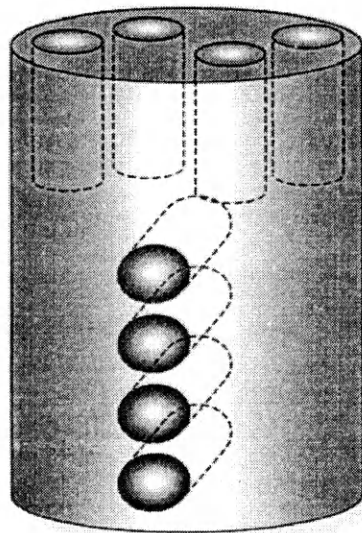
Figure 48: Re-coring of eight-inch core retrieved for tunnel

6.3 Testing Program

Physical property tests conducted on the core samples received from the tunnel to establish database to verify the rock mass boreability index. Also, the data could be used to obtain the coefficients for the influencing parameters such as, Uniaxial Compressive Strength (UCS), Brazilian Tensile Strength (BTS), and the Acoustic Velocities (P&S wave). The measured P and S wave velocities were utilized to calculate the dynamic elastic constants, the Young's Modulus and the Poisson's ratio. The RQD values were obtained from the geologist log of cores as they were retrieved from the tunnel to match the rock at coring locations. The geologist log sheets are given in appendix A. This data also includes the bedding direction for each core. The average value for joint spacing and conditions were considered from the geological investigation report of 1989, as it was not possible to observe the joint sets due to installation of wall lining in machine tail shield. The summary of the total number of different tests performed on the cores is given in Table 8. These tests were subsequently used to establish the required database for further analysis of effect of geological parameters on TBM performance.

Test Performed	Number of tests
Uniaxial Compressive Strength	133
Acoustic Velocity (For E and v)	113
Brazilian Tensile Strength	176
Total	**422**

Table 8: Summary of the number of tests performed.

6.4 Sample Acquisition and Logging

The core samples were received from the site in batches including cores from longitudinal and radial direction at each location. The core samples were analyzed and tested with a systematic approach as explained in the following.

6.4.1 Sample Logging

Each sample received from the tunnel was individually logged, and closely examined for planes of weakness, joints, fractures, veins and filling material to be sketched on the core log forms. The samples were then placed on a machinist flat and the surface roughness, together with straightness of the cores were checked. Figure 49 shows a sample sheet of the data sheet used for core logging with all the information recorded (i.e. diameter, approximate length, and geological features present). After logging, type and number of test to be performed on each sample was selected and the samples were prepared for testing. Figures 50 and 51 shows photographs of some samples received.

6.4.2 Sample Preparation and Testing Procedures

Detailed sample preparation and testing procedures were prepared for the entire test program for core samples received from the Boston Outfall Tunnel. The established ASTM standards were used for testing where applicable. A detailed description of the procedures employed for each test is given in the applicable ASTM standards.

6.5 Description of Tests Performed

The following sections contain the purpose and description of the tests performed.

6.5.1 Uniaxial Compressive Strength (UCS)

UCS is one of the most basic parameters and the most common test performed for determination of rock strength for tunnel boreability evaluations. It is measured in

accordance with the procedures recommended in ASTM-D2938. The samples are prepared to satisfy the requirements of ASTM D4543.
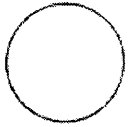
Figure 49: The core logging data sheet with recorded information.

Figure 50: Photograph of batch of core samples as received for testing.
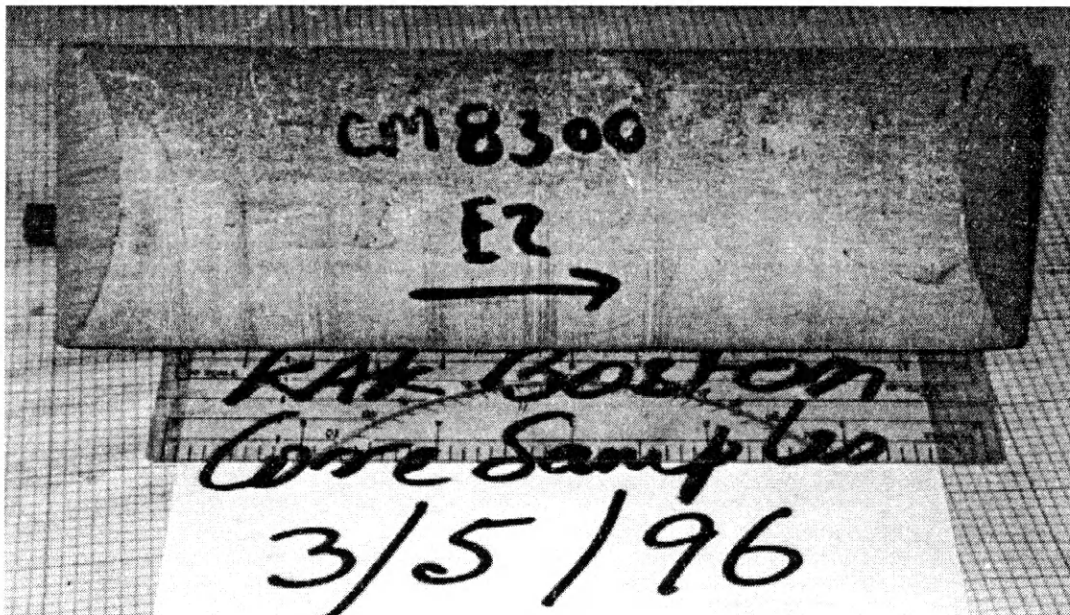
Figure 51: Photograph of a core sample after logging.

UCS measurements were made using an electronic-servo controlled MTS stiff testing machine with a capacity of 220,000 lbs. as shown in Figure 52. Loading data and other test parameters were recorded with a computer based data acquisition system, which were subsequently reduced and analyzed with a customized spread sheet program.

Due to the existence of a high degree of banding, clay fillings and jointing in a large number of samples, special attention was paid to observing and recording the sample mode of failure the testing. For the samples where failure was found to occur along existing weakness in the rock, the sample was classified to have undergone a structural failure. Where any existing rock feature did not control sample failure, the result is recorded as a normal or non-structural failure. This classification of test results was of significant importance since structural failure does not represent the intact strength of the rock. Figures 53 and 54 are typical examples of failure in the non-structural and the structural modes respectively. Figure 53 shows a sample failing in tension with lateral pieces, where the failure is not controlled by any rock weakness. On the other hand, Figure 54 shows a sample that failed along an existing discontinuity, hence resulting in a structural failure.

The UCS of a rock specimen is calculated as follows:

$$UCS^* = \frac{F\max}{A}$$

Where:

UCS* is measured Uniaxial Compressive Strength (psi)

Fmax is maximum load on the sample before failure (lbs.)

A is cross-sectional area of the sample in square inches
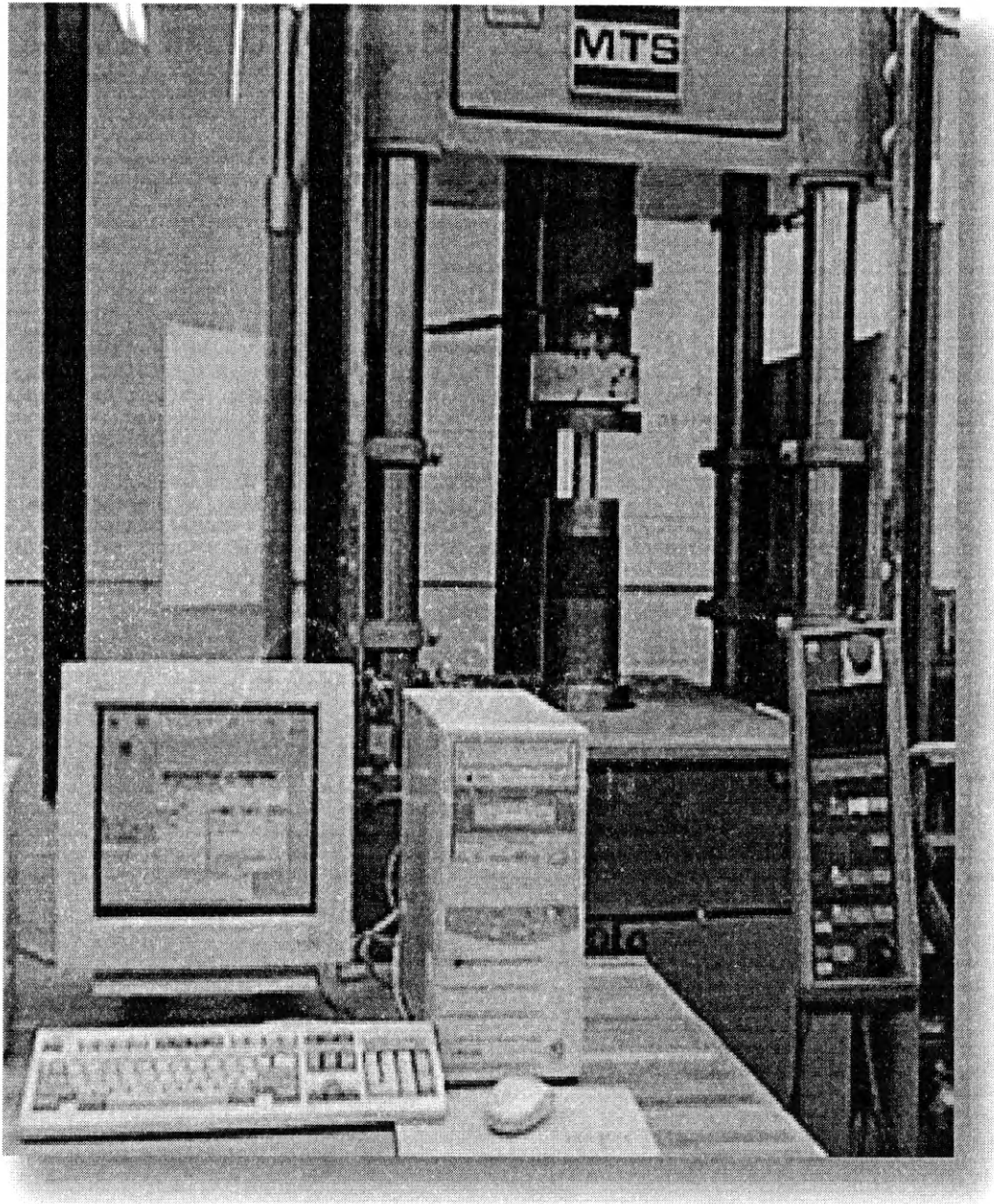
Figure 52: The MTS machine used for Compressive Strength Testing

Figure 53: Typical non-structural sample failure for UCS testing

Figure 54: Typical structural sample failure for UCS testing

If the size of the core sample was different than 2 to 1 length to diameter ratio, the measured UCS was corrected to a L/D ratio of 2 using the following equation:

$$UCS = \frac{UCS*}{0.88 + 0.24\left(\dfrac{D}{L}\right)}$$

Where:

UCS is corrected Uniaxial Compressive Strength (psi)

UCS* is measured Uniaxial Compressive Strength (psi)

D is sample diameter in inches

L is sample length in inches

6.5.2. Brazilian Tensile Strength

Indirect or Brazilian tensile strength (BTS) provides a measure of rock tensile strength. This parameter was measured according to procedures set forth in ASTM D3967. The tensile strength testing was performed on the same test machine used for UCS testing as shown in Figure 52. The detail test procedures are given in ASTM standards.

Using the core measured dimensions and failure load, the Brazilian indirect tensile strength was determined as follows:

$$BTS = \frac{2P}{\pi LD}$$

Where:

BTS is Brazilian Tensile Strength (psi)

P is maximum load at failure (lbs.)

D is diameter of the sample in inches

L is thickness of the sample in inches

In order to investigate any directional properties present in argillite, the tensile strength samples were tested in two orientations, perpendicular and parallel to the bedding strike. Typical sample failures in two different directions are shown in Figures 55 and 56. As expected, the samples showed a higher strength when loaded in the direction perpendicular to the bedding orientation. The samples were closely examined as to determine the mode of failure. The samples found to fail along an existing joint, fracture plane or bedding were classified as structural failures. The samples where a typical vertical split failure occurred were recorded as being normal or non-structural.
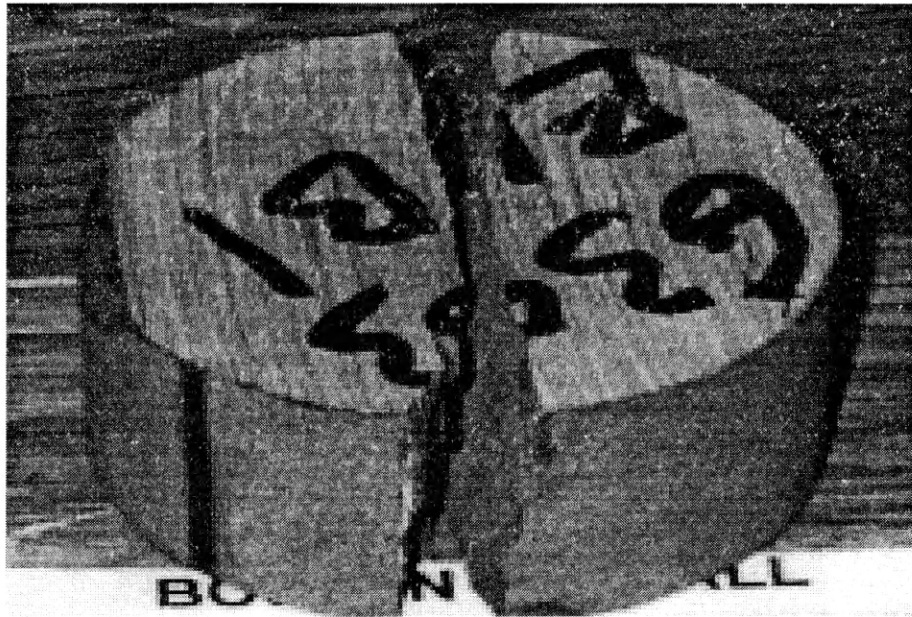
Figure 55: Typical failure when sample loaded parallel to bedding strike
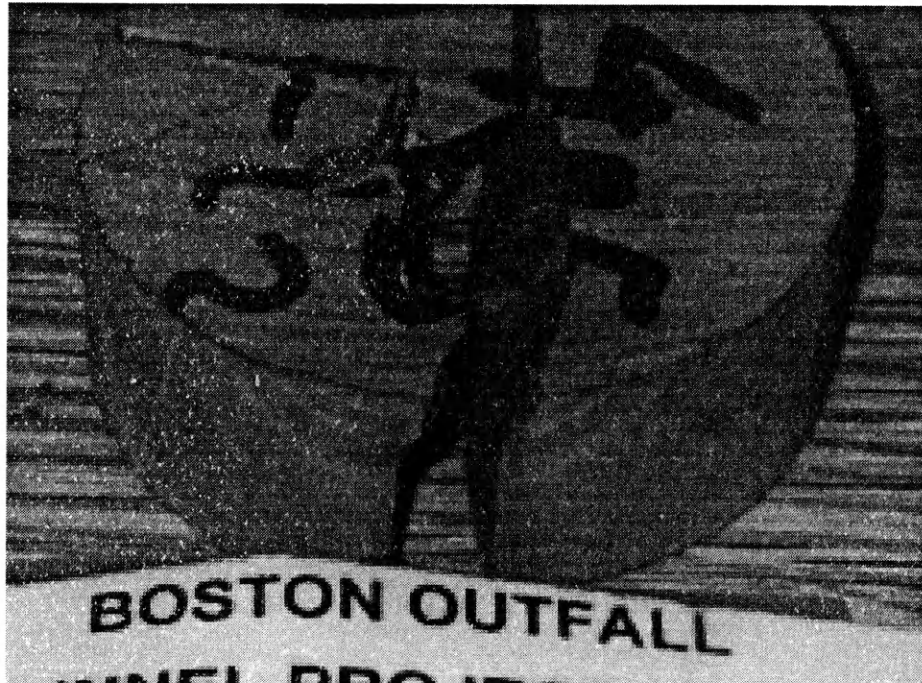
Figure 56: Typical failure when sample loaded perpendicular to bedding strike

6.5.3. Acoustic Velocity or Dynamic Modulus Test

This test measured the acoustic wave velocities through a rock sample. The wave velocities, P-wave (pressure wave) and S wave (shear wave) can be used to determine the dynamic elastic constants of the rock. These constants include the Young's modulus and the Poisson's ratio of the material. This test was performed in accordance with the procedures recommended by ASTM-D2845 on core samples prepared for UCS testing. The equipment used for acoustic velocity measurements is shown in Figure 57. To conduct a test, set of piezoelectric transducers were attached to the sample using Phenyl Salcylate solution. A signal generated by a function generator was then transmitted through the sample and the arrival time for the P and S wave was recorded.

The velocities for P and S wave were calculated as follows:

$$V = \frac{L * 10^{\wedge}5}{T}$$

Where:

V is velocity of P or S wave (m/sec)

L is length of the specimen (cm)

T is time of arrival for P or S wave (μsec)

The dynamic elastic modulus and the Poisson's ratio were calculated from the measure wave velocities and the sample bulk density, as follows:

$$E = \frac{\rho Vs^2 \left(3Vp^2 - 4Vs^2\right)}{Vp^2 - Vs^2}$$

$$v = \frac{Vp^2 - 2Vs^2}{2\left(Vp^2 - Vs^2\right)}$$

Where:

Vs is shear wave velocity (m/sec)

Vp is compressive wave velocity (m/sec)

E is elastic modulus of rock (MPa)

v is Poisson's ratio of rock

ρ is density of rock (kg/m^3) = 4W/LπD^2

W is weight of the rock sample (g)

D is diameter of the rock sample (cm)

L is length of the rock sample (cm)
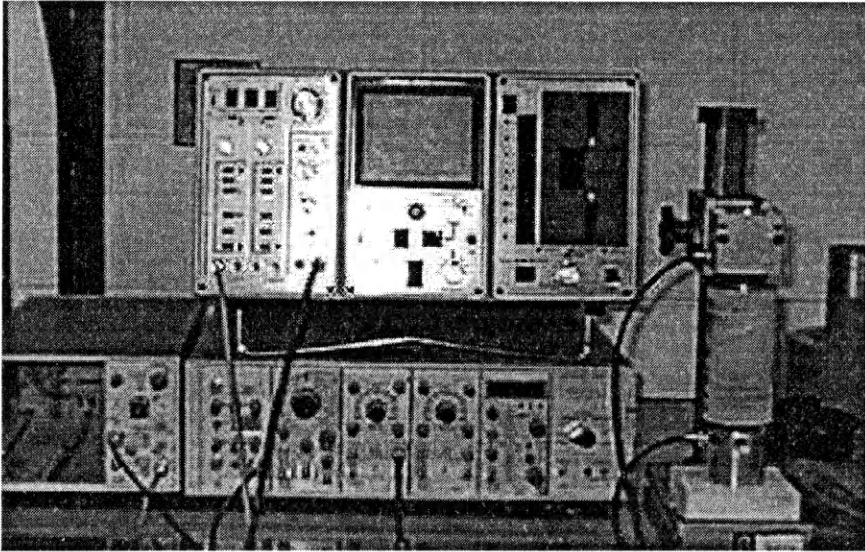
Figure 57: Equipment used for the Acoustic Velocity measurements

6.6 Summary of Laboratory Test Results

The overall test results of all the tests performed to evaluate mechanical strength of rock are given in the appendix B. These tests include uniaxial compressive strength, tensile strength, elasticity modulus, and Poisson ratio. The density of the rock was also measured, as it is required to calculate the dynamic constants. In this section average result for each test is briefly discussed.

Table 9 provides a summary of the average UCS test results for the radial and longitudinal cores. As can be seen, the average non-structural (intact) strength for all tests performed is 19,047 psi. The average for samples failed in structural mode is around 11,000 psi. It is also observed during the uniaxial compressive strength testing that there is essentially no difference in the strength of cores tested in radial and longitudinal direction. This is due the foliation direction that is at an angle to the tunnel axis. The results also show that there is a big difference in values of samples failed in structural mode and non-structural mode. These shows that the classification of test

results is of significant importance since structural failures do not represent the intact strength of the rock. The intact strength of rock is important for any performance prediction as it represents the true strength of the rock to be bored.

Table 9: Summary of Uniaxial Compressive Strength Testing Results.

Direction	Structural Failures (psi)	Intact Failures (psi)
Longitudinal	11,358	18,851
Radial	10,614	19,142
Average	10,963	19,047

Table 10 summarizes the results of tensile strength tests for the structural and non-structural failures in radial and longitudinal direction. As can be seen, the tensile strength for longitudinal direction is 23 % higher than the strength in radial direction, confirming the directional properties of the rock. Table 11 shows the average test results for P and S wave velocities, dynamic elastic modulus and the Poisson's ratio. The results show that the elasticity modulus and the Poisson's ratio of the rock is higher in the radial direction which is direction of tunnel axis. Higher modulus of elasticity and Poisson ratio indicates that the rock can be harder to bore and more ductile in this direction, which is the direction machine was excavating the rock.

Table 10: Summary of Tensile Strength Testing Results

Direction	Structural Failures (psi)	Intact Failures (psi)
Longitudinal	852	1,864
Radial	795	1,523
Average	818	1,687

Table 11: Summary of Acoustic Velocity Test Results.

Direction	Primary Wave (ft/sec)	Secondary Wave (ft/sec)	Elasticity Modulus (ksi)	Poisson's ratio ν
Longitudinal	16,570	9,962	8,878	0.21
Radial	18,023	10,408	9,928	0.24
Average	17,432	10,226	9,501	0.23

6.7 Discussion of Test Results

The test results clearly illustrated the variability of the rock along the tunnel, which can subsequently be used to develop an understanding of the impact of rock variability on the TBM performance. Also, the test results clearly indicated the existence of the directional properties in the rock. As expected, this was more pronounced in tensile strength test results. The variation in the uniaxial compressive strength measured on samples in different directions was not significant. This was partly due to the fact that core samples were not oriented exactly along the bedding/foliation. Therefore, the tests could not be performed parallel or perpendicular to the direction of foliation. The existence of an angle between 30 to 60 degree between foliation and core axis and sometimes variation of foliation/bedding orientation even within one sample has somewhat reduced the difference in the UCS and to lesser extend BTS test results between radial and longitudinal cores.

In general the testing indicated that tests such as UCS are less sensitive to the directional properties of the rock samples. The preferred test for measuring the directional properties of the rock was found to be tensile strength, as expected. This test and similar splitting tests such as point load index test capture the directional properties of the rock sample and thus, hint the engineers to take them into account in their analysis.

The screening process to separate the structural failures in testing from the normal failure has proved to be useful, as this process allows an objective assessment of the rock strength for boreability prediction. This was especially true for Cambridge argillite, which contained many secondary fractures and filled calcite veins.

The final results from this entire extensive laboratory testing for rock can be summarized as follows:

1. The actual intact strength of the rock was measured to be around 19,000 psi. The intact tensile strength of the rock was as an average 1,687 psi with maximum average strength of 1,864 psi in longitudinal direction.

2. Argillite was found to exhibit significant directional properties as determined by difference in tensile strength measurements on the samples from different directions. Due to existing foliation / bedding, rock tensile strength was found to be higher acting in the direction of machine advance.

3. The average dynamic modulus of elasticity was measured at 9,501 ksi, which was high side for this type of rock. The average dynamic Poisson's ratio of this rock was 0.23.

All the measured rock properties in the testing program were used to establish the required database. This information was subsequently used to verify the developed concept for using rock mass boreability index in predicting performance of tunnel boring machines in jointed / foliated rock formations.

7. TBM PERFORMANCE EVALUATION AND ANALYSIS

7.1 Introduction

As stated earlier, the objective of this study was to try and correlate machine performance with geological conditions. Obviously, when performance prediction is conducted for a TBM in a given geology, it is assumed that machine is working at its maximum capacity. However, there are conditions that machine does not use its full thrust or power capacity due to the nature of the rock.

TBMs are known to run power limited in softer rocks, merely due to the fact that for a given level of thrust or cutter load, it penetrates deeper into the rock and thus it takes relatively higher rolling force, torque and power. The opposite happens in harder rock formations where machine typically runs thrust limited because it takes more thrust to penetrate the rock. Commonly, in such cases machine still has excess power which is not used.

To fully understand the effect of geological factors on the machine performance, the level of thrust and power used to penetrate at certain rate into the rock must be estimated or measured. This means that the magnitudes of cutter load, rate of penetration, consumed power and rock properties have to match. In other words, in a given geology and for a machine with certain cutterhead design and profile, there is only one point where all these parameters converge to determine machine performance. Clearly, for a given conditions, as the cutterhead thrust is increased the penetration will increase and so is the power consumption. Therefore, to compare effect of varying geological conditions on the machine performance, the rate of penetration must be normalized with respect to cutter load. This concept has been considered in the past and was introduced by Nelson(1985). The amount of thrust required to achieve unit penetration, which is

termed field penetration index (FPI) was developed to allow normalizing the rate of penetration with cutter load. FPI is determined by dividing the cutter load for a given rate of penetration per revolution. By using this factor, effect of machine diameter and RPM on the rate of penetration is separated and by using the cutter load, the effect of thrust on penetration is normalized. In such case the index, which is expressed in kips/in or kN/mm can be used to differentiate between rocks with different strength or other characteristics.

The same logic holds true for any TBM field performance evaluation and analysis. Since applied cutter load and power is variable from point to point, to determine the effects of changing rock type and formations on machine performance, one should normalize the TBM performance data. This means that machine operating parameters should be monitored at certain points, in this case coring locations, to allow objective evaluation of effect of geological parameters on TBM performance.

This can be achieved by variety of means, including monitoring and measurement of propel pressure, power consumption and rate of penetration. Using these parameters, cutter load can be estimated and used in the analysis.

7.2 Applied Thrust and Cutter Load

The cutter load is a term commonly used to represent the magnitude of normal force applied on the cutter to penetrate the rock. These forces are provided by the thrust or propel cylinders. Hence, to estimate the cutter load, machines gross thrust generated by propel cylinders has to be determined. This is simply done by multiplying the applied propel pressure by the total area of the thrust cylinders. In the case of Boston tunnel machine the lattice design of double shield was used with 10 thrust cylinders each at certain angle with the tunnel axis. The total area of cylinders was about 1,540 square inches and the correction factor for the angle of cylinders with the tunnel axis was

determined to be as an average 0.88 for full stroke. These parameters and the pressure of propel cylinder was used to estimate the magnitude of gross thrust of the machine.

A part of the gross thrust goes to cancel the frictional forces acting on the shield. The friction between the shield and the ground is typically evaluated at about 50% of machine weight. Another component of gross thrust is the tow forces which is used to pull the backup system behind the machine. Once these two components are subtracted, net thrust can be estimated to determine cutter load.

Therefore, estimating the drag or friction of the TBM as it moves forward over the excavated rock surface is an essential component for evaluating the actual thrust delivered to the cutter head. This friction is a function of the weight of the TBM and its bearing area on the rock surface as shown in Figures 58 and 59. In simple words, the thrust used in dragging the TBM is not available to thrust the cutters against the rock face. This effect is well known as shield drag and is measured with drag tests, which is run to estimate the magnitude of the drag forces. The common procedure to perform a drag test is to pull the front shield back from the face, set the propel pressure to zero and propel the machine forward toward the face. The propel pressure at which machine starts moving forward is recorded and in this case the gross thrust estimated for the given pressure is equivalent to shield drag. This test is repeated several times and the pressure is similarly recorded to arrive at an average propel pressure which starts the shield motion. To avoid additional friction caused by cutters touching the walls and damage to gage cutters, the head is turned and sometimes the gage cutters are removed. The assumption is that since the cutters are not pushed against the face, all the generated thrust is used to react to tow force, which is more or less constant and to over come the frictional forces acting on the shield.

There are many details in performing a drag test that is beyond the scope of this study. It also must be noted that the amount of drag is reduced by the vibration of the

head while cutting the rock, this refers to "dynamic drag" which could be as low as 50 to 60% of the measured drag from the drag test, which represents the static drag forces. Once the amount of drag is estimated, the net thrust can easily be determined by subtracting drag from gross thrust at any propel pressure.
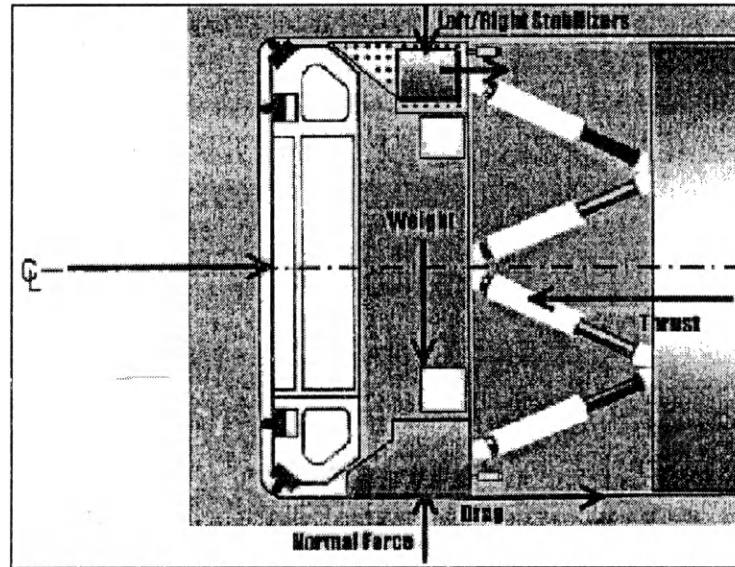
Figure 58: Schematic drawing of the TBM showing the forces in effect while boring (Side view).
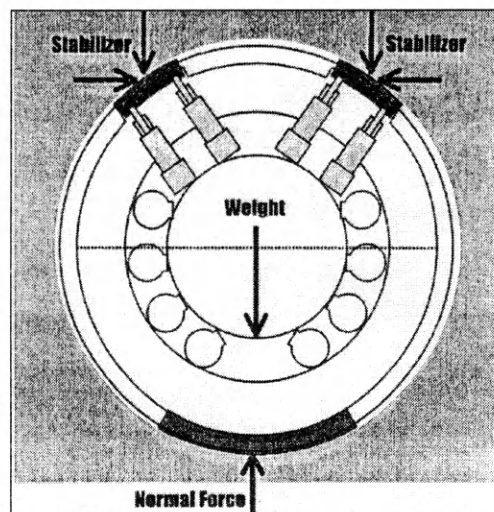
Figure 59: Schematic drawing of the TBM showing the forces in effect while boring (Rear view).

Once the shield drag of a machine can be estimated, the magnitude of cutter load can be assessed and used for performance evaluation of the system. An additional test that has proven very useful is the thrust-penetration test. In this test machine is fully engaged and the rate of penetration is measured while changing the applied propel pressure in incremental steps. This test eliminates the effect of dynamic friction and includes the dynamic drag in machine operation. Practically the cutter head is engaged and pushed into the face while operator maintains a certain level of propel pressure. The amount of machine advance or stroke is measured on propel cylinders for the elapsed period of time. Then the propel pressure is increased to the next level and similarly the rate of penetration is measured. When the data is plotted on the proper chart, the relationship between applied thrust and rate of penetration can be derived.

A total of 10 thrust-penetration tests were conducted with varying rates of advance of the machine. Five tests were performed at a slow advance rate. Three tests at 50% propel rate (2 in/min) and 2 tests at 100% propel rate (4 in/min). The propel pressure was obtained from the monitoring system discussed in the following sections.

Based on the results of these drag tests the total machine friction was calculated to be 613 kips, as shown in Table 12.

Drag	500 kips
Tow force while boring	115 kips
Total drag and tow	613 kips

Table 12: Results of Drag test to estimate the friction.

7.3 TBM Performance Monitoring

To monitor the performance of the machine it was decided to install a monitoring system to measure some of the important operating parameters on the machine. For this purpose a strip chart recorder was installed to record machine parameters including propel pressure, cutter head motor amps and stroke of the propel cylinder. The data for the strip chart was obtained from machine's main electronic control system or PLC by connecting to the respective data channels. This information was then transmitted through a digital/analog data transmission and control system to strip chart recorder.

These strip charts in addition to shift reports could be used to determine machine operational parameters throughout the tunnel. Since the geological data was available at 250-ft increment through the coring locations, it was decided to select the strip charts related to machine performance at these locations. Therefore, at each coring location a total of 9 pushes were selected to include the station where the core was obtained as well as 4 strokes before and 4 strokes after that spot. Each stroke was equal to the width of the concrete lining ring, which was 5-ft (1.5 m).

The purpose of the analysis of the machine operational parameters at these locations was two fold:

1. To determine average propel pressure, ROP, and cutter head motor power represented by motor amps

2. To combine these results with the results of measured geological paramters obtained from the rock testing program to develop relationship between geological parameters and machine performance.

7.4 Strip Charts Analysis

7.4.1 Description of Strip Chart Recordings

Figure 60 shows a typical example of actual recording performed by the strip-chart recorders. The blue trace represents the motor amp. The motor Amps varied from 0 when the motors where shut down, to 32 amps when they were running under no load to a maximum allowable 335 amps. This covers the entire range of performance of the 420-hp electrical motors powering the cutterhead. The total installed cutterhead power was 3,360 hp provided by 8 motors. The strip chart recorder was set to plot Amps within the range of 0 to 500 amps, covering the operational range of the motors. The propel pressure (red trace) was also monitored to measure the machine applied thrust. The transducers were initially set up on the lower hydraulic rams. The range of pressure recorded was between 0 to 4000 psi. This was a combination of the cutterhead thrust and the pressure applied in the lower rams for steering and to prevent the head from diving.

This setting was later modified to monitor the average pressure applied to all the rams for propelling the head. Thus, the effect of differential pressure on the rams in the crown and invert was taken out. The data recorder was therefore set for measuring pressure from 0 to 5,000 psi at the beginning and from 0 to 2,500 psi and 0 to 3,000 after modification for electricians and office charts, respectively. The propel pressure ranged between 0 to a maximum of 2,000 psi with the average operating range of about 1,700 psi. The stroke indicator (green trace) was set up to read from 0 to 100 inches of stroke. The actual range of stroke was within 0-60 inches or 5 ft of advance per push. During the course of the project, several strip chart-recording speeds were used, including 50, 60, 100, 120, and 300 mm/hr.

The strip charts selected for the analysis correspond to the pushes at the coring locations. The coring locations as mentioned earlier were 250 ft apart and related pushes

were identified from the date and tunnel stations bored per day. The selected parts of strip charts consist of the push including the ring number on the coring location in addition to 4 pushes before and 4 pushes after the coring location. This means that a total of 9 pushes (centered on the coring locations) were selected out of each roll of strip charts. These sections were color copied and used for the current analysis.
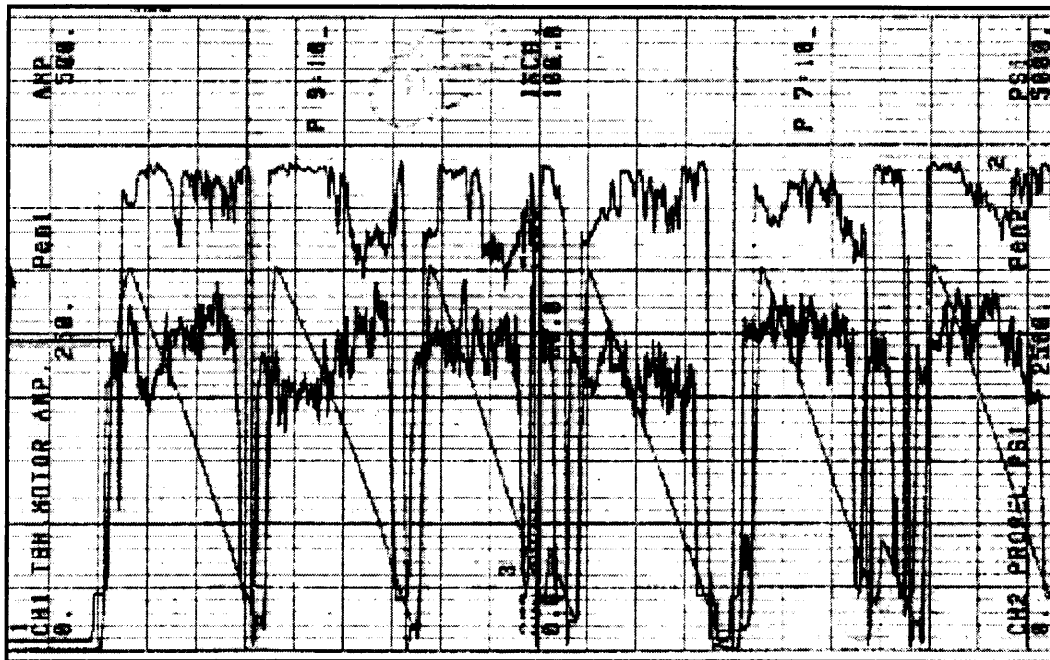
Figure 60: Sample of the strip chart recordings used in the analysis.

7.4.2 Scanning

The strip charts were first scanned to create an electronic image of the file for digitization and further analysis. The scanner used was capable of scanning images with a resolution of 300 data points per inch of spacing (dpi). This was far more than the resolution needed to follow the traces since the typical width of a trace was over 0.05 inch. This means that the width of the trace was approximately 15 pixels. The image

files were saved in the TIF format. A uniform procedure was used for naming the files. Each file was assigned a name including [RN]#. TIF, where RN stands for 4 digit ring number. The # represents the number of the chart for the selected section since in some coring locations, more than one sheet image was selected to include 9 pushes. The image files were then fed into the digitizing program.

7.4.3 Digitizing

The program used for digitizing of the strip charts was Nueralog® developed by Neuralog Inc. of Houston Texas. This program is window based and was specifically developed for application in the oil well drilling industry and well logging analysis. It is a widely used program for the digitizing and analysis of the logging data for identification of geological formations or features recorded by geophysical logging devices. The program is designed to accept the image files in a variety of formats. The image files of the strip chart recordings were loaded into the Neuralog program for further analysis and digitizing of the traces. Figure 61 shows a typical image file in the Neuralog program.

The file was digitized by first defining the coordinate system on the image file. This was accomplished by selecting the origin and entering coordinates of a few points in the image file into the program. Any skew of the axis was taken out by choosing a non-rectangular set of axis. The horizontal axis or the time axis was identified and a set of vertical lines was drawn at equal distance to mark the time increments. The units used for digitizing the strip charts were the 10-mm (centimeter) marks on the charts. The vertical full scales were input separately for individual traces, 500 for Amps, 2,500 for propel pressure (or 5,000 in some cases as previously discussed), and 100 for stroke. This information was taken out of each individual chart and was read off the status reports printed on the charts in special time increments.
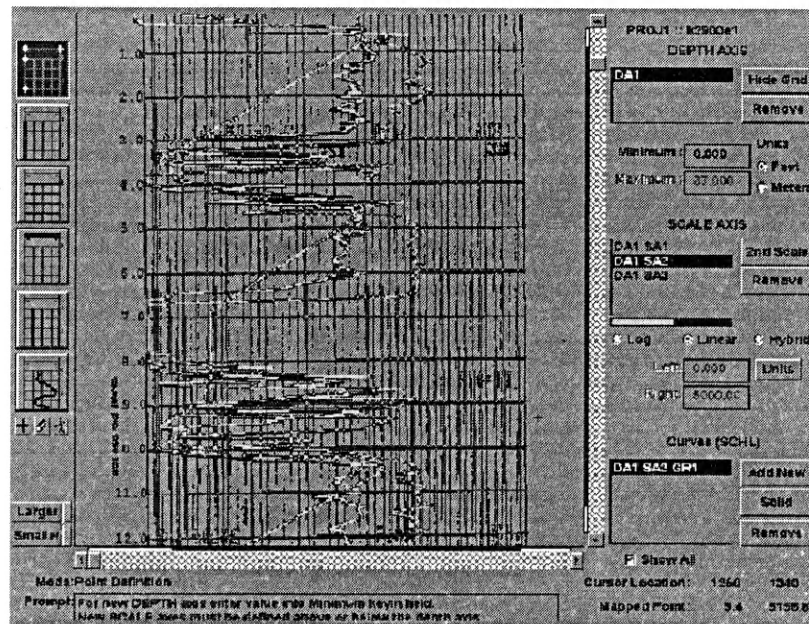
Figure 61: View of the Neuralog program.

The digitizing process in the program needed a path to be defined for each trace. The path can be defined by the user manually or set by the program automatically. For the automatic mode, the user has to place the pointer on the trace and allow the program to follow the trace. The path is shown on the screen in an active color and is superimposed on the trace. Since the strip charts contained cross over of several traces and also the strip chart grids, at times manual control became necessary when logic of the program would stop the automatic tracing at points where it could not identify the direction to continue. This was typically encountered when several traces/grids crossed. In addition, the width of the traces was such that sometimes it was difficult for the program to follow the trace. In such cases, the operator was required to redirect the program. Moreover, in cases when the path deviated from the trace, the operator corrected the path to ensure its match to the actual trace.

After defining the path, the Neuralog program created a file containing the digitized data for all the traces. This file was in ASCII format with the file extension of "LAS", which contained all the detailed information about the image file and the digitizing. The user defined the resolution used to record the data. For this project, the resolution of 100 points per unit was selected which corresponded to 10 points per mm or roughly 250 points per inch (dpi). The digitized information included the X and Y coordinates of the points on the defined path. The program selected these points by determining the Y values for the points on the path corresponding to the X values at the increments conforming to the selected resolution.

The Neuralog program was also capable of reloading the LAS files and superimposing the paths on the traces of the image file. This feature was very useful to verify the accuracy of the digitizing. Also, the same feature was used to modify the path and over-write the LAS file if any mismatch was found. These files can be read and exchanged with a variety of programs such as spreadsheets, editors, etc.

Prior to the analysis of the strip charts and digitizing the records, several trials were made to verify the capabilities of the program and select the right resolution for saving digitized data. These trials included feeding the plot of a sine wave into the system and reproducing the plot from the digitized data. This test proved the ability of the program to reproduce the simple trace. Using the actual strip charts followed the trials. In this case, the program required some corrections and redirections by the operator; nonetheless it did produce a nearly perfect reconstructed image of all the traces. Several different resolutions were tried for storing the digitized information. This included 0.1, 0.01, and 0.001 resolution (or 10, 100, 1000 points per unit or centimeter) per trace. The regenerated graphs showed that beyond 0.01 resolution or 100 point there was no major difference or improvements in the resolution of the recreated graph compared to the original chart recordings, nor did it affect the result of analysis and averaging. As noted

earlier, even at 0.01 resolution the digitization would supercede the resolution of the scanning and the line thickness of the traces.

7.4.4 Data Reduction

To reduce the digitized data from the strip charts, a special program was developed in the EXCEL spreadsheet environment. This program was written to allow for importing of data from multiple files, combining the charts into one file, and allowing the operator to select and specify individual pushes. The bulk of the calculations were performed by a Macro and use of a floating template to temporarily import the data, organize it and create a variety of graphical presentations.

The program was starting with a dialog box to receive the general information about the strip chart from the user. As shown in Figure 62, the ring number, number of pushes, and the type of the chart constitute the first information entered into the program. Also, the number of pages of strip charts (or the number of files) corresponds to that station was provided to the program. The program then proceeds with opening the appropriate data files and importing the digitized data into a template. In the template file, the data files were merged to create a consistent set of data for graphical representation of the strip charts. The offset of the pens were accounted for by shifting the respective columns to ensure that the three indicators were synchronized and correspond to the correct time. The thrust offset was matched by moving the data by the offset difference whish was 0.2 units.

After combining the respective data files a subsequent dialog box allowed the user to select an individual push and the corresponding parameters to each push, as shown in Figure 63. The start and the end of the push were noted and some approximate values were entered into the program to allow the graphs to re-scale the chart and zoom in on the selected push. Depending on the type of push, the user selected a single or multiple

Figure 62: Dialog box for strip chart information.

Figure 63: Dialog box for individual shove information.

windows for data analysis. This allowed for analysis of data within one or two windows. The single window was suitable for the shoves without any interruption. Multiple windows were used for the shoves with interruption, such as re-grip or machine shut down. After the data was entered, the program activated the graph and zoomed in on the part of the chart predefined by the user as the start and the end of that particular push.

Figure 64 shows an example of the graph containing the selected part of a strip chart for data analysis with a single window. Figure 65 shows an example of a push with multiple windows for data reduction and analysis. The purpose was to allow the user to identify and select parts of the push for more detailed analysis.
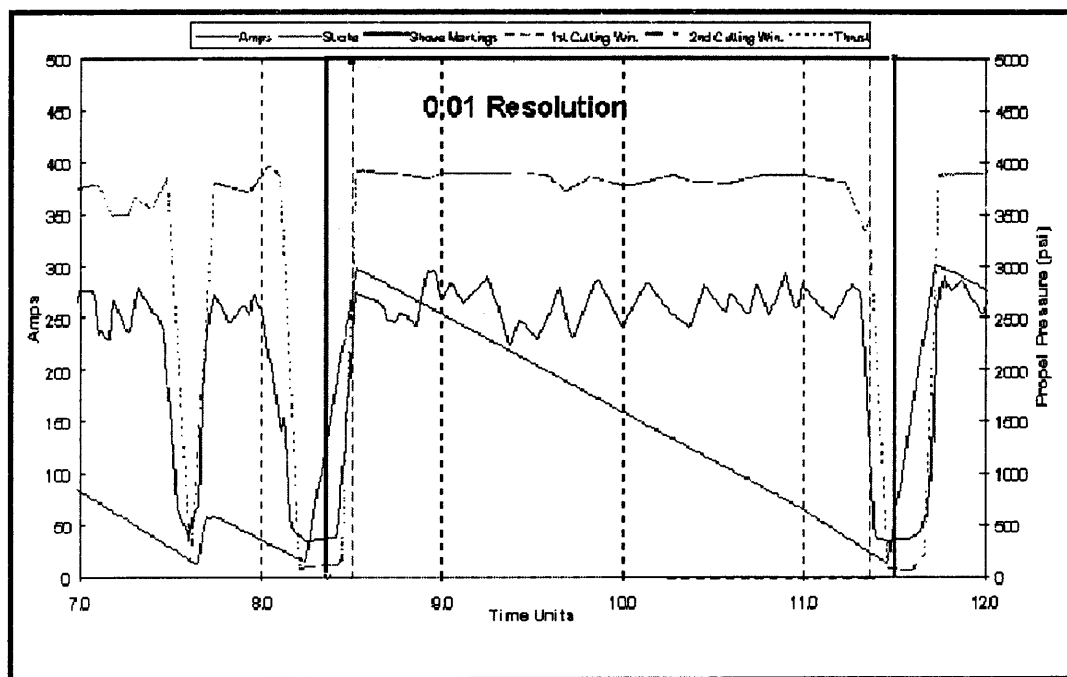
Figure 64: Example of the data analysis graph reproduced from strip charts with single window.
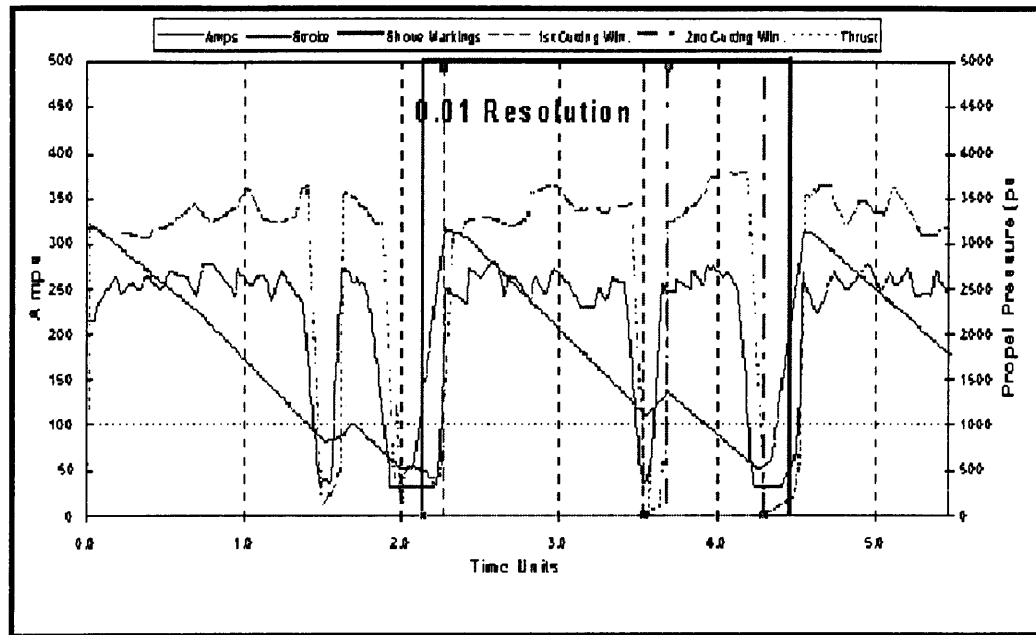
Figure 65: Example of the data analysis graph reproduced from strip charts with multiple data analysis windows.

Use of this feature provided for selection of any segment for the analysis and elimination of the sections when the machine was not mining. If for any reason, user needed to change the limits, shift the graph or work on other segments, change the classification, etc. the dialog box for that push was repeated and proper adjustments were made.

The template file was simultaneously updated to include the selected windows and the points were passed on to the main program for further analysis. The analysis of this strip charts results are discussed as follows

7.5 Strip Chart Results

The machine performance was analyzed by reducing the strip chart obtained from the machine. The analysis started with the calculation of amps, propel pressure and the

rate of penetration for the pressures above 500 psi as the machine clock was set to start as the propel pressures exceeding this pressure. Thus, the program followed the propel pressure within the specified PUSH START and PUSH STOP and averaged the amps, propel pressures and rate of penetration while the pressure remained above 500 psi. When pressure droped below 500 psi, it continued to follow the pressure until pressure rised above the 500 psi when it resumed averaging. This process continued until the stop point was reached where the program terminated the calculations and returned the calculated averages to the summary sheet.

The program subsequently performed the analysis of data for the actual mining cycle. This routine used the defined windows to determine the average amps and propel pressure. In addition, it calculated the ROP within the specified windows. If the multiple window option was used, then the program calculated the averages for each window independently. It subsequently determined the span for each window and performed weighted average for each parameter. Those weighted averages were the machine's operational parameters while fully engaging in rock. All of the resultant information is then transferred to a data summary sheet.

7.5.1 Cutter Load from Propel Pressure

The mentioned earlier, the propel pressure is the parameter measured from the strip charts to determine the gross thrust of the machine. The cutter load can be calculate from propel pressure in following steps.

First the gross thrust of the machine was calculated from propel pressure by multiplying by cylinder area and average cylinder skew. Second step was to determine the drag of the machine as discussed in previous section. Subtracting drag from gross thrust gave the resultant cutterhead thrust or net. The resultant cutter head thrust was then divided by equivalent number of cutters to calculate the cutter load on each cutter.

The equivalent number of cutters was the number of cutters which at loads equal to face cutters would require same net thrust. This was due to the fact that gage cutters carry less load since they are installed at an angle fron the tunnel axis. The average propel pressure measured from strip charts was 1967 psi. The equation used to determine the cutter load from propel is as follows:

$$CL = \frac{(PAc) - D}{N}$$

Where:

CL = Cutter load

P = Propel pressure

A = Cylinder area

c = Correction factor for skew

D = Drag

N = Equivalent number of cutters

Using the above relationship and the 1,967 psi average propel pressure measured from the strip chart analysis, the average cutter load was calculated at 48.9 kips, as shown in Table 13.

7.5.2 Rate of Penetration

The average penetration rate from the strip chart analysis was measured to be 8.8 ft /hr. The measured rate of penetration was further used to estimate the cutter load from amps as discussed in the following section.

Average propel pressure (net of tow load)	1967 psi
Thrust cylinder area (10 cylinders)	1539 sq. in
Average lattice cylinder skew	0.90
Gross thrust	2,723 kips
Using thrust	2,700 kips
Less Drag	500 kips
Cutter head thrust	2,200 kips
Equivalent number of cutters	45
Load on each cutter	48.9 kips

Table 13: Calculation of Cutter load using Propel pressure.

7.5.3 Cutter Load from Motor Amps

The calculation of TBM cutter loads from amp measurements is based on the proven relationship between the cutter rolling and normal or thrust forces. This relationship commonly known as the rolling or cutting coefficient is a function of cutter size, geometry and depth of penetration and is independent of the rock type being cut. Extensive laboratory and field studies of rock fragmentation with disc cutters have established reliable equations for determining the rolling coefficient based on these parameters. Once this ratio is determined for a given rate of penetration, calculation of average cutter load from drive motor Amps is a simple mathematical process, as follows: First, the motor amps increased as the cutters engaged the rock face. The measured motor amps at full cutterhead engagement and number of motors running was converted

to cutterhead power by using manufacturer supplied motor power curves. The cutterhead torque was then calculated from the power, by utilizing the cutterhead rotational speed (rpm). The number of cutters and the average moment arm was taken into account to arrive at an average value of rolling force on the cutters, measured torque (Figure 66). The calculated rolling force was then divided by the rolling coefficient to determine average thrust force acting on the cutter. These calculations could be performed manually or more precisely with a computer program containing the actual cutter layout pattern modeled to allow calculation of exact loading on individual TBM cutters. The flow chart of this method to calculate cutter load from strip chart is shown in Figure 67.
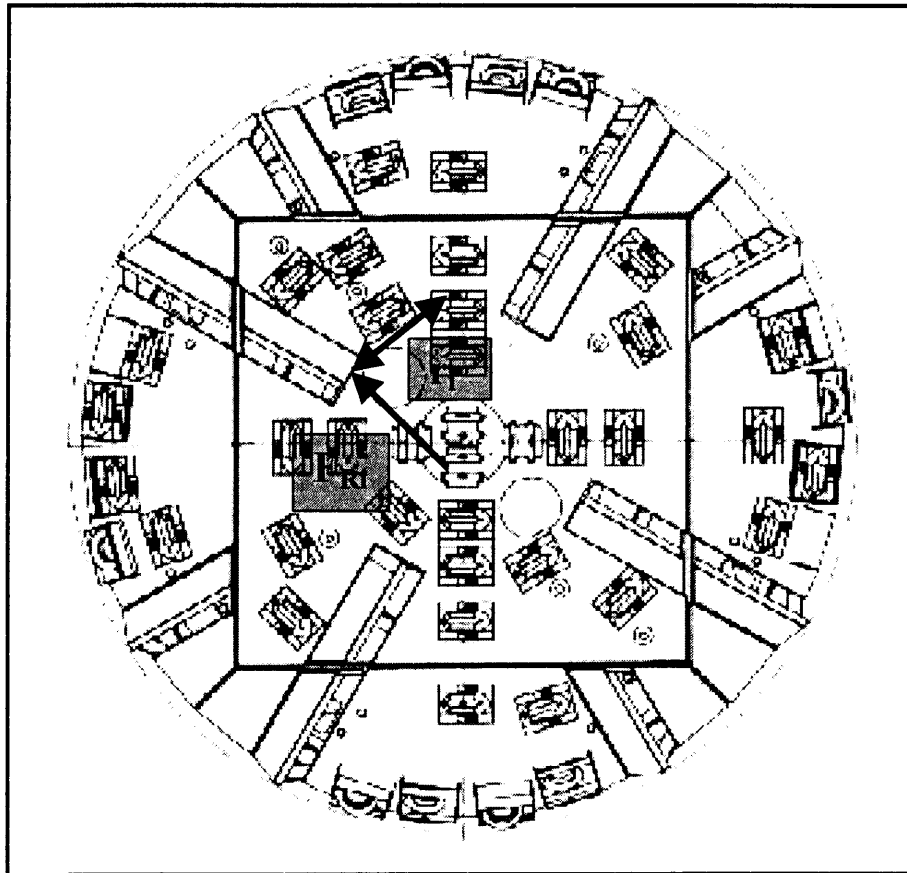
Figure 66: Estimation of Cutter head Torque
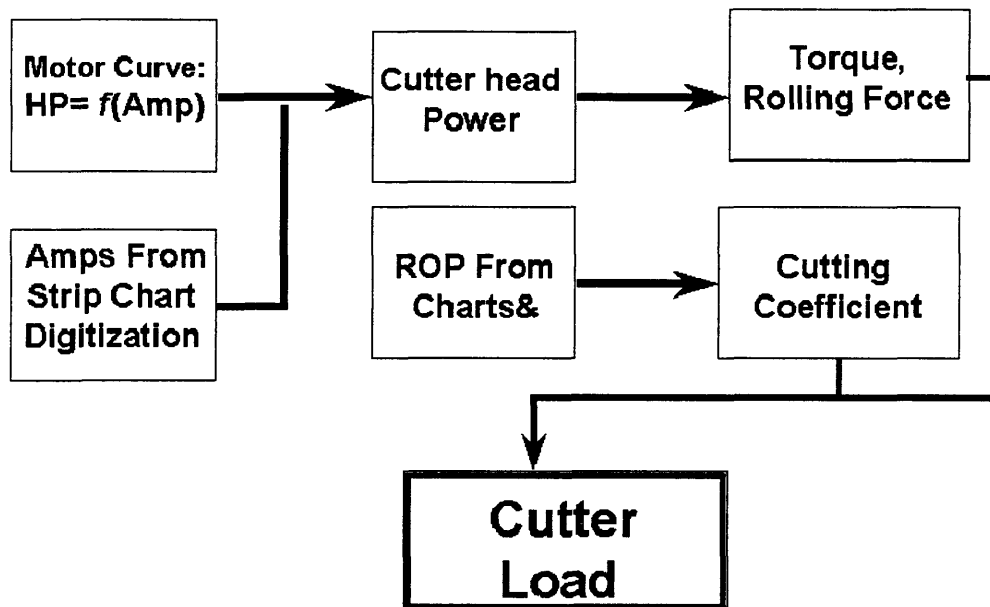
Figure 67: The flow chart showing method to calculate cutter load from amps.

The data summary sheets contained formulae to calculate the cutter-loads from Amp measurements and the ROP. This was accomplished by using the formulae explained in the following. The power output of each motor as a function of the amp draw was determined from the bench tests performed by the motor manufacturer. Therefore, the power consumption of the machine was calculated from the number of motors and the average Amps recorded. Using the appropriate rolling (or cutting) coefficient, as shown below then this equation was used to calculate the actual average cutter load:

$$CutterLoad \approx \frac{Amps}{R.C.} \approx \frac{Amps}{ROP}$$

Where:

Amps = Average Amps from the charts

R.C. = Rolling coefficient on the cutters = $\dfrac{F_R}{F_N}$

ROP = Rate of penetration (for that push)

F_N = Normal force or cutter load

F_R = Rolling force

The Rolling coefficient was calculated as follows:

$$R.C. = Tan\left(0.45\,\phi\right)$$

Where:

Φ = Angle of theoretical contact area = $\cos^{-1}\left(\dfrac{Dc-2p}{Dc}\right)$

The cutter head available horsepower was calculated from the measured Amps of the motors by using the results of bench tests performed by the motor manufacturer. In bench tests, the motor Amps for a single unit were measured versus the output power, while measuring the rotational speed (RPM) and the torque on the motor monitor the power. The test for the motors used on the Boston Outfall TBM was performed by manufacturer (P&H) and the results can be found in Figure 68, where the motor power as a function of the motor Amps was plotted. This figure includes the data points and the resultant best-fit line to the data. The equation used for calculation of the power from the motor Amps is as follows:

$$HP_{motor} = 8.02 + 1.375\ Amps$$

The cutter head power requirement is expressed by:

$$HP_{cн} = \frac{Torque \times RPM}{\eta}, \quad \text{or}$$

$$Torque = \frac{HP_{TBM} \times \eta}{RPM}$$

Where:

HP_{CH} = Total cutter head power = $HP_{motors} * N_{motors}$

N_{motors} = Number of motors running

η= Efficiency of the system (combined mechanical and electrical efficiency) @ 90 % for TBM

RPM = Cutter head RPM, 6.4 for Boston Outfall Tunnel TBM.
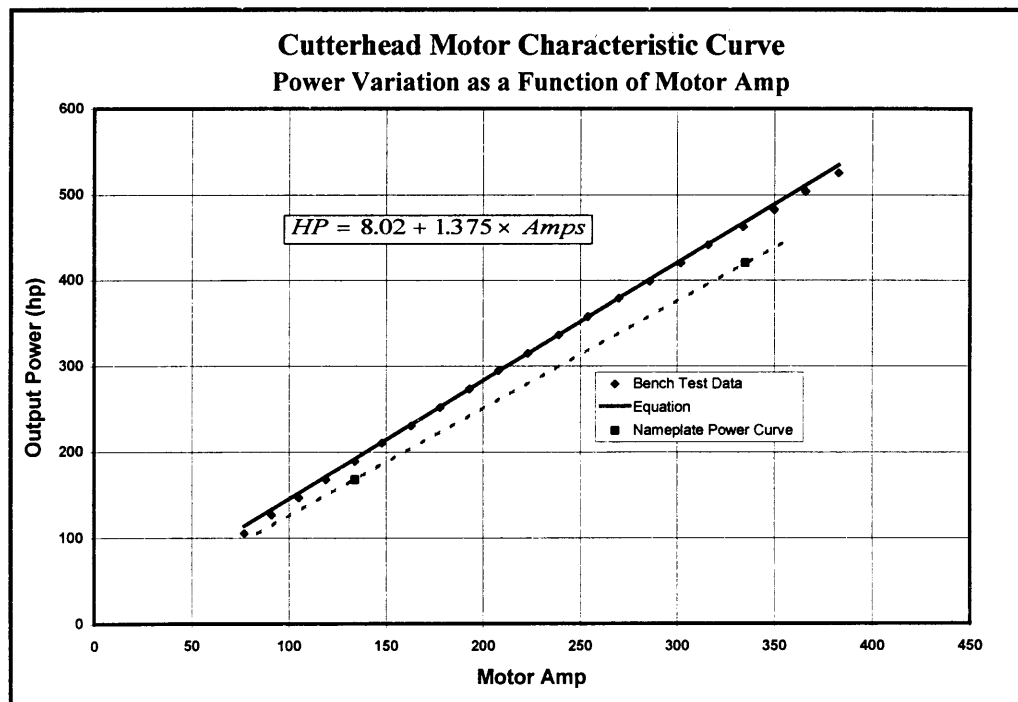
Figure 68: Result of bench tests of the TBM motors by manufacturer.

Torque = Cutter head torque requirements, also calculated as

$$Torque = \sum R_i . F_{R_i} = N . F_N . R_c \, 0.27 \, D_{TBM}$$

Where:

R_i = Radius of individual cutters

F_{Ri} = Rolling force for individual cutters

F_N = Average cutter load (or Normal Force)

N = Number of cutters on the head

R_c = Rolling coefficient

D_{TBM} = TBM diameter

As can be seen, the cutter head torque is related to the average cutter load through the rolling (cutting) coefficient. The average moment arm for the Boston TBM was calculated at 54 % of the radius ($0.27*D_{TBM}$). The above formula was simplified by using the actual TBM diameter of 26.5 ft. and the RPM of 6.4. Also, the number of cutters used in the formula was 45 at full average load, which was equivalent to 50 cutters installed on the machine at various loads in different positions. The simplified formula then becomes:

$$Torque = 328.22 . F_N . R_c$$

or

$$Torque = 328.22 . F_N . R_c = 738 . HP_{TBM}$$

Solving this equation for F_N yields:

$$F_N = 2.25 \, \frac{HP_{TBM}}{R_C}$$

Using the number of motor running, and replacing HP by its equivalent from the Amp formula, the final equation relating the average cutter load to the motor Amps was derived as follows:

$$F_N = (3.1.N_{motors}) \frac{Amps + 5.83}{R_C}$$

The additional information used in the calculation of the cutter load included the number of motors running and the Amp offset. The number of motors operating during each push was extracted from the shift reports and entered into the data summary sheets. The calculated cutter loads were then adjusted proportionally to the number of motors. In addition, the Amp offset, which was the position of the Amp recording pen from the horizontal chart axis (or zero line), was determined for each push from the strip charts. This number gives the reading of the Amp channel while motors were shut down. The Amp readings for each push were then adjusted for the measured value of Amp offset. Finally, the calculated Amp values from the strip charts were adjusted to account for the signal losses in the data transmission line as calibrated and measured by field-testing.

The values of losses in Amp data used in the current analysis were 12% until first 3.8 miles of the tunnel and 18% thereafter based on actual field tests. The difference (12 to 18 percent) was due to the addition of an Opt-link repeater in the data transmission system around that location. Hence, an adjustment of 12% or 18% was made to the Amp values read from the charts depending on the station number.

The available charts for all coring stations were analyzed to develop an overall summary of information. For each coring location, the results were analyzed to arrive at the machine operating parameters at that station.

7.6 Summary of Strip Chart Analysis

The parameters pertaining to machine performance during the course of mining the Boston Outfall tunnel at the coring locations were obtained from the summary of the strip chart Amps analysis. Table 14 presents the summary of the results obtained from strip-chart analysis showing the measured average values for amps, penetration rate, and propel pressure. The summary of average cutter loads calculated from propel pressure and motor amps are shown in Table 15.

Average measured Amps	259 amps
Average measured Propel pressure	1967 psi
Average measured Penetration rate	8.8 ft/hr

Table 14: Summary of the Results of Operating Parameters.

Parameter	Cutter Load
Propel Pressure	48.9 kips/cutter
Motor Amps	47.2 kips/cutter

Table 15: Summary of Cutter Load from Operating Parameters

Based on the findings of this unprecedented effort to analyze and evaluate the TBM performance and operational parameters, the following conclusions can be drawn regarding the operation and cutter loading of the Boston Outfall Tunnel TBM:

1. The average cutter load was calculated around 48,900 lbs. using the propel pressure and drag measurements.

2. The average cutter load was calculated at about 47,200 lbs. using the amp measurements

3. The machine-clock rate of penetration was found to average 8.8 ft/hr based on the analysis of strip-chart recordings.

In addition this analysis generated a sizable database of machine performance and operational parameters for further studies and correlation with geological data. The measured values of amp, propel pressure, and rate of penetration yielded the corresponding values of cutter load at coring locations. Thesr parameters were in turn used to determine the normalized values of thrust/penetration or penetration index to be used in subsequent analysis for evaluation of impact of variation of geological parameters on rock boreability and machines ability to achieve certain rate of penetration under given operational conditions.

8. MODEL RESULTS WITH ROCK MASS BOREABILITY INDEX

8.1 Introduction

As discussed earlier, the current study is an attempt to include the rock mass properties in the existing CSM predictor model to improve its accuracy in predicting the performance of tunnel boring machines in joint rock mass. To verify the validity of developed index, the extensive field and laboratory data collected from the Boston Outfall Tunnel, including unconfined compressive strength, indirect tensile strength, modulus of elasticity, Poisson's ratio, as well as the rock mass properties such as rock quality designation, joint spacing and conditions, obtained from geologist log and geotechnical data report (GDR) were utilized. This was accomplished through the use of the size reduction factor as explained in previous chapter.

8.2 Establishing the Database

The extensive field and laboratory testing presented in previous chapters was used to establish a database of rock properties as shown in appendix D. The field observed properties include measured size reduction factor.

Figures 69 to 73 shows histograms of the variables in the database. These histograms show the range of each parameter presently contained in the database. Figure 69 shows the range of elasticity modulus, which is between 5,000 to 13,000 ksi. Figure 70 shows the range of Poisson's ratio, which is between 0.05 to 0.35. Figure 71 shows the range of size reduction factor, which is between 0.02 to 0.25. Figure 72 shows the range of unconfined compressive strength of rock influencing the size reduction factor, which was between 2,000 to 30,000 psi. Figure 73 shows the other parameter, RQD of rock, which influence the size reduction factor ranging between 30 to 100 percent.
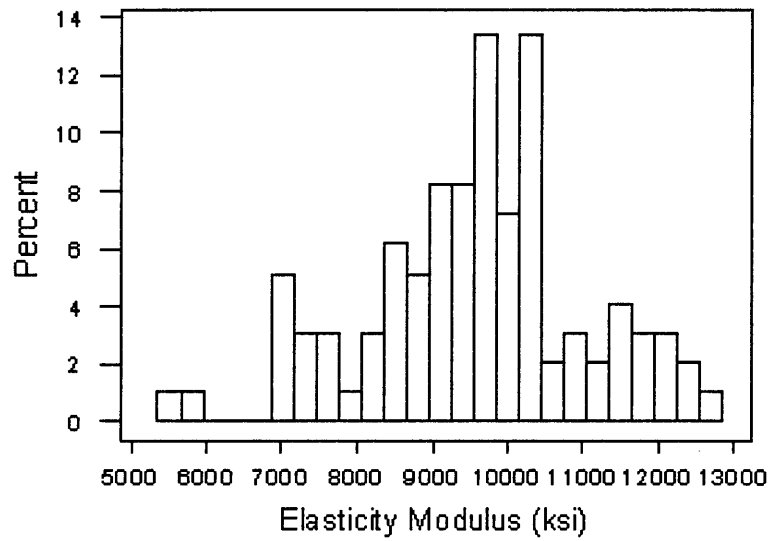
Figure 69: Histogram of Elasticity Modulus variation in the database.
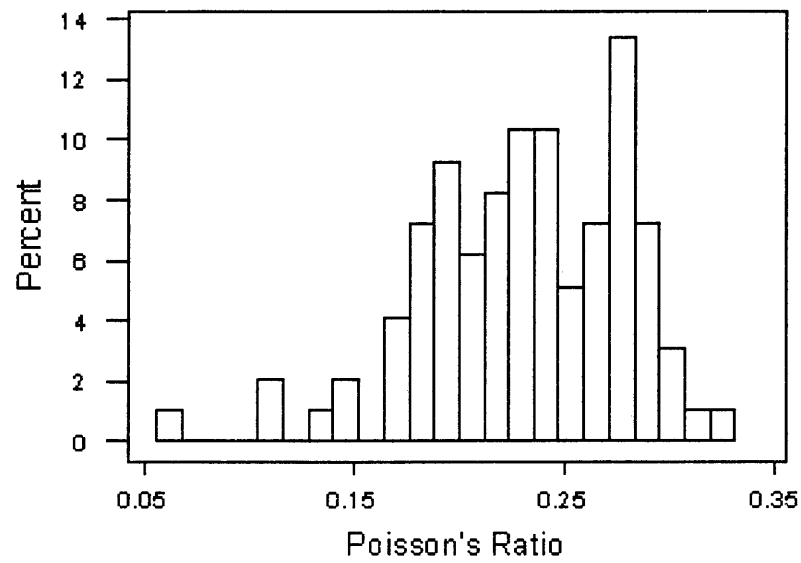
Figure 70: Histogram of Poisson's Ratio varaition in the database.
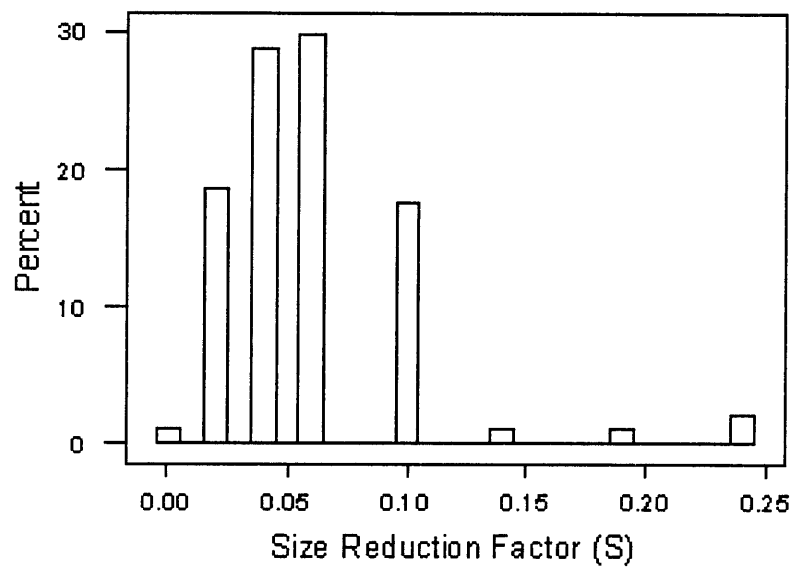
Figure 71: Histogram of Size Reduction Factor variation in the database.
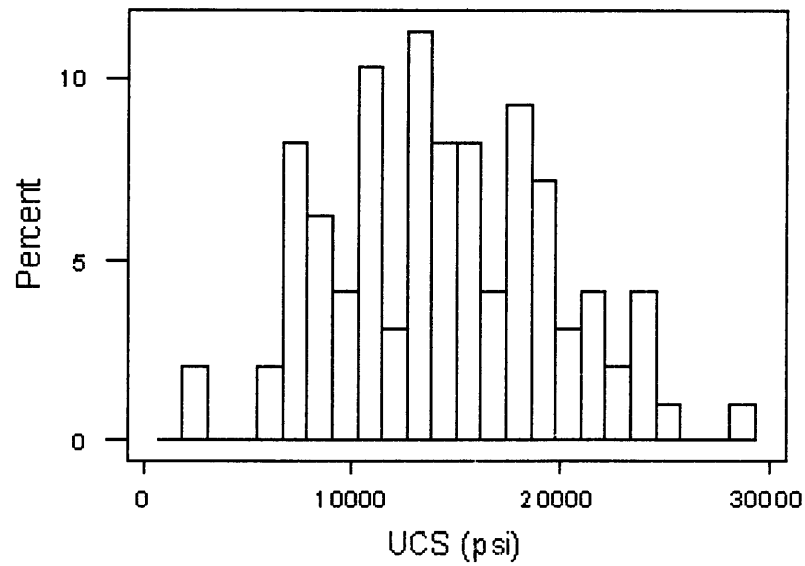
Figure 72: Histogram of unconfined compressive strength variation in the database.
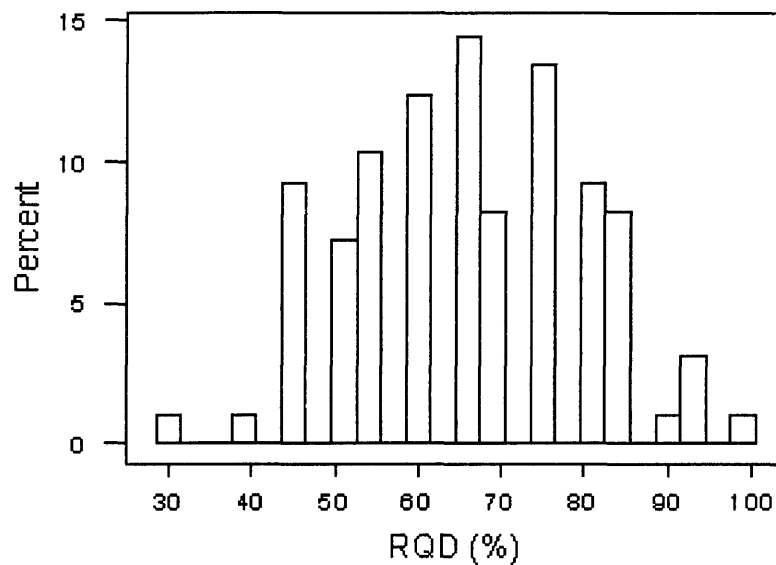
Figure 73: Histogram of rock quality designation variation in the database.

8.3 Regression Analysis Results

A relationship between the parameters was developed by establishing a database of independent parameters including modulus of elasticity, Poisson's ratio and size reduction factor obtained from geological strength index. The database shown in appendix D was arranged in sets of columns. By performing multiple regression analysis by using professional version of MINITAB®, which is a commercial software package for standard statistical analysis, to find the best combination of parameters to develop a relationship between the rock mass strength and the input parameters. Normally, the relationships found between the parameters are linear functions. In other words, the program finds the best-fit regression between the parameters in a linear combination.

The nonlinear relation between the parameters was determined by defining a new set of variables in the program from the original set of variables. For example a new variable Y was defined as a function of original parameter X $(Y = f(X))$. This method

variable Y was defined as a function of original parameter X (Y= f (X)). This method was used for logarithmic analysis and using the logarithm of each parameter in a linear relationship. This allowed obtaining the correct power for each parameter using the characteristics of logarithmic function.

The simplest formula includes the linear relationship between the parameters. The equation gives erroneous answers when the value of the parameters is near boundary conditions (i.e. if any of the parameters are set to zero). The linear relationship for the rock strength index estimation is as follows: (Correlation Coefficient R^2 = 73%)

$$RMBI = 8659 + 0.338E + 11614S - 434v$$

Where:

$RMBI$ = Rock Mass Boreability Index (psi)

E = Elasticity Modulus (ksi)

S = Size Reduction Factor

v = Poisson's Ratio

Also, when the analysis is performed in a logarithmic scale, the relationships includes power functions instead of linear functions. The result of the logarithmic analysis produces the following equation: (Correlation Coefficient R^2 = 85%)

$$RMBI = 26900 * E^{0.097} * S^{0.444} * v^{-0.066}$$

As can be seen, this equation offers a better correlation with the data. The negative power for Poisson's ratio shows that this parameter is inversely proportional to the strength of rock mass. Figures 74 and 75 shows the plot of measured versus estimated rock mass boreability index.
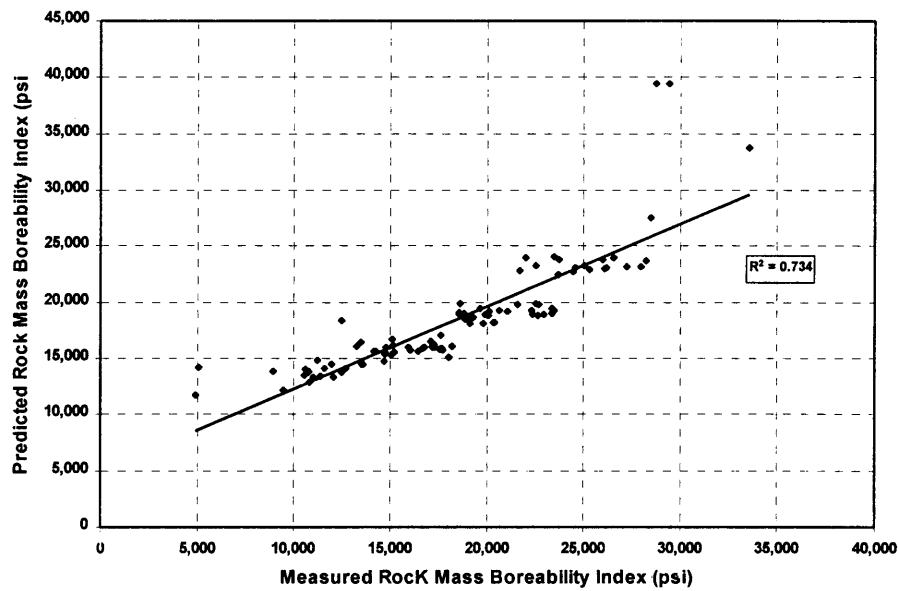
Figure 74: Comparison between the measured and predicted rock mass boreability for the linear equation.
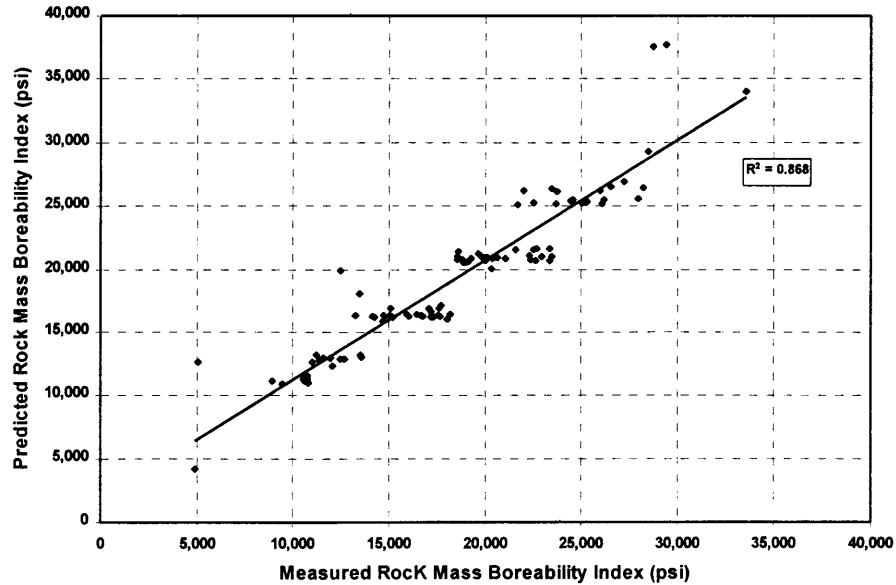
Figure 75: Comparison between the measured and predicted rock mass boreability index for the logarithmic (power function) equation.

8.4 Prediction of TBM Performance with New Model

The results for new model show that the machine should have achieved an average penetration of 11.85 ft/hr with average intact rock strength of 19,000 psi. with cutter load of 50,000 lbs. per cutter. The results of detailed machine analysis show using amp cutter load of 47,200 lbs. per cutter, instead of cutter load from propel during excavation, penetration rate of 11.2 ft/hr must have been achieved. The same analysis showed that machine's field penetration rate was 8.8 ft/hr. There is a difference of around 2.5 ft/hr between predicted and achieved penetration rate, which is due to rock mass behavior encountered during the excavation.

The parameters to evaluate the GSI and the value of GSI to determine size reduction factor S are given in Table 16 along with values and RMR for each category for this project. The minimum and maximum values for size reduction factor for this projects are 0.015 and 0.236 respectively.

The calculated size reduction factor (S) from average values of each parameter, average measured values for modulus of elasticity (E) and Poisson's ratio (v) are given in Table 17.

Item	Value	Rating
Uniaxial Compressive Strength (UCS)	19,000 psi	12
Rock Quality Designation (RQD)	75%	13
Joint Spacing (Js)	1 to 3 ft	20
Joint Conditions (Jc)	Slightly Rough	20
Water Condition	Dry	10
GSI		75

Table 16: Rock parameters for rock mass analysis

Parameters	Values
Modulus of Elasticity (E)	9,501 ksi
Poisson's Ratio (v)	0.23
SizeReduction Factor (S)	0.062

Table 17: Summary of Average Parameters for Rock Mass Strength

Substituting the values of parameters for Boston Outfall Tunnel project in the developed rock mass boreability index (RMBI) equation, the rock mass strength calculated is about 21,000 psi.

Comparison of the results for the machine is given in Table 18. As can be seen, using the new rock mass boreability index, the predicted rate of penetration differs only 4% from actual measurements as compared to a 25 percent difference obtained with only intact rock properties of the rock.

Prediction with Rock Mass Boreability Index (RMBI)	Actual Performance
RMSI = 21,000 psi	
CL = 47,200 lbs.	CL = 47,200 lbs
ROP = 9.15 ft/hr	ROP = 8.8 ft/ hr

Table 18: Summary of Predicted and Actual Performance.

The most important parameter in this new strength formula is size reduction factor as it includes the intact rock strength and other rock mass characteristics parameters including rock quality, joint spacing and joint conditions. This factor has a large impact on the performance of the machine. Due to this reason, this factor has to be estimated for each project to determine the strength of rock that will be encountered during excavation.

Other parameters, such as the modulus of elasticity and Poisson's ratio for the RMBI can be estimated from historical data of a particular rock type. These parameters can also be obtained from laboratory testing along with the unconfined compressive strength using ASTM standards.

8.5 Effect of Rock Mass Boreability Index Parameters on TBM Performance

The existing model has been discussed in previous chapters. The new developed index was incorporated into the CSM model to include the rock mass properties in place of intact rock strength of the rock. To study the behavior of parameters that drive the new rock mass boreability index equation effect on the performance of the tunnel boring machine, three cases were studied and parameters selected with following assumptions.

a) For the first case, rock conditions were such that the reduction factor and Poisson's ratio were held constant and the modulus of elasticity of the rocks was varied.

b) For the second case, the modulus of elasticity and reduction factor were held constant and the value of Poisson's ratio was varied.

c) In the third case the elasticity modulus and Poisson's ratio were held constant and the reduction factor in the rocks was varied.

The results of this study are presented in the following section.

8.5.1 Effect of Modulus of Elasticity

This is the analysis of the first case, in which the reduction factor and Poisson's ratio were held constant throughout the analysis of the Boston machine performance. The values for elasticity modulus were varied from 5,000 ksi to 15,000 ksi. Figure 76 shows the relationship between modulus of elasticity and Penetration Index. The analysis reveals that the rock modulus of elasticity has little effect on the rate of penetration when rock encounters numerous joints. Elasticity modulus effects the rate of penetration as the rock size reduction factor value reach around 0.1. As the value of the reduction factor increases, the effect of increase in an elasticity modulus on the penetration rate increases.
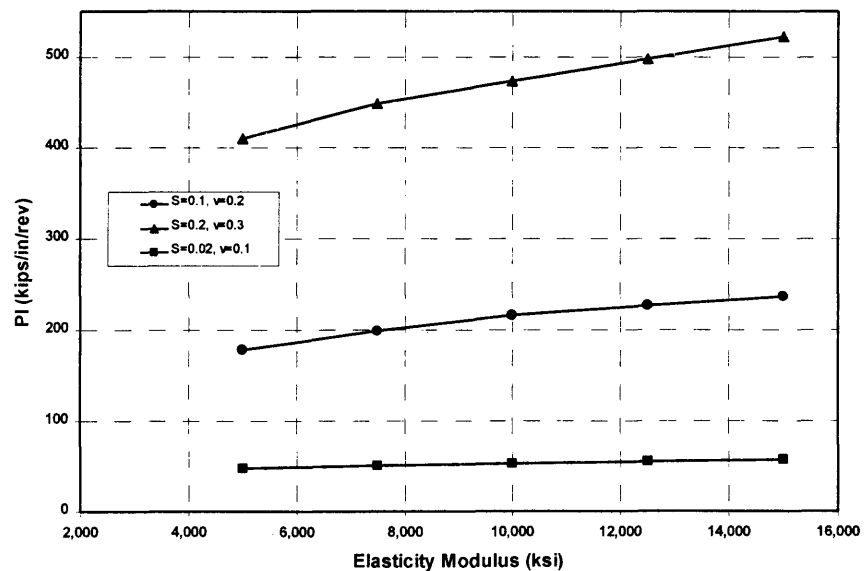
Figure 76: Effect of Elasticicty Modulus on Penetration Index.

8.5.2 Effect of Poisson's Ratio

In the second case, both the modulus of elasticity and the size reduction factor were kept constant throughout the analysis of the machine performance. The values for Poisson's ratio were varied from 0.1 to 0.3. Figure 77 shows the relationship between

Poisson's ratio and Penetration Index. The analysis shows that Poisson's ratio has small effect on penetration index at lower values of S and elastic modulus.

8.5.3 Effect of Reduction Factor

This is the analysis of third case, where the modulus of elasticity and Poisson's ratio were kept constant throughout the analysis of the machine performance. The values for reduction factor was varied from 0.02 to 0.2. Figure 78 shows the relationship between size reduction factor and Penetration Index. The analysis demonstrates that the effect of size reduction factor on the penetration index is significantly greater than that of the other parameters. It indicates that the machine performance depends strongly upon the joint conditions and spacing in foliated rock mass. The increase in this factor decreases the rate of penetration.
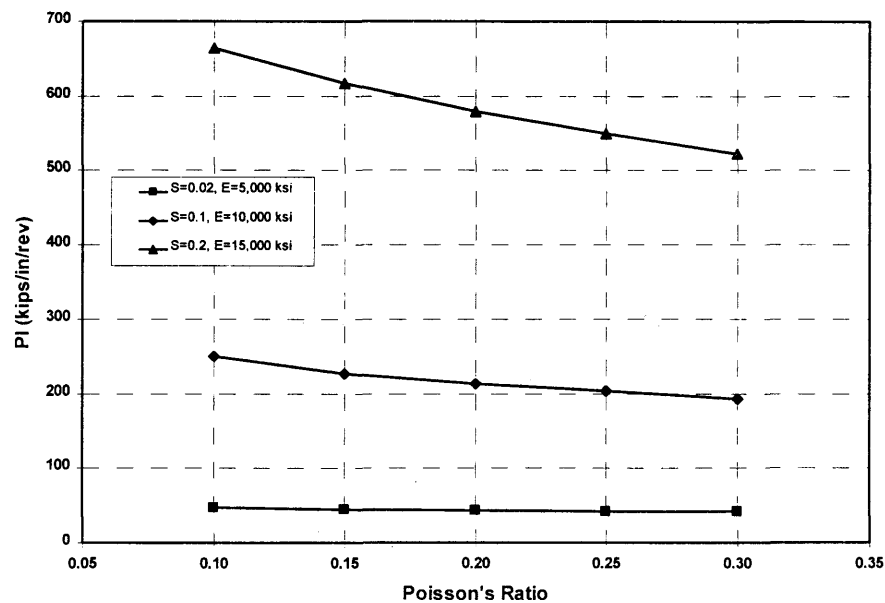
Figure 77: Effect of Poisson's Ratio on the Penetration Index.
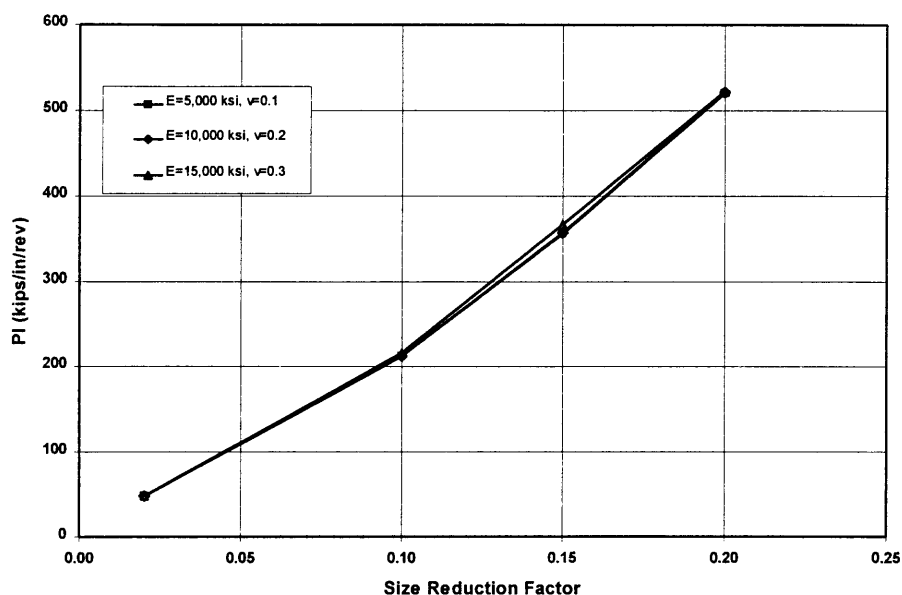
Figure 78: Effect of Size Reduction Factor on Penetration Index.

8.6 Model Calibration and Limitation

The developed model was used for estimation of the penetration rate in a tunneling project for the purpose of comparison and validation. The case presented in this section included an actual TBM project in Boston, Massachusetts. The reason for selection of this particular tunneling project was mainly due to the fact that it was the only project where rock samples were obtained systematically at certain intervals and the data were available on the foliated and jointed rock formations encountered in the tunnel. In addition, the machine operational parameters were monitored for a large portion of the tunnel and were available at the same locations as where the core samples were obtained. This allowed for a detailed evaluation of the performance of this TBM with the influence of joints / foliation and rock mass properties on the machine performance. In addition, the geology of the tunnel and the machine performance were studied in detail and reliable field performance data was collected for the project. The developed new index and the model was used to

predict the performance of the TBM and compare it with the actual field performance achieved by the machine for validation of the developed rock mass index concept.

However, in spite of the good correlation obtained in the comparison between the predicted and actual performance, it has to be noted that this model has been validated with only a single project. Therefore, the developed index should be applied with care until the results of some future tunneling projects in jointed / foliated rock formations are compared to further calibrate and adjust the model.

9. SUGGESTED GEOTECHNICAL INVESTIGATION AND ROCK TESTING FOR TBM PROJECTS

The complexity of rock mass as an engineering material and the limited possibility to actually observe the material represents great challenges in investigation and testing, interpretation of results and characterization of the site. The geological conditions may vary within wide limits. Each site has its own characteristics, and hence there is no standard investigation procedure, which can meet the requirements in all the cases. With this background in this chapter specific physical property tests and field investigation will be described briefly which are required to evaluate rock mass boreability index, then the additional tests that can be utilized in difficult conditions. The equation for rock mass boreability index is as follows:

$$RMBI = 26900 E^{0.097} S^{0.444} v^{-0.066} .$$

Where:

RMBI = Rock Mass Boreability Index

E = Modulus of Elasticity

v = Poisson's Ratio

S = Size Reduction Factor

The information required for this index can be collected from three sources.

a) Field Coring Program

b) Geological Mapping

c) Laboratory Rock Testing

Field Coring Program:

Core drilling is among the routine methods for subsurface exploration. Most commonly, NX size core drill is used. The drilling often has multiple purposes, of which the following are the most important:

- To obtain information on the rock type boundaries and degree of weathering.

- To obtain information on the orientation and character of discontinuities.

- To provide samples for the laboratory analysis.

The drilling should be carried out with the prime purpose to investigate major discontinuity zones crucial for the performance of the tunnel boring machines. The drill hole gives valuable information about the rock mass. A parameter linked to core drilling is the RQD, representing the total length of recovered core pieces greater than or equal to 4 inches divided by the length of the attempted core run expressed in percentage. Also if the cores are oriented with respect to tunnel axis, the information about joint orientation, joint spacing and joint conditions can be obtained.

Apart from drill hole testing, the recent development in this involves directional drilling makes it possible to core drill in any direction. Using this technique it is possible to gather information along the alignment of a planned tunnel. Technically this method is capable of producing longer and more deviated holes.

Geological Mapping:

Geological mapping is carried out by using simple tools like a geologist hammer, a compass with clinometer and thus is relatively inexpensive. Basic information on the rock can be obtained by observing and hitting the rock with the hammer.

Joint mapping is one of the key issues of fieldwork, since it is important parameter for the index. The information on the degree of jointing, joint orientation as well as joint conditions is crucial input data for performance prediction of tunnel boring machines.

Geological mapping to a great extent is a matter of experience, and the methodology and techniques have not changed much over the last few years. The major development has been the introduction of Global Positioning System (GPS) instruments, making positioning more reliable and enhancing the quality of mapping results in difficult locations.

Laboratory Rock Testing:

In all tunnels boring machine performance prediction efforts, careful sampling is a key factor. If the test samples are not representative of the actual field conditions, the predicted performance will not be very reliable. The laboratory testing for performance prediction of TBMs can be divided in two parts:

i)   Physical Property tests

ii)   Cutting tests

The physical property tests that are required to determine the rock mass boreability index are as follows:

Uniaxial Compressive Strength Test:

The most common test performed on rock for initial investigation is the uniaxial or unconfined compressive strength test commonly known as UCS. This is the ASTM standard test, performed on intact cylindrical rock specimen. The load is applied on the specimen with constant rate until the sample fails in compression. The values stated in pounds per square inches are regarded as standard units. The strength of the tested

specimen is considered to be a true representative of the intact rock if the specimen does not fail along the existing weakness present in the rock; in other words, it is not structural failure. This test alone is not enough to evaluate the strength of rock as different rock types of the same compressive strength behave differently due other material properties. Therefore further testing is recommended to determine other related rock properties which effect the performance of mechanical excavators like TBM, Road header and others. This is also a parameter required to calculate the size reduction factor for the rock strength index equation.

Elastic Constants:

The important rock elastic constants are modulus of elasticity (E) and Poisson's ratio (v). These two parameters characterize the rock toughness and brittleness. These parameters can be measured in two modes, static and dynamic.

The static determination of elastic constants related to unconfined compressive strength require strain gauges to be attached to the rock samples when the sample is subjected to load.

The dynamic elastic constants are determined by pulse velocities of compression waves and shear waves in the rock. This method is valid for wave velocity measurements in both an-isotropic and isotropic rocks although the velocities obtained in grossly an-isotropic rocks may be influenced by such factors as direction, travel distance, and diameter of transducers. The ultrasonic or dynamic elastic constants are calculated from the measured wave velocities and the bulk density.

It is important to exercise care in core drilling, sawing, grinding and lapping the test specimen to minimize the mechanical damage caused by stress and heat. Liquids other than water are prevented from contacting the specimen, except that necessary as a

coupling medium between specimen and transducer during the test. The surface area under each transducer should be sufficiently planed.

Tensile Strength Test:

Tensile strength of rock determines boreability of rock. The higher the tensile strength of rock, the more difficult it is to bore through the rock as it takes high energy to chip. By definition the tensile strength is obtained by the direct uniaxial test. This means instead of compressing the cylindrical specimen, it is pulled with some method until it fails in tension. This tensile test is difficult and expensive for routine applications. The splitting tensile commonly known as the indirect tensile test appears to offer a desirable alternative, because it is much simpler and inexpensive. The strength results from an indirect tensile test are determined by testing the rock by diametrical line compression of a disk till it fails. If the rock has directional properties due to foliation or other discontinuities, it is recommended that the disk obtained from the core should be oriented during testing to obtain the effect of anistropic condition on the rock strength. This test is an essential parameter for existing and newly developed models for performance prediction of tunnel boring machines.

Additional Testing:

Following are some additional tests that can provide more information about the behavior of rock to be expected during underground construction with mechanical excavators.

Indentation or Punch Penetration Test:

The punch test is a reliable means of evaluating rock toughness and brittleness. A standard conical indentor is pressed into a rock sample cast into a steel ring to provide confinement during this test. The load and displacement of the indentor is recorded with

a computer system. The particular shape and slope of the load-penetration curve provides a reliable basis for estimating the excavating ability of the rock in the form of energy needed for efficient chipping.

Abrasivity Test:

The Cerchar test provides a reliable measure of rock abrasivity for cutter wear estimation. The test is performed by scratching a freshly broken rock surface with a sharp pin of heat-treated alloy steel as shown in Figure 79. The Cerchar Abrasivity Index (CAI) is calculated as the average diameter of the abraded tip of the steel pin after recommended distances travel across the rock surface. The test can be performed on irregular rock pieces.

The CAI value is related directly to cutter life in the field. The CAI values for various rock types are listed in Table 19.
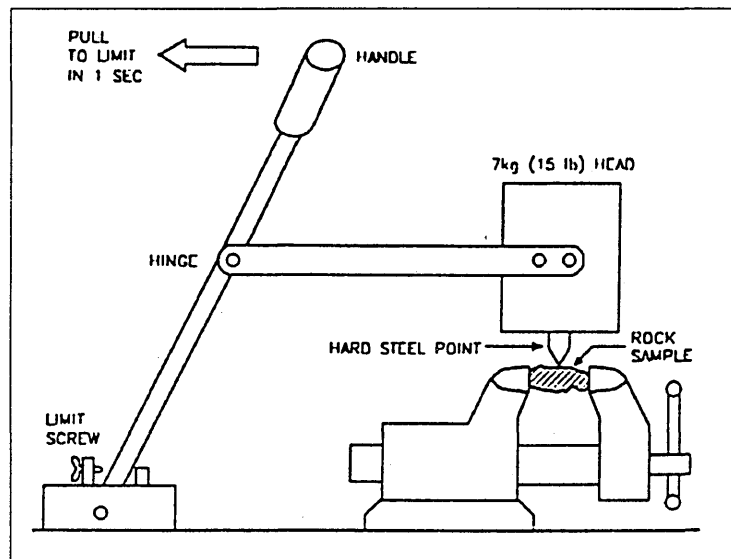
Figure 79: Schematic drawing of Cerchar test apparatus.

ROCK NAME	CAI	COMMENT
Sandstone	0.3	Fontenelle
Shale	0.9	Rochester, New York
Shale	1.1	Cleveland, Ohio
Dolomitic limestone	1.1 to 1.5	Chicago, Illinois
Sandstone	1.3	Navajo
Phyllite	1.3	Norway
Micaschist	2.2	Washington D.C.
Andesite	2.3	Buckskin tunnel
Quartz diorite	3.2	Norway
Red sandstone	3.6	Kentucky
Amphibolite	3.6	Norway, 14% quartz
Gabbro	3.7	0% quartz
Amphibolite	4.0	8% quartz
Öjeby granite	4.0	Sweden, 30% quartz
Gneiss	4.1	Atlanta, Georgia
Quartzitic gneiss	4.3	40% quartz
Quartzite	4.3	East Africa
Gneiss	4.4	Norway, 18% quartz
Gneiss	4.4	Norway, 27% quartz
Sandstone	4.7	Kentucky
Quartzitic gneiss	4.8	Norway
Granitic gneiss	4.8	Norway, 38% quartz
Granite	4.8	Atlanta, Georgia
Micaschist	5.3	New York
Granitic gneiss	5.3	13% quartz
Quartzite	5.9	Norway

Table 19: Measured values of CAI for some rock types.

Petrographic Analysis:

A reliable determination of mineral content, and detail study of rock texture can be obtained by thin section analysis. A thin section analysis is a study of a specially prepared transparent section of the rock under a microscope. For TBM projects, the following characteristics are usually observed with this analysis:

1. Type and content of hard minerals

2. Grain orientation, size, shape and directional properties

3. Grain interlocking

4. Unusual microscopic features

All these characteristics affect the boring ability of machine in the rock. In particular grain interlocking significantly increases the difficulty of boring.

Point Load Test:

The point load test is mean to obtain a reasonable estimate of uniaxial compressive strength of the rock. In this test a piece of core is loaded across its diameter between two hardened steel points. The load required to break a rock core under point load conditions is many times less than the load required for failure of a specimen subjected to uniaxial compressive stress, the point load equipment is light and is ideal for use in the field during logging of the core.

Moh's Hardness:

This test determines the relative hardness of the rock. The hardness of the rock is obtained by scratching the mineral of known hardness from Moh's hardness scale to the

surface of the rock to determine if it is harder or softer than the mineral of known hardness.

Laboratory Cutting Tests:

The punch test or the petrographic analysis can identify the existence of unusual behavior of rock. When this condition exists, the laboratory-cutting test can provide more accurate data on the cut-ability of the particular rock formation. The most common test in this respect is the linear cutting test, which is routinely performed by several institutions around the world including the Colorado School of Mines.

In the linear cutting test, the rock sample is cast with concrete in a heavy steel box to provide the necessary confinement. A servo controlled hydraulic actuator forces the sample under the cutter at preset penetration and spacing as shown in Figure 80. Thus, various combinations of penetration and spacing can be tested with this apparatus to evaluate the conditions which produces the largest volume of rock chips using the least amount of cutting energy.

This test uses full size cutters and is capable of generating the full range of cutter loads and penetrations experienced in field boring. As a result, the test results can be directly applied to field performance prediction since no scaling of results is needed. This test has been used extensively over the last 20 years and has proven highly reliable for accurately predicting field TBM performance.

The cuttings generated from linear cutting tests can be used to determine chip size distributions to evaluate their use as tunnel invert backfill or as road base material.

Rotary cutting test can be performed on a 2-meter diameter computer-controlled rotary cutting machine available at Colorado School of Mines and shown in Figure 81.
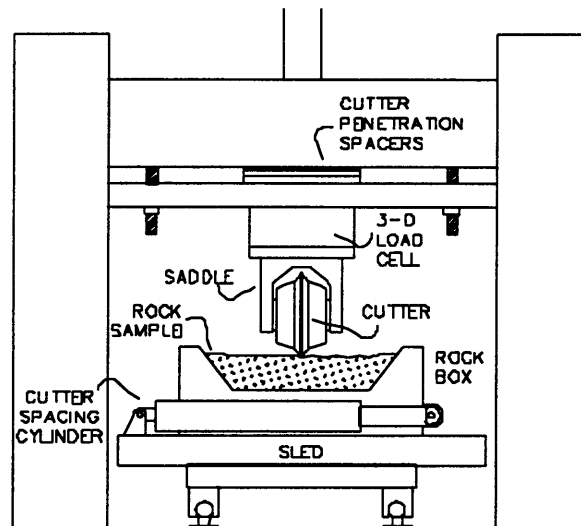
Figure 80: Schematic drawing of Linear Cutting Machine used by CSM
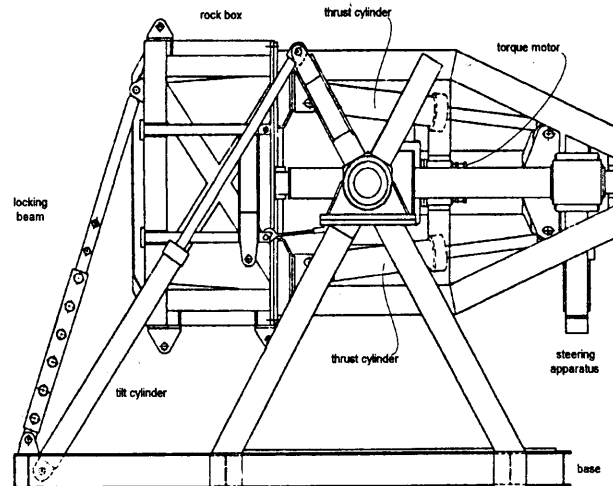
Figure 81: Schematic drawing for Rotary Cutting Machine at CSM

This test fixture allows the testing of new cutterhead designs to evaluate different cutter types, spacing, rpm, thrust and input power under field simulated conditions.

10. CONCLUSIONS

An extensive field and laboratory-testing program was performed to develop a database of TBM performance in various rock conditions. This database was used to derive a rock mass boreability index to reflect the influence of geological factors in the existing CSM predictor model and to allow for more accurate performance prediction for tunnel boring machines in jointed and / or foliated rock formations.

This study comprised three major phases. The first phase involved a literature study to identify the parameters that can characterize the strength of rock from a boreability viewpoint. The second phase was the collection of the data from a tunneling project in Boston to evaluate the effects of rock mass characteristics on machine performance. This included extensive field and laboratory testing to establish a database of machine performance as a function of intact rock and rock mass properties. This information was subsequently applied towards development of an equation for a new rock mass boreability index to be used for boreability evaluations. The third phase of the study dealt with the comparison of the actual and the predicted machine performance using the newly developed model and the evaluation of the effect of rock mass boreability index parameters on the performance of the machine.

A database of TBM field performance was developed to allow for the study of the impact of rock mass properties on the machine rate of penetration. This database included intact rock and rock mass properties, as well as machine operational parameters at fixed intervals through the 10 mile long tunnel to represent a systematic sampling of these parameters along the tunnel. To develop this database, an extensive laboratory testing program was conducted. This included the sampling of rock at every 250-ft along the tunnel and measuring the physical properties of the intact rock. This was coupled

with the analysis of machine operational parameters at the same locations. In addition, the pre-construction geologic data together with logging of the cores taken along the tunnel were analyzed to develop the required information about rock mass characteristics.

The findings of this study can be summarized as follows:

1. The systematic sampling of rock along the tunnel clearly showed that the intact rock properties and strength of rock mass varies from location to location for the same rock type. This impacted the machine performance along the tunnel even under constant machine operational parameters.

2. The analysis of the measured physical properties of the intact rock showed that the structural failures must be excluded from the test data when performing TBM boreability assessment.

3. The test results showed that the Argillite encountered in the tunnel exhibited strong directional properties which caused about a 40 percent increase in the indirect tensile strength when measured perpendicular to foliation.

4. In order to determine the average cutter load for performance prediction purposes, a set of thrust-penetration tests were conducted to measure the thrust loss due to TBM friction. The analysis of the test results showed about an average cutter load of 48 kips during boring.

5. An alternative method was developed to determine the average cutter load from motor amp measurements. The analysis of this data also showed that the machine was operated at average cutter loads of 47 kips or higher throughout the tunnel.

6. A Rock Mass Boreability index (RMBI) was developed to more accurately reflect the effects of geologic features on TBM performance. The new index

was then incorporated into the existing CSM predictor model with the purpose of improving the accuracy of TBM performance predictions in jointed / foliated rock formations.

7. The most important factor in the developed RMBI is the size reduction factor S, which is based on unconfined compressive strength, RQD, joint spacing and conditions. This factor is determined from Geological Strength Index (GSI) which was introduced by Hoek to represent the strength of rock mass in the design of underground structures.

8. The foliation effects in the model are accounted for by the rock tensile strength. It is of crucial importance that in foliated rock, the indirect tensile measurements are performed in the same direction as the machine advance with respect to foliation.

9. The modulus of elasticity and the Poisson's ratio are also included in the developed RMBI to provide a measure of rock brittleness / plasticity from a boreability viewpoint.

10. A very close correlation was obtained between the actual machine performance and that predicted using the developed rock mass boreability index.

11. RECOMMENDATIONS

Based on the findings and conclusions of this thesis, the following areas are recommended for future studies. The recommendations are made in three categories; first, the pre-bid geotechnical investigation, second, collecting the data during construction, third further studies of the developed index.

a) The recommendations for pre-bid investigation:

Since preliminary investigations typically consist of a limited number of boreholes, it is recommended that future projects should consider the following:

1. To the extent possible the exploration boreholes should be spread more or less evenly along the proposed tunnel alignment.

2. The results of the physical property testing should be carefully screened to exclude structural failures for boreability evaluation.

3. The testing program should include special provisions to identify any directional properties of rock and its potential impact on machine performance.

4. If access to the underground location is feasible or if the same formation has unweathered outcrop, consideration should be given to performing laboratory cutting tests.

5. The geological data, such as RQD, joint orientation, joint spacing and any existing foliation should be recorded from each hole.

b) Recommendations for collecting data during construction:

1. Continues recording TBM operational data should be carried out in future projects. This should include power, thrust, torque and the penetration rate. This information can be used in future studies to improve the accuracy of predictor models.

2. Together with recording the machine performance, cores should be retrieved in the tunnel to establish a database of rock properties actually encountered.

c) Recommendations for further development of the rock mass boreability index:

1. The TBM database used for the model calibration needs to be expanded to include more data from other projects with a more extensive variety of rock types and rock mass features.

2. Using the expanded database and frequently updating it with new project information, the effects of rock mass properties on machine performance can be further studied. This should also include other rock mass boreability parameters such as brittleness / porosity, etc. in the developed model for more accurate estimation of machine penetration rate in various rock formations.

12.REFERENCES AND SELECTED BIBLIOGRAPHY

Aeberli U. and Wanner H. "On the influence of geologic conditions at the application or tunnel boring machines". In *Proc. 3rd Int. Congr. Int. Assoc. Eng. Geol.,* Madrid, section III, vol.2, pp.7-14 (1978).

Aziz N,I., Schmidt L.C., 1992, "Rock Cutting Study Using Linear Elastic Fracture Mechanics". Engineering Fracture Mechanics, Vol. 41, No. 5, pp 771-778.

Bamford W. E. " Rock Toughness Index For Excavatability Assessment". In Proc. IX Australian Tunneling Conference, Sydney, Australia, August 1996.

Bamford W. F. "Rock test indices are being successfully correlated with tunnel boring machine performance". In *Proc. 5th Australian Tunnelling Conference,* Melbourne, vol.2, pp.19-22. (1984).

Barosh, Patrick, 1984, "Regional Geology and Tectonic History of Southeastern New England", Geology of the Coastal Lowlands Boston, MA to Kennebunk, ME, Hanson, L.S. ed., NEIGC Guidebook, Dept. of Geology, Salem State College, Salem, MA.

Barton, N.R. and Bandis, S.C. 1982. "Effects of block size on the shear behaviour of jointed rock" *23rd US. symp. on rock mechanics,* Berkeley, 739-760.

Barton, N.R and Bandis, S.C. 1990. "Review of predictive capabilities of JRC-JCS model in engineering practice" In *Rock joints, proc. mt. symp. on rock joints.,* Norway, (eds N. Barton and 0. Stephansson), 603-610. Rotterdasn:

Barton, N.R. and Chouhey, V.1977. "The shear strength of *rock* joints in theory and practice". *Rock Meck* 10 (1-2), 1-54.

Barton, N.R., Lien, R. and Lunde, J. 1974. "Engineering classification of rock masses for the design of tunnel support". *Rock Mech.* 6(4), 189-239.

Barton, N., Lien, R. and Lunde, J. 1980. "Application of the Q-system in design decisions". In *Subsurface space,* (ed. M. Bergman) 2, *553-561.* New York: Pergamon.

Bieniawski, ZT. 1967. "Mechanism of brittle fracture of rock", parts I, II and III. *Int. J. Rock Mech. Min. Sc & Geomech. Abstr.* 4(4), 395430.

Bieniawski, Z.T. 1973. "Engineering classification of jointed rock masses". *Trans S. Afr. Inst Civ. Engrs 15,335-344.*

Bieniawski, ZT. 1974. "Geomechanics classification of rock masses and its application in tunnelling". In *Advances in rock mechanics* 2 (A), 27-32. Washington, D.C.: Nat. Acad. Sci.

Bieniawski, Z.T. 1976. "Rock mass classification in rock engineering". In *Exploration for rock engineering, proc. of the symp.,* (ed. Z.T. Bieniawski) 1, 97-106. Cape Town: Balltem

Bieniawski, Z.T. 1979. "The geomechanics classification in rock engineering application" *Proc. 4th. congr., Int. Soc. Rock Mech.,* Montreux 2, 41-48.

Bieniawski, Z,T. 1989. *"Engineering rock mass classafications".* New York: Wiley.

Benjumea R. , Sikarskie D.L., 1969, "A note on the penetration of a rigid wedge into a nonisotropic brittle material". Int. J. of Rock Mech. &Mining Sci. & Geomech. Abs., Vol.6. 1969.

Billings, M. P., 1976, "Geology of the Boston Basin", Studies in New England Geology, Lyons, P. C., and Brownlow, A. H., eds., Geological Society America, Memoir 146, pp. 5-30.

Brady B. H. *G.* and Brown E. T. "Rock Mechanics for Underground Mining" Allen and Unwin, London *(1985).*

Brook N. "Estimating the triaxial strength of rocks". *Int. J. Rock Mech. Min. Sci. & Geomech. Abstr.* 16, 261-264 (1979).

Brown E. T. (Ed.) International Society for Rock Mechanics (ISRM) "Rock Characterization and Monitoring Methods". Pergamon Press, Oxford (1981).

Bruland, A., Dahlo T., Nilsen, B., 1995, "Tunneling Performance Estimation Based on Drillability Testing". Proceedings of 8th International Congress of Rock Mechanics, Sep. 25-30, Tokyo, Japan.

Cook, N.G.W. , Hood M., Tsai F. 1984, " Observation of crack growth in hard rock loaded by an indentor". Int. J. of Rock Mech. &Mining Sci. & Geomech. V.21, No.2, pp97-107.

Deere D. V. and Miller R. P. "Engineering Classification and Index Properties for Intact Rock". University of Illinois, US Department of Commerce, National Technical Information Service (1966).

Deering K., Dollinger G. L., Kranter D. and Roby J. A. "Development and performance of large diameter cutters for use on high performance TBMs". In *Proc. Rapid Excavation and Tunneling Conference,* Seattle, WA, pp.807-814 (1991).

Dollinger 0. L. "Hard rock tunnel boring: A summary of recent developments". In *Proc. Rapid Excavation and Tunneling Conference,* Chicago, IL, pp. 89-105. (1983).

Farmer I. W. and Glossop N. H. "Mechanics of disc cutter penetration". *Tunnels and Tunnelling* 12(6), 22-25(1980).

Geological Society Working Party Report. "The logging of rock cores for engineering purposes". Q. J. *Eng. Geol.* 3, 1-24 (1970).

Griffith, A~. 1921. "The phenomenon of rupture and flow in solids". *Phil Trans. Roy. Soc.,* London A221, 163-198.

Griffith, A.A. 1924. *"Theory* of rupture". *Proc. 1st congr. applied mechanics,* Delft, 55-63. Delft: Technische Bockhandel en Drukkerij.

Handewith, H., 1995, "Hard Rock Fracture", Hard Rock Mechanical Excavation Technology Survey communicated with EMI, CSM. June 1995.

Hatheway, Allen W. and Paris, William C., 1979, "Geologic Conditions and Considerations for Underground Construction in Rock, Boston, Massachusetts", Engineering Geology in New England, Hatheway, A. W., ed., ASCE Preprint No. 3602.

Hoek E. and Brown E. T. "Underground Excavations in Rock". Institution of Mining and Metallurgy, London (1980).

Hoek:, E. 1983. Strength of jointed rock masses, 23rd. Rankine Lecture. *G~otechnique'* 33(3), 187-223.

Hoek:, E. and Bray, L W. 1981. *Rock slope engineering.* 3rd edn. London: Instn Mm. Metall.

Hoek, E., and Brown, E.T. 1980a. *Underground excavations in rock.* London: In stn Min. Metall.

Hoek, E and Brown, E.T. 1980b. Empirical strength criterion for rock masses. *L Geotech, Engng Div., ASCE* 1O6(GT9), 1013-1035.

Hoek, E. and Brown, E.T. 1988. The Hock-Brown failure criterion - a 1988 update. In *Rock engineering for underground excavations, proc. 15th Canadian rock meck symp., (ci* J.C. Curran), 31-38. Toronto: Dept. Civ. Engineering, University *of* Toronto.

Hock, E., Wood, D. and Shah, S. 1992. A modified Hoek-Brown criterion for jointed rock *masses. Proc. rock characterization, symp. Int Soc. Rock Mech. Eurock '92, (ed.* LA. Hudson), 209-214. London: Brit. Geol. Soc.

Hoek E. "Estimating Mohr-Coulomb friction and cohesion values from the Hoek-Brown failure criterion -Technical note". *Int. J. Rock Mech. Min. Sci. & Geomech. Abstr.* 27, 227-229 (1990).

Howarth D.F., Roxborough F.F., 1982, "Some fundamental aspects of the use of disc cutters in hard-rock excavation". J. of S. African Institute of Mining and Met. Nov. 1982, pp 309- 315.

Hudson J. A. " Comprehensive Rock Engineering – Principles, Practice and Projects". Vol. 3, pp 41-85, 105-117 (1993)

Hudson J. A. " Comprehensive Rock Engineering – Principles, Practice and Projects". Vol. 4, pp 261-311 (1993)

ISRM "Suggested method for determining tensile strength of rock materials". *Int. J. Rock Mech. Min. Sci. & Geomech. Abstr.* 15, 99-103(1978).

ISRM "Suggested methods for quantitative description of discontinuities in rock masses". *Int. J. Rock Mech. Min. Sci. & Geomech. Abstr.* 15, 319-368 (1978).

Jeager, J.C., Cook, N.G.W., 1976, "Fundamentals of Rock Mechanics". Second Edition, Chapman and Hall, A Halsted Press Book., John Wiley & Sons Inc., New York.

Kaiser, P., McCreath, D., 1994, "Rock Mechanics Considerations for Drilled or Bored Excavations in Hard Rock". Tunneling and Underground Space Technology, Vol. 9, No. 4, pp 425-437, Pergaman Press, Elsevier Science Ltd.

Kaye, C. A., 1967, "Outline of Pleistocene Geology of the Boston Basin", Geology of Southeastern New England, Cameron, Barry, ed., a guidebook for field trips; 68th Annual Meeting N. E. I. G. C., Science Press, Princeton, New Jersey, pp. 46-63.

Kaye, C. A., 1980, "Bedrock Geologic Maps of the Boston North, Boston South, and Newton Quadrangles, Massachusetts", U. S. Geol. Survey Misc. Field Studies Map MF-1241, scale 1:24,000.

Kaye, C. A., 1982, "Bedrock and Quaternary Geology of the Boston Area, Massachusetts", Geological Society of America: Reviews in Engineering Geology, Vol. V., pp. 25-40.

Kaye, C. A., 1984, "Boston Basin Restudied", Geology of the Coastal Lowlands Boston, MA to Kennebunk, ME, Hanson, L. S., ed., NEIGC Guidebook, Dept. of Geology, Salem State College, Salem, MA.

Korbin G. "Tunnel Boring Machine Performance Assessment Report Metrowest Water Supply Tunnel" MWRA, Boston, November 1995

Korbin G. E. "Factors influencing the performance of full face hard rock tunnel boring machines". US Dept. of Transportation, UMTA-CA-06-0122-79-1, available from National Technical Information Service. Number PB80-12378 (1979).

Korbin G. E., 1992, " Cowles Mountain Tunnel Geotechnical Report On Differing Site Conditions", Report Prepared for Trylor Bros. Inc. Nov. 1992.

Korbin G., Ilsley R., Dollinger G. "Evaluation of KAK's Reduced Penetration Rate Claim" for Boston Harbor Outfall Tunnel, MWRA, March 1998

Korbin G., Ilsley R., Dollinger G. "Reduced Penetration Rate Claim Supplemental Report" for Boston Harbor Outfall Tunnel, MWRA, May 1998

Lindqvist P.A., 1992, "Rock fragmentation by indentation and disc cutting". Doctoral Thesis, Univ. of Lulea, Lulea, Sweden.

McFeat-Smith I. and Tarkoy P. J. "Site investigations for machine tunneling contracts". *Tunnels and Tunnelling* 12, 36-39 (1980).

Morrel, R., Larson, D., 1974, "Tunnel Boring Technology". Report of Investigation RI-7961, US Bureau of Mines.

Nelson P. N., O'Rourke T. D., Flanagan R. F., Kulhawy F. H., Ingraffea A. R. " Tunnel Boring Machine Performance Study". Final Report National Technical Information Service, UMTA Technical Assistance Program, June 1984

Nelson P. P. "Tunnel boring machine performance in sedimentary rocks". Doctoral dissertation, Dept. of Civil Engineering, Cornell University, p. 448. Ann Arbor, Michigan, USA (1983).

Nelson P. P., Ingraffea A. R. and O'Rourke T. D. "Technical Note: TBM performance prediction using rock fracture parameters". *Int. J. Rock Mech. Min. Sci. & Geomech. Abstr.* 22, 189-192 (1985).

Nelson P. P., O'Rourke T. D. and Glaser S. D. "TBM system downtime causes, frequency and duration on six tunnel projects". In *Proc. Rapid Excavation and Tunneling Conference,* New York, vol.2, pp.751-770 (1985).

Nelson, P.P., Abd Al-jalil, Y., Laughton, P.E., 1994, "Tunnel Boring Machine Project Data Bases and Construction Simulation". Report to MIT, Geotechnical Engineering Report GR94-4, Geothechnical Engineering Center, Departmenet of Civil Engineeing, The University of Texas at Austin, Dec. 1994.

Nelson, P.P., O'Rourke, 1983a, "Tunnel Boring Machine Performance in Sedimentary Rocks". Report to Goldberg-Zoino Associates of New York, P.C. by School of Civil Engineering, Cornell University, Ithaca, New York, Feb 1983.

Nelson, P.P., O'Rourke, T.D., Kulhawy F. H., 1983b, "Factors Affecting TBM Penetration Rates in Sedimentary Rocks". 24th U.S. Symposium on rock mechanics, June 1983, pp227-237.

Norwegian Institute of Technology. "Hard rock tunnel boring. Project Report 1-88" Trondheim, Norway, p 183 (1988).

Norwegian Institute of Technology. "Hard rock tunnel boring. Project Report 1-94" Trondheim, Norway, p 164 (1995).

Ozdemir L. (Ed). "Mechanical Excavation and Ground Support". Short Course, NAT Conference 1994

Ozdemir L. (Ed). "Mechanical Mining Technology". Short Course, at Colorado School of Mines, June 11, 1995

Ozdemir L. (Ed). "Mechanical Mining". Short Course, at Colorado School of Mines, March 19-21, 1997

Ozdemir L. (Ed). "Mechanical Tunneling". Short Course, at Colorado School of Mines, October 2-4, 1995

Ozdemir L. and Wang F. "Mechanical tunnel boring, prediction, and machine design". Final report by CSM to NSF, NSF/RA-790161, available from National Technical Information Service under accession number PB8O-101660, p.204. (1979).

Peng S.S., Goldsmith W., Hood M., 1989, "A force-indentation model for brittle rocks". Rock Mechanics & Rock engineering, Vol.22, pp 127-148.

Parsons, Brinkerhoff, Quade, & Douglas, 1990, "Geotechnical Design Summary Report".

Parsons, Brinkerhoff, Quade, & Douglas, 1989, "Geotechnical Interpretive Report".

Rahm, D.A., 1962, "Geology of the Main Drainage Tunnel, Boston, Massachusetts", Journal of the Boston Society of Civil Engineers, V. 49, pp. 310-368.

Reichmuth D. R. "Point-load testing of brittle materials to determine tensile strength and relative brittleness". In *Proc. 9th US Symp. Rock Mech.,* University of Colorado, pp.134-159 (1968).

Rostami J. "Development of a Force Estimation Model for Rock Fragmentation with Disc Cutters Through Theoretical Modeling and Physical Measurement Of Crushed Zone Pressure". Doctoral dissertation, Dept. of Mining Engineering, Colorado School of Mines, p. 382. Golden, Colorado, USA (1997).

Rostami J., Ozdemir L., 1993b "A new model for performance prediction of hard rock TBMs". RETC 93 Proceedings, Chapter 50, pp. 793-809, June 13-17, Boston MA.

Rostami, J. Ozdemir, L. 1993c, " Computer Modeling For Cutterhead Design and Layout Of Mechanical Excavators". Proceedings of Annual Technical Meeting of the Institute of Shaft Drilling Technology (ISDT), Las Vegas, May 3-5, 1993.

Rostami, J. Ozdemir, L. Neil, D. 1994, "Performance Prediction, A Key Issue In Mechanical Hard Rock Mining". Mining Engineering, SME, Vol. 46, No. 11, November 1994.

Rostami, J. 1991, "Design optimization, performance prediction, and the economic analysis of TBM application for the construction of proposed Yucca Mountain nuclear waste repository". Thesis # 3941, Colorado School of Mines.

Rostami, J. 1993a, "Study of the Effects of Rock Fracture Parameters on the Cutting Forces Acting on a Disc Cutter". Prepared for CVEN-6831, Intro. to Engineering Fracture Mechanics. Submitted to Dr. Victor Saouma, Dept. of Civil and Architectural Eng. Colorado Univ. at Boulder (unpublished).

Rostami, J. Ozdemir, L. 1996, "Computer Modeling of Mechanical Excavators Cutterhead". Proceedings of the World Rock boring Association 1996 Conference, "Mechanical Excavation's Future Role in Mining", Sep. 17-19, Laurentian University, Sudbury, Ontario, Canada.

Roxborough F. F. "Research in mechanical rock excavation: progress and prospects". In *Proc. Rapid Excavation and Tunneling Conference,* New York, vol.1, pp. 225-244. (1985).

Roxborough F. F. and Phillips H. R. "Rock excavation by disc cutter". *Int. J. Rock Mech. Min. Sci.& Geomech. Abstr.* 12, 361-366 (1975).

Samuel A. F. and Scow L. P. "Disc force measurements on full face tunnel boring machines". *Int. J. Rock Mech. Min. Sci. & Geomech. Abstr.* 21, 83-96 (1984).

Sanio H. P. "Prediction of the performances of disc cutters in anisotropic rock". *Int. J. Rock Mech. Min. Sci & Geomech. Abstr.* 22, 153-161 (1985).

Sato K., Gong F., Itakura K., "Prediction of disc cutter performance using a circular rock cutting rig", Proceedings 1st International Mine Mechanization and Automation symposium, June 1991, Colorado School of Mines, Golden Colorado, USA.

Sharp W. and Ozdemir L. "Computer modeling for TBM performance prediction and optimization". In *Proc. Int. Symp. Mine Mechanization and Automation,* Golden, Co, vol.1, pp.4.57-4.66. CSM and U.S. Bur. Mines (1991).

Tarkoy P. J. "Practical geotechnical and engineering properties for tunnel-boring machine performance analysis and prediction". *Transportation Research Record* 1087, Transportation Research Board, National Research Council, pp.62-78 (1987).

Tarkoy P. J. 1991, "Difficult rock comminution and associated geological conditions".

Tierney, F.L., Billings, M.P., and Cassidy, M.M., 1968, "Geology of the City Tunnel, Greater Boston, Massachusetts", Journal of Boston Society of Civil Engineers, V. 55, pp. 60-96.

University of Trondheim, 1994, "Hard Rcok Tunnel Boring". Project Report 1-94, University of Trondheim, The Norwigian Institute of Technology, Trondheim, Norway.

Wanner H. "On the influence of geologic conditions at the application of tunnel boring machines". *Bull. Int. Assoc. Eng. GeoL* 12, 21-28 (1975).

Wanner H. and Aeberli H. U. "On the influence of discontinuities at the application of tunnel boring machines".

Wanner H. and Aeberli U. "Tunnelling machine performance in jointed rock". In *Proc. Int. Cong. ISRM,* Montreaux, vol.1, pp.573-580. (1979).

APPENDIXES

APPENDIX A

Summary of Core Recovery Logging Data

Table 1 CORE SAMPLE RECOVERY SUMMARY												
Ring No.	Station No.	Date	Length Recovered	Cores Possible	Rock Type	Liner Inclination	Hole Inclination	Bedding Inclination	Dip Direction	Apparent Inclination	True Inclination	Driller
153	11095	10/02	0.30	1	Argillite	35	62	60	NNE	N75W60NE	294 34	Jim
153A	11095	10/02	1.80	8	Argillite	36	61	60	NNE	N75W60NE	295 33	Jim
201	11335	10/02	1.45	7	Argillite	35	62	70	N	EW70N	270 42	John
251	11585	10/02	0.00	0	Argillite	34	63	60	N	EW60N	270 33	John
251A	11585	10/03	0.00	0	Argillite	33	64	60	NNE	N75W60NE	293 35	John
253	11595	10/03	1.50	8	Argillite	33	64	70	N	EW70N	270 44	John
297	11815	10/03	0.80	5	Argillite	31	66	70	N	EW70N	270 46	Jim
297A	11815	10/03	1.30	7	Argillite	30	67	70	NNE	N75W70NE		Jim
299	11825	10/03	0.20	1	Argillite	32	65	65	N	EW65N	270 40	Jim
352	12090	10/04	0.70	3	Argillite	31	66	65	NE	N45W65NE	327 50	John
352A	12090	10/04	1.00	5	Argillite	34	63	65	NNE	N75W65NE	292 39	John
401	12335	10/04	0.40	1	Argillite	30	67	75	NE	N45W75NE	322 60	Jim
401A	12335	10/04	0.50	2	Argillite	30	67	60	NE	N45W60NE	329 46	Jim
403	12345	10/04	1.90	7	Argillite	30	67	50	N	EW50N	27027	Jim
449	12575	10/04	Abandoned									John
453	12595	10/05	1.00	2	Argillite	35	62	NV	NV			John
453A	12595	10/05	1.20	6	Diabase	35	62	NV	NV			John
454	12600	10/06	0.8	2	Argillite	34	63	50	N	EW50N	270 23	John
552	13090	10/05	0.80	1	Argillite	31	66	30	N	EW30N	270 06	Jim
552A	13090	10/05	1.00	4	Argillite	30	67	35	N	EW35N	270 12	Jim
600	13330	10/05	1.00	2	Argillite	33	64	50	N	EW50N	270 24	Jim
650	13580	10/06	0.00	0	Diabase	32	65	NM	NM			John
651	13585	10/10	1.45	7	Diabase	32	65	NM	NM			John
652	13590	10/06	0.50	2	Diabase	32	65	NM	NM			John
652A	13590	10/10	0.70	4	Diabase	32	65	50	NE	N45W50NE	338 36	John
698	13820	10/06	0.00	0	Argillite	30	67	NM	NM			Jim
700	13830	10/06	0.50	2	Argillite	30	67	50	N	EW50N	270 27	Jim
702	13850	10/06	1.00	5	Argillite	30	67	60	N	EW60N	270 37	Jim
702A	13850	10/10	0.50	2	Argillite	29	68	75	N	EW75N	270 53	Jim
704	13850	10/10	1.00	5	Argillite	29	68	70	N	EW70N	270 48	Jim
751	14085	10/10	1.45	8	Argillite	31	66	60	N	EW60N	270 36	John
801	14335	10/11	0.65	4	Argillite	32	65	65	N	EW65N	270 40	Jim
802	14340	10/10	0.70	3	Argillite	30	67	65	N	EW65N	270 42	Jim
802A	14340	10/10	0.75	4	Argillite	32	65	65	N	EW65N	270 40	Jim
846	14560	10/12	0.00	1	Argillite	33	64	50	N	EW50N	270 24	John
848	14570	10/11	0.60	3	Argillite	34	63	65	N	EW65N	270 40	John
848A	14570	10/12	0.00	0	Argillite	35	62	60	N	EW60N	270 35	John
850	14580	10/11	0.00	0	Argillite	34	63	60	N	EW60N	270 36	John
851	14585	10/11	0.00	0	Argillite	35	62	70	N	EW70N	270 48	John
900	14830	10/11	0.00	0	Argillite	34	63	NM	NM			Jim
901	14835	10/11	0.00	0	Argillite	33	64	NM	NM			Jim
902	14840	10/12	0.00	0	Argillite	36	61	NM	NM			John
903	14845	10/12	0.50	0	Argillite	35	62	60	N	EW60N	270 36	Jim
905	14845	10/11	0.00	0	Argillite	33	64	NV	NV			Jim
951	15085	10/12	0.80	4	Argillite	33	64	50	N	EW50N	270 24	John
951A	15085	10/13	0.60	3	Argillite	30	67	60	N	EW60N	270 37	John
999	15325	10/13	0.90	5	Argillite	35	62	80	SE	N45E80SE	225 80	Jim
1000	15330	10/12	0.80	4	Argillite	33	64	80	SE	N45E80SE	225 81	Jim
1051	15585	10/13	1.45	8	Argillite	31	66	80	SE	N45E80SE	225 83	John
1101	15835	10/13	1.00	5	Argillite	30	67	60	S	EW60S	90 83	Jim
1302	16840	10/16	0.40	1	Argillite	33	64	55	NE	N45W55NE	335 40	Jim
1399	17325	10/16	0.00	0	Argillite	35	62	NM	NM			Jim
1399A	17325	10/17	0.55	2	Argillite	36	61	75	NNE	N75W75NE	290 47	Jim
1403	17345	10/17	0.00	0	Argillite	34	63	NM	NM			Jim
1405	17355	10/17	0.35	1	Argillite	33	64	NV	NV			Jim
1449	17575	10/16	0.50	2	Argillite	34	63	55	NNE	N75W55NE	296 30	John
1551	18085	10/16	1.40	7	Argillite	35	62	70	N	EW70N	270 42	John
1699	18825	10/18	0.75	3	Argillite	31	66	20	E	NS20E	48 31	Jim
1699A	18825	10/18	0.80	4	Argillite	31	66	50	E	NS20E	48 31	Jim
1804	19350	10/17	0.00	0	Argillite	35	62	NM	NM			John
1805	19355	10/17	0.00	0	Argillite	34	63	NV	NV			John
1805A	19355	10/17	1.00	5	Argillite	34	63	NV	NV			John
1806	19360	10/17	0.00	0	Argillite	35	62	NV	NV			John
1847	19565	10/18	0.00	0	Argillite	35	62	NM	NM			Jim
1849	19575	10/18	0.00	0	Argillite	33	64	NM	NM			Jim
1853	19595	10/19	0.70	0	Argillite	35	62	35	SW	N45W35SW	119 58	Jim
1853A	19595	10/19	0.80	3	Argillite	33	64	20	N	EW20N	90 56	Jim
1854	19600	10/19	0.70	3	Argillite	32	65	30	S	EW30S	90 55	Jim
1855	19605	10/19	0.60	2	Argillite	35	62	20	S	EW20S	90 48	Jim
1901	19835	10/18	1.30	7	Argillite	34	63	20	E	NS20E	51 33	John
1902	19840	10/18	1.10	4	Argillite	30	67	45	SE	N45E45SE	56 63	John

Table 1 CORE SAMPLE RECOVERY SUMMARY

Ring No.	Station No.	Date	Length Recovered	Cores Possible	Rock Type	Liner Inclination	Hole Inclination	Bedding Inclination	Dip Direction	Apparent Inclination	True Inclination	Driller
1903	19845	10/18	0.80	4	Argillite	32	65	40	E	NS40E	27 46	John
1945	20055	10/20	0.40	1	Argillite	30	67	25	SE	N45E25SE	65 44	Jim
1947	20065	10/20	1.40	5	Sandy A	33	64	30	SSE	N75E30SE	81 56	Jim
1950	20080	10/20	0.30	1	Argillite	33	64	20	SE	N45E20SE	69 42	Jim
1951	20085	10/20	0.40	1	Argillite	30	67	40	SE	N45E40SE	58 58	Jim
1999	20325	10/19	0.00	0	Argillite	32	65	NM		NM		John
2000	20330	10/19	1.20	3	Argillite	34	63	40	E	NS40E	28 47	John
2000A	20330	10/20	2.20	8	Argillite	34	63	20	SE	N45E20SE	69 43	John
2003	20345	10/19	0.00	0	Argillite	33	64	65	ESE	N15E65SE	24 74	John
2099	20825	10/23	0.50	1	Argillite	34	63	20	S	EW20S	90 47	John
2100	20330	10/20	0.45	1	Argillite	33	64	25	SSE	N75E25SE	82 51	John
2100A	20330	10/20	0.55	2	Argillite	32	65	30	SSE	N75E30SE	81 55	John
2103	20845	10/23	0.60	2	Argillite	35	62	20	SE	N45E20SE	70 44	John
2151	21085	10/23	0.00	0	Argillite	33	64	30	SE	N45E30SE	63 51	Jim
2151A	21085	10/23	1.10	5	Argillite	29	68	35	SE	N45E35SE	59 53	Jim
2199	21325	10/23	0.40	2	Argillite	34	63	40	SSE	N75E40SE	80 66	John
2200	21330	10/23	0.60	3	Argillite	35	62	40	SE	N45E40SE	59 62	John
2203	21345	10/24	1.00	4	Argillite	35	62	30	S	EW30S	90 58	John
2251	21585	10/23	1.00	3	Diabase	35	62	NM		NM		Jim
2348	22070	10/25	0.80	3	Argillite	35	62	40	S	EW40S	90 68	Jim
2351	22085	10/24	0.60	2	Argillite	30	67	40	S	EW40S	90 63	Jim
2353	22095	10/24	0.00	0	Argillite	33	64	NM		NM		Jim
2354	22100	10/24	0.30	1	Argillite	33	64	35	SE	N45E35SE	61 56	John
2399	22325	10/24	1.30	7	Argillite	35	62	30	SE	N45E30SE	64 53	John
2400	22330	10/24	0.40	1	Argillite	35	62	30	S	EW30S	90 58	John
2450B	22580	10/25	1.10	5	Argillite	34	63	40	SE	N45E40SE	59 62	Jim
2452	22590	10/25	0.30	1	Argillite	36	61	40	SE	N45E40SE	59 63	John
2649	23575	10/25	0.60	2	Argillite	38	59	30	SE	N45E30SE	65 56	Jim
2655	23605	10/25	0.70	2	Argillite	35	62	30	S	EW30S	90 58	Jim
2700	23830	10/25	0.80	3	Argillite	33	64	Fold		Fold		John
2700A	23830	10/26	0.80	3	Argillite	34	63	Fold		Fold		John
2700B	23830	10/26	1.20	5	Argillite	36	61	90	Vert			John
2897	24815	10/26	0.90	3	Argillite	35	62	40	E	NS40E	29 47	Jim
2899	24825	10/26	0.00	0	Argillite	31	66	NM		NM		Jim
2901	24835	10/26	0.00	0	Argillite	33	64	90	SE	N45E Vert.	222 72	Jim
3101	25835	10/26	0.70	3	Argillite	34	63	25	E	NS25E	4 36	John
3049	25575	10/27	0.50	1	Argillite	35	62	75	S	EW75S	270 77	Jim
3049A	25575	10/27	1.10	5	Argillite	34	63	50	SE	N45E50SE	55 71	Jim
3100	25830	10/27	0.00	0	Argillite	34	63	30	S	EW30S	90 57	John
3103	25845	10/27	1.00	5	Argillite	31	66	45	SE	N45E45SE	56 64	John
3154	26100	10/27	0.60	3	Argillite	35	62	10	E	NS10E	69 30	Jim
3199	26325	10/30	0.75	4	Argillite	39	58	10	S	EW10S	90 42	John
3200	26330	10/30	0.00	0	Argillite	35	62	NV		NV		John
3200A	26330	10/30	0.90	5	Argillite	39	58	NV		NV		John
3249	26575	10/30	0.50	2	Argillite	32	65	NV		NV		Jim
3250	26580	10/30	0.85	4	Diabase	31	66	NM		NM		Jim
3251	26585	10/31	1.20	5	Diabase	32	65	NM		NM		Jim
3300	26830	10/31	0.65	3	Argillite	36	62	15	E	NS15E	60 32	John
3300A	26830	10/31	1.00	5	Argillite	38	59	20	SE	N45E20SE	71 47	John
3350	27080	10/31	0.00	0	Diabase	33	64	NM		NM		Jim
3351	27085	11/01	0.00	0	Diabase	33	64	NM		NM		Jim
3353	27095	11/01	1.10	5	Felsite	33	64	NM		NM		Jim
3349	27075	11/02	0.40	1	Felsite	36	61	NM		NM		Jim
3353A	27095	11/02	0.00	0	Felsite	35	62	NM		NM		Jim
3401	27335	11/02	0.70	3	Argillite	35	62	30	E	NS30E	39 40	John
3449	27575	11/03	1.10	6	Argillite	35	62	20	E	NS20E	52 34	John
3499	27825	11/02	2.25	8	Argillite	39	58	20	E	NS20E	56 37	John
3699	28825	11/03	1.30	6	Argillite	35	62	10	E	NS10E	69 30	John
3753	29095	11/06	0.00	0	Argillite	38	59	15	NE	N45W15NE	62 23	John
3847	29565	11/06	0.50	2	Argillite	39	58	20	NE	N45W20NE	50 22	John
3847A	29565	11/06	0.75	2	Argillite	38	59	20	NNE	N75W20NE	49 22	John
3896	29810	11/06	0.40	1	Argillite	40	57	20	ENE	N15W20NE	53 33	John
3995	30305	11/07	1.10	3	Argillite	36	61	10	NNE	N75W10NE	82 20	John
3995A	30305	11/07	1.00	5	Argillite	35	62	10	E	NS10E	69 30	John
3997	30305	11/07	1.10	3	Argillite	36	61	10	ENE	N15W10NE	69 28	John
4101	30835	11/07	0.40	1	Argillite	36	61	10	NNE	N75W10NE	82 20	Jim
4103	30845	11/07	1.20	6	Argillite	34	63	5	NNE	N75W5NE	87 22	Jim
4149	31075	11/08	1.35	6	Argillite	35	62	20	E	NS20E	52 34	John
4200	31330	11/08	1.20	5	Argillite	35	62	15	E	NS15E	60 32	Jim
4251	31585	11/09	0.75	4	Argillite	35	62	10	E	NS10E	69 30	John
4301	31835	11/09	0.00	0	Argillite	35	62	NM		NM		Jim

Ring No.	Station No.	Date	Length Recovered	Cores Possible	Rock Type	Liner Inclination	Hole Inclination	Bedding Inclination	Dip Direction	Apparent Inclination	True Inclination	Driller
Table 1 CORE SAMPLE RECOVERY SUMMARY												
4305	31855	11/09	0.00	0	Argillite	34	63	NM	NM			Jim
4351	32085	11/09	0.00	0	Argillite	38	59	30	NE	N45W30NE	22 22	John
4352	32095	11/09	1.25	6	Argillite	30	67	15	NNE	N75W15NE	66 09	John
4452	32090	11/13	0.80	5	Argillite	35	62	5	ENE	N15W5NE	79 27	John
4452A	32590	11/13	1.40	7	Argillite	35	62	5	NE	N45W5NE	82 25	John
4496	32810	11/13	0.00	0	Argillite	34	63	5	SSE	N75E5SE	88 32	Jim
4502	32840	11/13	0.00	0	Argillite	35	62	NM	NM			Jim
4596	33310	11/14	1.15	4	Argillite	35	62	15	NE	N45W15NE	58 20	John
4602	33340	11/13	0.45	1	Argillite	34	63	10	E	NS10E	69 29	John
4605	33355	11/13	0.50	1	Diabase	34	63	NM	NM			John
4649	33575	11/13	0.90	5	Argillite	34	63	10	NNE	N75W10NE	81 18	Jim
4649A	33575	11/14	0.80	4	Argillite	34	63	15	NE	N45W15NE	56 19	Jim
4652	33590	11/13	0.00	0	Argillite	33	64	15	ENE	N75W15NE	71 12	Jim
4753	34095	11/14	0.80	4	Argillite	34	63	10	E	NS10E	69 29	John
4753A	34095	11/14	1.15	6	Argillite	37	60	10	E	NS10E	71 32	John
4799	34325	11/14	0.00	0	Felsite	32	65	NM	NM			Jim
4799A	34325	11/14	0.80	4	Felsite	38	59	NM	NM			Jim
4799B	34325	11/15	1.40	8	Sandston	38	59	NV	NV			Jim
4850	34580	11/15	0.60	2	Argillite	35	62	15	E	NS15E	60 32	John
4900	34830	11/15	0.90	4	Argillite	30	67	15	E	NS15E	56 27	John
5000	35330	11/16	2.25	8	Argillite	30	67	10	E	NS15E	56 27	John
5050	35580	11/15	0.40	1	Diabase	30	67	NM	NM			Jim
5098	35820	11/17	1.10	3	Argillite	33	64	20	SE	N45E20SE	69 42	Jim
5098A	35820	11/17	0.00	0	Argillite	35	62	NV	NV			Jim
5100A	35830	11/17	Abandoned									
5101A	35835	11/16	Abandoned									
5300A	36830	11/16	0.90	5	Argillite	33	64	15	ESE	N75E15SE	84 41	John
5349C	37075	11/16	1.15	6	Argillite	32	65	15	SE	N45E15SE	72 37	Jim
5449	37575	11/17	1.50	8	Argillite	34	63	20	ESE	N15E20SE	57 37	John
5450	37580	11/17	0.40	1	Argillite	35	62	20	E	NS20E	52 34	John
5498	37820	11/17	0.70	3	Argillite	35	62	15	NE	N45W15NE	58 20	John
5598A	38320	11/20	0.00	0	Argillite	34	63	NM	NM			John
5599	38325	11/20	0.95	5	Argillite	34	63	20	NE	N45W20NE	41 19	John
5599A	38325	11/20	0.00	0	Sandston	36	61	NV	NV			John
5601A	38325	11/20	0.00	0	Sandston	37	60	NV	NV			John
5605A	38355	11/21	0.75	4	Sandston	34	63	NV	NV			John
5696	38810	11/22	0.80	4	Argillite	30	67	15	E	NS15E	56 27	John
5701A	38835	11/21	0.95	5	Sandston	31	66	NV	NV			John
5701B	38835	11/21	0.00	0	Argillite	30	67	NM	NM			John
5705	38855	11/21	0.00	0	Argillite	33	64	NV	NV			John
5705A	38855	11/21	0.00	0	Sandy A	33	64	NV	NV			John
5745	39055	11/20	0.60	2	Argillite	33	64	NV	NV			Jim
5745A	39055	11/20	0.90	4	Argillite	32	65	5	E	NS5E	78 26	Jim
5746	39060	11/20	0.50	2	Argillite	32	65	5	N	EW5N	90 20	Jim
5750	39080	11/20	0.35	1	Argillite	34	63	10	ENE	N15W10NE	68 26	Jim
5802C	39340	11/21	0.00	0	Argillite	30	67	NV	NV			Jim
5901	39835	11/21	1.05	6	Argillite	33	64	15	E	NS15E	59 30	Jim
6052	40590	11/22	0.75	4	Argillite	31	66	NV	NV			Jim
6052A	40590	11/22	1.10	6	Argillite	33	64	40	NE	N45W40NE	351 27	Jim
6250A	41580	11/22	0.00	0	Argillite	33	64	NV	NV			John
6251B	41585	11/22	0.50	2	Argillite	33	64	NV	NV			John
6300	41830	11/22	0.65	3	Argillite	31	66	15	E	NS15E	57 28	Jim
6303	41845	11/27	1.00	5	Argillite	33	64	15	E	NS15E	59 30	Jim
6305	41855	11/27	0.00	0	Argillite	30	67	NV	NV			Jim
6351	42085	11/27	1.25	6	Sandy A	35	62	NV	NV			John
6450	42580	11/27	1.35	7	Sandy A	35	62	30	E	NS15E	60 32	John
6500	42830	11/28	1.00	5	Argillite	33	64	20	E	NS20E	50 32	Jim
6601	43335	11/28	0.60	2	Argillite	35	62	15	E	NS15E	60 32	John
6605	43355	11/28	0.55	2	Argillite	34	63	5	E	NS5E	79 27	John
6606	43360	11/28	0.85	4	Argillite	36	61	10	E	NS10E	70 31	John
6702	43840	11/28	1.15	4	Argillite	30	67	5	ESE	N15E5SE	78 25	Jim
6748	44070	11/28	0.30	1	Argillite	31	66	30	ESE	N15E30SE	44 42	Jim
6748A	44070	11/29	0.30	1	Argillite	31	66	5	E	NS5E	78 25	Jim
6750B	44080	11/29	0.80	3	Argillite	35	62	30	E	NS30E	39 40	Jim
6750C	44080	11/30	1.20	4	Argillite	33	64	30	E	NS30E	37 39	Jim
6850	44580	11/29	0.50	2	Argillite	30	67	30	SE	N45E30SE	62 49	Jim
6950A	45080	11/30	0.00	0	Argillite	31	66	NM	NM			John
6951A	45085	11/30	0.90	3	Argillite	32	65	25	E	NS25E	42 35	John
7000	45330	11/30	0.30	1	Argillite	35	62	NV	NV			Jim
7101	45835	12/01	0.00	0	Argillite	33	64	NV	NV			John
7102	45840	12/01	1.25	3	Argillite	33	64	NV	NV			John

Ring No.	Station No.	Date	Length Recovered	Cores Possible	Rock Type	Liner Inclination	Hole Inclination	Bedding Inclination	Dip Direction	Apparent Inclination	True Inclination	Driller
7149	45840	12/01	1.25	3	Argillite	33	64	10	E	NS10E	68 28	Jim
7196	46310	12/08	0.40	2	Argillite	35	62	45	N	EW45N	270 17	Jim
7202A	46340	12/08	0.50	2	Argillite	38	59	15	E	NS15E	63 35	Jim
7202B	46340	12/08	0.30	0	Argillite	35	62	15	E	NS15E	60 32	Jim
7203A	46345	12/08	0.35	1	Argillite	33	64	15	E	NS15E	59 30	Jim
7345	47055	12/05	0.00	0	Argillite	30	67	NM	NM			Jim
7347	47065	12/05	0.00	0	Argillite	40	57	NM	NM			Jim
7348B	47070	12/04	Abandoned									Jim
7351	47085	12/04	0.00	0	Argillite	32		NM	NM			Jim
7401B	47335	12/11	1.10	6	Argillite	35		30	E	NS30E	39 40	Jim
7500A	47830	12/11	0.95	5	Argillite	33		10	ENE	N15W10NE	67 25	Jim
7549A	48075	12/11	1.30	7	Argillite	34		40	NE	N45W40NE	353 27	Jim
7595	48305	12/14	0.00	0	Argillite	40	57	NV	NV			Jim
7597	48315	12/14	0.00	0	Argillite	35	62	NV	NV			Jim
7600	48330	12/11	0.00	0	Argillite	33	64	NM	NM			Jim
7602	48340	12/13	0.50	1	Argillite	32	65	20	NW	N45E20NW	144 18	John
7604	48350	12/14	0.00	0	Argillite	40	57	30	NE	N45W30NE	26 23	Jim
7605	48355	12/13	0.00	0	Argillite	34	63	30	ENE	N15W30NE	30 34	Jim
7647	48565	12/14	1.60	8	Argillite	35	62	30	N	EW30N	270 02	John
7652	48590	12/13	0.00	0	Argillite	33	64	35	NNE	N75W35NE	317 12	John
7653	48595	12/14	0.00	0	Argillite	35	62	60	NE	N45W60NE	334 43	John
7654	48600	12/14	0.50	2	Argillite	35	62	50	NNE	N75W50NE	299 24	John
7700B	48830	12/15	1.40	8	Argillite	38	59	55	N	EW55N	270 24	Jim
7847	49565	12/18	0.60	2	Argillite	35	62	NV	NV			John
7850	49580	12/15	0.00	0	Argillite	34	63	NV	NV			John
7851A	49585	12/15	0.00	0	Argillite	34	63	NV	NV			John
7852	49590	12/18	0.00	0	Argillite	35	62	NV	NV			John
7854	49600	12/18	0.00	0	Argillite	33	64	NM	NM			John
7896	49810	12/18	0.75	3	Argillite	35	62	30	N	EW30N	270 02	Jim
7900	49830	12/15	0.55	2	Argillite	35	62	NV	NV			Jim
7902	49840	12/18	0.40	1	Argillite	35	62	NV	NV			Jim
7903	49845	12/18	0.30	1	Argillite	37	60	NV	NV			John
7950	50080	12/19	1.30	7	Argillite	34	63	10	N	EW10N	90 17	John
7950A	50080	12/19	1.05	6	Argillite	34	63	15	N	EW15N	90 12	John
8000	50330	12/19	0.90	5	Argillite	37	60	25	N	EW25N	90 05	Jim
8000A	50330	12/19	1.15	6	Argillite	37	60	NV	NV			Jim
8103	50845	12/21	1.00	5	Argillite	30	67	30	W	NS30W	34 37	Jim
8103A	50845	12/21	1.00	4	Argillite	37	60	30	N	EW30N	270 00	Jim
8150	51080	12/22	1.00	5	Argillite	35	62	30	N	EW30N	270 02	Jim
8150A	51080	12/26	1.00	4	Argillite	33	64	45	N	EW45N	270 19	Jim
8149	51075	12/27	1.30	6	Argillite	35	62	45	N	EW45N	270 17	Jim
8200	51330	12/21	0.00	0	Argillite	33	64	60	E	NS60E	14 63	John
8200A	51330	12/26	1.60	8	Argillite	35	62	55	N	EW55N	270 29	John
8205	51355	12/21	0.50	2	Argillite	34	63	45	N	EW45N	270 18	John
8205A	51355	12/22	1.60	8	Argillite	34	63	45	N	EW45N	270 18	John
8300	51830	12/26	1.70	8	Argillite	36	61	60	N	EW60N	270 31	John
8350	52080	12/27	1.50	8	Argillite	35	62	15	N	EW15N	90 13	John
8395	52305	12/28	0.00	0	Argillite	32	65	NM	NM			Jim
8400	52330	12/27	0.00	0	Argillite	32	65	NM	NM			Jim
8445	52555	12/28	0.70	4	Argillite	38	59	45	NW	N45E45NW	58 70	John
8445A	52555	12/28	1.50	8	Argillite	38	59	NV	NV			John
8450	52580	12/28	1.10	2	Argillite	36	61	60	NNE	N75W60NE	295 33	John

Table 1 CORE SAMPLE RECOVERY SUMMARY

Note: Length recovered is useable test length/NM = not measured/NV = not visible

APPENDIX B

Summary of Physical Property Testing Data

Earth Mechanics Institute   Colorado School Of Mines

Physical Property Testing Results for the tunneling project to evaluate rock strength

Sample No.	Density ρ (gr/cm^3)	Uniaxial Compressive Strength (MPa)	(psi)	Brazilian Tensile Strength (MPa)	(psi)	Seismic Velocities P-wave (ft/sec)	S-wave (ft/sec)	Dynamic Constants Modulus (ksi)	Poisson's Ratio	Notes
RN-250-L2										
Brazilian	2.66			15	2,182					Parl to bedding strike (Normal failure)
RN-297-E1										
UCS	2.75	142	20,411							Tensile failure
Acoustic	2.75					17,540	10,210	9,545	0.24	
Brazilian	2.73			8	1,092					Perp to bedding strike (Normal failure)
RN-500A-L2										
Brazilian	2.74			12	1,741					Parl to bedding strike (Normal failure)
RN-0600-E2										
Brazilian	2.71			15	2,217					Parl to bedding strike (Normal failure)
RN-600-L2										
Brazilian	2.69			15	2,223					Perp to bedding strike (Normal failure)
RN-650-E1										
UCS	2.96	91	13,108							Structural failure
Acoustic	2.96					17,711	10,941	11,327	0.19	
Brazilian	2.96			13	1,845					Massive bedding (Normal failure)
RN-702-E2										
UCS	2.70	147	21,213							Tensile failure
Acoustic	2.70					17,306	10,631	9,794	0.20	
Brazilian	2.70			13	1,905					Perp to bedding strike (Normal failure)
RN-704-L2										
UCS	2.71	115	16,515							Tensile failure
Acoustic	2.71					16,656	9,734	8,540	0.24	
Brazilian	2.71			14	1,967					Parl to bedding strike (Normal failure)
RN-800A-E2										
Brazilian-1	2.66			8	1,187					Parl to bedding strike (Normal failure)
Brazilian-2	2.68			11	1,568					Parl to bedding strike (Normal failure)
RN-800A-L2										
UCS	2.73	92	13,194							Tensile failure
Acoustic	2.73					17,400	10,649	9,956	0.20	
RN-951A-L2										
UCS	2.69	95	13,704							Tensile failure
Acoustic	2.69					15,897	10,520	8,843	0.11	
Brazilian	2.69			14	2,077					Perp to bedding strike (Normal failure)
RN-1000-E2										
UCS	2.69	115	16,623							Tensile failure
Acoustic	2.69					17,718	9,951	9,056	0.27	
Brazilian	2.68			6	835					Parl to bedding strike (Structural failure)
RN-1000-L2										
UCS	2.69	105	15,074							Tensile failure
Acoustic	2.69					16,941	10,464	9,420	0.19	
Brazilian	2.67			7	941					Parl to bedding strike (Structural failure)
RN-1051-E2										
UCS	2.73	153	22,032							Tensile failure
Acoustic	2.73					17,570	10,268	9,570	0.24	
Brazilian	2.73			7	1,023					Parl to bedding strike (Normal failure)
RN-1100-E2										
UCS	2.73	103	14,862							Tensile failure
Acoustic	2.73					16,551	9,364	8,097	0.26	
RN-1304-E4										
Brazilian	2.60			8	1,096					Parl to bedding strike (Normal failure)
RN-1400-E2										
Brazilian-1	2.53			5	660					Parl to bedding strike (Structural failure)

Earth Mechanics Institute									Colorado School Of Mines
Physical Property Testing Results for the tunneling project to evaluate rock strength									
Sample	Density	Uniaxial Compressive		Brazilian Tensile		Seismic Velocities		Dynamic Constants		
No.	ρ	Strength		Strength		P-wave	S-wave	Modulus	Poisson's	Notes
	(gr/cm^3)	(MPa)	(psi)	(MPa)	(psi)	(ft/sec)	(ft/sec)	(ksi)	Ratio	
Brazilian-2	2.54			6	901					Parl to bedding strike (Normal failure)
Brazilian-3	2.54			10	1,398					Parl to bedding strike (Normal failure)
RN-1450A-E2										
UCS	2.67	79	11,445							Structural failure
Acoustic	2.67					19,560	10,744	10,610	0.28	
RN-1450A-L2										
UCS	2.66	94	13,527							Tensile with Top Cone
Acoustic	2.66					13,612	9,020	6,418	0.11	
Brazilian	2.65			10	1,461					Perp to bedding strike (Normal failure)
Brazilian	2.67			7	1,067					Parl to bedding strike (Normal failure)
RN-1500B-E4										
UCS	2.69	68	9,724							Structural failure
Acoustic	2.69					17,954	10,928	10,390	0.21	
Brazilian	2.67			6	887					Perp to bedding strike (Normal failure)
RN-1700- L2										
UCS	2.57	49	7,038							Structural failure
RN-1753-E2										
Brazilian	2.58			5	718					Perp to bedding strike (Structural failure)
RN-1855- L2										
UCS	2.69	62	8,986							Structural failure
RN-1901-E3										
UCS	2.71	78	11,303							Tensile failure
Acoustic	2.71					16,493	9,689	8,422	0.24	
Brazilian	2.69			8	1,161					Massive bedding (Normal failure)
RN-1947-E2										
UCS	2.74	51	7,343							Structural failure
Acoustic	2.74					14,429	8,969	7,008	0.19	
Brazilian	2.73			9	1,307					Perp to bedding strike (Structural failure
Brazilian	2.73			9	1,244					Parl to bedding strike (Structural failure)
RN-2000A-E3										
UCS	2.69	147	21,183							Tensile failure
Acoustic	2.69					17,559	10,034	9,141	0.26	
RN-2051- E2										
UCS	2.71	67	9,635							Structural failure
Acoustic	2.71					17,325	11,826	10,786	0.06	
Brazilian	2.64			16	2,334					Massive bedding (Normal failure)
RN-2100-E2										
Brazilian	2.45			9	1,319					Perp to bedding strike (Normal failure)
Brazilian	2.45			6	830					Parl to bedding strike (Structural failure)
Brazilian	2.46			7	1,016					Perp to bedding strike (Structural failure
Brazilian	2.44			6	808					Parl to bedding strike (Structural failure)
RN-2100-L2										
UCS	2.55	41	5,871							Structural failure
Acoustic	2.55					12,936	8.416	5,476	0.13	
Brazilian	2.53			6	801					Perp to bedding strike (Structural failure
RN-2151-L1										
Brazilian	2.66			12	1,687					Parl to bedding strike (Normal failure)
Brazilian	2.67			12	1,669					Perp to bedding strike (Normal failure)
RN-2201A-E2										
UCS	2.70	75	10,871							Structural failure
Acoustic	2.70					18,542	10,301	9,806	0.28	
Brazilian	2.69			7	1,069					Perp to bedding strike (Normal failure)
RN-2203-L2										

Earth Mechanics Institute									Colorado School Of Mines
Physical Property Testing Results for the tunneling project to evaluate rock strength									
Sample No.	Density ρ	Uniaxial Compressive Strength		Brazilian Tensile Strength		Seismic Velocities		Dynamic Constants		Notes
						P-wave	S-wave	Modulus	Poisson's	
	(gr/cm^3)	(MPa)	(psi)	(MPa)	(psi)	(ft/sec)	(ft/sec)	(ksi)	Ratio	
UCS	2.68	34	4,895							Structural failure
Acoustic	2.68					15,973	10,435	8,816	0.13	
Brazilian	2.95			12	1,739					Massive bedding (Normal failure)
RN-2251- E2										
Brazilian	2.77			11	1,580					Massive bedding (Normal failure)
RN-2251- L2										
Total Hardness										
Brazilian	2.78			9	1,356					Massive bedding (Normal failure)
RN-2301- E2										
UCS	2.69	54	7,717							Structural failure
Brazilian	2.66			6	936					Parl to bedding strike (Structural failure)
RN-2401A- E2										
UCS	2.68	53	7,684							Structural failure
Acoustic	2.68					14,784	9,338	7,313	0.17	
Brazilian	2.64			11	1,548					Parl to bedding strike (Normal failure)
RN-2450A-L1										
Brazilian	2.67			12	1,762					Perp to bedding strike (Normal failure)
RN-2499- L2										
UCS	2.74	50	7,129							Structural failure
Acoustic	2.74					15,046	9,305	7,559	0.19	
RN-2550- E2										
UCS	2.69	61	8,832							Structural failure
Acoustic	2.69					16,023	10,531	8,958	0.12	
Brazilian	2.66			6	817					Parl to bedding strike (Normal failure)
RN-2551- L2										
UCS	2.68	60	8,602							Structural failure
Acoustic	2.68					15,613	9,170	7,482	0.24	
RN-2700B-E2										
UCS	2.74	83	12,012							Structural failure
Acoustic	2.74					18,130	10,072	9,496	0.28	
Brazilian	2.73			12	1,740					Perp to bedding strike (Normal failure)
RN-2700-L1										
UCS	2.73	83	12,019							Structural failure
Acoustic	2.73					16,989	10,561	9,669	0.19	
RN-2751-L3										
Brazilian	2.72			2	326					Perp to bedding strike (Structural failure)
Brazilian	2.66			5	717					Parl to bedding strike (Structural failure)
RN-2755- E2										
UCS	2.73	35	5,074							Structural failure
RN-2805- E2										
UCS	2.74	109	15,626							Tensile failure
Acoustic	2.74					18,581	10,883	10,767	0.24	
Brazilian	2.72			8	1,159					Perp to bedding strike (Structural failure)
RN-2849-L2										
UCS	2.72	62	8,879							Structural failure
Acoustic	2.72					17,167	10,347	9,493	0.2147067	
Brazilian	2.74			6	803					Perp to bedding strike (Structural failure
RN-2950- L2										
UCS	2.73	48	6,878							Structural failure
Acoustic	2.73					16,601	10,461	9,377	0.17	
Brazilian	2.70			8	1,117					Perp to the bedding strike (Normal failur
RN-3155-E2										
UCS	2.74	128	18,423							Tensile failure

217

Sample No.	Density ρ (gr/cm^3)	Uniaxial Compressive Strength (MPa)	(psi)	Brazilian Tensile Strength (MPa)	(psi)	Seismic Velocities P-wave (ft/sec)	S-wave (ft/sec)	Dynamic Constants Modulus (ksi)	Poisson's Ratio	Notes
Acoustic	2.74					19,672	11,623	12,233	0.23	
Brazilian	2.72			7	969					Perp to bedding strike (Structural failure
RN-3155- L2										
Brazilian	2.72			13	1,911					Parl to bedding strike (Normal failure)
RN-3200A-L1										
UCS	2.74	57	8,196							Structural failure
Acoustic	2.74					18,029	10,713	10,349	0.23	
Brazilian	2.74			11	1,547					Massive bedding (Normal failure)
RN-3250-L1										
Brazilian	2.92			7	994					Massive bedding (Structural failure)
Brazilian	2.93			6	853					Massive bedding (Structural failure)
RN-3251-E4										
Brazilian	2.94			11	1,564					Massive bedding (Normal failure)
Brazilian	2.94			13	1,935					Massive bedding (Normal failure)
RN-3300-L2										
UCS	2.74	67	9,676							Structural failure
Acoustic	2.74					17,415	11,012	10,401	0.17	
Brazilian	2.73			16	2,326					Perp to bedding strike (Normal failure)
RN-3353-E2										
UCS	2.81	145	20,882							Tensile failure
Acoustic	2.81					19,521	10,197	10,274	0.31	
Brazilian	2.79			11	1,631					Massive bedding (Normal failure)
RN-3401-L2										
UCS	2.72	104	14,959							Tensile failure
Acoustic	2.72					16,985	9,539	8,429	0.27	
RN-3450A-E2										
UCS	2.74	48	6,931							Structural failure
Acoustic	2.74					19,216	10,980	11,141	0.26	
Brazilian	2.73			7	1,074					Parl to bedding strike (Normal failure)
RN-3545A-E2										
UCS	2.74	38	5,425							Structural failure
Acoustic	2.74					17,820	11,105	10,700	0.18	
Brazilian	2.71			3	471					Parl to bedding strike (Structural failure)
RN-3555-L2										
UCS	2.75	61	8,746							Structural failure
Acoustic	2.75					17,203	10,659	9,965	0.19	
RN-3601-L2										
UCS	2.74	134	19,229							Tensile failure
Acoustic	2.74					17,882	11,210	10,866	0.18	
Brazilian	2.73			12	1,798					Perp to the bedding strike (Normal failur
Brazilian	2.72			10	1,423					Parl to the bedding strike (Normal failure
RN-3650-L2										
Brazilian	2.72			11	1,535					Perp to bedding strike (Normal failure)
RN-3700-L2										
UCS	2.75	14	2,029							Structural failure
Acoustic	2.75					15,948	9,941	8,608	0.18	
Brazilian	2.74			12	1,779					Parl to bedding strike (Normal failure)
RN-3847-L2										
UCS	2.72	109	15,711							Tensile failure
Acoustic	2.72					14,063	9,078	6,853	0.14	
Brazilian	2.70			9	1,246					Parl to bedding strike (Normal failure)
RN-3950A-L2										
UCS	2.70	105	15,092							Tensile failure

Earth Mechanics Institute — **Colorado School Of Mines**

Physical Property Testing Results for the tunneling project to evaluate rock strength

Earth Mechanics Institute									Colorado School Of Mines
Physical Property Testing Results for the tunneling project to evaluate rock strength									
Sample	Density	Uniaxial Compressive		Brazilian Tensile		Seismic Velocities		Dynamic Constants		
No.	ρ	Strength		Strength		P-wave	S-wave	Modulus	Poisson's	Notes
	(gr/cm^3)	(MPa)	(psi)	(MPa)	(psi)	(ft/sec)	(ft/sec)	(ksi)	Ratio	
Acoustic	2.70					14,557	8,986	6,962	0.19	
Brazilian	2.71			14	2,015					Parl to bedding strike (Normal failure)
RN-3995-E1										
UCS	2.71	35	5,066							Structural failure
Acoustic	2.71					15,734	9,730	8,174	0.19	
RN-4005-L2										
UCS	2.72	120	17,252							Tensile failure
Acoustic	2.72					14,143	8,983	6,830	0.16	
Brazilian	2.68			4	635					Perp to bedding strike (Structural failure)
RN-4049-L2										
UCS	2.61	75	10,795							Structural failure
Acoustic	2.61					13,669	8,410	5,908	0.20	
Brazilian	2.60			12	1,791					Perp to bedding strike (Normal failure)
RN-4100-E2										
Brazilian	2.74			8	1,179					Perp to bedding strike (Normal failure)
RN-4203-E2										
Brazilian	2.69			8	1,217					Perp to bedding strike (Normal failure)
Brazilian	2.68			4	589					Parl to bedding strike (Structural failure)
RN-4251A-L2										
UCS	2.70	113	16,303							Tensile failure
Acoustic	2.70					14,568	9,212	7,167	0.17	
RN-4255A-E2										
Brazilian	2.71			7	1,017					Parl to bedding strike (Normal failure)
RN-4350A-L2										
UCS	2.67	62	8,970							Structural failure
Acoustic	2.67					13,243	9,584	6.253	-0.05	
RN-4452A-E1										
Brazilian	2.50			5	676					Perp to bedding strike (Structural failure
Brazilian	2.50			3	439					Parl to bedding strike (Structural failure)
Brazilian	2.50			1	87					Perp to bedding strike (Structural failure
RN-4595A-L1										
UCS	2.74	132	19,031							Tensile failure
Acoustic	2.74					16,461	9,602	8,406	0.24	
Brazilian	2.70			14	2,018					Perp to bedding strike (Normal failure)
RN-4596-E3										
UCS	2.74	36	5,168							Structural failure
Acoustic	2.74					17,020	10,157	9,263	0.22	
Brazilian	2.71			5	681					Parl to bedding strike (Normal failure)
RN-4649-L3										
Brazilian	2.72			10	1,433					Perp to bedding strike (Normal failure)
Brazilian	2.73			14	2,043					Perp to bedding strike (Normal failure)
Brazilian	2.68			8	1,144					Parl to bedding strike (Normal failure)
RN-4649-E2										
Brazilian	2.73			4	539					Parl to bedding strike (Structural failure)
RN-4700-L2										
UCS	2.72	106	15,230							Tensile failure
Acoustic	2.72					16,413	9,759	8,510	0.23	
Brazilian	2.73			10	1,413					Perp to bedding strike (Normal failure)
Brazilian	2.70			8	1,146					Parl to bedding strike (Normal failure)
RN-4753A-L2										
Brazilian	2.74			9	1,294					Perp to bedding strike (Normal failure)
Brazilian	2.73			10	1,420					Parl to bedding strike (Normal failure)
Brazilian	2.70			15	2,096					Perp to bedding strike (Normal failure)

Earth Mechanics Institute										Colorado School Of Mines
Physical Property Testing Results for the tunneling project to evaluate rock strength										
Sample No.	Density ρ	Uniaxial Compressive Strength		Brazilian Tensile Strength		Seismic Velocities		Dynamic Constants		Notes
						P-wave	S-wave	Modulus	Poisson's Ratio	
	(gr/cm^3)	(MPa)	(psi)	(MPa)	(psi)	(ft/sec)	(ft/sec)	(ksi)	Ratio	
RN-4755-E1										
UCS	2.75	115	16,577							Tensile failure
Acoustic	2.75					18,974	10,508	10,386	0.28	
Brazilian	2.74			6	845					Parl to bedding strike (Structural failure)
RN-4801-E2										
UCS	2.80	92	13,253							Tensile failure
Acoustic	2.80					19,531	10,453	10,638	0.30	
Brazilian	2.77			9	1,339					Perp to bedding strike (Structural failure)
RN-4801A-L1										
Brazilian	2.78			2	353					Massive bedding (Structural failure)
RN-4851A-E3										
UCS	2.76	38	5,429							Structural failure
Acoustic	2.76					18,545	10,677	10,543	0.25	
Brazilian	2.73			8	1,169					Parl to bedding strike (Structural failure)
RN-4851-L2										
Brazilian	2.76			8	1,198					Perp to bedding strike (Normal failure)
Brazilian	2.72			12	1,700					Parl to bedding strike (Normal failure)
RN-4904-E3										
UCS	2.74	99	14,197							Tensile failure
Acoustic	2.74					17,913	10,384	9,875	0.25	
Brazilian	2.73			10	1,423					Perp to bedding strike (Normal failure)
RN-4904-L3										
Brazilian	2.73			11	1,588					Massive bedding (Normal failure)
RN-4952-L2										
UCS	2.75	101	14,525							Tensile failure
Brazilian	2.75			14	2,024					Massive bedding (Normal failure)
Brazilian	2.74			23	3,252					Massive bedding (Normal failure)
RN-5000-E1										
Brazilian	2.72			7	1,013					Massive bedding (Normal failure)
RN-5049-L1										
Brazilian	2.97			16	2,376					Massive bedding (Normal failure)
RN-5098-L2										
Brazilian	2.73			9	1,352					Massive bedding (Normal failure)
Brazilian	2.73			8	1,176					Massive bedding (Normal failure)
Brazilian	2.71			9	1,252					Massive bedding (Normal failure)
RN-5101-E2										
Brazilian	2.72			6	830					Perp to bedding strike (Structural failure
Brazilian	2.67			7	968					Parl to bedding strike (Normal failure)
Brazilian	2.62			7	951					Perp to bedding strike (Normal failure)
Brazilian	2.67			6	839					Perp to bedding strike (Structural failure
RN-5151-L2										
UCS	2.75	122	17,504							Tensile failure
Brazilian	2.74			16	2,356					Parl to bedding strike (Normal failure)
RN-5200-E2										
Brazilian	2.71			14	2,081					Perp to bedding strike (Normal failure)
RN-5205-L2										
UCS	2.73	80	11,567							Structural failure
Brazilian	2.71			14	2,088					Massive bedding (Normal failure)
RN-5252A-L4										
Brazilian	2.75			14	2,086					Parl to bedding strike (Normal failure)
RN-5252-E4										
UCS	2.75	141	20,277							Tensile failure

Earth Mechanics Institute										Colorado School Of Mines
Physical Property Testing Results for the tunneling project to evaluate rock strength										
Sample No.	Density ρ	Uniaxial Compressive Strength		Brazilian Tensile Strength		Seismic Velocities P-wave	S-wave	Dynamic Constants Modulus	Poisson's Ratio	Notes
	(gr/cm^3)	(MPa)	(psi)	(MPa)	(psi)	(ft/sec)	(ft/sec)	(ksi)	Ratio	
Brazilian	2.75			11	1,562					Perp to bedding strike (Normal failure)
RN-5301-E4										
UCS	2.73	117	16,843							Tensile failure
Brazilian	2.72			16	2,275					Perp to bedding strike (Normal failure)
RN-5305-L2										
Brazilian	2.75			16	2,286					Perp to bedding strike (Normal failure)
RN-5348-E1										
UCS	2.75	119	17,112							Tensile failure
Brazilian	2.74			11	1,512					Parl to bedding strike (Normal failure)
RN-5349A-L1										
Brazilian	2.75			15	2,107					Parl to bedding strike (Normal failure)
RN-5402A-E2										
Brazilian	2.77			11	1,631					Perp to bedding strike (Normal failure)
RN-5402-L4										
UCS	2.76	89	12,765							Structural failure
Brazilian	2.75			12	1,719					Parl to bedding strike (Normal failure)
Brazilian	2.75			8	1,136					Perp to bedding strike (Normal failure)
RN-5449A-E1										
UCS	2.70	72	10,306							Structural failure
Acoustic	2.70					16,652	9,907	8,699	0.23	
RN-5555-L3										
Brazilian	2.77			18	2 580					Massive bedding (Normal failure)
RN-5555-E3										
UCS	2.77	125	17,944							Tensile failure
Brazilian	2.76			12	1,684					Massive bedding (Normal failure)
RN-5599-E3										
Brazilian	2.77			12	1,699					Massive bedding (Normal failure)
Brazilian	2.76			3	425					Massive bedding (Structural failure)
RN-5651-L2										
UCS	3.03	129	18,564							Tensile failure with top cone
Acoustic	3.03					18,036	10,978	11,792	0.21	
RN-5745A-E3										
UCS	2.73	76	10,903							Tensile failure
Acoustic	2.73					18,365	10,263	9,824	0.27	
Brazilian	2.73			4	541					Massive bedding (Structural failure)
RN-5802-L1										
Brazilian	2.74			17	2,495					Massive bedding (Normal failure)
RN-5806-E2										
UCS	2.77	78	11,259							Structural failure
Acoustic	2.77					18,979	10,303	10,161	0.29	
Brazilian	2.75			19	2,666					Massive bedding (Normal failure)
RN-5849-E1										
UCS	2.75	94	13,601							Tensile failure
Acoustic	2.75					20,153	11,836	12,751	0.24	
RN-5901-L1										
UCS	2.79	126	18,202							Tensile failure
Acoustic	2.79					18,006	10,526	10,270	0.24	
Brazilian	2.78			10	1,421					Massive bedding (Normal failure)
Brazilian	2.77			12	1,707					Massive bedding (Normal failure)
RN-5949-E2										
UCS	2.74	171	24,562							Tensile failure
Acoustic	2.74					19,649	10,371	10,322	0.31	

Earth Mechanics Institute										Colorado School Of Mines
Physical Property Testing Results for the tunneling project to evaluate rock strength										
Sample	Density	Uniaxial Compressive		Brazilian Tensile		Seismic Velocities		Dynamic Constants		
No.	ρ	Strength		Strength		P-wave	S-wave	Modulus	Poisson's	Notes
	(gr/cm^3)	(MPa)	(psi)	(MPa)	(psi)	(ft/sec)	(ft/sec)	(ksi)	Ratio	
Brazilian	2.75			12	1,708					Massive bedding (Normal failure)
RN-5998-L3										
UCS	2.76	175	25,223							Tensile failure
Acoustic	2.76					18,707	10,365	10,170	0.28	
Brazilian	2.74			14	1,985					Parl to bedding strike (Normal failure)
Brazilian	2.73			18	2,548					Parl to bedding strike (Normal failure)
RN-6049-E2										
Brazilian	2.77			14	2,003					Massive bedding (Normal failure)
RN-6049-L1										
UCS	2.77	97	14,008							Tensile failure
Acoustic	2.77					14,664	8,876	7,080	0.21	
RN-6103-L2										
Brazilian	2.77			18	2,651					Perp to bedding strike (Normal failure)
Brazilian	2.75			18	2,590					Parl to bedding strike (Normal failure)
RN-6103-E2										
UCS	2.77	124	17,915							Tensile failure
Acoustic	2.77					19,492	11,573	12,182	0.23	
Brazilian	2.76			12	1,799					Massive bedding (Normal failure)
RN-6152-L3										
UCS	2.76	113	16,205							Tensile failure
Brazilian	2.75			18	2,547					Massive bedding (Normal failure)
RN-6152-E2										
Brazilian	2.78			15	2,104					Massive bedding (Normal failure)
RN-6201-L2										
Brazilian	2.75			12	1,753					Massive bedding (Normal failure)
RN-6201A-E2										
Brazilian	2.74			16	2,314					Massive bedding (Normal failure)
Brazilian	2.73			16	2,292					Massive bedding (Normal failure)
RN-6250-L1										
Brazilian	2.75			12	1,689					Massive bedding (Normal failure)
RN-6251A-E3										
UCS	2.73	111	16,051							Tensile failure
Acoustic	2.73					18,453	10,441	10,087	0.26	
RN-6303-E1										
UCS	2.74	88	12,732							Tensile failure
Acoustic	2.74					17,549	10,134	9,438	0.25	
Brazilian	2.74			7	995					Perp to bedding strike (Normal failure)
RN-6349-E2										
UCS	2.77	101	14,593							Structural failure
Acoustic	2.77					19,783	11,487	12,193	0.25	
RN-6350-L2										
Brazilian	2.75			12	1,743					Massive bedding band (Normal failure)
RN-6395-E4										
UCS	2.76	66	9,456							Structural failure
Acoustic	2.76					18,654	10,336	10,095	0.28	
Brazilian	2.76			11	1,534					Parl to bedding strike (Normal failure)
RN-6399-L2										
Brazilian	2.76			11	1,549					Massive bedding (Normal failure)
RN-6455-L1										
UCS	2.78	122	17,524							Tensile failure
Acoustic	2.78					19,028	11,473	11,899	0.21	
Brazilian	2.72			18	2,591					Massive bedding (Normal failure)

Earth Mechanics Institute									Colorado School Of Mines

Physical Property Testing Results for the tunneling project to evaluate rock strength

Sample No.	Density ρ	Uniaxial Compressive Strength		Brazilian Tensile Strength		Seismic Velocities		Dynamic Constants		Notes
						P-wave	S-wave	Modulus	Poisson's	
	(gr/cm^3)	(MPa)	(psi)	(MPa)	(psi)	(ft/sec)	(ft/sec)	(ksi)	Ratio	
RN-6455-E2										
Brazilian	2.76			10	1,499					Massive bedding (Normal failure)
RN-6499-L3										
UCS	2.76	103	14,810							Tensile failure
Acoustic	2.76					18,184	10,102	9,646	0.28	
Brazilian	2.74			14	1,957					Massive bedding (Normal failure)
RN-6553-L2										
Brazilian	2.80			14	1,981					Perp to bedding strike (Normal failure)
RN-6553-E3										
UCS	2.78	15	2,144							Structural failure
Acoustic	2.78					18,567	10,079	9,765	0.29	
Brazilian	2.75			13	1,917					Perp to bedding strike (Normal failure)
Brazilian	2.77			15	2,232					Perp to bedding strike (Normal failure)
RN-6606-E2										
UCS	2.75	111	16,018							Tensile failure
Acoustic	2.75					16,741	9,991	9,013	0.22	
Brazilian	2.73			16	2,241					Massive bedding (Normal failure)
RN-6651A-E2										
UCS	2.76	92	13,223							Structural failure
Acoustic	2.76					18,732	10,105	9,765	0.29	
Brazilian	2.72			13	1,814					Perp to bedding strike (Normal failure)
RN-6698-L4										
Brazilian	2.74			18	2,583					Massive bedding (Normal failure)
RN-6699-E2										
UCS	2.72	160	23,081							Tensile failure
Acoustic	2.72					16,501	10,912	9,635	0.11	
Brazilian	2.72			13	1,887					Perp to bedding strike (Normal failure)
RN-6750-E2										
Brazilian	2.75			11	1,621					Parl to bedding strike (Normal failure)
RN-6750-L2										
UCS	2.75	165	23,789							Tensile failure
Acoustic	2.75					17,792	10,356	9,846	0.24	
Brazilian	2.78			12	1,759					Massive bedding (Normal failure)
Brazilian	2.76			11	1,567					Massive bedding (Normal failure)
RN-6803-L2										
UCS	2.75	60	8,709							Structural failure
Acoustic	2.75					18,552	10,336	10,053	0.27	
Brazilian	2.75			14	2,051					Parl to bedding strike (Normal failure)
RN-6851A-L2										
Brazilian	2.82			5	724					Parl to bedding strike (Structural failure)
Brazilian	2.77			5	655					Parl to bedding strike (Structural failure)
RN-6852A-E2										
UCS	2.77	128	18,452							Tensile failure
Acoustic	2.77					19,439	10,259	10,201	0.31	
Brazilian	2.77			10	1,493					Perp to bedding strike (Normal failure)
RN-6900-E2										
UCS	2.68	43	6,204							Structural failure
Acoustic	2.68					18,561	10,365	9,818	0.27	
Brazilian	2.75			4	577					Parl to bedding strike (Structural failure)
RN-6901-L1										
Brazilian	2.72			14	2,040					Massive bedding (Normal failure)
RN-6901-L1										
UCS	2.73	101	14,612							Tensile failure

Earth Mechanics Institute										Colorado School Of Mines
Physical Property Testing Results for the tunneling project to evaluate rock strength										
Sample	Density	Uniaxial Compressive		Brazilian Tensile		Seismic Velocities		Dynamic Constants		
No.	ρ	Strength		Strength		P-wave	S-wave	Modulus	Poisson's	Notes
	(gr/cm^3)	(MPa)	(psi)	(MPa)	(psi)	(ft/sec)	(ft/sec)	(ksi)	Ratio	
Acoustic	2.73					15,345	9,246	7,601	0.21	
RN-6950-E2										
UCS	2.63	58	8,295							Tensile failure (weak rock sample)
Acoustic	2.63					15,650	8,814	6,951	0.27	
Brazilian	2.60			2	302					Massive bedding (Structural failure)
RN-7003-E3										
UCS	2.76	39	5,679							Structural failure
Acoustic	2.76					15,501	9,965	8,424	0.15	
Brazilian	2.74			11	1,641					Perp to bedding strike (Normal failure)
RN-7003-L2										
UCS	2.75	111	15,963							Tensile failure
Acoustic	2.75					16,239	9,402	8,133	0.25	
RN-7051-L2										
UCS	2.76	106	15,291							Tensile failure
Acoustic	2.76					12,039	9,665	4,094	-0.41	
Brazilian	2.75			14	2,072					Massive bedding (Normal failure)
Brazilian	2.75			15	2,195					Massive bedding (Normal failure)
RN-7051-E1										
UCS	2.76	96	13,778							Tensile failure
Acoustic	2.76					17,468	9,947	9,229	0.26	
Brazilian	2.71			17	2,379					Perp to bedding strike (Normal failure)
Brazilian	2.72			13	1,885					Parl to bedding strike (Normal failure)
RN-7102-L2										
UCS	2.77	141	20,323							Tensile failure
Acoustic	2.77					16,156	9,694	8,502	0.22	
Brazilian	2.77			10	1,479					Massive bedding (Normal failure)
RN-7155-E3										
UCS	2.77	169	24,314							Tensile failure
Acoustic	2.77					18,497	10,064	9,684	0.29	
Brazilian	2.76			12	1,670					Perp to bedding strike (Normal failure)
Brazilian	2.77			14	1,963					Parl to bedding strike (Normal failure)
RN-7155-L2										
Brazilian	2.73			14	1,966					Massive bedding (Normal failure)
Brazilian	2.74			10	1,482					Massive bedding (Normal failure)
RN-7250-L4										
UCS	2.78	102	14,667							Tensile failure
Acoustic	2.78					12,525	9,703	5,252	-0.25	
Brazilian	2.76			8	1,218					Massive bedding (Normal failure)
RN-7300-E2										
UCS	2.75	92	13,314							Tensile failure
Acoustic	2.75					18,614	10,128	9,745	0.29	
Brazilian	2.72			13	1,837					Perp to bedding strike (Normal failure)
RN-7401-E2										
UCS	2.75	111	15,971							Tensile failure
Acoustic	2.75					17,813	9,896	9,207	0.28	
Brazilian	2.73			17	2,400					Perp to bedding strike (Normal failure)
RN-7450-E2										
UCS	2.76	129	18,538							Tensile failure
Acoustic	2.76					17,622	9,790	9,047	0.28	
Brazilian	2.68			8	1,224					Massive bedding (Normal failure)
RN-7503-E1										
UCS	2.74	204	29,342							Tensile failure
Acoustic	2.74					18,267	10,088	9,579	0.28	
RN-7549-E2										

Earth Mechanics Institute									Colorado School Of Mines

Physical Property Testing Results for the tunneling project to evaluate rock strength

Sample No.	Density ρ	Uniaxial Compressive Strength		Brazilian Tensile Strength		Seismic Velocities		Dynamic Constants		Notes
	(gr/cm^3)	(MPa)	(psi)	(MPa)	(psi)	P-wave (ft/sec)	S-wave (ft/sec)	Modulus (ksi)	Poisson's Ratio	
UCS	2.75	113	16,298							Tensile failure
Acoustic	2.75					18,441	9,719	9,113	0.31	
Brazilian	2.74			10	1,428					Massive bedding (Normal failure)
Brazilian	2.76			12	1,778					Massive bedding (Normal failure)
RN-7549-L3										
UCS	2.75	131	18,895							Tensile failure
Acoustic	2.75					16,477	9,612	8,453	0.24	
Brazilian	2.74			13	1,923					Massive bedding (Normal failure)
RN-7604-L1										
UCS	2.78	127	18,268							Tensile failure
Acoustic	2.78					17,744	9,966	9,393	0.27	
RN-7654-L2										
UCS	2.76	118	16,997							Tensile failure
Acoustic	2.76					18,786	10,346	10,142	0.28	
RN-7700-E2										
UCS	2.79	89	12,797							Tensile failure
Acoustic	2.79					18,176	10,127	9,762	0.27	
Brazilian	2.78			6	890					Massive bedding (Structural failure)
RN-7750-E1										
UCS	2.76	95	13,749							Tensile failure
Acoustic	2.76					18,349	10,163	9,762	0.28	
Brazilian	2.74			14	2,064					Massive bedding (Normal failure)
RN-7750-L2										
UCS	2.76	94	13,604							Tensile failure
Acoustic	2.76					17,940	10,025	9,455	0.27	
Brazilian	2.72			16	2,339					Parl to bedding strike (Normal failure)
RN-7800-E2										
UCS	2.76	129	18,558							Tensile failure
Acoustic	2.76					18,351	9,940	9,438	0.29	
Brazilian	2.74			8	1,109					Massive bedding (Normal failure)
RN-7801-L2										
UCS	2.76	139	19,976							Tensile failure
Acoustic	2.76					18,092	10,051	9,525	0.28	
RN-7851-E2										
UCS	2.74	134	19,351							Tensile failure
Acoustic	2.74					18,701	10,519	10,314	0.27	
Brazilian	2.72			11	1,609					Massive bedding (Normal failure)
Brazilian	2.73			13	1,881					Massive bedding (Normal failure)
RN-7896-E1										
Brazilian	2.75			9	1,311					Massive bedding (Normal failure)
Brazilian	2.74			9	1,300					Massive bedding (Normal failure)
RN-7950-L3										
UCS	2.77	94	13,578							Tensile failure
Acoustic	2.77					16,790	9,977	9,075	0.23	
Brazilian	2.74			12	1,746					Massive bedding (Normal failure)
RN-8000-L4										
UCS	2.74	136	19,574							Tensile failure
Acoustic	2.74					15,470	9,282	7,702	0.22	
Brazilian	2.73			13	1,875					Massive bedding (Normal failure)
RN-8103-L2										
UCS	2.77	89	12,756							Structural failure
Acoustic	2.77					17,209	10,107	9,390	0.24	
Brazilian	2.76			13	1,907					Parl to bedding strike (Normal failure)
RN-8103-E3										

Earth Mechanics Institute										Colorado School Of Mines
Physical Property Testing Results for the tunneling project to evaluate rock strength										
Sample	Density	Uniaxial Compressive		Brazilian Tensile		Seismic Velocities		Dynamic Constants		
No.	ρ	Strength		Strength		P-wave	S-wave	Modulus	Poisson's	Notes
	(gr/cm^3)	(MPa)	(psi)	(MPa)	(psi)	(ft/sec)	(ft/sec)	(ksi)	Ratio	
UCS	2.76	113	16,318							Tensile failure
Acoustic	2.76					18,729	10,552	10,442	0.27	
Brazilian	2.75			8	1,132					Massive bedding (Normal failure)
Brazilian	2.75			6	867					Massive bedding (Structural failure)
RN-8150-L1										
Brazilian	2.74			12	1,657					Parl to bedding strike (Normal failure)
Brazilian	2.72			13	1,811					Perp to bedding strike (Normal failure)
RN-8150-E1										
Brazilian	2.73			11	1,516					Perp to bedding strike (Normal failure)
Brazilian	2.73			7	1,004					Parl to bedding strike (Normal failure)
Brazilian	2.73			10	1,368					Perp to bedding strike (Normal failure)
RN-8250-E1										
UCS	2.75	75	10,839							Structural failure
Acoustic	2.75					15,335	9,503	7,914	0.19	
Brazilian	2.73			13	1,836					Perp to bedding strike (Normal failure)
RN-8300-E2										
UCS	2.76	152	21,943							Tensile failure
Acoustic	2.76					18,478	9,972	9,533	0.29	
Brazilian	2.75			8	1,106					Massive bedding (Normal failure)
Brazilian	2.73			8	1,215					Massive bedding (Normal failure)
RN-8350-E3										
Brazilian	2.73			5	769					Parl to bedding strike (Structural failure)
Brazilian	2.72			3	438					Parl to bedding strike (Structural failure)
Brazilian	2.73			9	1,360					Perp to bedding strike (Normal failure)
RN-8656-E4										
UCS	2.73	167	24,035							Normal Failure
Acoustic	2.73					18,557	11,518	11,509	0.19	
Brazilian	2.73			10	1,511					Normal Failure
Brazilian	2.71			16	2,279					Normal Failure
RN-8656-L1										
Brazilian	2.71			18	2,584					Normal Failure
RN-8753B-E3										
UCS	2.72	104	15,006							Normal Failure
RN-8753B-L1										
Brazilian	2.72			12	1,798					Tensile failure with structural effect
RN-8805-L1										
Brazilian	2.70			13	1,921					Structural failure
Brazilian	2.71			8	1,132					Structural failure along bedding
RN-8854-E3										
UCS	2.72	113	16,266							Normal failure, broken in many pieces
Acoustic	2.72					17,012	8,709	7,299	0.32	
Brazilian	2.70			13	1,817					Single Split tensile failure
Brazilian	2.70			7	943					Single Split tensile failure
RN-8903-E2										
Brazilian	2.74			6	861					Structural failure along bedding
Brazilian	2.71			9	1,362					Structural failure
RN-8903-L1										
UCS	2.73	49	7,095							Structural failure
Acoustic	2.73					17,309	11,148	10,407	0.15	
Brazilian	2.72			7	1,042					Tensile failure
RN-9003A-E2										
UCS	2.73	52	7,510							Normal Failure
Acoustic	2.73					18,479	11,395	11,350	0.19	
Brazilian	2.68			7	948					Tensile failure with structural effect

Earth Mechanics Institute									Colorado School Of Mines

Physical Property Testing Results for the tunneling project to evaluate rock strength

Sample No.	Density ρ	Uniaxial Compressive Strength		Brazilian Tensile Strength		Seismic Velocities		Dynamic Constants		Notes
	(gr/cm^3)	(MPa)	(psi)	(MPa)	(psi)	P-wave (ft/sec)	S-wave (ft/sec)	Modulus (ksi)	Poisson's Ratio	
RN-9052-L3										
Brazilian	2.66			16	2,291					Tensile failure
Brazilian	2.67			11	1,606					Tensile failure
RN-9077-E1										
UCS	2.76	136	19,631							Normal failure, bottom remained intact
Acoustic	2.76					19,092	11,326	11,634	0.23	
Brazilian	2.75			13	1,879					Single tensile split
RN-9077-L3										
Brazilian	2.75			10	1,377					Single Tensile Split
Brazilian	2.70			9	1,328					Structural Failure
RN-9116-E3										
UCS	2.72	78	11,171							Structural Failure, along calsite intrusion
Acoustic	2.72					18,914	11,540	11,689	0.20	
Brazilian	2.68			10 ·	1,377					Single Tensile Split
RN-9151A-E3										
UCS	2.71	84	12,155							Structural failure, along calcite intrusions
Brazilian	2.72			6	825					Structural failure, along micrfractures
RN-9203-E3										
UCS	2.76	111	15,971							Structural failure, along the bedding lines
Brazilian	2.75			5	786					Structural failure along the beeding
RN-9203-L4										
Brazilian	2.80			6	839					Tensile failure
Brazilian	2.78			9	1,295					Structural failure along bedding
Brazilian	2.75			5	699					Structural failure
RN-9250-E1										
UCS	2.74	118	16,969							Normal failure, as many pieces
Brazilian	2.71			9	1,342					Tensile failure with tructural effect
RN-9250-L4										
Brazilian	2.74			12	1,682					Tensile failure, broken into pieces
RN-9302-E4										
UCS	2.76	0	14							Structural failure, along the bedding
RN-9302-L3										
Brazilian	2.77			12	1,788					Double split tensile failure
RN-9350-E1										
UCS	2.77	152	21,836							Normal failure,
Acoustic	2.77					18,881	11,328	11,587	0.22	
Brazilian	2.74			17	2,427					Double Split Tensile failure
RN-9398-L3										
UCS	2.79	84	12,047							Structural failure,
RN-9449A-L4										
Brazilian	2.77			13	1,872					Tensile failure with directional properties
Brazilian	2.78			11	1,577					Structural failure, edge failure
RN-9502-E1										
Brazilian	2.74			10	1,385					Tensile failure
Brazilian	2.73			5	719					Structural failure
RN-9748-E1										
UCS	2.81	134	19,338							Normal failure, sevaral pieces
Acoustic	2.81					19,351	11,672	12,431	0.21	
Brazilian	2.77			6	930					Tensile failure
RN-9748-L1										
Brazilian	2.77			14	2,002					Tensile failure
Brazilian	2.76			15	2,200					Tensile failure

Earth Mechanics Institute										Colorado School Of Mines
Physical Property Testing Results for the tunneling project to evaluate rock strength										
Sample No.	Density ρ	Uniaxial Compressive Strength		Brazilian Tensile Strength		Seismic Velocities		Dynamic Constants		Notes
						P-wave	S-wave	Modulus	Poisson's	
	(gr/cm^3)	(MPa)	(psi)	(MPa)	(psi)	(ft/sec)	(ft/sec)	(ksi)	Ratio	
RN-9798-E1										
UCS	2.75	156	22,413							Normal Failure
Acoustic	2.75					19,259	11,804	12,304	0.20	
Brazilian	2.68			7	1,037					structural failure along calcite band
Brazilian	2.71			15	2,116					Tensile failure
RN-9847S-L3										
Brazilian	2.72			19	2,668					Tensile failure
Brazilian	2.75			8	1,193					Structural failure

APPENDIX C

Summary of TBM Performance Analysis

Machine Performance analysis from Strip Charts

Motor Amps	Propel Pressure Thrust	Penetration Rate	Cutter Load
(Amps)	(psi)	(ft/hr)	(lbs)
312	2,085	7.4	63,222
291	2,123	6.7	61,746
295	2,128	7.7	58,856
266	2,100	7.4	54,209
258	2,108	7.4	52,559
259	2,156	7.6	52,120
286	2,170	8.8	53,761
292	1,989	9.6	52,864
285	1,960	10.1	50,476
319	2,203	10.6	55,128
302	2,224	10.0	53,629
313	2,276	10.5	54,319
298	2,125	10.1	52,649
296	2,186	9.9	52,778
273	2,252	9.8	48,989
284	2,105	10.1	50,243
263	2,299	9.7	47,458
275	2,336	9.6	49,707
240	2,114	7.8	41,804
309	2,194	8.8	50,872
315	2,084	9.9	49,059
257	2,204	8.8	42,487
266	2,191	8.5	44,584
206	2,062	6.6	38,847
226	2,282	7.6	39,895
245	2,315	8.4	41,333
284	2,249	5.4	57,875
283	2,320	8.6	47,108
287	2,262	9.3	46,114
248	2,295	7.9	42,953
238	2,272	7.8	41,537
296	2,344	8.7	49,008

Machine Performance analysis from Strip Charts			
Motor Amps	**Propel Pressure Thrust**	**Penetration Rate**	**Cutter Load**
(Amps)	**(psi)**	**(ft/hr)**	**(lbs)**
288	2,275	8.3	48,734
292	2,323	8.7	48,245
293	2,249	8.9	48,030
289	2,302	8.8	47,520
295	2,232	8.9	48,354
282	2,301	8.7	46,756
268	2,280	8.2	45,557
270	2,222	8.5	45,126
270	2,259	10.5	41,123
264	2,226	9.7	41,716
261	2,287	9.6	41,408
273	2,159	9.7	43,065
265	2,265	8.4	44,618
290	2,272	8.1	49,492
244	2,273	9.1	39,768
231	2,204	8.5	38,784
248	2,207	10.5	37,736
287	2,256	11.4	42,033
260	2,228	10.5	39,630
255	2,244	10.7	38,653
260	2,182	10.4	39,824
276	2,212	10.8	41,599
267	2,100	10.9	39,901
275	2,216	11.3	40,513
278	2,198	12.3	39,371
279	2,055	13.0	38,564
213	2,089	10.4	37,485
241	2,238	11.1	41,042
215	2,224	9.4	34,612
288	2,197	11.0	48,938
301	1,973	10.8	51,516
295	2,113	11.4	49,244

Machine Performance analysis from Strip Charts

Motor Amps	Propel Pressure Thrust	Penetration Rate	Cutter Load
(Amps)	(psi)	(ft/hr)	(lbs)
291	2,180	10.8	49,850
299	2,157	10.6	51,775
275	2,222	9.5	50,082
289	2,277	9.3	52,964
265	2,211	9.0	49,501
285	2,234	9.2	52,724
292	2,218	12.3	47,212
280	2,185	9.8	50,295
273	2,083	10.8	47,004
283	1,985	11.2	47,795
290	1,908	12.5	46,534
282	1,913	11.5	46,944
275	2,002	11.6	45,819
289	1,863	11.1	49,004
287	1,994	11.4	48,047
279	1,967	13.1	43,942
300	1,880	11.8	49,414
293	2,154	10.6	50,658
308	1,940	9.3	56,439
298	2,127	10.7	51,338
308	2,236	11.0	52,344
293	2,149	10.8	50,142
290	1,919	11.3	48,623
268	2,012	10.8	46,057
218	1,649	10.9	37,546
202	1,680	11.6	33,947
236	1,669	11.6	39,477
242	1,755	11.2	41,020
210	1,927	10.6	32,070
195	1,829	10.0	30,646
305	2,041	12.4	42,864
312	2,174	12.6	43,483

Machine Performance analysis from Strip Charts			
Motor Amps	**Propel Pressure Thrust**	**Penetration Rate**	**Cutter Load**
(Amps)	**(psi)**	**(ft/hr)**	**(lbs)**
290	2,233	11.0	43,295
290	2,211	11.3	42,657
282	2,229	10.6	42,689
281	2,061	10.4	42,903
269	2,142	9.7	42,594
283	1,999	11.7	46,801
283	2,034	10.9	48,328
283	2,051	10.6	49,093
283	2,150	11.2	47,749
274	2,066	10.3	48,056
254	2,025	11.0	43,317
224	1,963	9.1	41,828
258	2,012	10.3	45,329
269	1,987	10.8	46,123
258	2,182	13.0	40,746
281	2,227	13 3	43,856
238	2,091	11.3	40,171
253	1,708	11.6	42,021
270	1,986	11.3	45,462
239	1,968	10.8	41,183
238	1,998	9.6	43,213
247	2,052	9.9	44,220
267	2,166	10.6	46,263
230	1,913	12.3	37,284
248	1,922	12.8	39,448
247	1,923	12.3	40,063
224	2,029	11.7	37,312
218	2,009	10.5	38,244
213	1,976	10.1	37,998
208	1,974	9.7	37,822
231	1,979	10.5	40,346
214	1,955	10.0	38,190

Machine Performance analysis from Strip Charts

Motor Amps	Propel Pressure Thrust	Penetration Rate	Cutter Load
(Amps)	(psi)	(ft/hr)	(lbs)
211	1,978	10.0	37,781
225	1,900	11.0	38,402
175	2,003	8.6	33,769
224	2,251	9.0	41,966
222	2,096	9.3	40,977
240	2,144	8.8	45,283
252	2,180	9.4	46,163
203	2,123	8.3	39,648
241	2,126	9.4	44,254
248	2,223	9.8	44,552
259	2,231	10.0	46,173
219	2,161	9.5	40,172
204	2,190	8.8	38,846
198	2,305	8.1	39,181
212	2,334	8.8	40,274
221	2,269	8.8	41,906
208	2,199	9.0	39,093
243	2,255	10.3	42,661
252	2,146	11.2	42,653
243	2,257	10.4	42,512
280	2,078	12.3	45,267
230	2,141	11.0	39,252
213	2,115	10.8	36,826
264	2,219	13.4	41,105
224	1,969	11.4	37,790
228	2,178	11.1	38,885
265	2,089	11.7	44,020
235	1,997	10.1	41,811
259	1,924	11.2	43,695
229	1,848	11.7	38,121
230	1,897	11.1	39,154
229	1,873	11.9	37,741

Machine Performance analysis from Strip Charts			
Motor Amps	Propel Pressure Thrust	Penetration Rate	Cutter Load
(Amps)	(psi)	(ft/hr)	(lbs)
229	1,908	11.9	37,813
238	1,896	11.7	39,593
221	1,999	10.5	38,580
299	1,926	15.9	42,921
254	1,996	14.1	38,552
256	2,001	15.3	37,459
211	1,271	11.7	26,402
199	1,491	10.2	26,553
262	1,760	12.8	31,307
238	1,280	11.5	29,960
235	1,674	10.5	30,737
236	1,483	11.2	30,036
248	1,603	11.3	31,444
231	1,510	10.5	30,265
230	1,600	10.4	30,349
231	1,887	10.4	40,415
222	1,845	10.4	38,978
222	1,836	10.2	39,248
233	2,046	11.6	38,966
221	2,005	12.5	35,608
217	1,812	12.8	34,760
223	1,880	14.2	33,906
208	1,914	13.3	32,708
233	1,902	14.4	35,110
259	2,013	9.5	41,248
279	2,038	10.8	41,975
294	2,132	10.6	44,506
266	2,061	9.4	42,580
263	1,958	9.3	48,400
251	1,939	10.3	44,069
263	2,050	11.0	44,801
270	2,019	9.8	48,593

Machine Performance analysis from Strip Charts

Motor Amps (Amps)	Propel Pressure Thrust (psi)	Penetration Rate (ft/hr)	Cutter Load (lbs)
301	2,180	9.7	54,174
267	2,083	9.1	49,579
296	1,889	9.8	52,943
299	2,131	10.6	51,692
292	2,003	9.9	52,112
247	2,066	8.7	46,813
287	1,852	9.8	51,487
295	2,064	9.9	52,680
296	2,016	9.6	53,500
295	2,123	9.7	53,071
299	1,474	9.5	54,253
318	1,636	10.2	55,911
319	1,972	10.0	56,495
308	1,791	9.8	55,107
262	1,939	8.8	49,341
232	1,938	7.9	46,033
255	2,059	8.9	47,776
274	1,997	9.4	50,122
242	1,944	9.0	45,288
271	2,044	11.3	45,536
269	2,015	12.4	43,344
271	1,997	12.3	43,826
273	2,033	12.1	44,516
287	2,009	11.6	47,668
263	2,097	11.6	43,642
283	1,967	10.5	49,209
271	1,991	11.0	46,213
268	2,003	10.7	46,273
292	1,945	8.0	57,285
295	2,152	8.9	55,112
317	2,237	9.3	58,121
256	2,209	7.9	50,627

Machine Performance analysis from Strip Charts			
Motor Amps	Propel Pressure Thrust	Penetration Rate	Cutter Load
(Amps)	(psi)	(ft/hr)	(lbs)
241	2,171	7.3	49,373
258	2,105	8.0	50,819
232	2,176	8.0	45,798
268	2,149	8.2	52,182
262	2,232	8.1	51,161
289	2,226	9.1	53,628
294	2,234	9.3	53,890
292	2,243	8.9	54,660
312	2,214	9.2	57,494
284	2,166	8.8	53,492
279	2,114	9.1	51,695
269	2,156	9.7	48,505
240	2,176	8.6	45,867
263	2,284	8.6	50,061
240	2,190	8.5	46,088
207	2,000	7.6	42,059
201	2,199	6.4	43,968
202	2,260	6.6	43,753
181	2,060	6.1	40,622
223	2,260	8.1	43,748
225	1,925	8.4	43,494
255	2,036	10.7	44,099
255	2,247	9.9	45,657
254	2,188	10.3	44,639
172	2,212	8.0	34,295
221	2,204	8.6	42,220
238	2,069	8.7	45,108
181	2,202	4.9	44,349
231	2,236	5.9	52,259
248	2,183	6.8	52,703
269	2,157	7.0	56,100
272	2,206	6.9	57,157

Machine Performance analysis from Strip Charts			
Motor Amps	**Propel Pressure Thrust**	**Penetration Rate**	**Cutter Load**
(Amps)	(psi)	(ft/hr)	(lbs)
263	2,210	6.6	56,322
250	2,212	6.5	54,128
261	2,192	6.6	56,062
243	2,203	5.8	55,201
266	2,180	7.0	48,671
259	1,996	7.2	46,775
241	2,237	6.5	45,637
260	2,215	7.0	47,486
235	2,165	6.9	43,459
208	2,195	6.3	39,894
248	2,189	7.7	43,650
253	2,196	8.4	42,670
272	2,180	8.8	44,865
275	2,215	7.6	55,281
277	2,161	7.7	55,320
265	2,227	7.8	52,685
225	1,981	7.8	44,901
159	1,838	6.8	34,279
200	1,825	8.7	38,197
291	2,058	9.5	52,857
294	2,221	8.6	56,052
297	2,159	7.8	58,931
270	2,088	7.5	54,832
289	2,127	6.9	60,779
310	2,200	7.1	63,974
332	2,109	7.2	68,311
279	2,236	7.0	58,402
272	2,207	7.7	54,281
281	2,162	8.2	54,787
279	1,922	8.2	54,290
290	2,238	6.5	62,317
301	2,106	7.0	62,799

Machine Performance analysis from Strip Charts			
Motor Amps	**Propel Pressure Thrust**	**Penetration Rate**	**Cutter Load**
(Amps)	(psi)	(ft/hr)	(lbs)
292	2,236	7.2	60,222
273	2,200	7.0	56,834
291	2,228	6.6	62,104
304	2,231	6.9	63,769
298	2,171	6.9	62,553
301	2,224	6.9	63,173
307	2,263	6.8	64,938
287	2,205	8.2	55,693
245	2,174	7.2	50,690
272	2,172	7.3	55,801
271	2,163	5.3	63,878
249	2,159	6.3	54,680
274	2,222	7.5	55,593
282	2,117	7.0	58,713
296	2,198	6.9	62,028
277	2,142	7.5	56,120
305	2,100	8.5	58,397
322	2,102	8.8	60,535
315	2,069	9.4	57,526
307	2,117	9.1	56,851
300	2,059	9.7	54,143
286	2,081	9.4	52,423
289	2,143	9.1	53,769
302	2,085	8.8	56,790
298	2,144	9.0	55,615
251	2,093	7.3	51,459
291	2,079	8.2	56,535
285	2,160	8.5	54,442
256	2,067	7.5	51,855
278	2,156	8.9	52,032
282	1,981	8.6	53,608
275	2,038	9.5	50,103

Machine Performance analysis from Strip Charts			
Motor Amps	**Propel Pressure Thrust**	**Penetration Rate**	**Cutter Load**
(Amps)	**(psi)**	**(ft/hr)**	**(lbs)**
314	1,963	10.4	54,641
281	2,030	10.2	49,408
252	1,851	10.2	44,541
294	1,739	10.0	52,356
261	1,706	8.5	50,033
307	1,724	8.9	57,477
294	1,810	8.3	56,976
282	2,034	8.0	55,457
296	2,175	7.7	59,208
309	2,090	8.2	59,983
297	2,041	7.9	58,588
320	2,092	8.1	62,310
304	2,073	8.4	58,419
316	2,136	8.5	60,277
295	2,103	8.3	56,856
344	2,146	8.7	64,509
320	2,122	8.2	62,060
294	2,176	8.0	57,728
276	2,214	7.8	54,844
270	2,161	6.7	57,305
240	2,053	9.2	44,610
264	1,979	9.7	47,703
254	1,932	9.6	46,167
218	1,815	7.5	44,308
197	1,983	7.3	40,607
178	1,938	6.3	39,463
292	2,009	8.9	54,812
289	1,924	9.5	52,521
296	1,932	8.8	55,779
278	1,867	8.5	53,182
277	1,840	9.1	51,567
276	1,888	8.4	53,206

Machine Performance analysis from Strip Charts

Motor Amps	Propel Pressure Thrust	Penetration Rate	Cutter Load
(Amps)	(psi)	(ft/hr)	(lbs)
277	1,974	8.3	53,539
273	1,859	7.8	54,321
269	2,045	9.1	49,950
258	1,882	9.0	36,082
231	1,871	8.5	33,403
225	1,899	9.0	31,654
244	2,012	8.9	34,340
245	2,037	6.8	38,949
247	1,884	8.0	36,493
199	1,885	6.5	32,445
220	1,908	4.6	41,440
276	2,137	10.1	48,822
293	2,132	9.9	52,218
285	2,104	9.4	52,233
309	2,108	9.9	55,117
319	2,152	10.4	55,591
279	2,164	9.9	49,846
230	1,857	9.1	42,876
242	1,829	10.7	41,968
216	1,512	9.8	39,018
276	2,148	7.7	55,283
274	2,194	7.0	57,039
241	2,174	6.8	51,137
258	2,100	7.0	53,812
297	2,097	7.8	59,030
284	2,140	7.9	56,065
289	2,127	8.0	56,967
301	2,142	8.5	57,415
295	2,146	8.7	55,748
237	1,369	7.5	48,317
241	1,325	7.6	48,544
273	1,406	7.8	54,293

Machine Performance analysis from Strip Charts

Motor Amps (Amps)	Propel Pressure Thrust (psi)	Penetration Rate (ft/hr)	Cutter Load (lbs)
272	1,359	7.9	53,667
230	1,292	7.1	47,818
276	1,303	8.4	53,140
286	1,294	9.3	52,668
304	1,341	8.9	57,036
286	1,392	8.6	54,334
193	1,212	5.7	44,393
224	1,191	6.8	47,424
209	1,276	6.5	45,242
221	1,316	6.5	47,903
232	1,284	6.4	50,714
207	1,223	6.1	46,176
246	1,317	7.5	49,869
221	1,276	7.2	45,894
221	1,314	5.7	44,340
199	1,344	5.1	42,125
196	1,245	5.0	41,769
242	1,242	6.8	44,815
233	1,211	6.6	43,902
237	1,297	6.7	44,246
224	1,251	7.3	40,279
232	1,276	6.7	43,215
252	1,295	6.6	47,174
246	1,212	7.4	43,935
242	1,235	7.0	44,454
239	1,287	6.7	44,746
238	1,274	6.7	44,310
244	1,284	7.2	44,145
206	1,216	5.8	41,189
242	1,215	5.4	49,598
191	1,173	4.4	42,877
202	1,186	4.8	43,531

Machine Performance analysis from Strip Charts

Motor Amps	Propel Pressure Thrust	Penetration Rate	Cutter Load
(Amps)	(psi)	(ft/hr)	(lbs)
209	2,116	8.5	40,177
200	1,862	8.8	37,903
224	1,854	10.3	39,401
187	1,874	9.1	35,162
245	2,294	10.3	43,114
212	2,122	9.5	38,950
259	2,162	10.2	45,744
235	2,326	10.1	41,832
225	2,137	8.9	42,290
274	2,076	10.2	48,335
281	1,959	10.0	49,979
239	1,925	9.6	43,412
247	1,840	9.9	44,275
244	1,914	9.8	43,970
218	1,865	8.9	41,002
235	1,835	9.6	42,659
242	1,817	9.4	44,450
229	1,804	9.4	42,080
249	1,950	8.6	47,621
260	1,993	10.4	45,401
235	2,052	9.0	44,062
230	2,086	8.5	44,194
214	2,064	7.1	44,659
233	2,064	7.4	47,627
224	2,077	7.3	46,009
238	2,113	7.9	47,327
254	1,765	8.9	47,823
313	2,287	10.6	54,105
295	2,292	10.2	51,850
313	2,329	10.3	54,923
303	2,376	10.1	53,555
271	2,218	9.7	49,039

Machine Performance analysis from Strip Charts			
Motor Amps	Propel Pressure Thrust	Penetration Rate	Cutter Load
(Amps)	(psi)	(ft/hr)	(lbs)
222	2,070	9.1	41,365
239	2,200	9.8	43,097
303	2,352	10.1	53,707
291	2,238	10.5	50,486
198	2,012	6.7	42,503
191	2,048	6.2	42,426
213	2,123	7.4	43,596
226	1,983	7.5	45,962
222	2,060	8.4	42,911
195	1,999	8.2	38,382
210	2,158	8.2	41,130
229	2,192	7.9	45,516
234	2,033	9.0	43,790
266	1,628	9.2	49,228
268	2,151	8.0	52,902
260	1,933	7.8	51,846
288	2,055	9.6	52,239
277	2,054	8.4	53,351
230	2,069	6.1	51,139
260	2,121	6.9	54,648
201	2,191	5.7	46,183
204	1,976	6.2	45,279
245	2,152	5.7	55,959
264	2,202	6.2	58,157
265	2,000	7.4	54,019
303	2,061	8.2	58,759
218	2,224	5.8	43,609
250	2,205	6.0	48,895
274	2,232	6.6	51,462
244	2,165	6.3	46,849
200	2,072	5.4	41,343
222	2,220	6.2	49,177

Machine Performance analysis from Strip Charts

Motor Amps	Propel Pressure Thrust	Penetration Rate	Cutter Load
(Amps)	(psi)	(ft/hr)	(lbs)
216	2,200	6.0	48,561
239	2,096	6.8	50,534
235	2,138	6.8	49,705
236	2,154	6.7	50,395
247	2,065	7.7	49,631
217	2,057	7.1	45,138
310	2,122	9.7	55,703
273	2,046	8.5	52,177
149	2,082	5.0	36,386
177	2,074	6.6	38,247
225	2,182	7.7	45,312
197	2,266	6.0	44,255
238	2,233	7.7	47,641
228	2,083	8.5	43,839
214	2,138	6.3	46,967
232	2,231	7.4	47,286
237	2,113	8.1	46,632
233	2,174	7.6	47,184
198	2,279	6.2	44,018
199	1,689	5.8	45,254
228	2,344	6.3	50,076
220	2,246	6.2	48,536
201	2,201	5.5	46,808
186	2,108	5.6	43,315
206	2,006	5.6	47,512
200	2,271	5.4	46,930
299	2,201	8.3	57,793
298	2,236	9.2	54,908
292	2,310	8.3	56,483
245	2,259	6.5	52,890
230	2,262	6.5	49,732
310	2,026	7.7	61,890

Machine Performance analysis from Strip Charts			
Motor Amps	Propel Pressure Thrust	Penetration Rate	Cutter Load
(Amps)	(psi)	(ft/hr)	(lbs)
294	2,044	7.7	58,884
286	1,943	8.2	55,699
284	1,814	8.9	53,244
280	1,855	9.2	51,751
283	1,949	8.8	46,688
264	1,883	8.6	44,060
249	1,923	8.1	42,814
271	1,616	7.6	47,839
227	1,322	7.6	45,769
254	1,435	8.4	48,988
274	1,419	10.2	36,313
264	1,528	9.3	36,557
279	1,772	7.3	42,815
298	1,813	7.3	45,679
286	1,721	7.0	59,459
328	1,786	7.8	65,052
356	1,891	8.3	68,182
286	1,895	8.3	48,463
297	1,882	8.7	49,165
300	1,863	8.7	49,788
314	1,855	10.1	48,616
314	1,600	11.1	46,512
302	1,764	11.5	43,940
289	1,802	9.6	45,773
279	1,723	8.9	45,900
301	1,885	10.2	46,372
281	2,220	7.5	56,831
299	2,314	8.1	58,392
292	2,142	8.1	57,048
256	2,091	7.2	53,028
250	2,008	6.7	53,367
242	2,033	6.5	52,431

Machine Performance analysis from Strip Charts

Motor Amps	Propel Pressure Thrust	Penetration Rate	Cutter Load
(Amps)	(psi)	(ft/hr)	(lbs)
249	1,945	7.0	52,145
265	2,014	7.3	54,449
265	2,019	6.9	55,831
275	1,878	8.9	45,007
291	1,858	8.6	48,321
289	1,860	9.8	45,313
261	1,791	8.6	43,635
313	1,695	11.7	45,173
309	1,901	8.2	60,000
330	2,052	8.5	62,940
285	2,119	7.5	57,591
279	2,087	7.5	56,659
282	1,698	7.2	58,099
322	1,600	11.7	53,126
302	1,782	10.8	51,894
317	1,816	11.0	53,779
320	1,913	10.9	54,722
293	1,919	10.8	43,958
308	1,789	11.1	45,645
244	1,738	9.3	39,305
265	1,751	12.1	37,856
253	1,682	10.8	38,200
257	1,735	9.2	41,643
240	1,561	9.4	38,506
242	1,590	9.6	38,543
285	1,699	10.9	42,635
274	1,664	8.9	44,941
308	1,700	11.5	44,931
324	1,570	12.0	46,268
312	1,484	12.4	43,904
314	1,883	9.1	58,030
275	1,832	9.0	51,222

Machine Performance analysis from Strip Charts

Motor Amps	Propel Pressure Thrust	Penetration Rate	Cutter Load
(Amps)	(psi)	(ft/hr)	(lbs)
207	1,299	8.1	40,813
218	1,696	8.5	41,878
197	1,576	8.4	38,157
221	1,235	12.5	31,259
233	1,458	13.6	31,516
274	36	9.1	44,437
249	38	8.9	40,887
273	39	8.5	45,703
290	39	7.9	50,076
311	37	8.4	52,166
299	41	7.9	58,964
315	41	9.0	58,600
249	36	6.2	54,717
269	35	6.8	56,815
271	1,920	9.2	50,035
303	1,712	11.3	50,902
287	1,817	9.4	52,329
326	1,994	9.7	58,556
320	1,848	10.4	55,904
241	1,433	9.4	44,250
336	2,103	8.1	65,550
364	2,191	9.2	66,468
363	2,183	9.5	65,555
331	1,982	9.6	59,647
288	1,953	8.7	54,392
279	1,938	8.4	53,719
280	1,872	8.7	52,927
342	1,936	9.3	62,516
314	1,957	9.4	57,367
340	2,213	8.7	64,070
307	2,241	8.6	58,432
220	2,378	8.9	41,507

Machine Performance analysis from Strip Charts			
Motor Amps	Propel Pressure Thrust	Penetration Rate	Cutter Load
(Amps)	(psi)	(ft/hr)	(lbs)
339	2,350	8.6	64,315
333	2,296	8.6	63,348
198	2,181	6.3	43,463
225	2,156	7.0	47,289
194	2,145	6.2	43,037
256	2,196	7.9	50,739
293	2,152	8.7	55,343
314	2,187	8.1	61,181
320	2,176	9.5	58,133
314	2,265	9.0	58,427
321	2,315	9.6	57,942
285	2,261	8.8	53,668
289	2,227	9.2	53,330
293	2,114	9.6	52,942
275	2,006	10.2	48,431
191	1,962	8.0	33,190
221	1,958	7.1	40,260
202	1,823	9.1	33,035
276	1,697	10.4	42,246
284	1,913	8.3	48,110
290	2,014	7.7	50,698
232	1,950	7.0	42,540
238	1,989	7.1	43,399
232	2,069	7.0	48,598
265	2,200	8.5	50,663
285	2,050	9.5	51,816
278	1,861	11.4	46,589
245	1,871	9.2	45,375
269	1,973	10.4	47,048
258	1,796	8.2	50,317
231	1,738	8.8	43,738
235	1,654	11.2	39,913

Machine Performance analysis from Strip Charts

Motor Amps	Propel Pressure Thrust	Penetration Rate	Cutter Load
(Amps)	(psi)	(ft/hr)	(lbs)
263	1,700	10.7	45,413
242	1,678	10.4	42,499
266	1,645	8.2	51,685
268	1,845	9.0	49,962
299	1,686	10.3	52,425
274	1,665	9.0	51,157
210	2,039	7.6	37,182
207	2,057	7.3	37,300
249	1,997	8.0	42,823
248	1,818	9.1	40,477
210	2,126	8.5	35,319
249	1,935	9.5	39,778
251	1,966	8.6	41,915
261	2,105	7.5	46,378
234	2,043	6.1	52,167
263	2,029	8.1	51,426
257	2,020	7.6	51,819
270	2,063	7.6	54,394
225	1,951	6.3	49,249
243	1,866	8.4	41,117
225	1,993	8.3	38,262
211	2,026	8.8	35,031
266	2,081	10.3	40,870
205	1,966	9.0	33,727
257	2,059	10.0	40,074
252	2,228	6.9	46,365
231	1,830	8.0	40,044
227	1,922	8.0	39,138
225	2,033	8.4	38,033
231	2,059	6.4	44,005
205	2,118	6.9	37,928
279	2,076	8.7	39,650

Machine Performance analysis from Strip Charts

Motor Amps	Propel Pressure Thrust	Penetration Rate	Cutter Load
(Amps)	(psi)	(ft/hr)	(lbs)
293	1,874	8.0	43,160
320	1,843	8.1	46,698
282	1,922	7.0	44,098
304	1,971	8.1	44,404
224	1,841	8.1	33,012
254	1,856	9.6	34,552
259	1,906	8.7	36,870
321	1,878	9.6	43,488
331	1,842	9.4	45,227
279	1,989	7.1	57,739
268	2,034	6.5	57,884
258	1,939	6.3	56,446
271	1,888	7.2	48,756
295	1,923	7.9	50,965
279	1,851	7.4	56,986
276	1,964	8.0	54,394
232	1,859	7.1	48,333
250	1,682	8.6	47,731
201	2,048	7.0	42,276
232	2,085	8.7	44,161
240	1,925	8.4	46,401
207	2,113	7.4	42,409
208	2,026	7.6	42,117
251	2,038	9.0	47,075
221	2,122	7.9	43,996
228	1,964	12.3	32,452
257	1,988	12.5	36,232
242	1,947	12.4	34,200
269	2,027	10.4	41,068
266	2,015	12.7	37,128
267	2,024	11.7	38,760
260	1,949	8.6	49,593

Machine Performance analysis from Strip Charts			
Motor Amps	**Propel Pressure Thrust**	**Penetration Rate**	**Cutter Load**
(Amps)	**(psi)**	**(ft/hr)**	**(lbs)**
234	1,858	8.3	45,520
253	1,845	9.9	45,276
199	1,994	8.2	34,161
196	1,986	6.8	36,642
218	2,024	8.0	37,733
199	1,927	5.4	40,981
319	1,929	10.1	56,381
253	1,813	10.3	44,546
223	1,832	9.6	40,652
250	1,867	14.3	37,823
208	1,834	13.4	32,519
220	1,915	13.9	33,884
211	2,010	6.4	46,066
228	2,050	6.5	49,346
284	2,058	7.8	56,543
240	2,108	7.0	50,405
243	2,116	7.6	49,094
219	2,088	7.6	44,481
227	1,985	8.2	44,394
247	1,829	8.6	47,079
210	2,039	6.8	44,849
232	2,063	6.4	50,563
215	1,990	5.9	48,465
208	1,932	8.9	34,333
198	1,831	7.9	34,472
246	1,887	8.1	42,231
246	1,956	8.1	42,093
196	1,769	8.0	33,922
227	1,616	9.7	35,976
218	1,451	10.2	33,739
215	1,643	8.2	36,853
220	1,726	8.8	36,392

Machine Performance analysis from Strip Charts

Motor Amps	Propel Pressure Thrust	Penetration Rate	Cutter Load
(Amps)	(psi)	(ft/hr)	(lbs)
226	1,850	8.7	42,942
231	1,882	7.6	46,535
235	1,849	8.8	44,556
226	1,787	8.9	42,496
172	1,937	6.1	38,536
200	2,008	6.9	42,204
180	2,114	6.7	38,649
211	2,090	7.0	44,275
148	2,041	5.4	35,069
178	2,134	5.9	40,465
185	2,054	6.9	39,102
168	1,984	5.6	39,094
190	1,929	7.3	39,188
163	2,069	6.7	35,065
223	1,981	6.5	48,314
189	2,103	6.2	41,821
198	2,086	4.8	48,972
241	2,013	7.2	49,679
253	1,909	5.1	60,508
283	1,944	7.9	55,994
299	2,040	7.9	59,177

APPENDIX D

Summary of Collected data for Regression Analysis

Rock Strength (psi)	Tensile Strength (psi)	UCS (psi)	Size Factor S	RQD (%)	Elastic Modulus (ksi)	Poisson's Ratio ν	Est RSI(Lin) (psi)
24550	1092	20411	0.097	80.00	9545	0.24377	23042
17091	1845	13108	0.036	60.00	11327	0.19161	16548
22978	1936	18864	0.062	75.00	9167	0.21882	18884
17179	1370	13194	0.036	60.00	9956	0.20068	16081
17704	2077	13704	0.036	60.00	8843	0.11043	15743
19904	1548	15849	0.062	70.00	9238	0.2306	18903
26194	1023	22032	0.097	85.00	9570	0.24065	23052
18894	1510	14862	0.062	65.00	8097	0.26458	18502
16449	1260	12486	0.036	60.00	8514	0.19626	15595
13575	887	9724	0.020	50.00	10390	0.20571	14459
15223	1161	11303	0.036	55.00	8422	0.23646	15546
11052	1276	7343	0.020	45.00	7008	0.18512	13325
25333	1712	21183	0.097	80.00	9141	0.25758	22900
13482	2334	9635	0.036	55.00	10786	0.06392	16420
9453	1060	5871	0.015	45.00	5476	0.13302	12155
11630	1404	7883	0.020	45.00	9311	0.20221	14096
11417	1548	7684	0.020	45.00	7313	0.1682	13435
10816	1056	7129	0.015	45.00	7559	0.19036	12835
12515	817	8717	0.020	50.00	8220	0.17822	13737
15963	1740	12016	0.036	60.00	9583	0.23095	15941
19676	1159	15626	0.062	65.00	10767	0.23889	19416
12686	803	8879	0.020	50.00	9493	0.21471	14152
10551	1117	6878	0.015	45.00	9377	0.17071	13458
22530	1911	18423	0.062	75.00	12233	0.23175	19915
11963	1547	8196	0.020	50.00	10349	0.22711	14436
13525	2326	9676	0.020	50.00	10401	0.16685	14479
25028	1631	20882	0.097	80.00	10274	0.31235	23259
18993	1514	14959	0.062	65.00	8429	0.2696	18612
10608	1074	6931	0.015	50.00	11141	0.25758	14016
10775	471	7086	0.015	45.00	10333	0.18538	13774
23349	1610	19229	0.062	75.00	10866	0.17633	19477
4900	1779	2029	0.002	30.00	8608	0.18221	11674
19824	1246	15771	0.062	65.00	6853	0.14272	18135
19129	2015	15092	0.062	65.00	6962	0.19219	18150
15074	1334	11159	0.036	55.00	7502	0.17614	15261
14695	1791	10795	0.036	55.00	5908	0.19524	14714
20368	1017	16303	0.062	70.00	7167	0.16685	18230
16050	2018	12100	0.036	60.00	8834	0.23277	15687
19271	1270	15230	0.062	65.00	8510	0.22655	18658
20648	1224	16577	0.062	70.00	10386	0.27876	19270

Rock Strength (psi)	Tensile Strength (psi)	UCS (psi)	Size Factor S	RQD (%)	Elastic Modulus (ksi)	Poisson's Ratio ν	Est RSI(Lin) (psi)
17240	846	13253	0.036	60.00	10638	0.29928	16268
8965	1310	5429	0.015	40.00	10543	0.25206	13817
18211	1506	14197	0.036	65.00	9875	0.24692	16033
14185	1285	10306	0.036	55.00	8699	0.22607	15645
22673	1639	18564	0.062	75.00	11792	0.20571	19777
14807	541	10903	0.036	55.00	9824	0.27296	16004
15178	2581	11259	0.036	55.00	10161	0.29109	16111
17598	1456	13601	0.036	60.00	12751	0.23673	17009
22305	1560	18202	0.062	75.00	10270	0.24038	19247
28754	1708	24562	0.236	92.00	10322	0.30695	39410
29422	2260	25223	0.236	92.00	10170	0.27852	39371
18017	2003	14008	0.036	65.00	7080	0.21093	15104
22013	2210	17915	0.097	80.00	12182	0.22775	23940
20111	1689	16051	0.062	70.00	10087	0.26458	19175
16703	995	12732	0.036	70.00	9438	0.24985	15884
18618	1743	14593	0.062	65.00	12193	0.24568	19895
13294	1542	9456	0.036	70.00	10095	0.27852	16093
21614	2045	17524	0.062	75.00	11899	0.21441	19809
18840	1957	14810	0.062	75.00	9646	0.27679	19021
5055	2028	2144	0.020	75.00	9765	0.29109	14210
20077	2241	16018	0.062	75.00	9013	0.22343	18830
17209	1814	13223	0.036	60.00	9765	0.29475	15975
27256	2235	23081	0.097	85.00	9635	0.11142	23130
27972	1646	23789	0.097	85.00	9846	0.24377	23144
12507	2051	8709	0.056	85.00	10053	0.27493	18400
22559	1493	18452	0.097	85.00	10201	0.30695	23237
14291	1309	10408	0.036	60.00	8710	0.24419	15640
12068	302	8295	0.020	50.00	6951	0.26771	13269
14722	1641	10821	0.036	55.00	8279	0.19787	15515
18558	2131	14535	0.062	65.00	9229	0.26006	18887
24461	1479	20323	0.097	80.00	8502	0.21875	22700
28503	1771	24314	0.135	92.00	9684	0.28971	27525
17303	1837	13314	0.036	65.00	9745	0.28971	15970
20029	2400	15971	0.062	65.00	9207	0.27679	18872
22647	1224	18538	0.062	75.00	9047	0.27679	18818
33578	1876	29342	0.189	100.00	9579	0.28061	33712
21689	1763	17597	0.097	80.00	8783	0.27491	22771
22372	1630	18268	0.062	75.00	9393	0.2696	18938
21077	1589	16997	0.062	70.00	10142	0.28233	19186
16770	890	12797	0.036	60.00	9762	0.27493	15983

Rock Strength (psi)	Tensile Strength (psi)	UCS (psi)	Size Factor S	RQD (%)	Elastic Modulus (ksi)	Poisson's Ratio ν	Est RSI(Lin) (psi)
17677	2202	13677	0.036	60.00	9609	0.27586	15930
23388	1109	19267	0.062	75.00	9481	0.28458	18962
23473	1750	19351	0.062	75.00	10314	0.26857	19250
17575	1746	13578	0.036	65.00	9075	0.22711	15771
23700	1875	19574	0.097	80.00	7702	0.21875	22430
18560	1520	14537	0.062	65.00	9916	0.25212	19123
14741	1836	10839	0.036	55.00	7914	0.18824	15395
26103	1160	21943	0.097	85.00	9533	0.29453	23016
28221	2240	24035	0.097	90.00	11509	0.18665	23731
20330	1380	16266	0.062	70.00	7299	0.32245	18208
10785	1202	7095	0.015	45.00	10407	0.14556	13817
11231	1088	7510	0.020	45.00	11350	0.19319	14789
23758	1914	19631	0.097	80.00	11634	0.2285	23755
15086	1377	11171	0.036	55.00	11689	0.20343	16665
25995	2427	21836	0.097	85.00	11587	0.21875	23743
23460	1516	19338	0.097	80.00	12431	0.21406	24030
26579	2116	22413	0.097	85.00	12304	0.19917	23994

Rock Strength Log	Tensile Strength Log	UCS Log	s Log	RQD Log	Elastic Modulus Log	Poisson's Ratio Log	Est RSI (pow) (psi)
10.1085	6.99577	9.92383	-2.3333	4.38203	9.16373	-1.4115	25490
9.74629	7.52023	9.48098	-3.3333	4.09434	9.33493	-1.6523	16891
10.0423	7.56838	9.84501	-2.7778	4.31749	9.12341	-1.5195	20993
9.75146	7.22257	9.48752	-3.3333	4.09434	9.20597	-1.6061	16630
9.78157	7.63868	9.52544	-3.3333	4.09434	9.08735	-2.2034	17101
9.89868	7.3446	9.67086	-2.7778	4.2485	9.13106	-1.4671	20936
10.1733	6.93049	10.0003	-2.3333	4.44265	9.16637	-1.4244	25518
9.84658	7.31962	9.60656	-2.7778	4.17439	8.9992	-1.3296	20483
9.70801	7.13887	9.43236	-3.3333	4.09434	9.04946	-1.6283	16404
9.51602	6.78784	9.18235	-3.8889	3.91202	9.24864	-1.5813	13028
9.63058	7.05704	9.33282	-3.3333	4.00733	9.03861	-1.442	16186
9.31035	7.15149	8.9015	-3.8889	3.80666	8.85481	-1.6868	12627
10.1399	7.44542	9.96095	-2.3333	4.38203	9.12055	-1.3564	25291
9.50912	7.75534	9.17316	-3.3333	4.00733	9.28597	-2.7502	18074
9.15413	6.96602	8.67778	-4.2222	3.80666	8.60812	-2.0172	10867
9.36131	7.24708	8.97246	-3.8889	3.80666	9.13897	-1.5984	12904
9.34287	7.34472	8.9469	-3.8889	3.80666	8.89739	-1.7826	12759
9.28881	6.96215	8.87193	-4.2222	3.80666	8.93053	-1.6589	10950
9.43469	6.70564	9.07303	-3.8889	3.91202	9.01435	-1.7248	12856
9.67801	7.46164	9.39399	-3.3333	4.09434	9.16773	-1.4655	16416
9.88716	7.05531	9.65669	-2.7778	4.17439	9.28427	-1.4317	21200
9.44828	6.68835	9.09144	-3.8889	3.91202	9.15828	-1.5385	12877
9.26397	7.0184	8.83608	-4.2222	3.80666	9.14606	-1.7678	11262
10.0226	7.55538	9.82136	-2.7778	4.31749	9.41188	-1.4621	21507
9.38956	7.34407	9.0114	-3.8889	3.91202	9.24462	-1.4823	12938
9.5123	7.75191	9.1774	-3.8889	3.91202	9.24964	-1.7907	13210
10.1277	7.39695	9.94664	-2.3333	4.38203	9.23734	-1.1636	25256
9.85182	7.32219	9.61307	-2.7778	4.17439	9.0394	-1.3108	20537
9.26938	6.97915	8.84376	-4.2222	3.91202	9.31842	-1.3564	11145
9.28502	6.15486	8.86588	-4.2222	3.80666	9.24306	-1.6853	11307
10.0583	7.38399	9.86417	-2.7778	4.31749	9.29338	-1.7354	21648
8.497	7.48381	7.6153	-6.4444	3.4012	9.06048	-1.7026	4146
9.89467	7.12769	9.66593	-2.7778	4.17439	8.83243	-1.9469	20992
9.85897	7.60837	9.62192	-2.7778	4.17439	8.84819	-1.6492	20615
9.6207	7.19611	9.32	-3.3333	4.00733	8.92287	-1.7365	16320
9.59525	7.49053	9.28684	-3.3333	4.00733	8.68401	-1.6335	15838
9.92173	6.92461	9.6991	-2.7778	4.2485	8.87725	-1.7907	20867
9.68344	7.60986	9.40096	-3.3333	4.09434	9.08638	-1.4577	16278
9.86634	7.14677	9.63102	-2.7778	4.17439	9.04898	-1.4848	20794
9.93538	7.10988	9.71577	-2.7778	4.2485	9.24826	-1.2774	20912

9.75499	6.74052	9.49198	-3.3333	4.09434	9.27215	-1.2064	16302
9.10105	7.17778	8.59951	-4.2222	3.68888	9.26324	-1.3781	11101
9.80979	7.31721	9.56079	-3.3333	4.17439	9.19779	-1.3987	16391
9.55992	7.15824	9.24048	-3.3333	4.00733	9.07098	-1.4869	16285
10.0289	7.40191	9.82898	-2.7778	4.31749	9.37516	-1.5813	21599
9.60287	6.29342	9.29679	-3.3333	4.00733	9.19259	-1.2984	16275
9.62757	7.85593	9.32892	-3.3333	4.00733	9.22635	-1.2341	16259
9.77556	7.28355	9.5179	-3.3333	4.09434	9.45334	-1.4408	16849
10.0126	7.35244	9.80929	-2.7778	4.31749	9.23698	-1.4255	21094
10.2665	7.44308	10.109	-1.4444	4.52179	9.24203	-1.1811	37537
10.2895	7.72312	10.1355	-1.4444	4.52179	9.2272	-1.2782	37725
9.79907	7.6024	9.54738	-3.3333	4.17439	8.86499	-1.5562	16036
9.99937	7.70075	9.79339	-2.3333	4.38203	9.40771	-1.4795	26218
9.90901	7.43189	9.68353	-2.7778	4.2485	9.21905	-1.3296	20924
9.72333	6.90274	9.45187	-3.3333	4.2485	9.15252	-1.3869	16307
9.83187	7.46336	9.5883	-2.7778	4.17439	9.40861	-1.4037	21417
9.49507	7.34084	9.1544	-3.3333	4.2485	9.21975	-1.2782	16296
9.9811	7.62315	9.77133	-2.7778	4.31749	9.3842	-1.5399	21559
9.84375	7.57917	9.60306	-2.7778	4.31749	9.17435	-1.2845	20772
8.52806	7.61481	7.67043	-3.8889	4.31749	9.18655	-1.2341	12656
9.90733	7.71468	9.68147	-2.7778	4.31749	9.10642	-1.4986	20929
9.7532	7.50329	9.48971	-3.3333	4.09434	9.18658	-1.2216	16183
10.213	7.712	10.0468	-2.3333	4.44265	9.17314	-2.1945	26866
10.239	7.4061	10.077	-2.3333	4.44265	9.19478	-1.4115	25567
9.43402	7.62608	9.07211	-2.8889	4.44265	9.21563	-1.2912	19860
10.0239	7.30854	9.82293	-2.3333	4.44265	9.23029	-1.1811	25268
9.5674	7.17702	9.25033	-3.3333	4.09434	9.07219	-1.4098	16205
9.39831	5.71043	9.02341	-3.8889	3.91202	8.84662	-1.3179	12313
9.59709	7.40306	9.28924	-3.3333	4.00733	9.02142	-1.6201	16350
9.82866	7.66435	9.58431	-2.7778	4.17439	9.13009	-1.3468	20768
10.1048	7.29912	9.91951	-2.3333	4.38203	9.04804	-1.5198	25386
10.2578	7.4793	10.0988	-2	4.52179	9.17822	-1.2389	29262
9.75863	7.51589	9.49657	-3.3333	4.17439	9.18449	-1.2389	16198
9.90493	7.78322	9.67853	-2.7778	4.17439	9.12768	-1.2845	20678
10.0278	7.10988	9.82758	-2.7778	4.31749	9.11019	-1.2845	20643
10.4216	7.53715	10.2868	-1.6667	4.60517	9.1673	-1.2708	33965
9.98454	7.47477	9.77548	-2.3333	4.38203	9.08056	-1.2913	25085
10.0156	7.39635	9.81291	-2.7778	4.31749	9.14775	-1.3108	20754
9.95593	7.37066	9.74079	-2.7778	4.2485	9.22446	-1.2647	20846
9.72734	6.79122	9.45697	-3.3333	4.09434	9.18626	-1.2912	16257
9.78	7.69712	9.52347	-3.3333	4.09434	9.17042	-1.2879	16229
10.06	7.01121	9.86615	-2.7778	4.31749	9.15708	-1.2567	20699
10.0636	7.46737	9.8705	-2.7778	4.31749	9.24128	-1.3146	20949
9.77422	7.46508	9.51621	-3.3333	4.17439	9.11325	-1.4823	16347

10.0732	7.53636	9.88196	-2.3333	4.38203	8.94928	-1.5198	25144
9.82878	7.32647	9.58445	-2.7778	4.17439	9.2019	-1.3778	20956
9.59836	7.51534	9.29091	-3.3333	4.00733	8.97635	-1.67	16333
10.1698	7.05618	9.9962	-2.3333	4.44265	9.1625	-1.2224	25171
10.2478	7.71423	10.0873	-2.3333	4.49981	9.35092	-1.6785	26419
9.91987	7.22984	9.69683	-2.7778	4.2485	8.89548	-1.1318	20015
9.28592	7.09174	8.86715	-4.2222	3.80666	9.25026	-1.9272	11497
9.32642	6.99189	8.92399	-3.8889	3.80666	9.33699	-1.6441	13194
10.0757	7.55695	9.88487	-2.3333	4.38203	9.36169	-1.4762	26095
9.62153	7.22766	9.32108	-3.3333	4.00733	9.36642	-1.5924	16876
10.1657	7.79441	9.99132	-2.3333	4.44265	9.35764	-1.5198	26160
10.0631	7.32383	9.86983	-2.3333	4.38203	9.42791	-1.5415	26377
10.1879	7.65728	10.0174	-2.3333	4.44265	9.4177	-1.6136	26477

APPENDIX E

Regression Analysis Results

The following is the output of the Minitab ® Statistical Analysis Software Package used for the Regression analysis of the data. The information includes the best subset regression and actual regression analysis for driving the rock strength index equation. The results are for both linear and logarithmic analysis, which yield power functions.

Best Subsets Regression: Linear Response with Rock Strength Index

Vars	R-sq	Adj. R-sq	C-p	s	E	v	S
1	72.6	72.3	2.6	2969.4			X
1	8.4	7.4	226.6	5428.9	X		
2	73.3	72.8	2.0	2944.3	X		X
2	72.6	72.0	4.6	2985.1		X	X
3	73.3	72.5	4.0	2960.0	X	X	X

The linear regression equation is

Rock Strength Index = 8659 + 0.338 Elastic Modulus - 434 Poisson's Ratio + 116144 Size Factor

Predictor	Coef	Stdev	t-ratio	p
Constant	8659	2305	3.76	0.000
Elastic Modulus	0.3377	0.2095	1.61	0.110
Poisson's Ratio	-434	6585	-0.07	0.948
Size Factor	116144	7995	14.53	0.000

s = 2960   R-sq = 73.3%   R-sq(adj) = 72.5%

Analysis of Variance

SOURCE	DF	SS	MS	F	p
Regression	3	2241702400	747234112	85.29	0.000
Error	93	814825472	8761564		
Total	96	3056527872			

Best Subsets Regression, Logarithmic Response with Rock Strength Index

Vars	R-sq	Adj. R-sq	C-p	s	L o g E	L o g v	L o g S
1	84.8	84.7	2.3	0.13550			X
1	6.5	5.5	494.6	0.33654	X		
2	85.0	84.7	3.2	0.13548		X	X
2	85.0	84.7	3.3	0.13553	X		X
3	85.2	84.7	4.0	0.13532	X	X	X

The logarithmic regression equation is

Log (RSI) = 10.2 + 0.097 Log (Elastic Modulus) + 0.444 Log (Size Factor)
            -0.066 Log (Poisson's Ratio)

Predictor	Coef	Stdev	t-ratio	p
Constant	10.1529	0.8278	12.26	0.000
Elastic Modulus	0.09696	0.08758	1.11	0.271
Size Factor	0.44423	0.02048	21.69	0.000
Poisson's ratio	-0.06633	0.05836	-1.14	0.259

s = 0.1894   R-sq = 83.6%   R-sq(adj) = 83.1%

Analysis of Variance

SOURCE	DF	SS	MS	F	p
Regression	3	9.8006	3.2669	178.41	0.000
Error	93	1.7029	0.0183		
Total	9	11.5034			